Shear Strength of Partially Grouted (PG) Masonry Shear Walls: Experimental and Analytical Studies

by

Amr Abubaker Ba Rahim

A thesis submitted in partial fulfillment of the requirements for the degree of

Doctor of Philosophy

in

STRUCTURAL ENGINEERING

Department of Civil and Environmental Engineering
University of Alberta

ABSTRACT

When subjected to in-plane loads, the shear behaviour of partially grouted (PG) masonry shear walls is complex due to the heterogeneous and anisotropic nature of the masonry materials and the nonlinear interactions among their constituents. For instance, insufficient shear strength will lead to a brittle failure mechanism, causing sudden failure and significant loss of life and property. Compared to the other wall systems, experimental studies aimed to investigate the resistance of PG walls against in-plane loads are limited, with some studies lacking features that are important when attempting a generalization of results (such as full-scale test specimens or realistic boundary conditions). Due to this lack of data, equations in North American codes (CSA.S304-14 2014; TMS 2016) for the shear strength prediction in PG walls are largely based on results obtained in fully grouted (FG) masonry walls, even when the nature and behaviour of two types of construction are fundamentally different. In consequence, arbitrary, semi-empirical strength reduction modifiers are required to fit the PG experimental data to the theory developed for FG walls. Unfortunately, it has been shown by Hassanli et al. (2014), Hung (2018), and Izquierdo (2021) that the current provisions in CSA S304 and TMS 402 for PG walls may result in uneconomical and/or unsafe designs in some circumstances.

In an attempt to advance the knowledge regarding PG wall construction, in this study, the in-plane strength of four full-scale PG walls is investigated through experimental and analytical studies. In a departure from some existing literature on the topic, these PG walls were designed and built to simulate and reproduce actual masonry construction practices, including wall geometry, reinforcement distribution, boundary conditions, and loading scenarios. All

the walls were subjected to a combination of constant vertical load and reverse in-plane lateral cyclic load that mimics conditions that may be found in actual walls. The variable design parameters investigated in this study were the aspect ratio and horizontal reinforcement type (bond beams or bed-joint reinforcement). The response of these walls and the role of the variable design parameters were evaluated in terms of hysteretic response, peak strength, energy dissipation, displacement ductility, and damage progression. The experimental peak strength of the specimens was compared to the predictions of North American code-based equations for walls that failed in diagonal shear and the general flexural analysis method for walls that failed in flexure.

The analytical component of the study consisted of the simulation of PG wall behaviour via an analysis model based on the finite element method. After validation with the experimental results obtained in this study and representative cases from the literature, a parametric study was conducted to investigate the role of the horizontal reinforcement types and their interaction with the aspect ratio, axial stress, vertical reinforcement, and compressive strength of masonry on the shear strength of PG walls. Finally, a stepwise regression analysis was performed on the parametric study results to propose an equation that resembles the CSA S304 equation to predict the diagonal shear strength of PG walls.

The experimental results revealed that the bed-joint reinforcement demonstrated to be a feasible economic option as a horizontal reinforcement in terms of energy dissipation, ductility, and crack size control when compared to the classical bond beam reinforcement, particularly in areas with low seismic hazard risk. In addition, the peak lateral load capacity attained by walls with similar aspect ratios had no significant difference regardless of the

reinforcement type used in terms of peak load. On the other hand, the lower the aspect ratio, the higher the peak strength. Regarding the analytical study, there was an acceptable agreement between the experimental and analytical results in terms of initial stiffness, peak load and its associated displacement. Based on the parametric study, the compressive strength of masonry and axial stress were found to significantly influence the shear capacity of PG walls. At the same time, there was a negligible effect of horizontal and vertical reinforcement amounts on shear strength. The proposed coefficients to the CSA S304 equation improved the precision and accuracy of the equation by 59% and 99%, respectively.

Preface

This thesis is the original work of Amr Abubaker Ba Rahim, executed under the supervision of Professor Dr. Carlos 'Lobo' Cruz Noguez. The identification and design of the research program was performed independently with direct supervision of Dr. Lobo. Four journal papers and three conference papers related to this thesis have been published or submitted and are listed below. This thesis is organized in paper format by following the paper-based thesis guidelines and including only the journal papers.

Journal Papers:

1. ***Amr Ba Rahim**, Clayton Pettit, Karren Izquierdo, and Carlos 'Lobo' Cruz-Noguez,* "Partially Grouted Masonry Shear Walls: State of the Art." [In preparation to be submitted to a journal]. I was responsible for the conceptualization, data collection, and analysis as well as the manuscript composition, review and editing. Clayton Pettit was involved with conceptualization, review and editing. Karren Izquierdo was involved with conceptualization, review and editing. Carlos 'Lobo' Cruz-Noguez was the supervisory author and was involved with conceptualization, review and editing.

2. ***Amr Ba Rahim**, Clayton Pettit, Carlos 'Lobo' Cruz-Noguez, and Cristián Sandoval,* "Partially Grouted Masonry Walls with Different Horizontal Reinforcement Types: Experimental Results." *Journal of Structural Engineering*, [Submitted to a journal and under review]. I was responsible for the conceptualization, data collection, and analysis as well as the manuscript composition, review and editing. Clayton Pettit was involved with conceptualization, review and editing. Carlos 'Lobo' Cruz-Noguez was the supervisory author and was involved with conceptualization, review and editing. Cristián Sandoval was the supervisory author and was involved with conceptualization, review and editing.

3. ***Amr Ba Rahim**, Clayton Pettit, Carlos 'Lobo' Cruz-Noguez, and Yong Li,* "Partially Grouted Masonry Shear Walls: Analysis Models using Macro-Modelling Approach."

[In preparation be submitted to a journal]. I was responsible for the conceptualization, data collection, and analysis as well as the manuscript composition, review and editing. Clayton Pettit was involved with conceptualization, review and editing. Carlos 'Lobo' Cruz-Noguez was the supervisory author and was involved with conceptualization, review and editing. Yong Li was the supervisory author and was involved with conceptualization, review and editing.

4. ***Amr Ba Rahim****, Clayton Pettit, Carlos 'Lobo' Cruz-Noguez, and Yong Li,* "Shear Strength of Partially Grouted Masonry Shear Walls: Parametric Study." [In preparation be submitted to a journal]. I was responsible for the conceptualization, data collection, and analysis as well as the manuscript composition, review and editing. Clayton Pettit was involved with conceptualization, review and editing. Carlos 'Lobo' Cruz-Noguez was the supervisory author and was involved with conceptualization, review and editing. Yong Li was the supervisory author and was involved with conceptualization, review and editing.

Conference Papers:

1. ***Amr Ba Rahim****, Jeffrey Hung, Clayton Pettit, and Carlos 'Lobo' Cruz-Noguez* (2019). "Effect of Interior Vertical Reinforcement on the Performance of Partially Grouted Masonry Shear Walls." Proceedings of 13th North American Masonry Conference, Salt Lake City, UT, US. I was responsible for the conceptualization, data collection, and analysis as well as the manuscript composition, review and editing. Jeffrey Hung was involved with conceptualization, review and editing. Clayton Pettit was involved with conceptualization, review and editing. Carlos 'Lobo' Cruz-Noguez was the supervisory author and was involved with conceptualization, review and editing.

2. ***Amr Ba Rahim****, Jeffrey Hung, Carlos 'Lobo' Cruz-Noguez, and Clayton Pettit* (2022). "Experimental Testing of Partially Grouted Masonry Shear Walls with Different

Horizontal Reinforcement Types." Proceedings of CSCE 2022 Annual Conference, Whistler, British Columbia. I was responsible for the conceptualization, data collection, and analysis as well as the manuscript composition, review and editing. Carlos 'Lobo' Cruz-Noguez was the supervisory author and was involved with conceptualization, review and editing. Clayton Pettit was involved with conceptualization, review and editing.

3. ***Amr Ba Rahim****, Clayton Pettit, Carlos 'Lobo' Cruz-Noguez, and Jeffrey Hung*. "An Analysis Model for Partially Grouted Shear Walls Using Macro-Modelling: Importance of Reporting Joint Shear." [Accepted for 14th North American Masonry Conference, OMAHA, NE, US, June 2023]. I was responsible for the conceptualization, data collection, and analysis as well as the manuscript composition, review and editing. Clayton Pettit was involved with conceptualization, review and editing. Carlos 'Lobo' Cruz-Noguez was the supervisory author and was involved with conceptualization, review and editing. Jeffrey Hung was involved with conceptualization, review and editing.

DEDICATION

To the soul of my grandpas, Mohamed Bamashmous and Abdularhaman Bazarah:
Thank you for the inspiration and wisdom I learned from you

To my parents, brothers, and sister

To my lovely wife, Khadega and my daughter, Alia

ACKNOWLEDGEMENTS

First of all, I thank Allah, the Sustainer, the Opener, the Knower of all, for giving me the strength, patience, and knowledge to complete this work.

The Prophet (peace and blessings of Allah be upon him) said, “He who does not thank people (for their favours) has not thanked Allah.” In this regard, I would like to express my deepest gratitude to my supervisor Dr. Lobo for his continuous guidance, valuable support, and motivating encouragement. Actually, his wisdom and passion for research inspired me and improved my skills as a researcher. Also, I am deeply grateful to my committee members, Dr. Douglas Tomlinson and Dr. Yong Li, for their constructive guidance, valuable advice, and cooperation.

I would like to express my sincere gratitude to Greg and Cam, the technicians at Morrison Structural Laboratory, for their patience and cooperation during all phases of the experimental work. Their dedication, especially during the challenging times of the Covid-19 lockdown, has been instrumental in the success of this project. I am also deeply thankful to all of my colleagues who provided invaluable assistance throughout the experimental program.

I would like to express my profound gratitude to Sheikh Abdullah Bugshan for his unlimited financial support from day one of my graduate studies (Master + PhD). Also, I would like to send my appreciation and gratitude to Hadhramout Foundation (HF) for awarding me the scholarship.

I want to thank the Canadian Masonry Design Centre (CMDC) for their assistance in funding the materials and for the valuable technical advice received. Also, I want to thank the Scorpio Masonry AB Inc. and Expocrete for constructing the tested walls.

Lastly, I would like to express my love and appreciation to my mother, father, grandma, sister, brothers, and all family members for their valuable prayers and motivating encouragement throughout my PhD program. I am grateful to my wife for her encouragement, endurance, and patience in this stressful journey of becoming a doctorate.

TABLE OF CONTENTS

LIST OF TABLES

LIST OF FIGURES

LIST OF SYMBOLS AND ABBREVIATIONS

The following parameters and symbols are used in this paper:

A_{net} Net cross-sectional area of a wall (mm^2)

A_{nv} Net shear area (mm^2)

$A_{h,bar}$ Cross-sectional area of (horizontal) shear reinforcement (mm^2)

A_s Reinforcement area (mm^2)

A_{vf} Total area of flexural (outer vertical) reinforcement (mm^2)

a Width of the compression block of masonry (mm)

b Width of the cross-section (mm)

c Location of neutral axis from the extreme fibre of cross-section (mm)

d Location of vertical reinforcing bar from the extreme fibre of cross-section (mm)

d' Location of compression vertical reinforcing bar from the extreme fibre of cross-section (mm)

d_v Effective depth of the cross-section, where $d_v \geq 0.8L$ (mm)

E_S Yong modulus of vertical reinforcing bar (MPa)

f'_m Compressive strength of masonry (MPa)

f'_{mg} Compressive strength of grouted masonry prism with h/t=5 (MPa)

f_{yh} Yield strength of horizontal reinforcement (MPa)

f_{yv} Yield strength of vertical reinforcement (MPa)

L Length of masonry wall, in direction of applied shear force (mm)

$\frac{M}{VL}$ Maximum moment at the section under consideration divided by the shear force times length,

which shall be taken as a positive number and need not be taken greater than 1.0

$\frac{M_f}{V_f d_v}$ Ratio of shear span to depth, $0.25 \leq \frac{M_f}{V_f L} \leq 1$, for the concurent moment, M_f and factored shear, V_f, at the section under consideration (unitless)

P Axial compressive load (kN)

s_h Spacing of horizontal reinforcement (mm)

$s_{v,ave}$ Average spacing between interior vertical reinforcement (mm)

t Wall thickness (mm)

$\alpha_1 \& \beta_1$ Compression stress block factors obtained using Hognestad's parabola

ε_m Compresssive strain of masonry where ε_m=0.003 at the ultimate state

ε_S Strain of reinforcing bar

γ_g Factor to account for partially grouted walls when calculating shear resistance, not greater than 0.5

$\gamma_{g,US}$ 0.75 for partially grouted shear walls and 1.0 otherwise.

1. INTRODUCTION

1.1 Background

In masonry constructions, load-bearing, partially grouted masonry shear walls (PG walls) are employed as a lateral force-resisting system. In contrast to fully grouted (FG) walls, which are grouted completely, PG walls are only grouted where reinforcing bars have been installed, such as vertically aligned cells with vertical flexural reinforcement or horizontal bond beams with shear reinforcement. Due to their lower labour and material costs, they provide an economic benefit over FG walls (Minaie et al. 2010; Dhanasekar 2011). In North America, PG walls are commonly seen in commercial and school buildings, college dormitories, hotels, and apartment buildings (Bolhassani et al. 2016b). Contrary to FG walls, which perform similarly to reinforced concrete, the shear response of PG walls under in-plane lateral loading is not yet fully known, making it difficult to estimate the shear strength of PG walls. As a result, North American code-based expressions used to predict the in-plane shear capacity were completely developed using FG wall data and then applied a reduction factor to PG walls in order to attain safety levels comparable to FG walls (Dillon P. and Fonseca 2017). Thus, the current design expressions have a limited degree of accuracy and, in some circumstances, are not conservative (Haider 2007; Minaie et al. 2010; Dhanasekar 2011; Hassanli et al. 2014; Bolhassani et al. 2016a; Izquierdo 2021).

An examination of the available literature shows that experimental programs on the shear behaviour of PG walls are limited compared to those on FG walls, and if available, they have unfortunately suffered from experimental constraints, which have hindered the use of their results. These have consisted of the inconsistent scale of test specimens and non-realistic boundary conditions.

This research presents the experimental and analytical results of four full-scale walls made of concrete masonry units (CMUs) to expand our understanding of PG wall construction. Unlike some of the current literature on the subject, these PG walls were designed and built to model and replicate actual masonry construction practices, including wall geometry, reinforcement detailing, boundary conditions, and loading settings. These walls were subjected to a combination of constant axial load and reverse cyclic in-plane lateral loads. The aspect ratio

and horizontal reinforcement types (bond beams and bed-joint reinforcement) were the variable design parameters in this research. The response of these walls and the role of the variable design parameters were studied in terms of hysteretic response, damage development, and peak strength. The experimental peak strength of the wall specimens was compared to the predictions of North American code-based equations for walls that failed in shear and the general flexural analysis method for walls that failed in flexure.

To interpret the data and investigate the effect of the design parameters, an analysis model based on the finite-element method was defined using the macro-modelling approach (i.e. treating the masonry assemblage as a region with averaged properties) to simulate the behaviour of the PG walls. Using a finite-element software that implements the modified compression field theory (MCFT) originally developed by Vecchio and Collins (1986) for reinforced concrete, the variant of the disturbed stress field model (DSFM) by Vecchio (2000, 2001) for reinforced concrete, and then upgraded by (Facconi et al. 2013) for masonry, aspects of the global behaviour such a peak strength, displacement at peak load, and initial stiffness were determined and compared to the experimental results from this study and other selected literature to determine the validity of this model. After validation, the analysis model was used to conduct a parametric study to study the effect of horizontal and vertical reinforcement, aspect ratio, level of axial load, and masonry compressive strength on the peak strength of PG walls. Finally, a stepwise regression analysis was conducted on a total of 442 experimental and numerical walls that failed or expected to fail in shear to propose an expression, resembling CSA S304 equation, to predict the in-plane shear strength of PG walls. Design recommendations based on the findings of the parametric study are developed. Design aids, methods, and tools for practicing engineers will be produced to aid in using, evaluating, and assessing these structural systems in real-life applications.

1.2 Problem Statement

Partially grouted walls are a cost-effective structural option to resist lateral loads in single-storey and low-rise buildings in areas with low seismicity. However, the literature review shows that the efforts to understand the shear response of PG walls subjected to in-plane loads and to develop models to predict their shear strength have been hindered by several factors. The first is the complex interaction among the material components of a PG wall, such as concrete blocks, mortar joints, reinforcement, and grouted/ungrouted cells. The second is related to the limitations in the experimental research discussed in the literature review, which leads to a comparatively small number of tests performed on PG walls than those conducted on FG walls. Compounding the problem, many PG walls in the literature are not representative of realistic masonry construction, and have issues regarding scale, vertical reinforcement ratio, boundary conditions, and loading protocols.

Therefore, there is a need to develop a new framework for investigating the in-plane shear capacity of PG walls, in which realistic design details, boundary conditions, and design variables are taken into account. In particular, the role of the horizontal reinforcement type should be clarified, as there is no clear consensus in the literature about its contribution to shear strength. While most of these studies conducted by Schultz (1994, 1996), Schultz et al. (1998), Baenziger and Porter (2011), Ramírez et al. (2016), Sandoval et al. (2018), and Stathis (2018) found that bed-joint reinforcement had superior performance over the bond beam in terms of cracking control and mitigating damage, Hidalgo and Luders (1986) and Hoque (2013) pointed out that the cracking patterns were more scattered in walls reinforced with bond beams. A study is warranted to investigate the advantages and limitations of each type and assess which system is the better option in terms of peak lateral capacity and post-peak performance.

The framework should include the definition of efficient analysis models, validated with experimental data, which can be used to extend the experimental results through parametric analysis. Regression analysis to determine improved design equations to predict the shear wall capacity of PG walls can be conducted on such expanded databases.

1.3 Objectives

To achieve the general objective of this investigation, the following objectives are identified:

1. To investigate PG walls experimentally with realistic details, incorporating the influence of major design variables.
    - *Specific goal 1:* Perform a literature review to identify the limitations and gaps in the experimental studies and reflect that into the design and construction of the walls tested in this study;
    - *Specific goal 2:* Design and build four full-scale walls, incorporating realistic construction details and design parameters;
    - *Specific goal 3:* Conduct a cyclic test on the walls to investigate the effects of horizontal reinforcement and aspect ratio on the hysteretic response, peak strength, damage progression, and failure mode;
    - *Specific goal 4:* Assess the predictive power of the current North American code-based expressions developed to capture the experimental peak lateral strength of the tested walls of this study.

2. To implement an analysis model for PG walls that captures their in-plane response against lateral loads.
    - *Specific goal 1:* Define a reliable macro-scale analysis model for the response of PG walls using the finite element method (FEM). This model implements a macro-modelling approach based on the concept of distributed cracking "smeared cracked" to model both plain concrete and unreinforced masonry and a discrete approach to model steel reinforcement;
    - *Specific goal 2:* Validate this model with the experimental results obtained in this study and selected results from the literature;

3. To conduct a parametric study using the analysis model to expand the range of variables and design parameters included in the experimental study.
    - *Specific goal 1:* Define a matrix of walls to be analyzed. This process considers the limited literature on the combined effect of more than one independent design

parameter, i.e. combining the effect of the horizontal reinforcement type with the axial loading, aspect ratio, vertical reinforcement, and masonry compressive strength on the dependent in-plane shear response of the PG wall;

- *Specific goal 2:* Generate a database of analytical relationships between the independent parameters chosen in *Specific goal 1* and the dependent shear strength of the walls. These relationships are compared and discussed in the context of available test data and findings from the literature;
- *Specific goal 3:* Conduct regression analyses using the stepwise regression technique to propose an equation, resembling CSA S304 equation parameters, to predict the in-plane shear strength of PG walls– and then evaluate its precision and accuracy against the current CSA S304 equation.

1.4 Scope

This research is limited to the study of shear- and flexure-critical PG (partially grouted) masonry shear walls built with concrete blocks. The lateral loads are applied in a cyclic, quasi-static manner, and as such the inertial effects are not investigated. The walls are solid, with no openings, and are assumed to be part of buildings located in areas with low seismicity. Therefore, the walls in this study are designed as conventional masonry construction, with no seismic detailing such as anchorage detailing.

The failure modes considered in this study are in-plane shear (for squat walls), including both diagonal shear and crushing of the masonry compressive struts, and flexural-shear (for slender walls). Other failure mechanisms (such as sliding shear or out-of-plane buckling) are precluded. Due to their relatively low aspect ratio and the fact that they are tested as cantilevers, the walls in this study are intended to represent an entire wall (from foundation to roof) in a low-rise building or a single-storey building.

1.5 Organization of Thesis

There are six chapters in this thesis:

- Chapter 1 introduces the research study and contains its problem statement, objectives and scope.

- Chapter 2 includes a comprehensive literature review of the experimental testing of PG shear-critical walls in terms of wall deign, loading setup, and types of horizontal reinforcement. Also, the analysis models of PG walls using finite element methods are reviewed.
- Chapter 3 describes the design and installation of wall specimens and the setup used for the full-scale cyclic test. Also, it introduces the experimental results in terms of the cracking pattern, hysteretic response, and peak strength. In addition, the prediction equations for flexural and shear strength are examined against the experimental peak strength of slender and squat walls, respectively.
- Chapter 4 presents the development of the finite element macro-model and validation of the developed model against experimental walls from various studies. In addition, numerical investigations were conducted on the failure mode and peak strength prediction of PG walls.
- Chapter 5 presents the results of the parametric analysis on 541 wall models that failed in a diagonal shear using the FE mode developed in Chapter 4. Besides, this chapter proposes a suggestion to improve the predictive ability of the CSA S304 equation by updating the equation coefficients.
- Chapter 6 describes the outcomes and recommendations based on the results of this research study.

2. LITERATURE REVIEW

Partially Grouted Masonry Shear Walls: State of the Art

Amr Ba Rahim [a], Clayton Pettit [a], Karren Izquierdo [a], and Carlos 'Lobo' Cruz Noguez [a]

[a] Department of Civil and Environmental Engineering, University of Alberta, 9211-116 Street, Edmonton, Alberta T6G 1H9, Canada

Abstract (194 Words)

Partially grouted (PG) masonry shear walls built using concrete blocks are widely used in construction, yet their behaviour under lateral loading remains an active area of research. This paper presents an overview of research on PG masonry shear walls, focusing on experimental testing and analytical modeling. The experimental section provides a critical review of wall design, loading setup, horizontal reinforcement types, and data reporting issues. The analytical section highlights the differences between two main modeling approaches using finite element methods: micro- and macro-modeling. It is concluded that there is a need to design and construct PG walls that more closely resemble realistic construction details, including wall size, reinforcement detailing, and boundary conditions. Furthermore, the function of horizontal reinforcement on the shear strength of PG walls needs to be clarified, as there is no clear consensus in the literature. The macro-modelling approach has been demonstrated to be practical for capturing peak strength and conducting parametric analyses to develop expressions predicting the peak strength of PG walls. These findings are important for improving the design and construction of PG masonry shear walls and for the development of improved modeling approaches that can inform building codes and design standards.

2.1 Introduction

Reinforced masonry (RM) shear walls are often used as the primary load-resisting system against lateral loads in low- and medium-rise masonry structures. RM walls can be fully grouted (FG) or partially grouted (PG), with the latter option being generally more economical and thus widely used in the masonry industry due to the ease of construction and low consumption of construction materials. Compared to FG walls, there is still a limited understanding of the response of PG walls against in-plane loads (Hamid et al. 2009; Banting and El-Dakhakhni 2012, 2014; Dillon 2015).

Several experimental studies demonstrate that several factors hinder the full understanding of the PG walls response, hence developing models to predict their strength. First are masonry materials' anisotropic properties and the complex interaction between unit block, mortar, grout, and reinforcing steel. This complex mechanism reflects in the arbitrary reduction factors adopted by CSA S304 and TMS 406 to add more conservatism compared to FG walls (Dillon and Fonseca 2017). Second, the limitations on experimental research, which result in fewer PG walls being tested than FG walls. Elmapruk et al. (2020) pointed out that experimental studies investigating the shear strength of partially grouted masonry walls are scarce, and the outcomes of many of these studies have not been adequately reported. Furthermore, various specimens tested in the literature did not adhere to the current minimum reinforcement requirements specified by building codes.

Besides the experimental tool, the numerical tool is used to study the PG wall response through the finite element (FE) methods, either using micro-modelling of the individual components of the masonry walls system or macro-modelling of the masonry wall system as a composite (Lourenco 2004). El-Dakhakhni and Ashour (2017) highlighted the importance of utilizing the macro-modelling approach as a key numerical tool used to predict the response of PG walls.

This paper is concerned with the experimental testing and analytical models of partially grouted (PG) masonry shear walls, utilizing the finite element (FE) method. The experimental section will provide an overview of the wall design, including the size effect and scaling, vertical reinforcement, and boundary conditions, as well as the implementation of axial and

lateral load setups. The paper will also discuss the performance of two horizontal reinforcement types used in PG walls based on experimental studies. The analytical portion will address the differences between micro- and macro-modelling approaches, followed by a review of relevant studies that have implemented these two approaches.

2.2 Experimental Testing of PG Shear-Critical Walls

2.2.1. Wall Design

Size Effects and Scaling

The majority of the experimental programmes have investigated PG walls that were smaller than the typical masonry shear wall found in a building (Minaie 2009a). Testing walls of realistic sizes is essential. Hamedzadeh (2013) pointed out that testing full-scale specimens is not always feasible due to space, cost, and loading device capacity constraints. Building a reduced-scale model of the planned full-scale prototype is one answer to these issues. Small-scale walls make up about 17% of the PG masonry walls that have been experimentally tested in the literature. Typically, scales of one-half or one-third blocks have been utilized (Izquierdo 2021).

One issue with reduced-scale models is the size effect, which shows that smaller size specimens have higher strength and more data scatter than their prototype counterparts (Maleki 2008). Sarhat and Sherwood (2015) found that masonry beam specimens with larger depths had smaller shear stress capacities and more brittle behaviour than smaller specimens due to greater crack widths.

Changing the physical dimensions of the model also influences the significance of several design parameters on the overall behaviour of the structure, such as the bond between reinforcement and mortar or grout and the adhesion between mortar and masonry units. It has been observed that the overall behaviour of the structural system and its global failure mechanism can be determined by testing small-scale masonry building models (Tomaževič and Velechovsky 1992; Long 2006). For instance, Long (2006) found that a reduced-scale model and prototype wall intended to fail in flexure were more similar than a model and prototype wall intended to fail in shear. This may be attributed to the cracking size effects, which were more noticeable in the walls failing in shear due to diagonal cracking.

Vertical Reinforcement

A number of walls tested in the literature also had details that are not commonly found in typical construction. For instance, a common way to promote shear failures is by designing

walls with very large vertical reinforcement ratios to ensure the moment capacity will not be reached before the walls fail in shear. A survey in the literature showed that the vertical reinforcement ratio ranged between 0.10 to 1.22% for most studies which is more than the common ratio usually adopted in masonry construction (0.045% - 0.09%) (CSA.S304-14 2014; Hatzinikolas et al. 2015). Besides being unrealistic, using large vertical reinforcement ratios is problematic because vertical reinforcement has been found to contribute to the shear strength by dowel action prior to yield. Shing et al. (1989, 1990) noted that specimens with higher amounts of vertical reinforcement exhibited higher shear strength than specimens with lower amounts. Shing et al. (1989, 1990) attributed the increased strength to the dowel action of the vertical reinforcement and truss action of the vertical and horizontal reinforcement, which reduced crack widening and therefore maintained aggregate interlock and integrity of the wall. Specimens with higher amounts of vertical reinforcement also showed slower strength degradation after reaching maximum lateral strength. Tomaževič (1999) and Haach et al. (2011), on the other hand, found that vertical reinforcement had no discernible impact on in-plane diagonal shear strength.

Boundary Conditions

The global deformation response of typical multi-storey buildings under lateral loads depends on the lateral force-resisting system (LFRS), as shown in Figure 2.1. Shear-dominated behaviour is seen in buildings that incorporate moment-resisting frame (MRF) systems, and flexural-dominated behaviour appears in buildings in which shear wall (SW) systems are used to resist lateral loads (Clough and Penzien 2003).

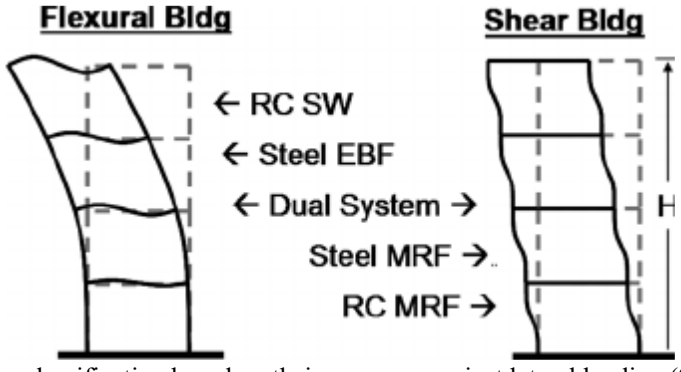

Figure 2.1 Buildings classification based on their response against lateral loading (Skolnik et al. 2011)

In masonry buildings, the LFRS consists of shear walls, and hence, the global deformation response of such a structure could be assumed to be flexurally-dominated. The moment profile experienced by the complete wall (from foundation to roof) under lateral loads, such as that arising from seismic demands, is shown in Figure 2.2.

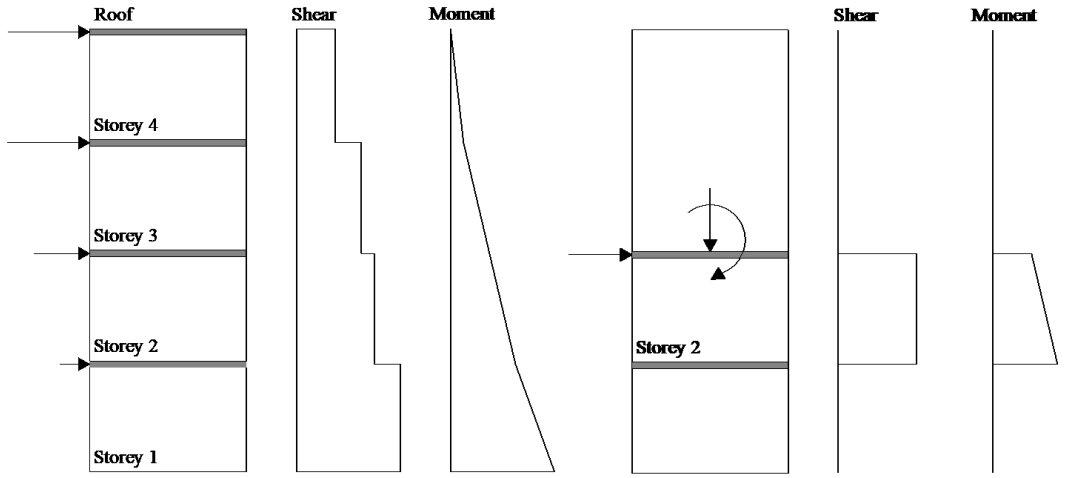

Figure 2.2 Distribution of forces in multi-storey masonry building adapted from Drysdale and Hamid (2005)

Figure 2.2 illustrates a common type of masonry construction used for multi-storey buildings, in which the walls are built storey by storey. Once a wall is laid up in a specific storey, the floor system (e.g., an RC slab or a precast beam floor system) is placed on top of the top course of the wall. Once the floor system is installed, another one-storey high wall segment is built on top of it. Adequate detailing is provided to ensure an adequate transmission of forces and moments between the floor system and the wall, and between the wall segments below and above the wall (Figure 2.3).

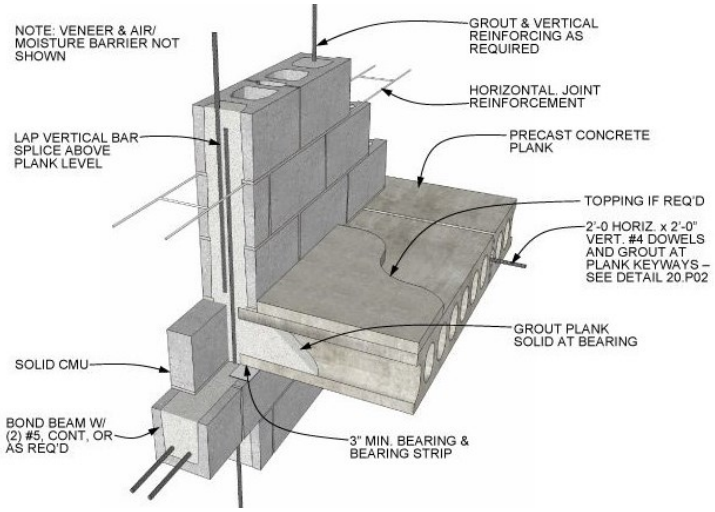

Figure 2.3 Wall-slab connection detailing at the intermediate storey (International Masonry Institute 2011)

Studies on the in-plane strength of wall systems are often aimed to capture a) global wall behaviour (from foundation to roof), b) inter-storey wall behaviour, or c) a subcomponent of the wall system, such as the wall segments that surround openings. In general, for global wall behaviour, the optimal boundary conditions are a cantilevered wall specimen (Figure 2.2). The same figure shows that for inter-storey wall behaviour, the most representative setup will be one that allows the wall to bend in single curvature, with a greater moment at the bottom than at the top. Finally, for piers or spandrels, it depends on the relative size of the opening with respect to the wall – for instance, a pier next to an opening may be constrained to bend in double curvature if the wall above and below the pier provides enough restraint (Figure 2.4).

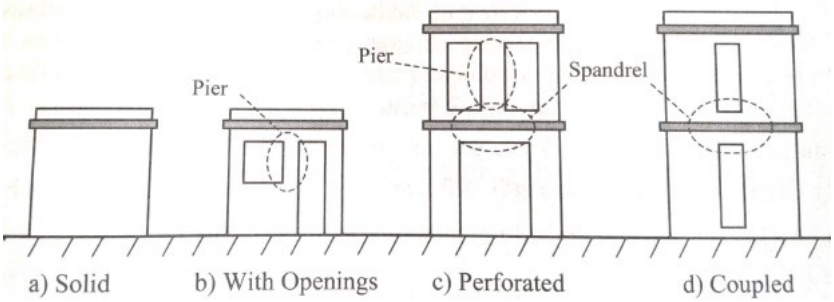

Figure 2.4 Elements in masonry shear walls (Hatzinikolas et al. 2015)

A survey of the literature shows a significant number of fixed-fixed walls (90 out of 205 tested walls documented by Izquierdo [2021]). One reason for this is practicality: it is easier to

promote a shear failure in walls tested under double curvature, as the shear force that develops in such a wall is higher than that developed in a wall tested as a cantilevered specimen.

Cantilevered setups (115 out of 205 walls), are popular due to their simplicity and less-specialized equipment requirement compared to fixed-fixed setups (Dillon 2015a).

2.2.2. Loading Setup

Lateral Loads

According to the literature, 200 out of 205 wall specimens have been tested under a quasi-static loading setup (Izquierdo 2021), as shown in Figure 2.5. Cyclic, quasi-static loads allow for the study of the hysteretic behaviour of structural systems in terms of crack tracking, damage propagation, and stiffness degradation. Dynamic tests, such as those conducted on shake table facilities, allow for the inclusion of inertial forces and the study of dynamic parameters such as strain-rate effects, response spectrum, damping ratio, natural frequencies, and mode shapes. However, dynamic tests are expensive and are seldom used.

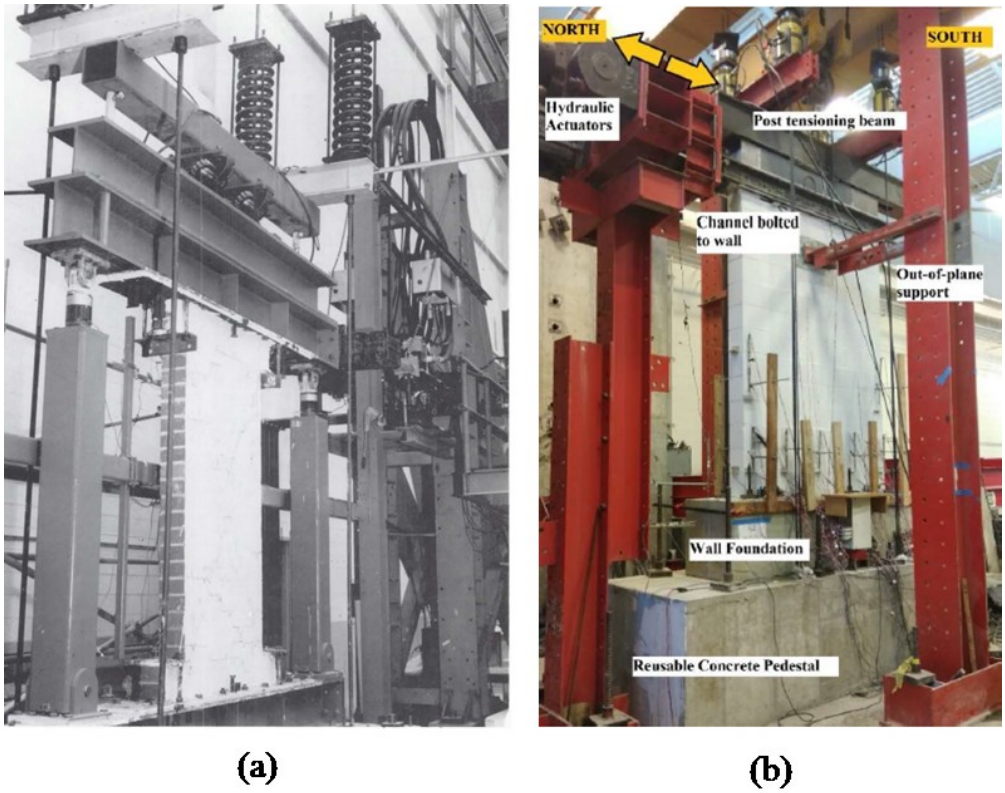

Figure 2.5 Overview of (a) Mayes et al. (1976) and (b) Mahmood et al. (2021) setup

Monotonic, incrementally-increasing cyclic (reverse cyclic), sequential-phased displacement, and simulated seismic loading histories have all been used to test walls (Tomaževič et al. 1996). Sample loading protocols are illustrated in Figure 2.6 (Tomaževič et al. 1996).

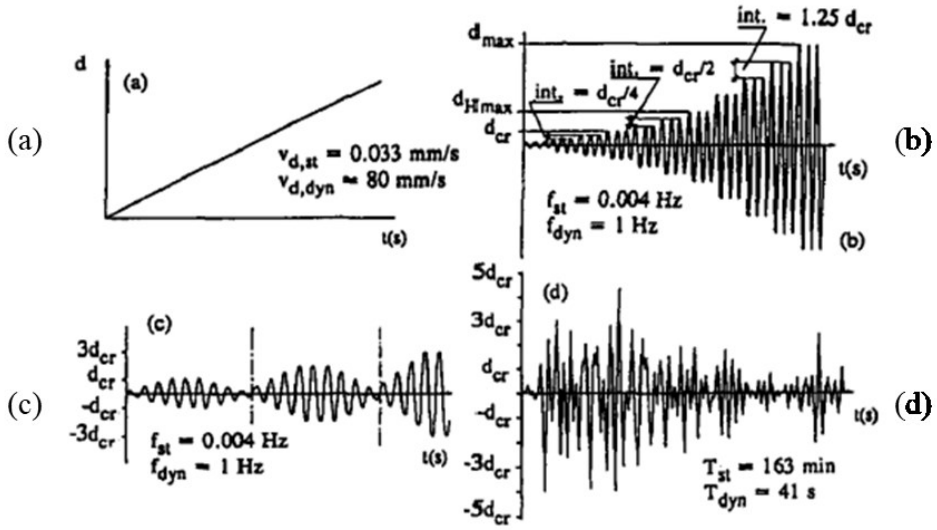

Figure 2.6 Displacement Time Histories protocols used to apply the lateral load; (a) Monotonic; (b) Reverse Cyclic; (c) Phased-Sequential; (d) Simulated Earthquake Response (Tomaževič et al. 1996)

Axial Loads

Axial loads on masonry walls arise from the occupancy loads, loads applied over the tributary areas, and load distributions coming from the floors and roof (Banting and El-Dakhakhni 2012). The axial stresses caused by gravity loads in a midrise reinforced masonry structure of three to eight stories in height would typically be expected to be less than 10% of the compressive strength of the concrete block unit (Banting and El-Dakhakhni 2012). According to the literature, the axial stress to the compressive strength of masonry ratio (σ/f'_m), adopted in the experimental studies, has ranged between 0.5 to 27.5% (Izquierdo 2021).

To simulate the gravity load acting on a wall specimen, post-tensioned bars and actuator systems are commonly used. Perhaps one of the most important features when designing an axial load system is that the axial load provided be constant throughout the lateral movement of the wall specimen.

Mobeen (2002), Moghimi (2013), and Dastfan and Driver (2015) used a system called gravity load simulator (Figure 2.7). This system maintains the verticality of the axial load throughout the lateral movement of the wall.

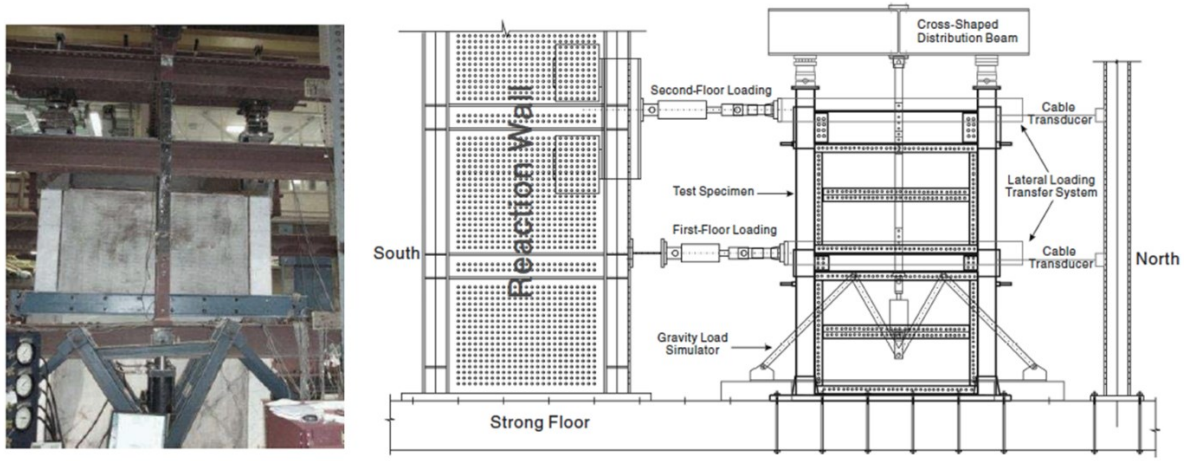

Figure 2.7 Test setup by Dastfan and Driver (2015)

2.2.3. **Types of Horizontal Reinforcement**

Two horizontal reinforcement types commonly used in masonry walls are bond beam and bed joint reinforcement. Bond beam reinforcement consists of horizontal steel bars placed at the centre of the masonry courses, supported on knocked-out webs and then filled these courses with grout. On the other hand, bed-joint reinforcement consists of a ladder-type steel reinforcement that is placed at the top of the masonry joints before applying mortar, as shown in Figure 2.8.

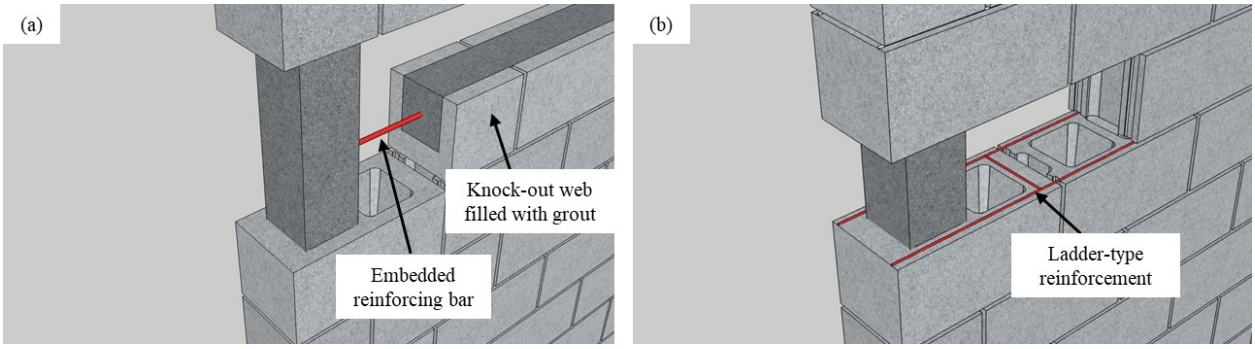

Figure 2.8 Types of horizontal reinforcement; (a) Bond beam reinforcement and (b) Bed-joint reinforcement

Bond beam reinforcement has a wide range in sizes (10M-25M) as per Clause 12.1.2 (CSA.S304-14 2014). TMS (2016) expands this range to include 30M as the maximum bar size as per Clause 9.3.3.1(a). On the other hand, bed-joint reinforcement has a limitation in size due to limited mortar thickness, which is typically 10 mm (Oan 2013; Calderon et al. 2021a). While TMS (2016) limits using the joint reinforcement to be at least 4.8 mm diameter as per Clause 9.3.3.1 (b), CSA.S304-14 (2014) bounds the joint reinforcement size between 3.0 mm and not less than one-half the mortar joint thickness or 5.0 mm, whichever is less as per Clause 12.1.4.

Tomaževič and Lutman (1988), Yancey and Scribner (1989), Schultz (1996), Schultz et al. (1998), Baenziger and Porter (2011), Hoque (2013), Bolhassani et al. (2016b), Stathis et al. (2018), Schultz and Johnson (2019), and Calderon et al. (2021a) investigated the influence of horizontal reinforcement types on the shear strength of PG walls. Hidalgo and Luders (1986), Wierzbicki (2010), and Hoque (2013) noted that bed-joint reinforcement is less effective than bond beam reinforcement as horizontal seismic reinforcement because it can readily fracture when subjected to several loading and unloading cycles. As a result, walls reinforced with a bond beam can be built to carry higher lateral capacities than those with bed-joint reinforcement.

On the other hand, Schultz et al. (1998), Baenziger and Porter (2011), Ramírez et al. (2016), Sandoval et al. (2018), Stathis et al. (2018) observed that bed-joint reinforcing played a major role in controlling the cracking distribution and improving the post-peak behaviour and wall ductility when compared to the bond beam reinforcement. This was attributed to the ability of bed-joint reinforcement to limit the propagation of existing cracks, forcing the creation of new cracks throughout the wall panel after reaching the peak lateral load.

In addition, this sub-section highlights the experimental studies and their outcomes that investigated both horizontal reinforcement types in one single study as follows.

Tomaževič and Lutman (1988)

Table 2.1 Properties of the tested walls (Yancey and Scribner 1989)

Total number of PG shear-critical walls in study: 10			Slovenia
Loading Type:	Reverse Cyclic	f'_m:	9.5 - 10.7 MPa
Loading Rate:	Quasi-Static	A_{net}/A_{gross}:	0.60
Support Type:	Cantilever	Net Axial Stress:	1.65 MPa
Scale:	0.5	Gross Axial Stress:	0.98 MPa
Height:	760 - 1405 mm	Flexural Reinf.:	0.26 - 0.52%
Length:	610 mm	Vertical (Interior) Reinf.:	0%
Thickness:	100 mm	Bond Beam Reinf.:	0%
H/L:	1.25 - 2.30	Joint Reinf.:	0 - 0.50%

Tomaževič and Lutman (1988) examined 16 PG masonry walls, with half measuring 760 mm in height and the other half measuring 1405 mm. The researchers used four horizontal reinforcement ratios (0%, 0.14%, 0.28%, and 0.50%) and two vertical reinforcement ratios (0.26% and 0.52%) for both the squat and slender wall groups. The study found that for slender walls with horizontal reinforcement, the walls' shear resistance improved significantly, resulting in flexure failure for six of the tested walls. The remaining ten walls failed in shear, including all the squat walls. Figure 2.9 presents the configuration and dimensions of the of the test specimens. More details about the tested PG walls are presented in Table 2.1.

According to Tomaževič and Lutman (1988), both vertical and horizontal reinforcement improved the seismic behavior of masonry walls (Figure 2.10). Specifically, horizontal reinforcement in the mortar joints led to enhanced shear capacity and ductility, resulting in some walls' vertical reinforcement yielding and a shift in failure mode from shear to flexure. The researchers also observed that, following wall cracking initiation, the horizontal joint reinforcement functioned in tension but did not yield, likely due to inadequate bond between mortar and reinforcement and concrete masonry block crushing, which prevented full

development of the reinforcement's tension capacity. At the peak load, the horizontal reinforcement was 41-66% effective, while at the maximum displacement (failure load), it was 61-83% effective. Tomaževič and Lutman further emphasized that quality masonry units and mortar, as well as sufficient reinforcement bond and anchorage, were necessary to activate the reinforcement fully.

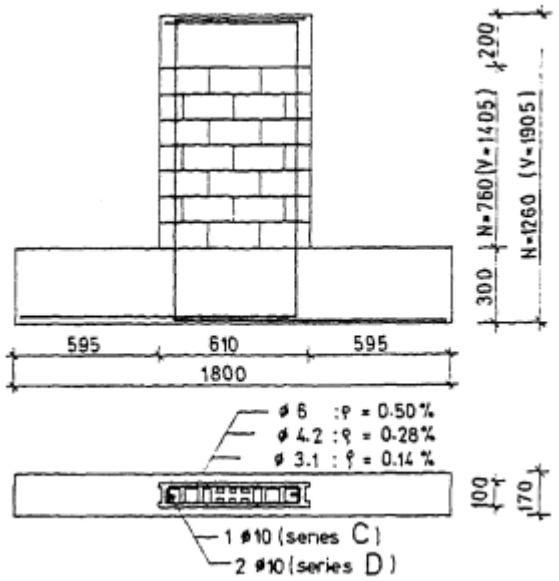

Figure 2.9 Details of test specimens

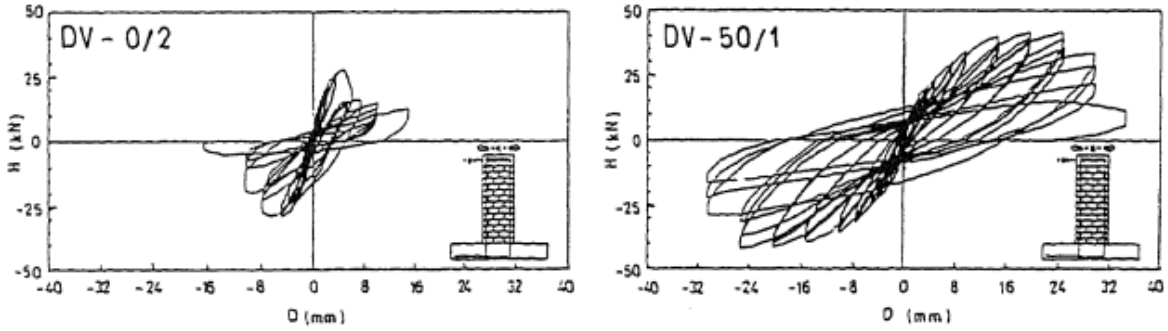

(a) (b)

Figure 2.10 Hysteretic response for (a) horizontally unreinforced and (b) horizontally reinforced walls

Yancey and Scribner (1989)

Table 2.2 Properties of the tested walls (Yancey and Scribner 1989)

Total number of PG shear-critical walls in study: 9			USA
Loading Type:	Reverse Cyclic	f'_m:	Unknown
Loading Rate:	Quasi-Static	A_{net}/A_{gross}:	0.54
Support Type:	Double Curvature	Net Axial Stress:	1.38 MPa
Scale:	1	Gross Axial Stress:	0.74 MPa
Height:	1422 mm	Flexural Reinf.:	0%
Length:	1219 mm	Vertical (Interior) Reinf.:	0%
Thickness:	194 mm	Bond Beam Reinf.:	0 - 0.22%
H/L:	1.17	Joint Reinf.:	0 - 0.06%

Yancey and Scribner (1989) tested 13 walls, three of them flexure-critical, and the other ten shear-critical. One of the ten shear-critical walls was unreinforced, while the other nine were PG walls. The study's goal was to see how changing the amount and distribution of horizontal reinforcement affected the results. Bed-joint reinforcement was used on two specimens, bond beams were used on five specimens, and a combination of joint and bond beam reinforcement was used on the remaining two specimens. More details about the tested PG walls are presented in Table 2.2. Figure 2.11 depicts the setup for the test. There was no vertical reinforcement on any of those walls, to single out the effect of the horizontal reinforcement type, which creates uncertainty about any possible interaction between the horizontal and vertical reinforcement. The translation of the results to actual practice, which requires a minimum vertical reinforcement in masonry walls, is therefore questionable.

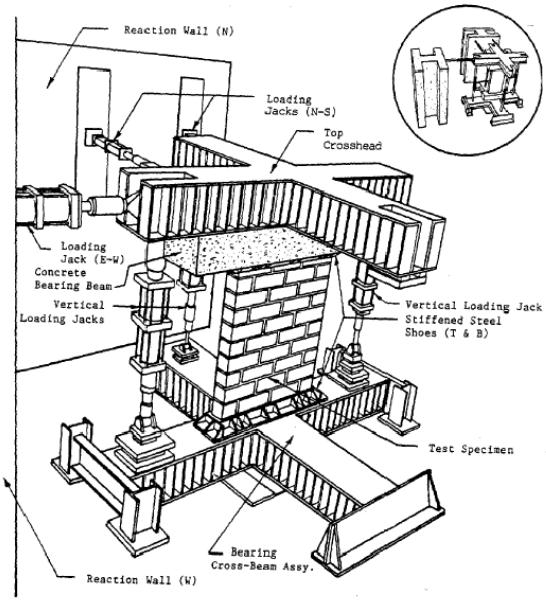

Figure 2.11 Test setup used by Yancey and Scribner (1989)

Yancey and Scribner (1989) concluded that increasing horizontal reinforcement increases shear strength but not proportionally to the amount of reinforcement added. They observed that bed joint reinforcement placed in alternating courses was as effective in increasing shear strength as bed joint reinforcement placed in each course, as shown in Figure 2.12. In addition, it is observed that the cracking pattern for walls reinforced exclusively with bond beam reinforcement had a more severe cracking pattern than those reinforced with bed-joint reinforcement in terms of block crushing, splitting, and spalling, as shown in Figure 2.13.

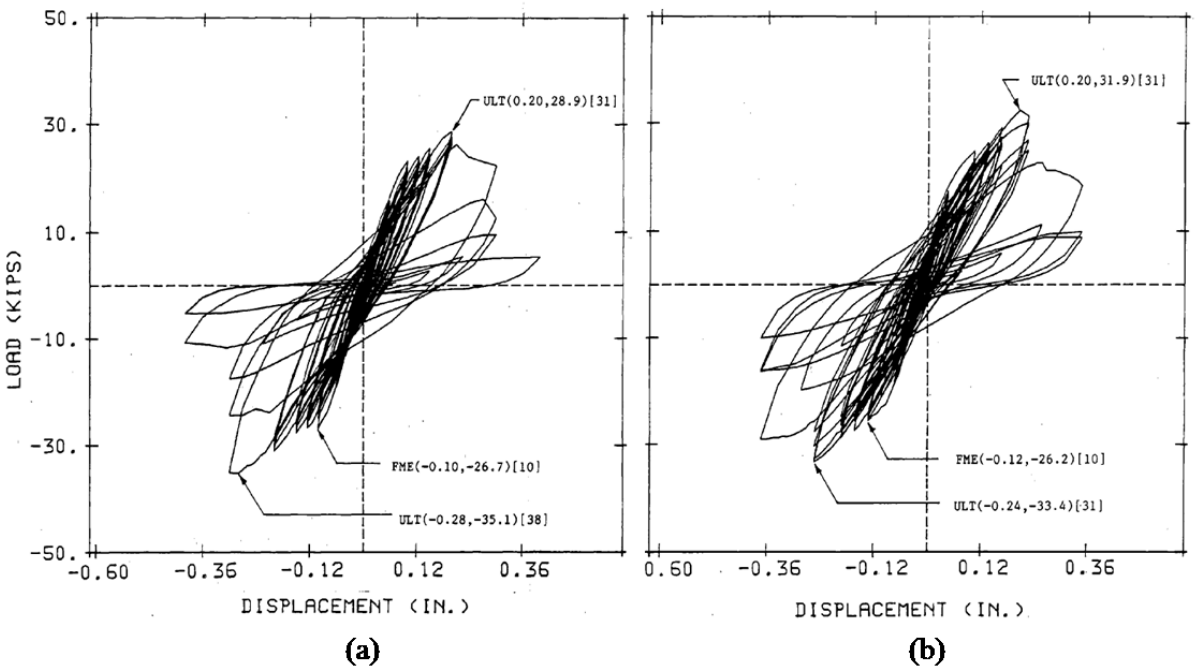

Figure 2.12 Load-Displacement curve for (a) wall reinforced with bed-joint in alternating courses and (b) wall reinforced at every course (Yancey and Scribner 1989)

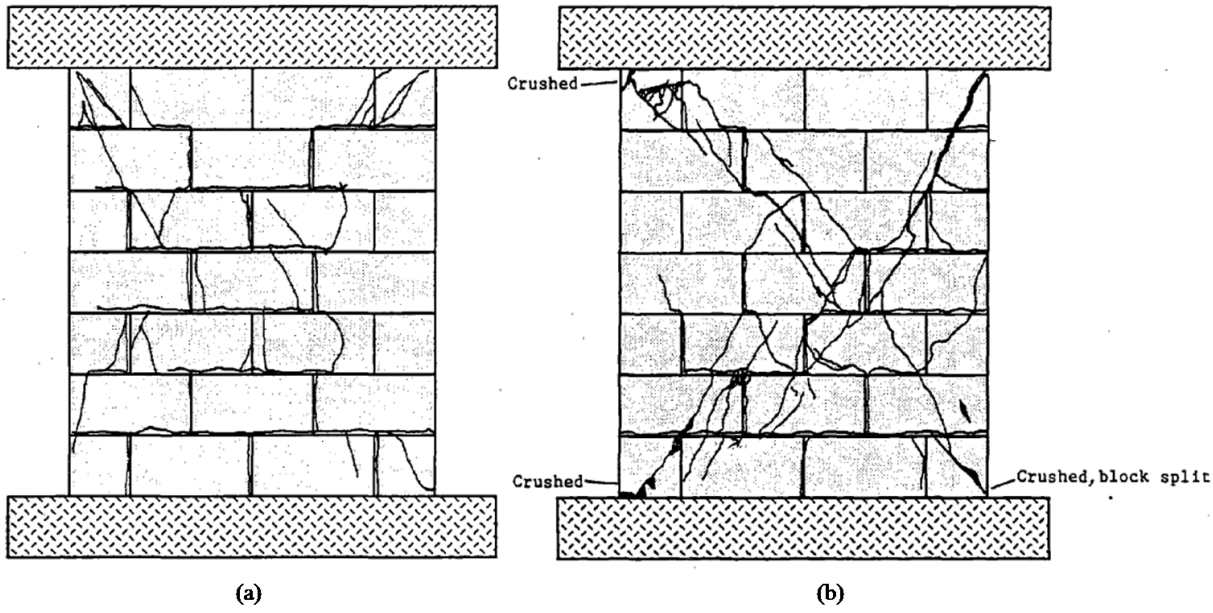

Figure 2.13 Cracking pattern for (a) wall reinforced with bed-joint reinforcement vs (b) wall reinforced with bond beam reinforcement (Yancey and Scribner 1989)

Schultz (1996) & Schultz et al. (1998)

Table 2.3 Properties of the tested walls (Schultz 1996; Schultz et al. 1998)

Total number of PG shear-critical walls in study: 12			USA
Loading Type:	Phased-Sequential	f'_m:	12-14 MPa
Loading Rate:	Quasi-Static	A_{net}/A_{gross}:	0.44 - 0.53
Support Type:	Double Curvature	Net Axial Stress:	0.90 - 1.10 MPa
Scale:	1	Gross Axial Stress:	0.45 - 0.48 MPa
Height:	1422 mm	Flexural Reinf.:	0.20 - 0.41 %
Length:	1422 - 2845 mm	Vertical (Interior) Reinf.:	0%
Thickness:	195 mm	Bond Beam Reinf.:	0.05 - 0.12 %
H/L:	0.5 - 1	Joint Reinf.:	0.06 - 0.11 %

Schultz (1996) and Schultz et al. (1998) studied the effect of horizontal reinforcement type and ratio with varying aspect ratios on the shear strength of PG walls. They tested six walls reinforced with bond beams and six walls reinforced with bed-joint reinforcement with the setup illustrated in Figure 2.14. More details about the tested PG walls are presented in Table 2.3.

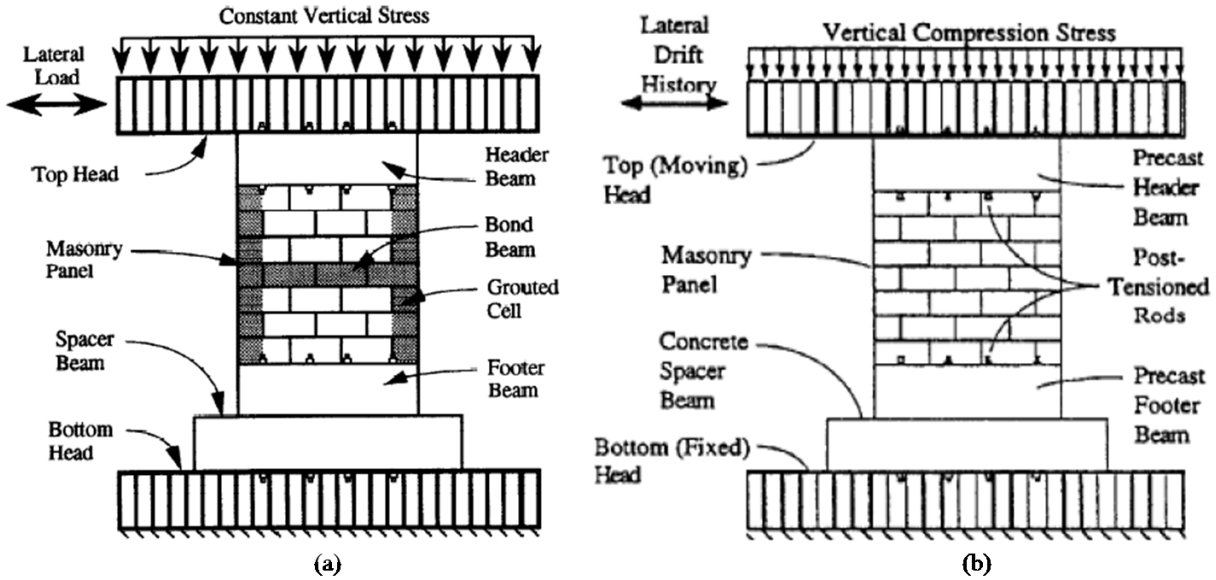

Figure 2.14 Test setup used by (a) Schultz (1996) and (b) Schultz et al. (1998)

They observed that there was no complete agreement between the walls reinforced with bond beam and walls reinforced with bed-joint in terms of the effect of the aspect ratio on the peak load. It is worth noting that PG walls had better stability and energy dissipation when joint reinforcement in each bed joint was used instead of a single bond beam located mid-height

and also served to bridge the vertical cracks and prevent interruption of stress transfer throughout the wall (Schultz et al. 1998). When comparing the shear response between two of the walls tested in this study; (a) wall reinforced with bond beam and (b) wall reinforced with bed-joint reinforcement in terms of load-displacement relationship as illustrated in Figure 2.15, it is noted that both walls had attained equal peak lateral load. However, the wall reinforced with bed-joint had double deformation capacity compared to the one reinforced with bond beam. It should be noted that both walls had similar properties in terms of length, aspect ratio, axial load, and horizontal reinforcement ratio. This concludes that the lateral load-resisting mechanism was improved in walls reinforced with bed-joint over those reinforced with bond beam (Schultz et al. 1998).

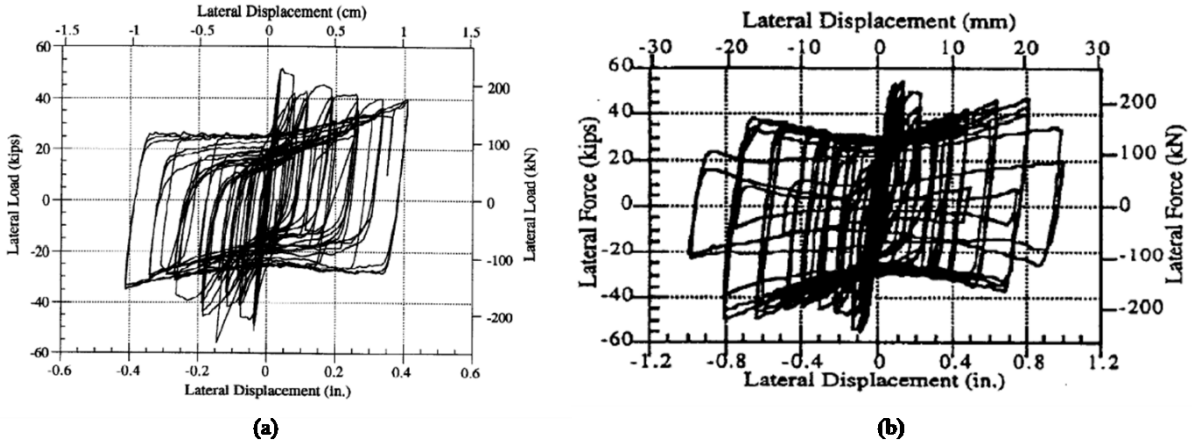

Figure 2.15 Force-displacement for (a) wall reinforced with bond beam and (b) wall reinforced with bed-joint reinforcement (Schultz 1996; Schultz et al. 1998)

Baenziger and Porter (2011)

Table 2.4 Properties of the tested walls (Baenziger and Porter 2011)

Total number of PG shear-critical walls in study: 8			USA
Loading Type:	Reverse Cyclic	f'_m:	13.9 - 19.8 MPa
Loading Rate:	Quasi-Static	A_{net}/A_{gross}:	0.56 - 0.65
Support Type:	Cantilever	Net Axial Stress:	0 MPa
Scale:	1	Gross Axial Stress:	0 MPa
Height:	2642 mm	Flexural Reinf.:	0.14 - 0.25 %
Length:	2845 - 4267 mm	Vertical (Interior) Reinf.:	0.05 - 0.06 %
Thickness:	194 mm	Bond Beam Reinf.:	0.05 - 0.11 %
H/L:	0.93 - 0.62	Joint Reinf.:	0 - 0.18 %

Baenziger and Porter (2011) tested ten full-scale walls, eight of which were PG and two of which were FG. The major goal of the study was to compare walls built with traditional bond beam reinforcement to walls built with bed-joint reinforcement. Top and bottom bond beams, as well as joint reinforcement at each bed joint (single ladder-type or double seismic style joint) or a bond beam at mid-height, were used to reinforce all walls horizontally. More details about the tested PG walls are presented in Table 2.4. Figure 2.16 depicts the setup for the test. This test, however, did not include the effect of the axial load.

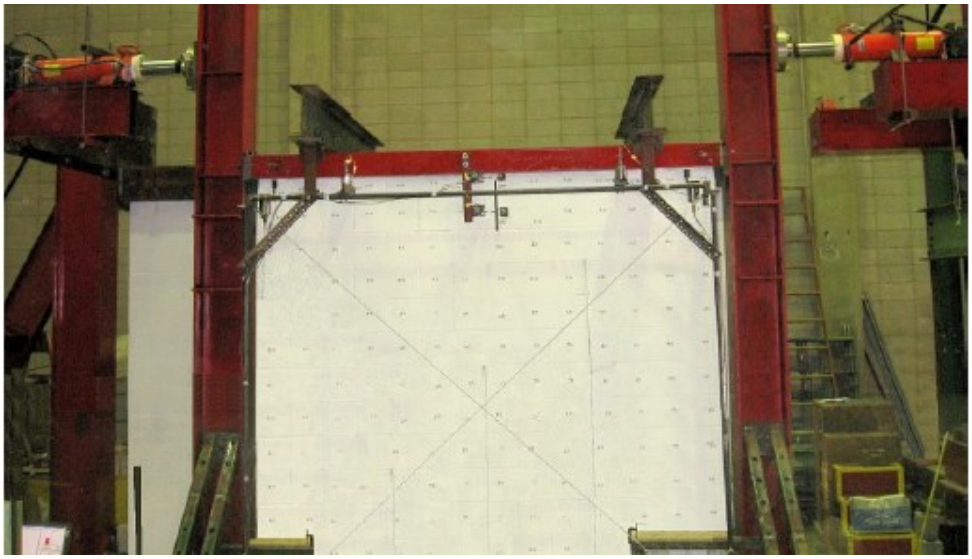

Figure 2.16 Test setup used by Baenziger and Porter (2011)

Baenziger and Porter (2011) observed that although wall reinforced with joint reinforcement attains a similar peak lateral load to the wall reinforced with bond beam, the wall reinforced with joint reinforcement performed better in terms of deformation capacity. As a result, they concluded that joint reinforcement was a viable option for horizontal reinforcement in masonry shear walls. Furthermore, horizontal reinforcement distributed evenly through the wall through joint reinforcement was found to provide better ductility and crack control than concentrated horizontal reinforcement in bond beams.

Hoque (2013)

Table 2.5 Properties of the tested walls (Hoque 2013)

Total number of PG shear-critical walls in study: 18			Canada
Loading Type:	Varied	f'_m:	16.6 MPa
Loading Rate:	Quasi-Static	A_{net}/A_{gross}:	0.58
Support Type:	Double Curvature	Net Axial Stress:	2.05 - 2.17 MPa
Scale:	1	Gross Axial Stress:	1.20 - 1.26 MPa
Height:	1800 mm	Flexural Reinf.:	0.12 %
Length:	1800 mm	Vertical (Interior) Reinf.:	0.06 %
Thickness:	190 mm	Bond Beam Reinf.:	0 - 0.17 %
H/L:	1.0	Joint Reinf.:	0 - 0.03 %

Hoque (2013) ran a testing campaign of 18 PG walls consisting of 8 groups; 4 groups with bond beams and four groups with bed-joint reinforcement. More details about the tested PG walls are presented in Table 2.5. These groups had variables of bond beam location, end anchorage conditions, presence of splice, and loading scenarios (monotonic or reverse cyclic lateral load and variable or constant axial load). The test setup is depicted in Figure 2.17. Several observations have been made on the wall specimens and the testing setup.

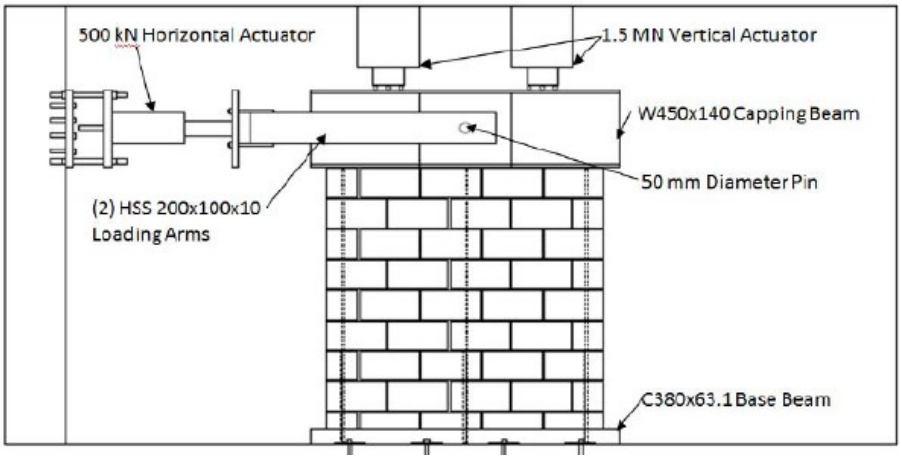

Figure 2.17 Test setup used by Hoque (2013)

She observed little difference in shear strength despite varying the horizontal reinforcement type. However, the cracking pattern was more distributed over the surface of the specimens containing a bond beam, while cracks concentrated into a large X-pattern in specimens containing joint reinforcement. In addition, she noted that the initial stiffness of walls with

bond beams was higher than those with joint reinforcement. On the other hand, similar levels of stiffness degradation and ductility were noticed through all walls regardless of horizontal reinforcement type, as shown in Figure 2.18. Finally, it will be interesting to see the aspect ratio effect in this study due to its significance according to most of the literature.

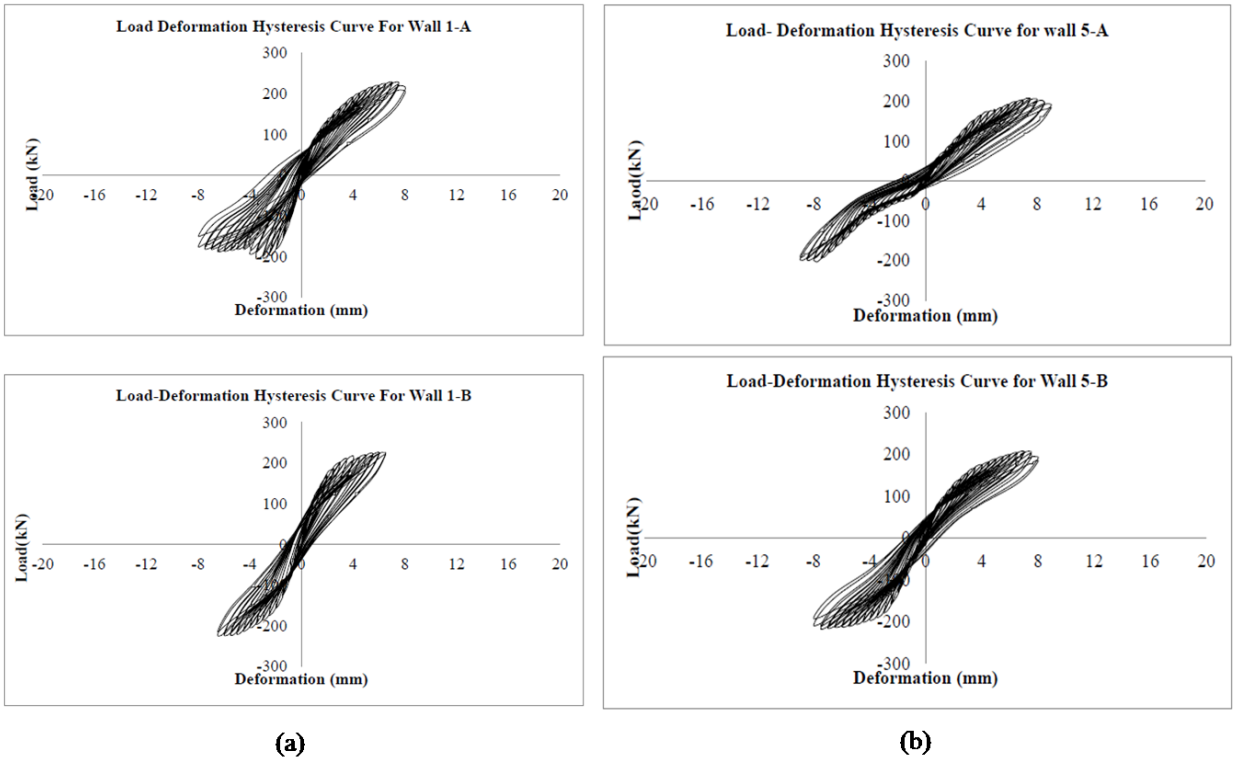

Figure 2.18 Hysteresis loop for (a) walls reinforced with bond beam vs (b) walls reinforced with joint reinforcement (Hoque 2013)

Bolhassani et al. (2016b)

Table 2.6 Properties of the tested walls (Bolhassani et al. 2016b)

Total number of PG shear-critical walls in study: 3			USA
Loading Type:	Reverse Cyclic	f'_m:	16.8 – 18.4 MPa
Loading Rate:	Quasi-Static	A_{net}/A_{gross}:	0.45 – 0.55
Support Type:	Cantilever	Net Axial Stress:	0.14 MPa
Scale:	1	Gross Axial Stress:	0.06– 0.08 MPa
Height:	3860 mm	Flexural Reinf.:	0.07 %
Length:	3860 mm	Vertical (Interior) Reinf.:	0.03 – 0.04 %
Thickness:	200 mm	Bond Beam Reinf.:	0.07 – 0.08 %
H/L:	1.0	Joint Reinf.:	0.03 %

Bolhassani et al. (2016b) used a cantilever setup to evaluate three square PG walls under cyclic lateral loads and continuous axial stresses, as shown in Figure 2.19. The conventional single-cell reinforcing distribution was used for the first of those walls using a bond beam as a horizontal reinforcement. A double-cell detailing was used for the second wall, with horizontal and vertical reinforcement placed in two adjacent cells rather than one isolated cell. The double-cell detailing was employed in the third wall, along with bed-joint reinforcement in every other course. More details about the tested PG walls are presented in Table 2.6. Two additional courses were added above the wall's targeted height to provide enough vertical rebar development length while properly transferring the horizontal load to the wall.

Figure 2.19 Test setup used by (Bolhassani et al. 2016b)

Although the wall with combined horizontal reinforcement had a greater horizontal reinforcement ratio than the other walls, the peak lateral load attained by all walls was not significantly different. On the other hand, the wall reinforced with a combination of bond-beam and bed-joint reinforcement showed better ductility and stiffness degradation when compared with the single-cell reinforcing wall (Figure 2.20). In addition, they observed that the use of distributed bed-joint reinforcement across the wall height allowed for stress distribution in hollow panels. As a result, the initial cracks caused by increased lateral displacement did not open significantly, and a new set of cracks spread at the top of the walls in contrast to the walls without bed-joint reinforcement (Figure 2.21). Finally, it should be noted that no walls tested were reinforced exclusively with bed-joint reinforcement in this study.

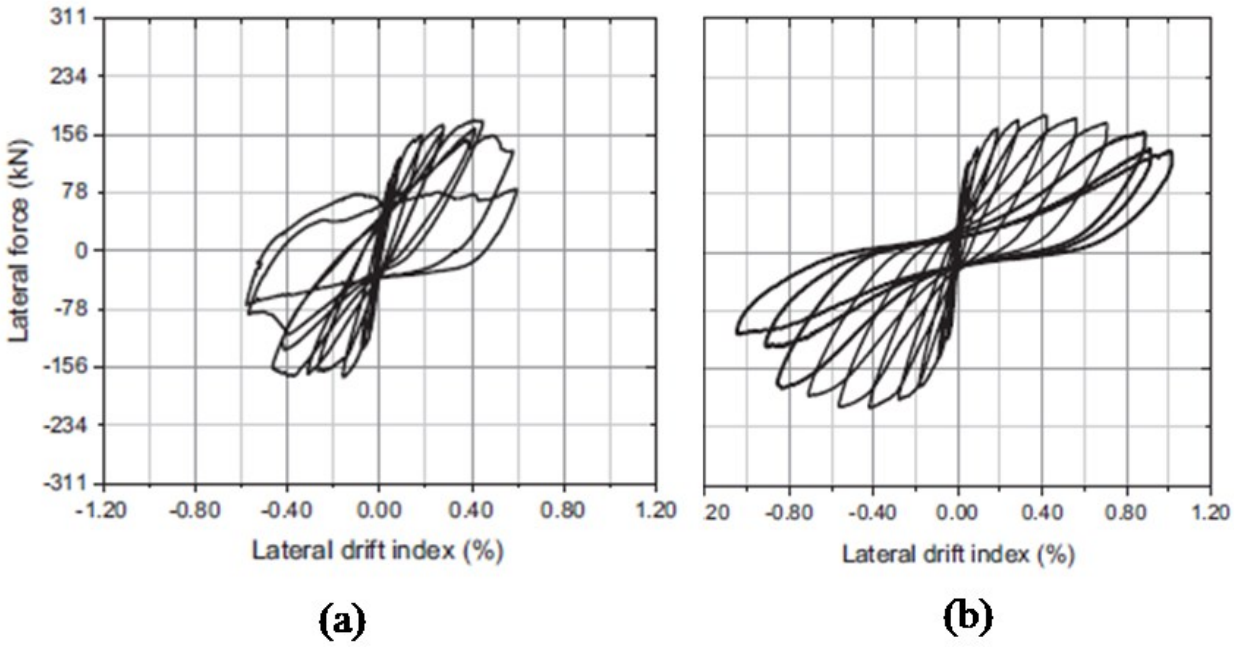

Figure 2.20 Lateral force displacement hysteresis loops for (a) single-cell wall reinforced only with bond beam vs (b) double-cell wall reinforced with combination of bond beam and bed-joint reinforcement (Bolhassani et al. 2016b)

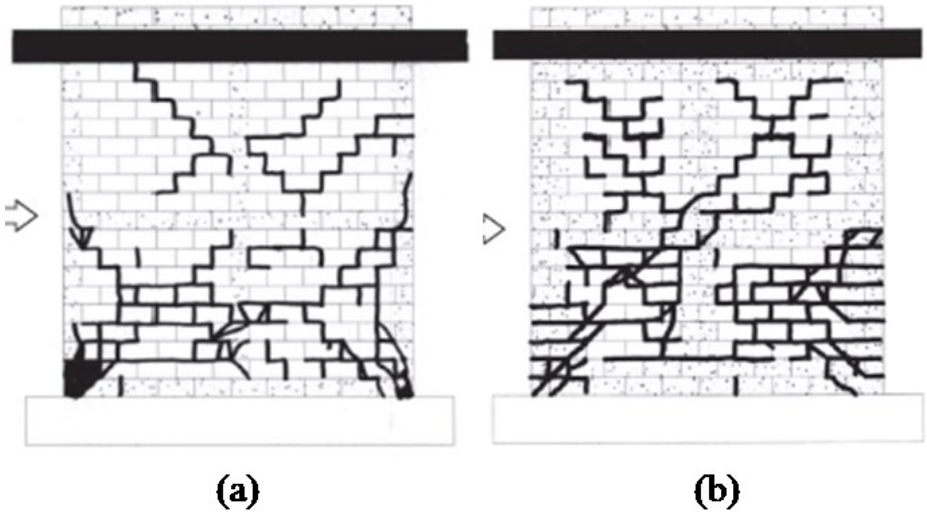

Figure 2.21 Cracking pattern for (a) single-cell wall reinforced only with bond beam vs (b) double-cell wall reinforced with combination of bond beam and bed-joint reinforcement (Bolhassani et al. 2016b)

Stathis et al. (2018)

Table 2.7 Properties of the tested walls (Stathis et al. 2018)

Total number of PG shear-critical walls in study: 8			Canada
Loading Type:	Reverse Cyclic	f'_m:	Unknown
Loading Rate:	Quasi-Static	A_{net}/A_{gross}:	0.55
Support Type:	Unknown	Net Axial Stress:	Unknown
Scale:	1	Gross Axial Stress:	Unknown
Height:	1800 mm	Flexural Reinf.:	0.12 %
Length:	1800 mm	Vertical (Interior) Reinf.:	0.06 %
Thickness:	190 mm	Bond Beam Reinf.:	0.09 %
H/L:	1.0	Joint Reinf.:	0.06 - 0.09 %

Stathis et al. (2018) tested eight PG walls. These walls were classified into four groups; one group was reinforced with bond beams, while the other groups were reinforced with different sizes of bed-joint reinforcement. They aimed to study the effect of horizontal reinforcement on the in-plane shear performance of PG walls using the setup depicted in Figure 2.22. More details about the tested PG walls are presented in Table 2.7. According to the study features tabulated in the above table, some essential parameters were not reported. They observed that the spacing of the horizontal reinforcement significantly influenced the crack pattern. Walls with bond beams exhibited larger, concentrated cracks that widened throughout the wall panel, causing a brittle shear failure. On the other hand, walls with bed-joint reinforcement exhibited smaller cracks spread all over the wall, causing a ductile shear failure. In addition, they found that walls with bed-joint reinforcement showed better energy dissipation, higher ductility, and slower stiffness degradation when compared with the walls reinforced with bond beams.

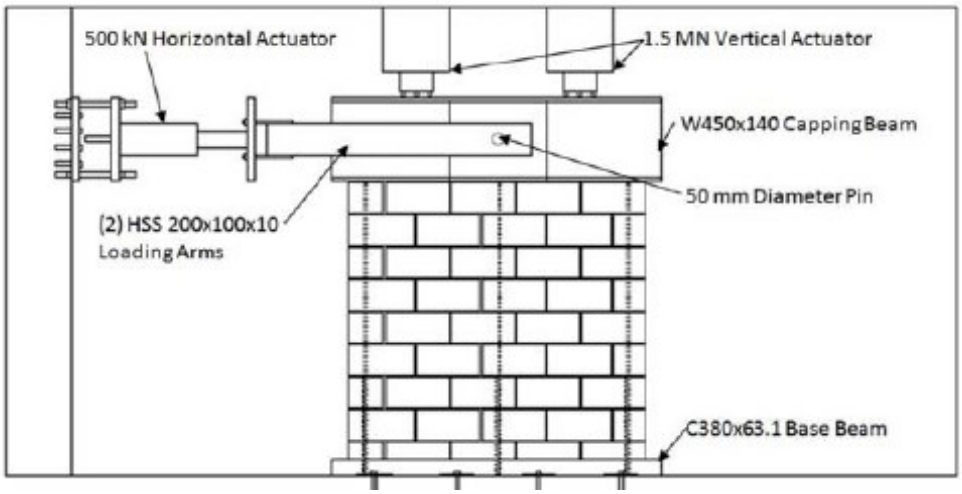

Figure 2.22 Test setup (Stathis et al. 2018)

Schultz and Johnson (2019)

Table 2.8 Properties of the tested walls (Schultz and Johnson 2019)

Total number of PG shear-critical walls in study: 2			USA
Loading Type:	Reverse Cyclic	f'_m:	17.3 – 23.1 MPa
Loading Rate:	Quasi-Static	A_{net}/A_{gross}:	0.42
Support Type:	Cantilever	Net Axial Stress:	0.013 MPa
Scale:	1	Gross Axial Stress:	0.05 MPa
Height:	4267.2 mm	Flexural Reinf.:	0.02 %
Length:	6500 mm	Vertical (Interior) Reinf.:	0.02 %
Thickness:	190 mm	Bond Beam Reinf.:	0.03 – 0.06 %
H/L:	0.67	Joint Reinf.:	0.05 %

Schultz and Johnson (2019) used a cantilever test setup to test two C-shaped PG shear walls with an aspect ratio of 0.67 under cyclic lateral loads and constant axial loads, as shown in Figure 2.23. Both walls have a window-like opening in the middle. Only bond beam reinforcement was used on one wall as a horizontal reinforcement, while bed-joint and bond-beam reinforcement were used on the second wall. These walls, however, have implemented reinforcement distributions of Bolhassani et al. (2016b). More details about the tested PG walls are presented in Table 2.8.

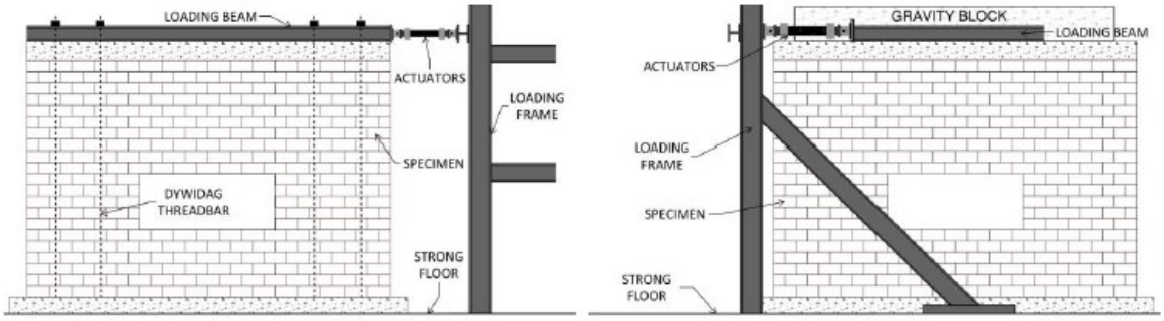

Figure 2.23 Test setup used by Schultz and Johnson (2019)

Schultz and Johnson (2019) observed that both walls attained approximately similar peak lateral load. However, wall reinforced with a combination of bond beam and bed-joint showed higher ductility by more than 138% of the wall reinforced with bond beam (Figure 2.24).

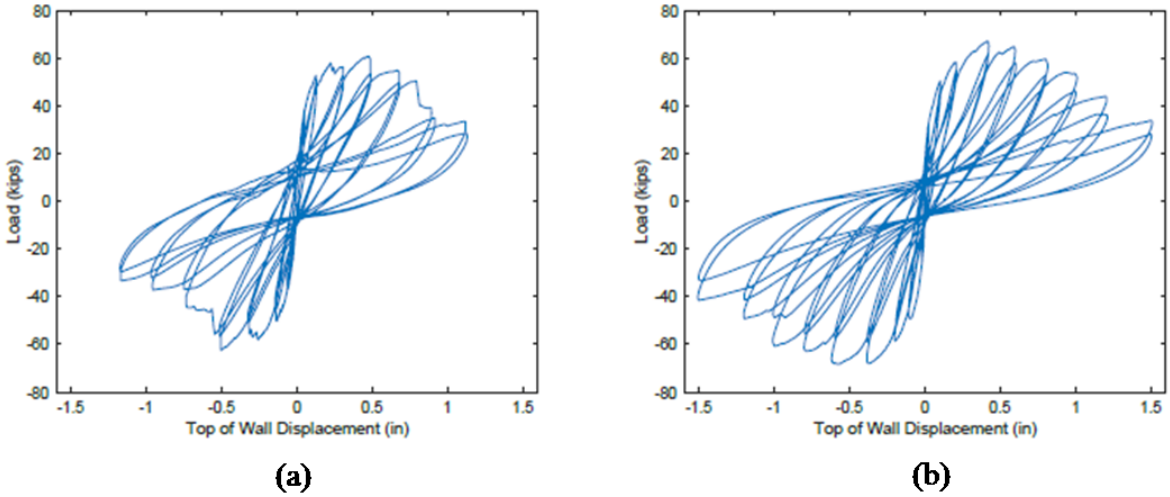

Figure 2.24 Load-displacement response for (a) wall reinforced with bond beam and (b) wall reinforced with a combination of bond beam and bed-joint reinforcement

Furthermore, they noted that the closer spacing of the bed-joint reinforcement allowed for more cracks to be crossed by the horizontal reinforcement. Accordingly, this forced the damage to move to other areas of the wall panel, therefore, utilizing more of the masonry than concentrating in one dominant crack. Consequently, the wall integrity was improved by adding the bed-joint reinforcement. (Figure 2.25). Finally, it is more interesting if there is a wall reinforced only with bed-joint reinforcement in the study to see its exclusive effect on the shear behaviour of PG walls.

(a) (b)

Figure 2.25 Crack size and distribution for (a) wall reinforced with bond beam and (b) wall reinforced with both bond beam and bed-joint reinforcement

Calderon et al. (2021a)

Table 2.9 Properties of the tested walls (Calderon et al. 2021a)

Total number of PG shear-critical walls in study: 4			Chile
Loading Type:	Reverse Cyclic	f'_m:	9.67 MPa
Loading Rate:	Quasi-Static	A_{net}/A_{gross}:	0.59
Support Type:	Cantilever	Net Axial Stress:	0.85 MPa
Scale:	1	Gross Axial Stress:	0.5 MPa
Height:	2270 mm	Flexural Reinf.:	0.21 %
Length:	2640 mm	Vertical (Interior) Reinf.:	0.21 %
Thickness:	140 mm	Bond Beam Reinf.:	0.06 – 0.1 %
H/L:	0.86	Joint Reinf.:	0.03 – 0.1 %

Calderon et al. (2021a) recently tested four PG walls with various horizontal reinforcing types in a cantilever test setup under constant axial and cyclic lateral loads, as shown in Figure 2.26. The first two walls had ladder-type bed-joint reinforcement, the third wall had steel rebars embedded in bond beams, and the fourth wall had a configuration that merged the two previous reinforcement types. All the walls had an approximate equal horizontal reinforcement ratio of 0.08%. Also, the two walls reinforced with bed-joint reinforcement had identical design specifications, including the horizontal reinforcement detailing and were tested following the same procedure to observe scattered results from such walls (Calderon et al. 2021a). More details about the tested PG walls are presented in Table 2.9.

They noticed that all walls attained nearly equal peak lateral load regardless of the horizontal reinforcement type. Also, the changes in the horizontal reinforcement layout did not affect the stiffness degradation. However, the wall reinforced with bed-joint reinforcement had a higher ductility and better deformation capacity when compared with the wall reinforced with bond beam (Figure 2.27).

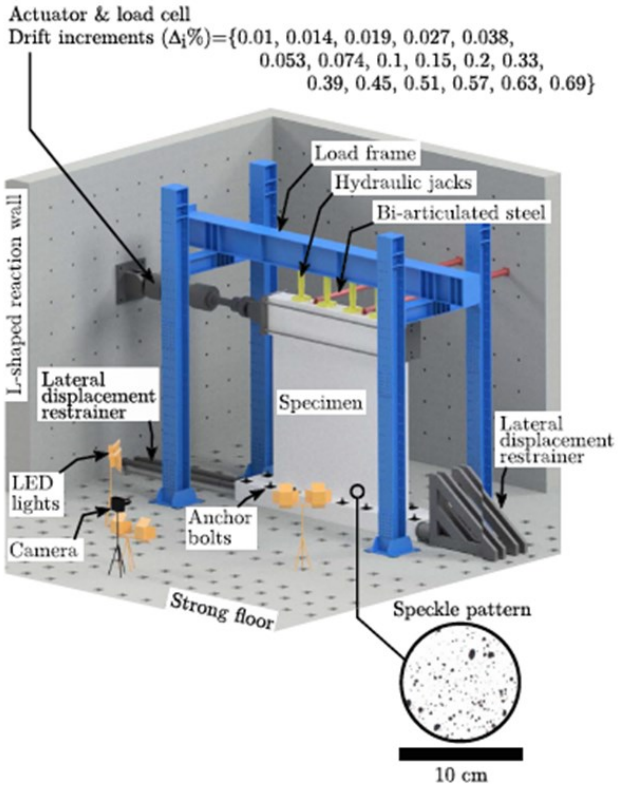

Figure 2.26 Test setup used by Calderon et al. (2021a)

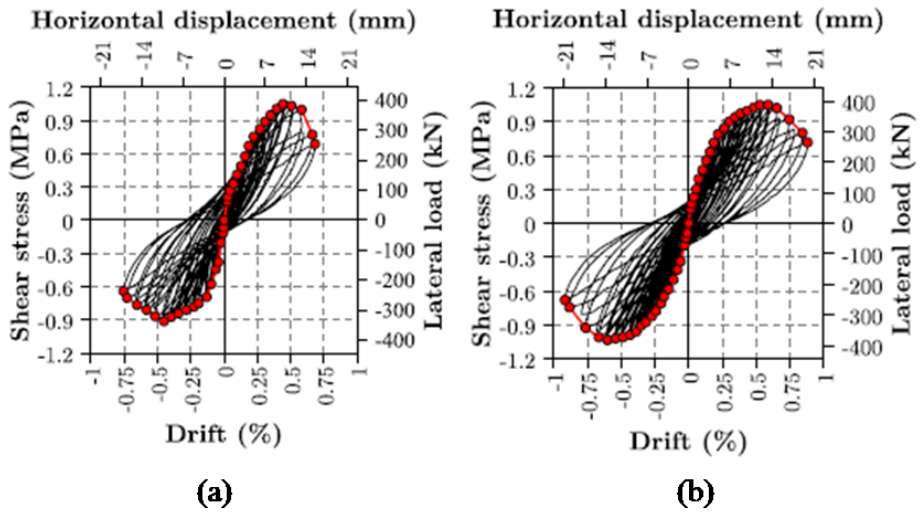

Figure 2.27 Hysteretic response of (a) wall reinforced with bond beam, and (b) wall reinforced with bed-joint reinforcement (Calderon et al. 2021a)

In addition, it was observed that using bed-joint reinforcement is superior in controlling the growth of crack width compared to bond beam reinforcement. The grout in bond beams prevented many cracks from forming in such zones, resulting in a few wide cracks crossing horizontal reinforcement in bond beams. Even when the walls were severely damaged, this impact was evident. On the other hand, the cracks were distributed throughout the wall panel, and the residual deformations were controlled by bed-joint reinforcement. As a result, bed-joint reinforcement provided integrity to the wall panel once the cracks were pronounced (Figure 2.28). Finally, the authors suggested studying whether the influence of the horizontal reinforcement type on the shear behaviour of PG walls can be similar to different aspect ratios, horizontal reinforcement ratios, and axial stresses.

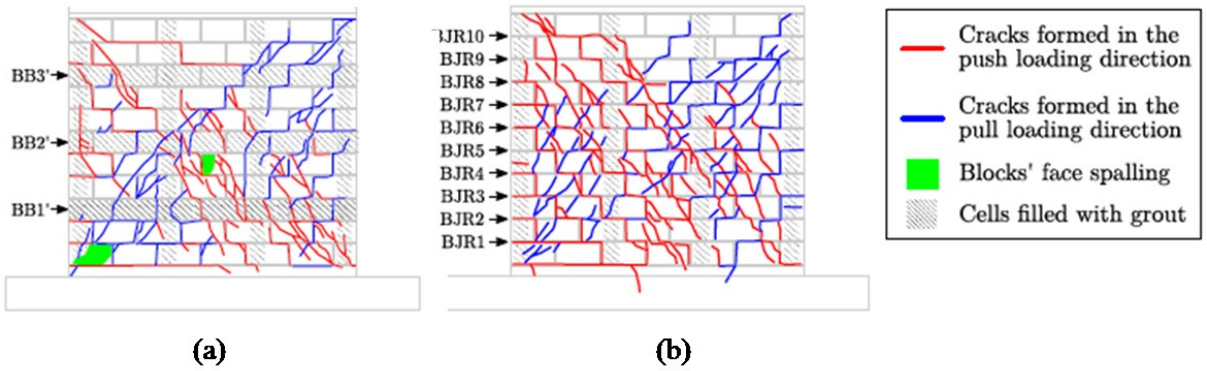

Figure 2.28 Crack patterns for (a) wall with bond beam and (b) wall with bed-joint reinforcement (Calderon et al. 2021a)

2.2.4. Missing Reported Data

The data acquisition system used by Hamedzadeh (2013) malfunctioned while testing one wall, leading to faulty results of axial loads. Because there was no way to determine the correct axial load value for this wall, it was removed from the final datasets. In addition, six of the studies (Meli et al., 1969; Thurston & Hutchison, 1982; Matsumura, 1987; Yancey & Scribner, 1989; Tomaževič et al., 1996; Voon & Ingham, 2006) did not report enough information for values of both ungrouted and grouted compressive strength of masonry to be determined. Finally, several studies (Ghanem et al., 1992; Ghanem et al., 1993; Schultz, 1996; Elmapruk, 2010; Baenziger and Porter, 2011; Nolph and ElGawady, 2012) failed to report enough information for one or more of block and mortar compressive and shear strength. Izquierdo et al. (2021) pointed out that variables such as the strength of block, mortar, and grout should be reported, and the methods used to test these materials should be clearly noted because of their significant influence on the shear strength of PG walls prediction.

2.2.5. Summary

Majority of PG walls built with full-scale blocks in the literature, experimentally tested are smaller than the typical masonry shear wall found in a building (Minaie 2009). Due to size limitations, masonry shear wall testing has often focused on single-storey walls that are not representative of multi-storey masonry buildings. On the other hand, some studies use smaller-scale units to try and test full-scale walls under laboratory constraints, so walls that are built with reduced-scale blocks make up about 17% of the PG masonry walls experimentally tested. Scales of one-half or one-third block size are the most common (Izquierdo 2021). One issue with reduced-scale models is the size effect, which shows that smaller size specimens have higher strength and more data scatter than their prototype counterparts (Maleki 2008). The difference extends to the failure mode; for instance, Long (2006) found that a reduced-scale model and prototype wall intended to fail in flexure were more similar than a model and prototype wall intended to fail in shear.

A literature survey shows a significant number of walls tested as fixed-fixed (90 out of 205 walls) (Izquierdo 2021). Even when double-curvature conditions may exist in segments of a wall around an opening, walls are usually tested in this fashion for practicality: it is easier to

promote a shear failure in walls tested under double curvature, as the shear force that develops in such a wall is higher than that developed in a cantilevered specimen. With the recent introduction of expansion/movement joints, masonry shear walls are uncouplers and act independently in a building, thus resulting in boundary conditions more reminiscent of a cantilever beam over fixed end conditions (Banting 2013). A number of walls tested in the literature also had details that are not commonly found in typical construction. For instance, a common way to promote shear failures is by designing walls with very large vertical reinforcement ratios to ensure the moment capacity will not be reached before the walls fail in shear. A survey in the literature showed that vertical reinforcement ratio ranged between 0.10 to 1.22% for most studies which means that some walls have higher reinforcement ratios than those usually found in masonry construction (0.045% - 0.09%) (CSA S304-14 2014; Hatzinikolas et al. 2015). The amount and location of the vertical reinforcement ratio are important since they determine the dowel action mechanism for shear resistance (Shing et al. 1989; 1990). Conversely, Tomaževič (1999) and Haach et al. (2011) reported that the vertical reinforcement had no significant effect on the in-plane diagonal shear strength.

Bond beam and bed joint reinforcement are two commonly used types of horizontal reinforcement in practice. However, despite numerous studies on this topic, there is still a lack of consensus on the role played by horizontal reinforcement type in determining the shear strength of PG walls.

Overall, more experimental studies are needed in order to revise and improve the accuracy of the current shear strength code equations since most of the available data are not well-documented and missing important information, leading to the assumption and correction option. Also, it should be noted that the available experimental data were from different places and periods, representing different construction practices.

2.3. Analysis Models of PG Walls using FEM

The finite element method (FEM) has been one of the most used numerical tools to simulate the structural behaviour of masonry during the last decades. The application of FEM has been carried out using mainly two modelling approaches. One is called macro-modelling, preferred for studying the global response of whole buildings or large structural systems. The other is micro-modelling, suited for studying the local response of smaller structural systems or components.

Macro-modeling represents masonry as a homogeneous composite material, where the constitutive relationships for units, mortar, and unit-mortar interface are averaged in a homogeneous continuum (Lourenço 2002). Its application allows for estimating the global structural response in terms of maximum resistance, displacement ductility and force-displacement relationship.

Micro-modelling consists of discretizing the masonry in a detailed or simplified way, explicitly modelling all (or the majority) of the constituent materials and interfaces in masonry units, mortar joints, grout, and the discontinuities between units and mortar joints (Lourenço et al. 1995). The behaviour of each discretized component is represented by a different constitutive law. The use of micro-modelling makes it possible to capture local failure mechanisms and obtain the response of an individual component or a part of it in terms of the local stresses and strains. A graphical representation illustrating the two approaches mentioned is illustrated in Figure 2.29.

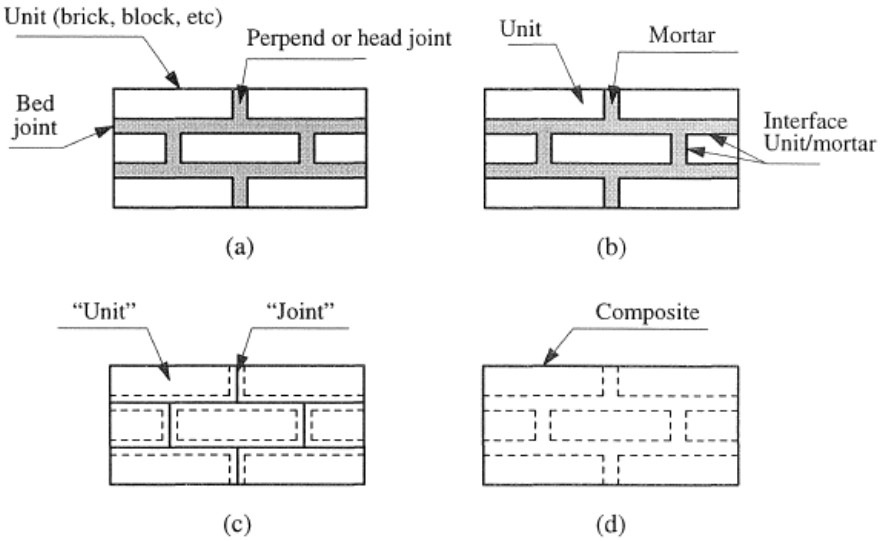

Figure 2.29 Modelling approaches for masonry walls (a) masonry sample, (b) detailed micro-modelling, (c) simplified micro-modelling, (d) macro-modelling (Lourenço et al. 1995)

There are scarce studies on the simulation of the monotonic and cyclic response of PG walls using any of the modelling approaches indicated above. On the other hand, many studies have been conducted on the simulation of FG walls. This is attributed to the fact that the existence of grout in every cell and reinforcement enhances the directional behaviour of masonry by creating continuity in the stress flow and thereby making the behaviour of FG walls similar to that of RC walls (Seif ElDin 2016).

2.3.1. Micro-Modelling Approach

Haach et al. (2011), Arnau et al. (2015), and Calderón et al. (2017) applied this approach to simulate the response of PG walls against cyclic loading using DIANA FEA software (DIANA 2014).

Haach et al. (2011) used a simplified micro-modelling approach to reproduce the monotonic response of five PG walls tested at reversible cyclic mode using a 2D numerical model. The model proposed by Lourenço and Rots (1997) for the monotonic simulation of masonry structures was implemented. The simulated walls were built with an aspect ratio of 0.66, and hollow concrete blocks were used. These walls were part of an experimental campaign previously carried out by Haach (2009). As a result of this work, the investigation reported excellent agreement between the monotonic numerical and experimental enveloping curves,

yielding errors in predicting the maximum lateral resistance of the order of 10%. Similarly, the numerical cracking patterns obtained were consistent with experimentally observed damage. An example of these results is shown in Figure 2.30, where the monotonic numerical curve, the experimental cyclical response and the numerical damage pattern can be seen for one of the walls studied.

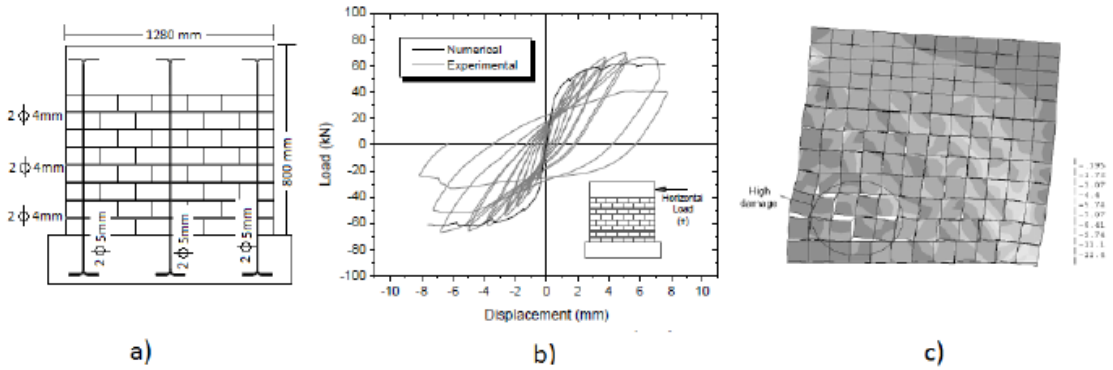

Figure 2.30 Numerical simulation results. a) N60-3C-B1-PA wall, b) Force-displacement diagrams, c) Numerical damage pattern (Haach et al. 2011)

Arnau et al. (2015) and Calderon et al. (2017) used the detailed micro-modelling approach. Arnau et al. (2015) developed a 2D numerical model to reproduce the monotonic response of two PG reinforced masonry walls tested at reversible cyclical displacements in their in-plane direction. For the construction of the model, the authors used results from their experimental tests and derived other data numerically from modelling small masonry assemblies. The simulated walls were built with an aspect ratio of 0.97 using multi-perforated clay bricks. These walls were part of an experimental campaign carried out by Sandoval et al. (2018). As a result of this work, the research reported great matching in terms of monotonic curves, cracking patterns and failure mechanisms. An example of these results is shown in Figure 2.31, where the comparison between the experimental and numerical monotonic curve can be seen for one of the walls studied, and, in addition, the pattern of numerical damage obtained is indicated.

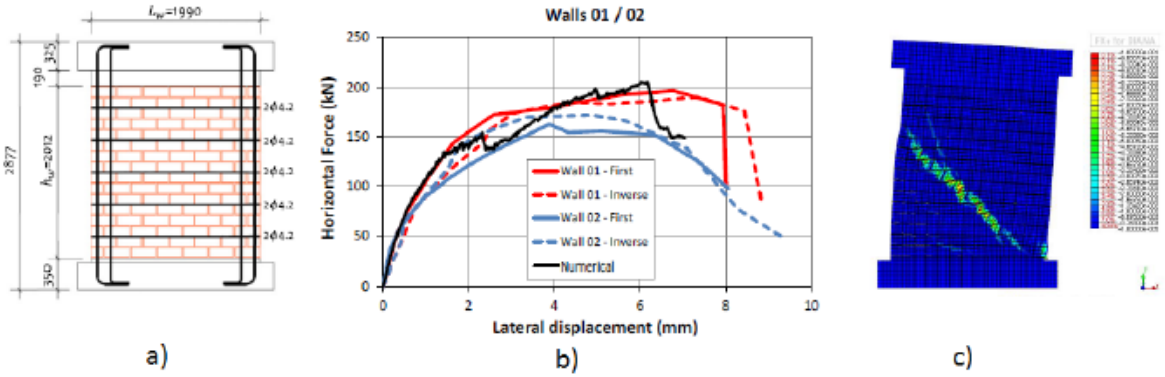

Figure 2.31 Numerical simulation results. a) Wall W 01/02, b) Enveloping curves. b) Numerical damage pattern. (Arnau et al. 2015)

In addition, Calderón et al. (2017) developed a 2D numerical model to reproduce the monotonic response of three PG reinforced masonry walls tested at reversible cyclical in-plane displacements, one solid and two with openings in the central part. For the construction of the model, the authors used their experimental results and numerical values derived from simulations of small masonry assemblies. The simulated walls were built with multi-perforated clay bricks and aspect ratios of 1.03 for the solid wall and 1.05 and 1.73 for the wall piers with central openings. As a result of this research, a good matching between the monotonic numerical and experimental envelope curves was reported. Also, a good agreement between maximum strengths, ultimate displacements and cracking patterns was obtained. An example of these results is shown in Figure 2.32, where it is depicted for one of the simulated walls, the comparison between the monotonic curves and the numerical damage pattern.

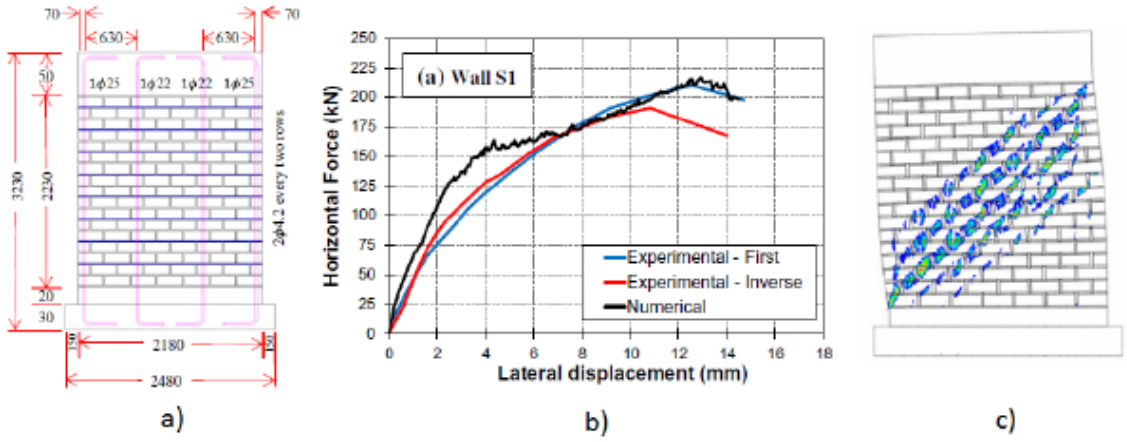

Figure 2.32 Numerical simulation results. a) Solid wall, b) Enveloping curves, b) Damage pattern. (Calderón et al. 2017)

Using the concrete-damaged plasticity model, Minaie et al. (2014) developed a 3D numerical model using the ABAQUS program to simulate the cyclic response of PG walls. They noticed that some might explicitly model each constituent material and precisely replicate the element's geometry. Others may smear all constituent materials into a single material and employ a 2D planar model. Therefore, their model aimed to strike a balance between these two approaches and to provide an efficient model capable of capturing the macro-level in-plane and the out-of-plane response of reinforced masonry shear walls (Minaie et al. 2014). Using the ABAQUS program, they simulated the hysteretic response of the PG and FG walls built with hollow concrete blocks and aspect ratios of 1.37. These walls were part of an experimental campaign carried out by the same author, Minaie et al. (2010).

As a result of this investigation, a good agreement between the numerical and experimental results was reported regarding cyclic curve shapes, failure modes, cracking patterns, and maximum lateral strength. An example of these results is shown in Figure 2.33, where for the PG wall studied, the comparison between the numerical and experimental hysterical curves and the numerical damage pattern obtained can be seen.

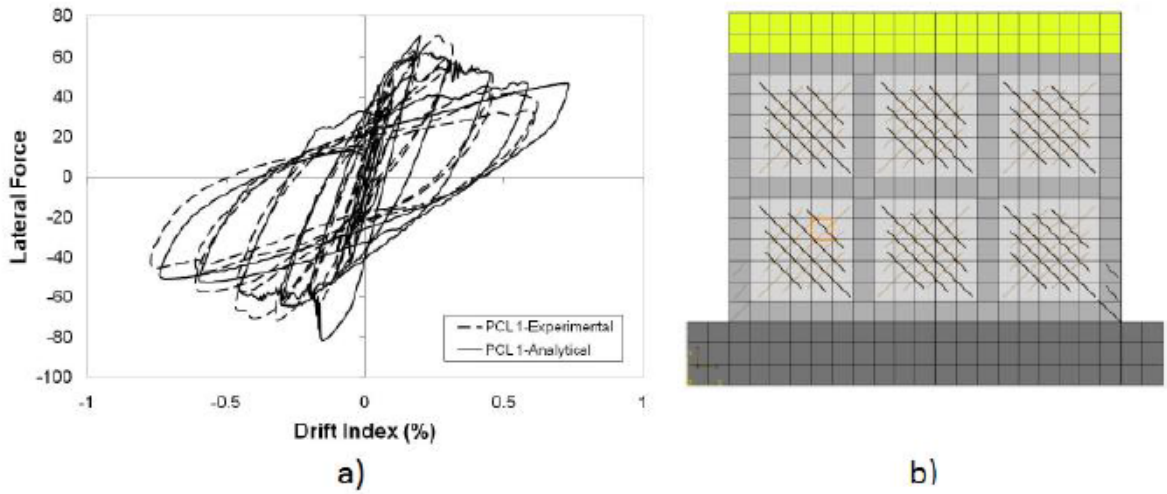

Figure 2.33 Numerical simulation results. a) Numerical and experimental cyclical curves, b) Numerical damage pattern (Minaie et al. 2014)

2.3.2. Macro-Modelling Approach

Seif ElDin (2016), Hung (2018), and Bolaños (2020) used the macro-model approach to develop 2D analysis models for PG walls subjected to cyclic loads using the VecTor2 program (VecTor Analysis Group, 2019).

Seif ElDin (2016) utilized this model approach only to analyze the FG walls, where he simulated nine FG walls that had been experimentally tested in his study. He found a good agreement between the numerical model and the experimental results. Also, he noticed that the mesh size significantly impacted the accuracy of the numerical simulation, especially when using the smeared approach to model the reinforcing bars. Using a more refined mesh size reduced the error in predicting the lateral load capacity for simulated walls from 13% to less than 2% (Seif ElDin 2016). Figure 2.34 shows an example of one of his simulated walls results with the comparison of the hysteric response between the experimental and the model.

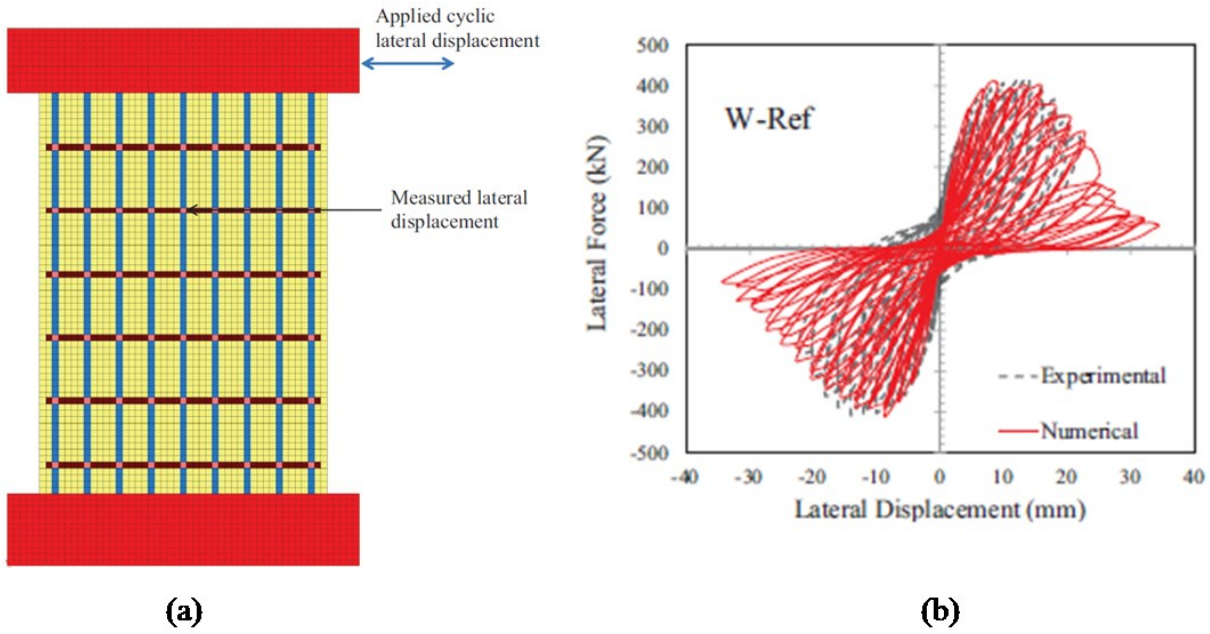

Figure 2.34 (a) FE model for the wall (b) Experimental vs. numerical cyclic lateral load-displacement response of tested wall

Hung (2018) applied this model approach to developing a 2D numerical model to reproduce the monotonic and cyclic response of one wall of reinforced masonry PG tested at reversible cyclical displacements in its own plane. The simulated wall was part of Maleki's (2008) experimental campaign, in which the wall was built with hollow concrete blocks with an

aspect ratio equal to 1.00. Hung (2018) found that the 'Joint Shear Strength Ratio,' the ratio between the shear strength of the joints and the maximum compressive strength of masonry, was observed to have the largest influence on the predicted response after conducting several parametric analyses. As a result of the numerical investigation, a good approximation between the experimental and numerical envelope curves was reported, and a reasonable simulation of the hysterical behaviour. In terms of maximum resistance and displacement ductility, the values of the numerical envelope curve reflected errors of less than 10%. Figure 2.35 shows the wall tested by Maleki (2008), the wall model developed by (Hung 2018), and a comparison between the numerical curve envelope and the experimental hysteric cycles. It should be noted that (Maleki 2008) walls were half-scale and lacked bed-joint reinforcement.

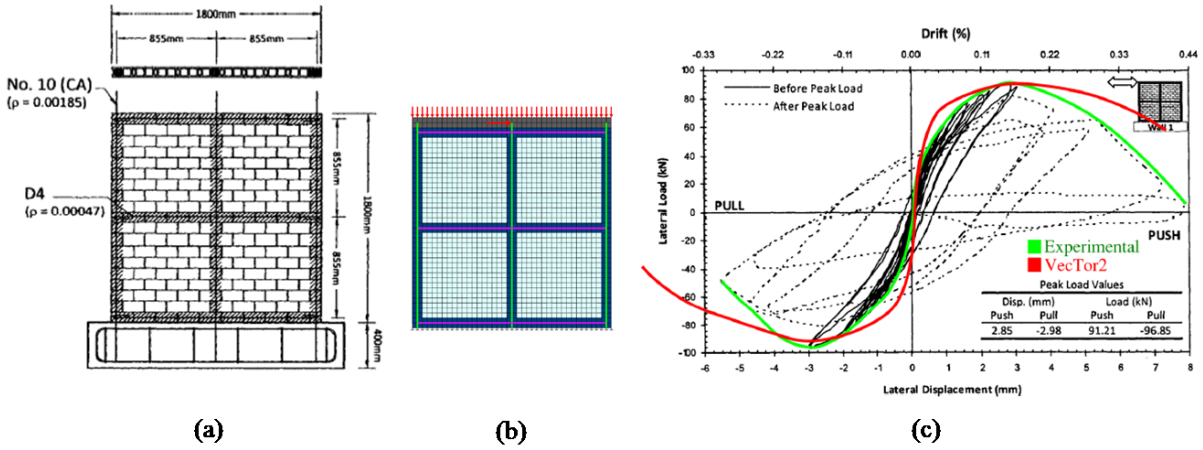

Figure 2.35 (a) Maleki (2008) wall tested experimentally, (b) wall model developed by Hung (2018), and (c) comparison between the experimental hysteresis loop envelope outlined in green with VecTor2 model hysteresis loop envelope outlined in red [adapted from Maleki (2008)]

Bolaños (2020) reproduced the monotonic response of eight PG walls that were tested at cyclic displacements in their plane and failed due to shear stresses with diagonal cracking. Monotonic curves and numerical cracking patterns were compared to the experimental envelope curves, and observed damage mechanisms to validate the developed model. Similarly, the model's predictive capacity for maximum resistance and associated lateral displacement were compared with the reported respective experimental values. He found that the numerical model could capture elastic stiffness for all simulated walls appropriately. Also, it was found that the prediction of the numerical model in terms of maximum strengths and their associated lateral displacements had a margin of error of less than 28%, except for one of the simulated walls, where an error in estimating the lateral displacement was 59.1%.

Finally, it was noticed that the numerical model tended to underestimate the maximum resistance in walls with an aspect ratio (H/L) ≥1, while walls with H/L<1, it tended to overestimate them. Figure 2.36 shows the model developed and the comparison of the monotonic numerical result with the experimental envelope.

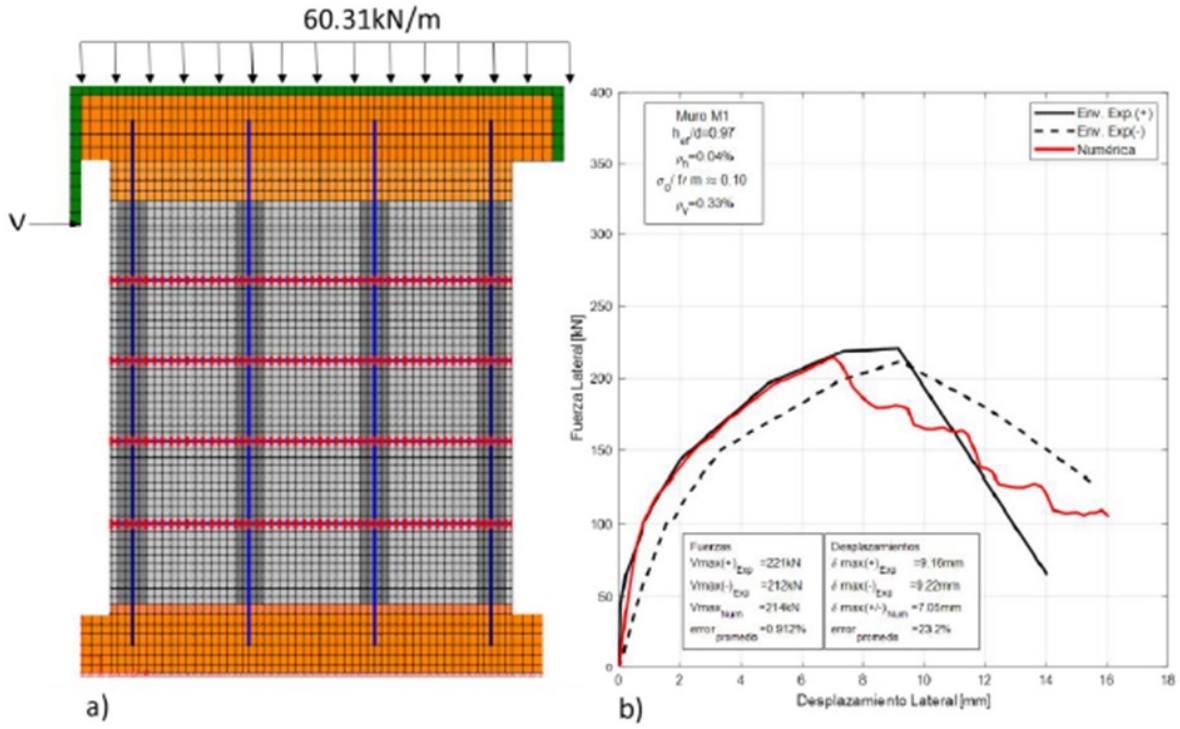

Figure 2.36 a) Model b) Comparison of lateral loads vs lateral displacement (Bolaños 2020)

2.3.3. Summary

To summarize, one modelling approach cannot be favoured over the other because both approaches have different applications (Lourenço et al., 1995). Micro-modeling studies are required to have a better knowledge of masonry local behaviour. This form of modelling is valid for structural details and modern building systems, where window and door openings frequently require piers just a few blocks long. Individual modelling of the blocks and joints is then preferred because these components are likely to govern the behaviour of the overall wall. Therefore, this approach requires extensive material characterization testing to define each constituent material exclusively in sophisticated software, which is not feasible in terms of time and cost. In addition, this type of modelling involves a prolonged running time.

On the other hand, when a structure is made up of solid walls with sufficiently large dimensions, macro-models can be used to ensure that stresses across or along a macro-length are practically uniform. Because of the reduced time, memory requirements, and user-friendly mesh generation, macro-modelling is more practical than micro-modelling. When a balance of accuracy and efficiency is required, this form of modelling comes in handy (Lourenço et al. 1995).

2.4 Conclusions

A brief review of the experimental and analytical studies of PG walls subjected to in-plane loads was presented. From all of the above, the following conclusions can be drawn:

- Small-scale models have higher strength and more data scatter than their prototype counterparts due to the size effect. PG walls are usually tested as fixed-fixed for practicality (easier to get higher shear). However, the fixed-free was found to be the most realistic boundary conditions due to the use of the modern movement joints. It alos found that some experimental walls have higher vertical reinforcement ratios than those usually found in the field. The purpose of elevating the vertical reinforcement was to ensure the shear dominant behaviour. However, this addition of vertical reinforcement may effect the resistance of PG walls against shear in terms of dowel action. In light of the findings, it is necessary to build PG walls that reflect practical construction characteristics in terms of wall size, reinforcement detailing, and boundary constraints.
- Since there is no clear agreement in the literature regarding how horizontal reinforcement type affects the shear strength of PG walls, that role needs to be explained. In particular, testing walls with higher aspect ratios and axial stress in accordance with what was found in the recent literature.
- Finally, the macro-modelling approach succeeded in capturing the peak strength, corresponding displacement, and initial stiffness. It therefore becomes a crucial tool for executing many parametric analyses required to develop expressions for predicting the shear strength of PG walls.

3. EXPERIMENTAL STUDY

Partially Grouted Masonry Walls with Different Horizontal Reinforcement Types: Experimental Results

Amr Ba Rahim [a], Clayton Pettit [a], Carlos 'Lobo' Cruz Noguez [a], and Cristián Sandoval [b]

[a] *Department of Civil and Environmental Engineering, University of Alberta, 9211-116 Street, Edmonton, Alberta T6G 1H9, Canada*

[b] *Department of Structural and Geotechnical Engineering; Pontificia Universidad Católica de Chile, Casilla 306, Correo 22, Santiago, Chile*

Abstract (262 Words)

The type of horizontal reinforcement can play a major role in the shear response of partially grouted (PG) masonry walls, particularly in the damage pattern and the post-peak behavior. Bond beam reinforcement and bed joint reinforcement are the two reinforcement types most used in practice; however, there is a lack of comparative studies between these two reinforcement strategies. To advance the knowledge on this matter, this paper presents the results of an experimental study made up of 4 full-scale walls tested under cyclic lateral loading. Two height-to-length aspect ratios (H/L=1.0, 1.86) and two reinforcement types per aspect ratio were considered. These walls were designed to reflect practical details and construction practices for PG walls in low seismic hazard areas.

Lateral load tests showed that the peak strength of walls with similar aspect ratios had no significant difference regardless of the reinforcement type used. Bed-joint reinforcement demonstrated to be a vital option as a shear reinforcement in controlling the crack width and improving the energy dissipation and ductility. The preliminary assessment of in-plane strength prediction equations of PG walls revealed that the general flexural analysis method provides a satisfactory estimation of flexural strength. In contrast, code-based equations had a highly conservative prediction of shear strength when imposing the upper limit. In addition, CSA and TMS equations used to predict the in-plane shear strength had a noticeable discrepancy in the contribution of the equation's parameters, particularly in the axial stress, horizontal reinforcement, and the upper limit, which highlighted the need to revise and reconsider the contribution of each design parameters used by these expressions.

3.1 Introduction

Loadbearing, partially grouted (PG) masonry shear walls are commonly used as a lateral force-resisting system in masonry structures. Unlike fully grouted (FG) masonry walls, PG walls are grouted only at the locations where either vertical or horizontal reinforcement bars are placed. As a result, they offer an economic advantage over FG walls due to reduced material and labor costs (Minaie et al. 2010; Dhanasekar 2011). PG walls are common in North America, especially in commercial and residential construction (Bolhassani et al. 2016b), but their response under in-plane lateral loading is not yet well understood, in contrast to FG construction (Banting and El-Dakhakhni 2012, 2014). For instance, North American code expressions for PG wall shear capacity are based on those developed for FG masonry, adding an arbitrary strength reduction factor to achieve safety levels comparable to FG walls (Dillon and Fonseca 2017). Consequently, the current design expressions are of limited accuracy, and in some cases, non-conservative (Haider 2007 Minaie et al. 2010; Dhanasekar 2011; Hassanli et al. 2014; Aguilar et al. 2016; Bolhassani et al. 2016a; Izquierdo 2021).

The North American standards for masonry incorporate guidelines for reinforced masonry walls in seismic zones, including specifications for reinforcement ratios, detailing, and anchorage. However, adhering to these regulations for constructing masonry walls in regions with low seismic hazards may lead to increased materials and construction costs. In areas with low seismic risks, such as the Canadian Prairies (which encompass Alberta, Saskatchewan, and Manitoba), designers prioritize cost-effectiveness over seismic performance when designing masonry walls, as illustrated in Figure 3.1. Yancey and Scribner (1989), Minaie et al. (2010) and Nolph and ElGawady (2012) showed experimentally that PG walls can be used effectively in low to moderate seismic hazards areas. Maleki (2008) and Kasparik et al. (2014) found that the PG walls, employing minimum reinforcement below the seismic demand (nominally reinforced), had the potential to be a cost-effective lateral resisting system in low to moderate seismic zones. In addition, anchorage detailing is an important aspect in seismic design where CSA S304 (2014) limits the use of 180 degrees hook in areas with a high level of plastic deformations. Sveinsson et al. (1985) found that proper anchoring of horizontal reinforcement around the extreme vertical reinforcement (180 degrees) is more effective than walls with hooks (90 degrees) in terms of ductility, strength degradation, and shear failure

mode, which was confirmed recently by Rizaee (2015) using strain gauges. On the other hand, 90 degrees hook can be an acceptable option where a low level of deformations was expected (Seif ElDin and Galal 2018).

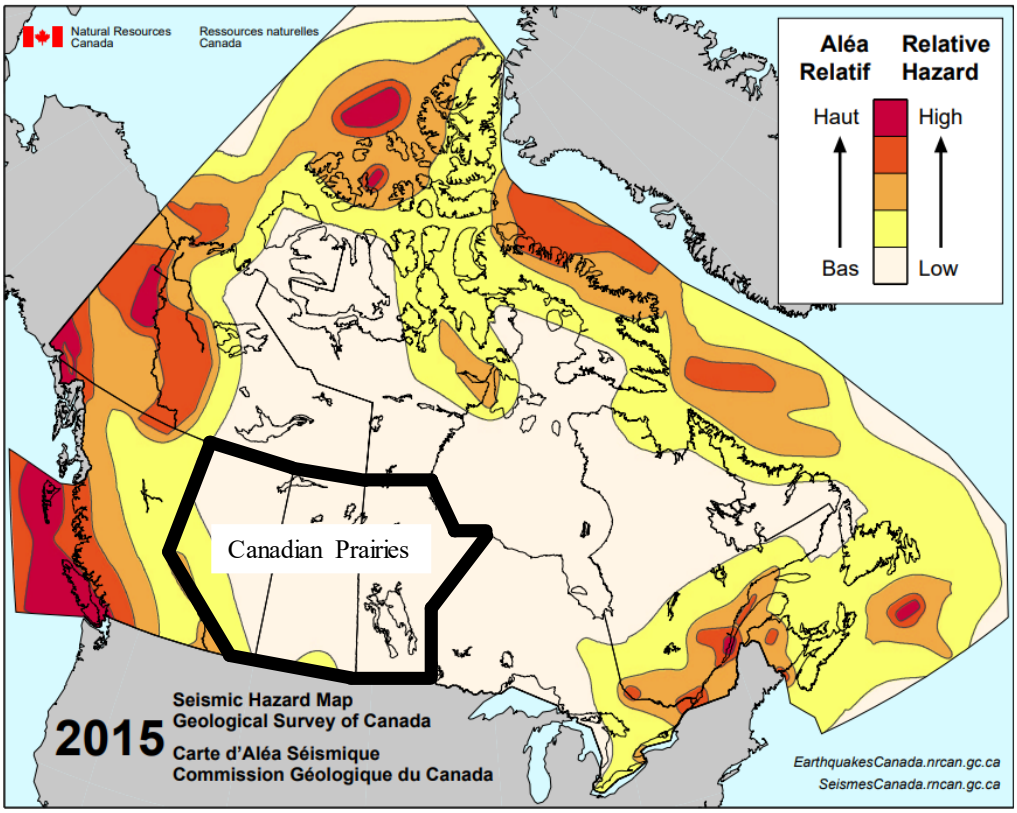

Figure 3.1 Seismic hazard map of Canada adapted from Earthquakes Canada (2021)

The literature shows that the type of horizontal reinforcement plays a major role in the response of PG walls. There are two horizontal reinforcement types commonly used in practice: bond beam and bed joint reinforcement (Figure 3.2). Bond beam reinforcement (Figure 3.2a) consists of horizontal steel bars placed at the centre of a masonry course, which is then filled with grout. Bed-joint reinforcement (Figure 3.2b) consists of a ladder- or truss-type steel reinforcement that is embedded in the horizontal mortar joints. Tomaževič and Lutman (1988), Yancey and Scribner (1989), Schultz (1996), Schultz et al. (1998), Baenziger and Porter (2011), Hoque (2013), Bolhassani et al. (2016b), Stathis et al. (2018), Schultz and Johnson (2019), and Calderon et al. (2021a) conducted comparative studies on the influence of horizontal reinforcement types (bond beam vs bed-joint) on the shear strength of PG walls. All the researchers mentioned above used an aspect ratio $H/L \leq 1$, except for Tomaževič and

Lutman (1988) and Yancey and Scribner (1989) where the latter had an aspect ratio close to one (h/L=1.17) while the former employed two aspect ratios (H/L=1.25 and 2.3).

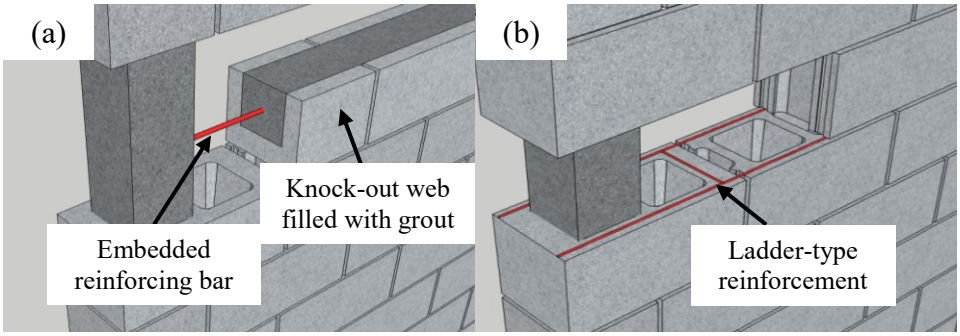

Figure 3.2 Types of horizontal reinforcement; (a) Bond beam reinforcement and (b) Bed-joint reinforcement

Hidalgo and Luders (1986), Wierzbicki (2010), and Hoque (2013) noted that bed-joint reinforcement is less effective than bond beam reinforcement as horizontal seismic reinforcement because it can readily fracture when subjected to several loading and unloading cycles. As a result, walls reinforced with a bond beam would be stronger than those reinforced with bed-joint reinforcement. Schultz et al. (1998), Baenziger and Porter (2011), Ramírez et al. (2016), Sandoval et al. (2018), and Stathis et al. (2018) observed that bed-joint reinforcing was effective in controlling the cracking distribution and improving the post-peak behavior and wall ductility when compared to the bond beam reinforcement. This is attributed to the ability of bed-joint reinforcement to limit the propagation of existing cracks, forcing the creation of new cracks throughout the wall panel after reaching the peak lateral load.

Bolhassani et al. (2016b) observed that the peak lateral load attained by all walls was not significantly different regardless of the horizontal reinforcement type, which was confirmed recently by Schultz and Johnson (2019) and Calderón et al. (2021a). Bolhassani et al. (2016b) used a cantilever setup to evaluate three square (H/L=1) PG walls under cyclic lateral loads and constant axial stresses of 0.14MPa (based on net area). Two of the walls were reinforced with a bond beam, while the last one was reinforced with a mix of bed-joint and bond beam reinforcement. While all the walls had approximately equal vertical reinforcement ratio of 0.075%, the wall with mixed horizontal reinforcement had a higher ratio of 0.1% than the other two walls of 0.075% (based on bar size area /spacing x thickness). They noticed that a wall reinforced with a combination of bond-beam and bed-joint reinforcement showed better ductility and stiffness degradation when compared with a wall reinforced only with bond

beam. They observed that the use of distributed bed-joint reinforcement across the wall height allowed for the distribution of stress in hollow panels. As a result, the initial cracks caused by increased lateral displacement did not open significantly, and a new set of cracks spread at the top of the walls in contrast to the walls without bed-joint reinforcement. The ability of bed-joint reinforcement to control crack progression had already been observed by Yancey and Scribner (1989), when they noticed that walls reinforced exclusively with bond beam reinforcement had a more severe cracking pattern than those reinforced with bed-joint reinforcement in terms of block crushing, splitting, and spalling.

Calderón et al. (2021a) recently tested four PG walls with various horizontal reinforcing types and layouts in a cantilever test setup, applying axial stress of 0.5MPa (based on gross area). The first two walls had ladder-type bed-joint reinforcement, the third wall had steel rebars embedded in bond beams, and the fourth wall had a combination of the two reinforcement types. It is worth noting that the horizontal and vertical reinforcement ratios of all walls were nearly identical at 0.1% and 0.34%, respectively (based on bar size area /spacing x thickness). In addition, all walls had a similar aspect ratio (H/L) of 0.86. The authors observed that the grout limited the development of cracks near the bond beams, resulting in a few wide cracks crossing horizontal reinforcement in bond beams. In contrast, the authors noticed that the cracks were better distributed throughout the wall panel and the residual deformations were controlled by bed-joint reinforcement. All the walls exhibited comparable shear strength, while the highest ductility was observed in the wall with ladder-type bed-joint reinforcement. Finally, these authors suggested studying whether the influence of the horizontal reinforcement type on the shear behaviour of PG walls follows the same trend when different aspect ratios, horizontal reinforcement ratios, and axial load levels are investigated.

The literature shows that there is a lack of comparative studies of bond beam vs bed-joint reinforcement that incorporate walls having aspect ratios greater than 1.0 with higher levels of axial load and with reinforcement distribution following the conventional construction practice, such as vertical reinforcement ratios. Therefore, the main objective of this research is to expand the understanding of the influence of the two horizontal reinforcement types used in PG wall construction. For this purpose, four full-scale PG walls with two different height-to-length aspect ratios (H/L=1.0; 1.86) and two different horizontal reinforcement types per

aspect ratio were subjected to cyclic lateral loading. Therefore, the wall aspect ratio and the horizontal reinforcement type (bond beams and bed-joint reinforcement) were the design parameters investigated in this research.

In this paper, the walls were made of concrete masonry units (CMUs) and were subjected to a constant axial load and reversible cyclic lateral load during the test. The response of these walls and the role of the variable design parameters were analyzed in terms of damage development, hysteretic response, shear strength, energy dissipation, and displacement ductility. The reinforcement layouts have followed the standard masonry code regulations and conventional construction practices. In addition, flexural strength prediction using the general flexural analysis method and in-plane shear strength predictions of the code-based equations from North America's leading codes were compared to the experimental results.

3.2 Experimental Program

3.2.1. Test Specimens

Four full-scale wall specimens were tested under constant axial load and cyclic in-plane lateral loads that were gradually increased up to failure. Each specimen had three parts – a cap-beam, a wall panel, and a foundation. The RC cap-beams and the foundations were designed to remain in the elastic range. Following the literature survey, two aspect ratios (wall height to wall length) H/L were investigated – 1.86 and 1.00. The walls termed as BB slender (bond-beam) wall and BJ slender (bed joint) wall are those with H/L of 1.86. Similarly, BB squat (bond-beam) wall and BJ squat (bed-joint) wall are the walls with H/L equal to 1.00. Table 3.1 shows the main characteristics of the walls, while Figure 3.3 provides the details of the reinforcement schemes of each wall. The wall specimens were designed following the provisions for PG walls subjected to combined axial and in-plane lateral loads of the North American codes CSA S304 (2014) and TMS 402 (2016). The design intended to reflect practical details and construction practices for PG walls in the Canadian Prairies area. Low amounts of reinforcement (both in the vertical and horizontal directions), satisfying the minimum requirement ratios in CSA S304 and TMS 402, were used to represent a design scenario governed by the economy factor over the seismic performance.

Table 3.1 Design details of specimens

	Specimen ID	Specimen Dimensions h mm	l mm	t mm	Aspect Ratio h/l	Vertical Reinforcement Vertical layout	ρ_v (%)	Horizontal Reinforcement Horizontal layout	ρ_h (%)	Axial Stress σ^* (MPa)
Slender walls	BB slender	2600	1400	190	1.86	15M@1200	0.09	10M@600	0.09	1.9
	BJ slender	2600	1400	190	1.86	15M@1200	0.09	3.7mm@400 + 1-10M	0.05	1.9
Squat walls	BB squat	2600	2600	190	1.00	15M@1200	0.09	10M@1200	0.04	1.9
	BJ squat	2600	2600	190	1.00	15M@1200	0.09	3.7mm@400 + 1-10M	0.05	1.9

** Based on gross area*

All walls had a vertical reinforcement ratio of 0.09%, using a 15M bar (Grade 400 steel) with a horizontal spacing of 1200 mm (Figure 3.3). The bars were continuous in the wall panel, anchored at the wall base and the cap beam.

Shear reinforcement formed by bond beams is a complex design parameter in North American codes. While CSA S304 (2014) limits the spacing of shear reinforcement to not more than 2400 mm or half of the wall length, whichever is less, TMS 402 (2016) sets the maximum spacing of shear reinforcement to be the lesser of half-length of the wall or 1219 mm. In this study, having the same amounts of horizontal reinforcement in the slender walls with bond beams and bed joint reinforcement would lead to designs that did not satisfy CSA S304 or TMS 402 on the walls with bond beams. Therefore, to obtain code-compliant walls, a reinforcement ratio of 0.09% was provided to the BB slender wall using five bond beams with a vertical spacing of 600 mm. Similarly, the BB squat wall was provided with a 0.04% reinforcement ratio through three bond beams spaced at 1200 mm. The bond beam reinforcement consisted of single 10M bar (Grade 400 steel), placed continuously throughout the wall length where it hooked using 90º hook around the edge of the boundary end cell as per CSA A23.1.

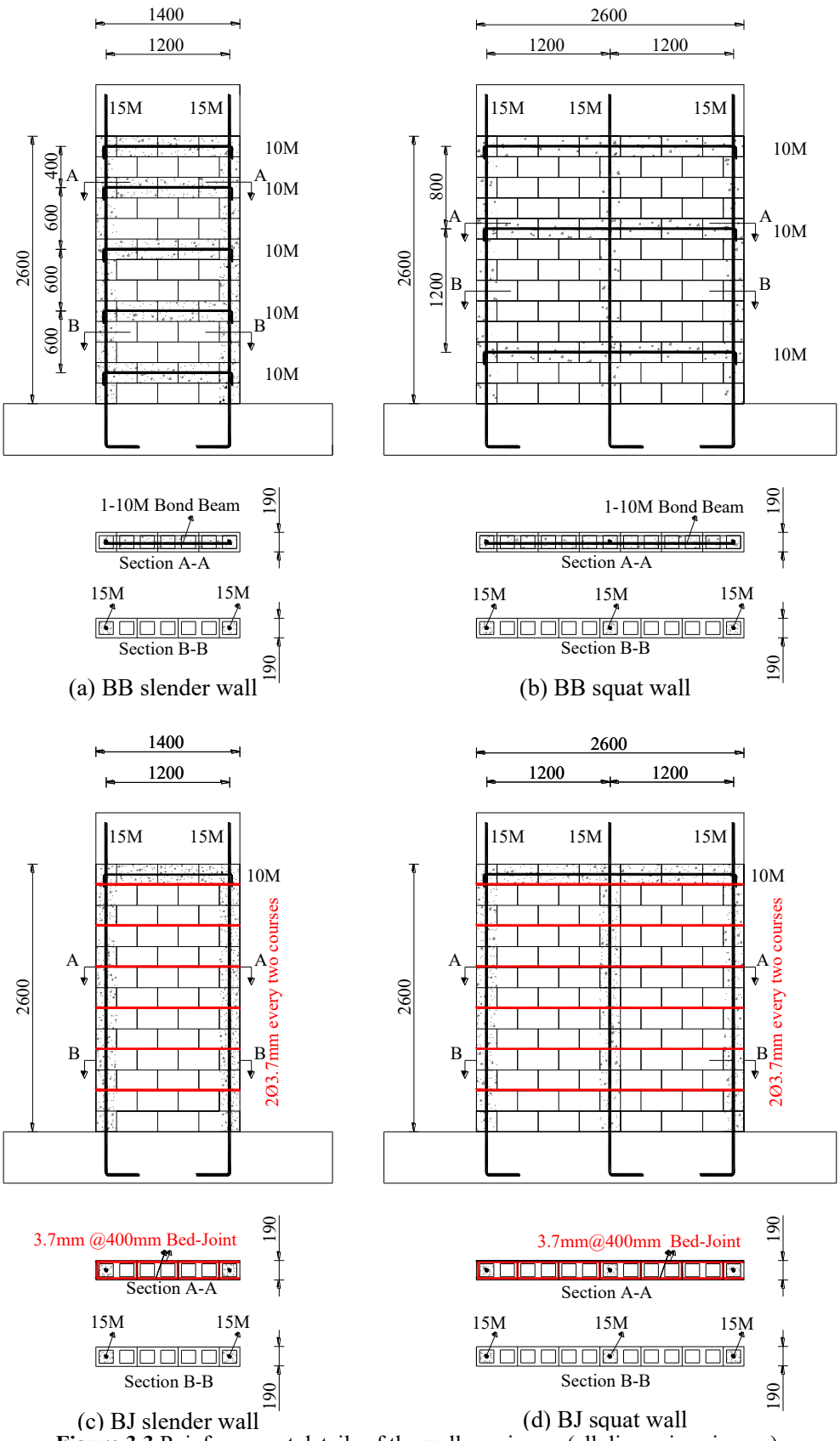

Figure 3.3 Reinforcement details of the wall specimens (all dimensions in mm)

Following the practical construction practice, the first bond beam was placed at a distance ($s_h/2$) from the base of the wall and after that, going up with the specified spacing so that the last bond beam was placed at the top (Figure 3.3), where s_h is the vertical spacing of the horizontal reinforcement. Dillon (2015) showed that bond beam placed at the base does not contribute to the wall strength, which reinforced by Izquierdo (2021) who pointed out that the majority of PG walls were reinforced with bond beams at the top and middle courses. Placing a bond beam at the top of all walls considers a conventional practice, to facilitate transferring the loads from the floor system.

For the walls with bed-joint (BJ) reinforcement, both BJ slender and BJ squat walls had a reinforcement ratio of 0.05% provided using the Standard: 9 Gauge Side Rods x 9 Gauge Cross Rods (ladder-type) reinforcement of 3.7 mm diameter with a vertical spacing of 400 mm (every other course). The vertical spacing complies with CSA S304 which directs the spacing not to exceed 600 mm for joint reinforcement. TMS 402 (2016) considers the provided vertical spacing (s_h=400 mm) as the maximum spacing permitted for joint reinforcement in areas with no- or low-seismic hazards.

The above code requirements led to the BB slender wall having approximately twice the amount of horizontal reinforcement ratio compared to the other walls. The implications of using different horizontal reinforcement ratios will be discussed in the Test Results section.

All walls were subjected to the same level of axial stress, which was approximately 1.9 MPa (based on gross area). This stress level is approximately 10% of masonry compressive strength. This applied axial stress was selected based on similar studies carried out in North America (Shing et al. 1989; 1990; Ahmadi et al. 2014; Rizaee 2015).

All wall specimens were constructed by professional masons using 20 cm standard hollow CMUs (with nominal dimensions 400x200x200 mm, using a running bond. Head and bed joint thickness of approximately 10 mm was implemented where Type S Portland Lime & Sand premixed mortar, which is commonly used at the masonry construction, was used throughout the joints. Core Fill Grout-Coarse was used to fill the vertical cells where vertical reinforcement placed and the bond beams along the whole length. The masonry walls were cured under laboratory environment control. The mechanical properties of the materials used

to build the wall specimens are summarized in Table 3.2. By applying material properties values, the flexural and shear capacities of the test specimens were computed as illustrated in Table 3.3. It is seen that the squat walls were expected to be a shear dominated while the slender walls were expected to be in flexure or mixed shear-flexure. For further details in the materials properties tests and the wall specimens design and construction, please refer to Appendix A.

Table 3.2 Summary of material properties

Property	Notation	Samples No.	Average (MPa)	CV (%)	Test Standard
Compressive strength of CMU*	f'_{cu}	5	19.0	6.8	CSA165-14
Compressive strength of mortar	f'_{cm}	6	14.8	16.7	CSA A179
Compressive strength of grout	f'_{cg}	6	30.6	8.1	CSA A179
Yield strength of 15M rebar	f_y	3	455	0.4	ASTM A615
Yield strength of 10M rebar	f_y	3	521	0.9	ASTM A615
Yield strength of BJR (3.7mm)	f_y	4	617	2.6	ASTM A951
Compressive strength of ungrouted prism*	f'_{ugm}	3	22.0	15.7	EN 1052-1
Compressive strength of grouted prism	f'_{gm}	3	16.4	16.1	EN 1052-1
Weighted compressive strength of masonry	f'_m	6	20.5	15.8	EN 1052-1
Shear strength of masonry joints (cohesion)	c	15	0.148	-	EN 1052-3

**Based on net area*

Table 3.3 Predicted capacities of the Test specimens

Specimen ID	BB slender wall	BJ slender wall	BB squat wall	BJ squat wall
V_m	77 kN	77 kN	140 kN	140 kN
V_p	65 kN	65 kN	118 kN	118 kN
V_s	58 kN	37 kN	54 kN	68 kN
$V_m+V_p+V_n$	200 kN	178 kN	312 kN	326 kN
V_r	192 kN	192 kN	350 kN	350 kN
V_f	166 kN	166 kN	554 kN	554 kN
V_f/V_n	0.9	0.9	1.8	1.7
Expected Failure Mode	Flexure	Flexure	Shear	Shear

Note: V_m, V_p, V_s and V_r are the masonry, axial stress, horizontal reinforcement contribution, and the upper limit using CSA S304 equation clause 10.10.2.1. V_n is the minimum of ($V_m+V_p+V_n$) and V_r. V_f is the flexural capacity using the general flexural analysis method.

3.2.2. Test Setup

The walls in this study were intended to represent an entire wall (from foundation to roof) of a low-rise or single-storey building. Therefore, the walls were tested in a cantilevered (fixed-free) setup (Figures 5 and 6). The bases and capping beams were designed to remain in the elastic range during the test. The out-of-plane displacements of the walls were restrained with rollers against the capping beam, allowing the in-plane displacements while restraining the

out-of-plane displacement. Two 800 kN actuators were used to apply reversed-cyclic load to the walls. The vertical load was applied to the top of the wall specimen through two sets of actuators which connected to the cruciform-shape beam at the top of the wall specimen via tension rods. Four actuators were mounted on four gravity load simulators (GLS), with two at each side of the wall specimen. The vertical load was monitored by load cells located within the tension rods, and it was cross verified by two load cells located in the cruciform-shape beam at the top of the wall specimen. This vertical load assembly was designed to maintain a constant axial load throughout the lateral movement of the wall.

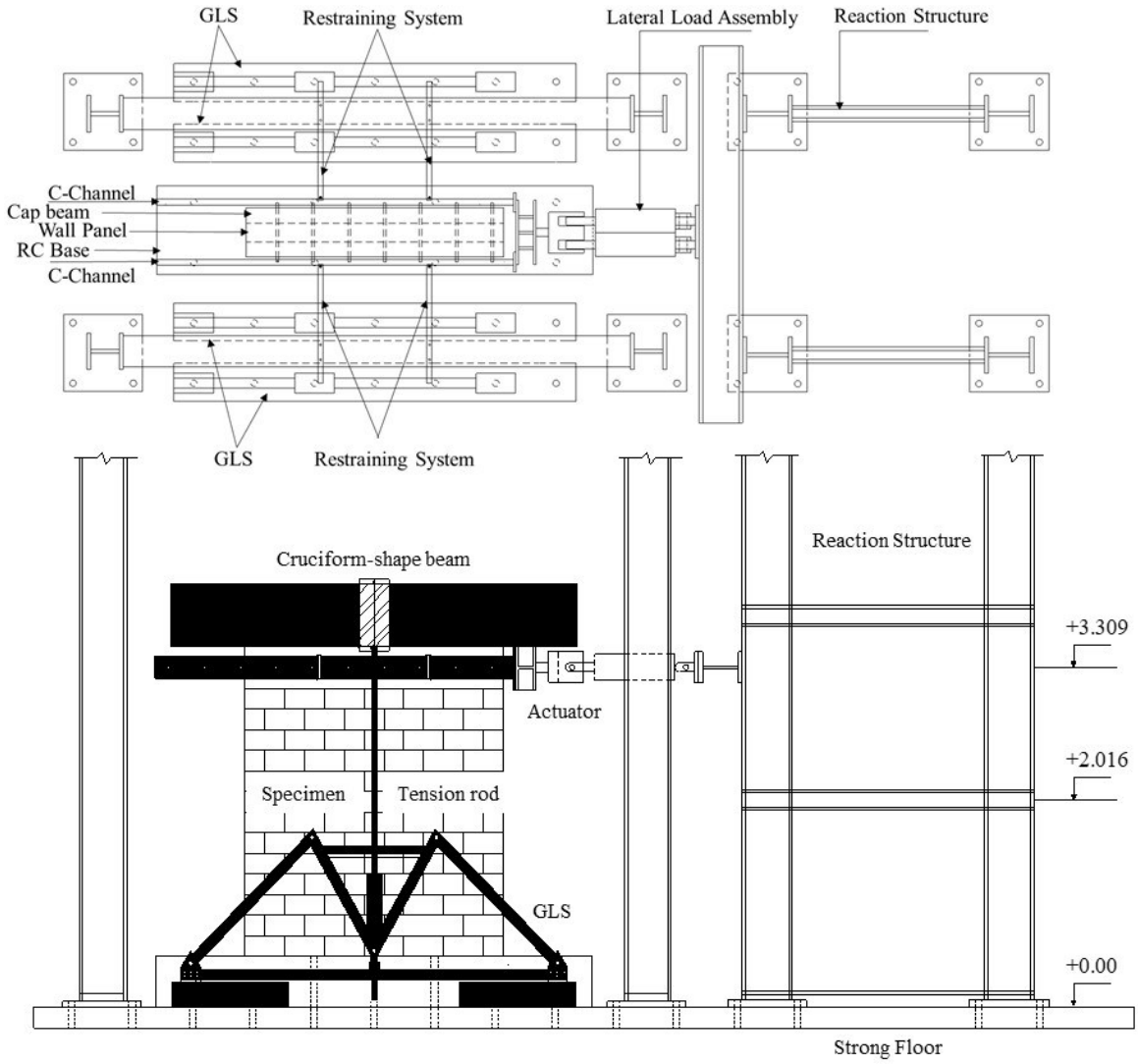

Figure 3.4 Schematic view of the test setup

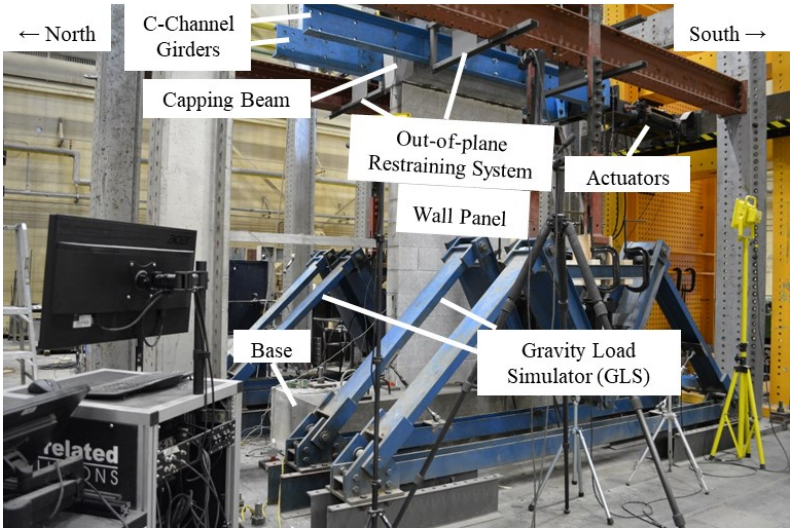

Figure 3.5 General view of the test setup

3.2.3. Instrumentation and Loading Procedure

Loads, strains, and displacements in the walls were measured using load cells, cable transducers, and Linear Variable Differential Transformers (LVDTs). Vertical and lateral loads were recorded via load cells. Lateral, vertical, diagonal, and out-of-plane displacements as well as the base slip were measured using cable transducers and LVDTs. In addition, strains in steel bars were recorded using strain gauges. Additional details about the instrumentations can be found in Appendix A.

Wall specimens were subjected first to axial stress (σ) ratio of $\sigma/f'_m \approx 0.1$ and kept constant. This translated into loads of 516 kN and 973 kN for wall specimens with an aspect ratio of 1.86 and 1.00, respectively. In-plane lateral loads were then applied in a reversal mode using a displacement-control protocol, as seen in Figure 3.6. The displacement levels for all cycles were based on the protocols followed by Nolph and ElGawady (2012) and Elmapruk et al. (2020). Each displacement level was repeated twice so that the stiffness degradation could be captured clearly (FEMA 461 2007). The Loading rate was 6 mm/min at the first displacement levels and then increased to 12 mm/min at the latter levels. Finally, the test was stopped when the lateral loads reached 80% of the peak lateral load that resulted from the test.

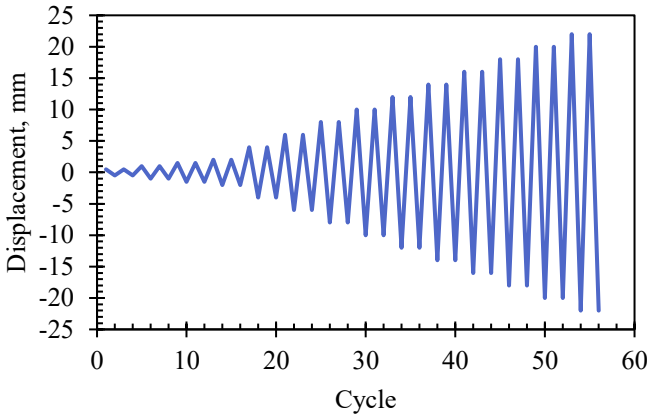

Figure 3.6 Loading Protocol

3.3 Test Results

3.3.1. Cracking Pattern and Failure Mode

The damaged state of the walls at peak load and failure is shown in Figure 3.7, where the average crack width is identified. Only one wall side is shown in Figure 3.7; in all walls, the other side had similar damage. For slender walls, BB slender wall developed less cracks than BJ slender wall. This can be attributed to the higher horizontal reinforcement of the BB slender wall (ρ_h of BB slender wall $\approx 2\rho_h$ of BJ slender wall), where the distribution of shear reinforcement (bed-joint) plays a more influential role in the degradation of the wall than the quantity of shear reinforcement (bond beam). More distributed bed-joint reinforcement limits the crack width but forms new cracks over the entirety of the wall rather than at select locations (bond beams). This was confirmed by the average crack width (Figure 3.7).

In squat walls, which had similar amounts of horizontal reinforcement, BJ squat wall showed less damage distribution than the BB squat at the peak load state (Figure 3.7). This is attributed to the distributed reinforcement, which limits the cracks' width from becoming visible. At the post-peak load state, both walls showed comparable damage, but the cracks in BJ squat wall distributed through the whole diagonal path of the wall panel in contrast to the BB squat wall (Figure 3.7), where no cracks appeared in the middle of the diagonal path of the wall panel, but they concentrated in the areas adjacent to the bond beams as observed by Calderon et al. (2021a).

In terms of the crack width, bed-joint reinforcement demonstrated to be viable in controlling the crack width in contrast to the bond beam, particularly in the post-peak load state (Figure 3.7). This is more visible in squat walls that failed in pure diagonal shear, where the cracks in BB squat wall had approximately three times the average width than the cracks found in BJ squat wall. This finding is in line with the studies of Tomaževič and Lutman (1988), Yancey and Scribner (1989), Bolhassani et al. (2016b), Schultz and Johnson (2019), and Calderon et al. (2021a).

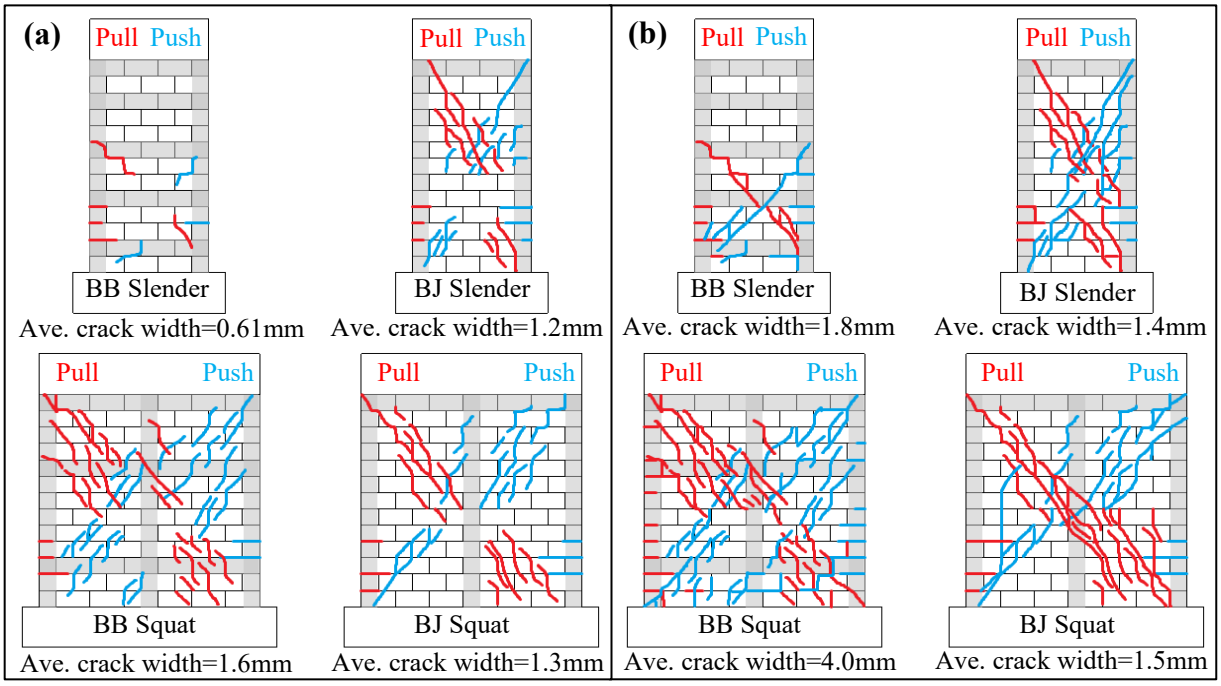

Figure 3.7 Cracking Patterns of Tested Walls at (a) peak load state and (b) final state

Regarding the failure mode, BB slender wall failed in flexure. Strains measured in the vertical reinforcement showed that the outermost vertical bars yielded before reaching the peak lateral load (Figure 3.8), a sign of flexural failure. BJ slender wall failed in mixed shear-flexure. Strains measured in the vertical bar did not yield but showed a sudden drop in the tension zone at the peak load state as shown in Figure 3.8. This drop may indicate a bond slip failure between the rebar and the grout. In addition, diagonal cracks were developed from the upper corner to the toe in BJ slender wall, which is a sign of mixed shear-flexure (Figure 3.7).

In the squat walls, there was no yielding in the vertical bars (Figure 3.8) as well as diagonal cracks throughout the wall surface occurred, indicating that both walls failed with diagonal

tension cracking, as shown clearly in Figure 3.7. Figure 3.9 shows that the damage to squat walls at the final state consisted of stair-stepped and diagonal cracking, cracking at the upper end and the wall toes, cracking of the vertical grout, and spalling of face-shell.

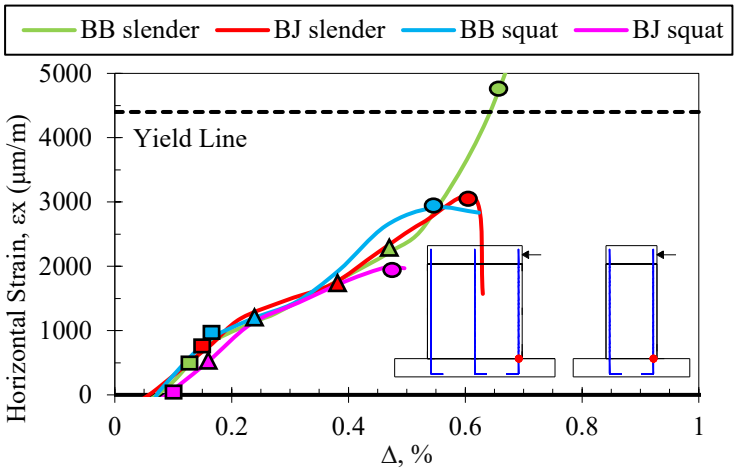

Figure 3.8 Strains at the bottom of the outermost vertical reinforcement

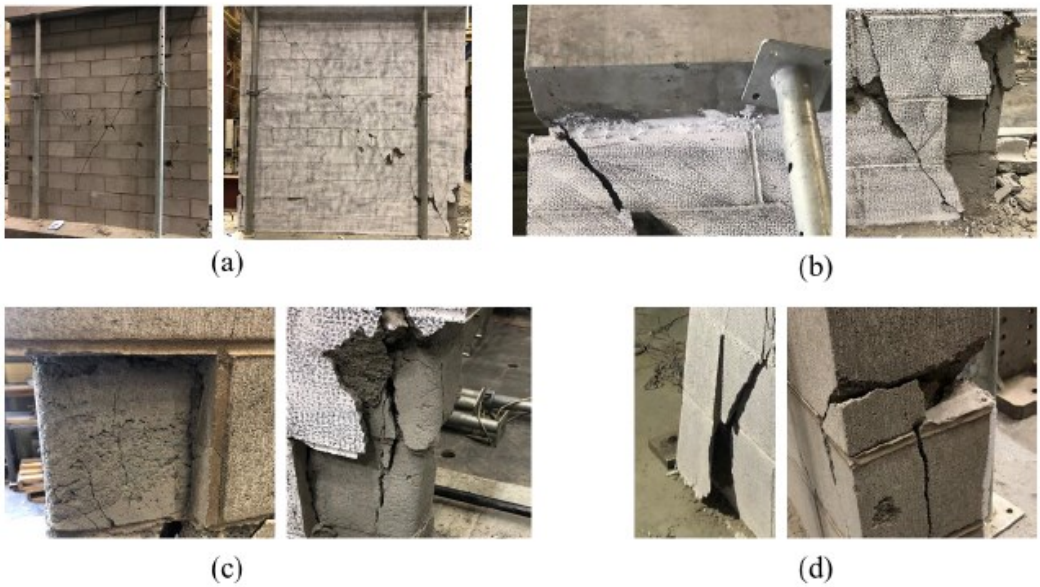

Figure 3.9 Typical damage for both squat walls at the point of failure (post-peak): (a) stair-stepped and diagonal cracking, (b) upper end and toe cracking, (c) vertical grout cracking, and (d) spalling of face-shell

3.3.2. Hysteretic Response

The lateral load was measured with the load cell placed between the wall specimen and the double-hydraulic jacks. The drift ratio was calculated as the ratio of the lateral displacement measured at the top of the wall over the wall height.

Figure 3.10 shows the hysteretic response of the walls. Table 3.4 provides the lateral load with associated lateral displacement and drift values at the key structural milestones. The first cracking was identified as the first slope change on the in-plane hysteresis curve. Following initial cracking, the next noticeable slope change in the in-plane hysteresis curve corresponds to the formation of a compressive strut in the walls, which carries most of the load at a stage in which the longitudinal steel has not yet been fully activated and the masonry has lost its tensile capacity due to cracking. The maximum load in the lateral load–drift ratio curve is termed the peak lateral load. Failure was defined as the point on the in-plane hysteresis curve where the lateral load dropped to 80% of the maximum lateral load recorded in the test.

Table 3.4 Summary of the test results

	Initial crack			**Strut formation**			**Peak lateral load**		
Specimen ID	Lateral Displacement (mm)	Drift Δ (%)	Lateral Force (kN)	Lateral Displacement (mm)	Drift Δ (%)	Lateral Force (kN)	Lateral Displacement (mm)	Drift Δ (%)	Lateral Force (kN)
BB slender	3.5	0.13	108	12.0	0.46	149	15.9	0.61	162
BJ slender	4.0	0.16	112	10.0	0.39	144	14.1	0.55	152
BB squat	4.0	0.16	242	6.1	0.23	269	14.9	0.58	406
BJ squat	2.2	0.09	227	4.1	0.16	301	12.0	0.46	416

**This table shows the average of lateral loads, lateral displacement, and drift in both loading directions*

3.3.1.1 Slender walls

Both walls experienced a linear elastic behaviour up to the occurrence of the first crack. This behaviour was characterized by narrow cycles and an approximately symmetric response with low dissipated energy. At the strut formation stage, the first diagonal cracks started to appear throughout the wall panels, and both walls started to exhibit nonlinear behaviour. Similar to the previous stage, both walls attained comparable lateral load.

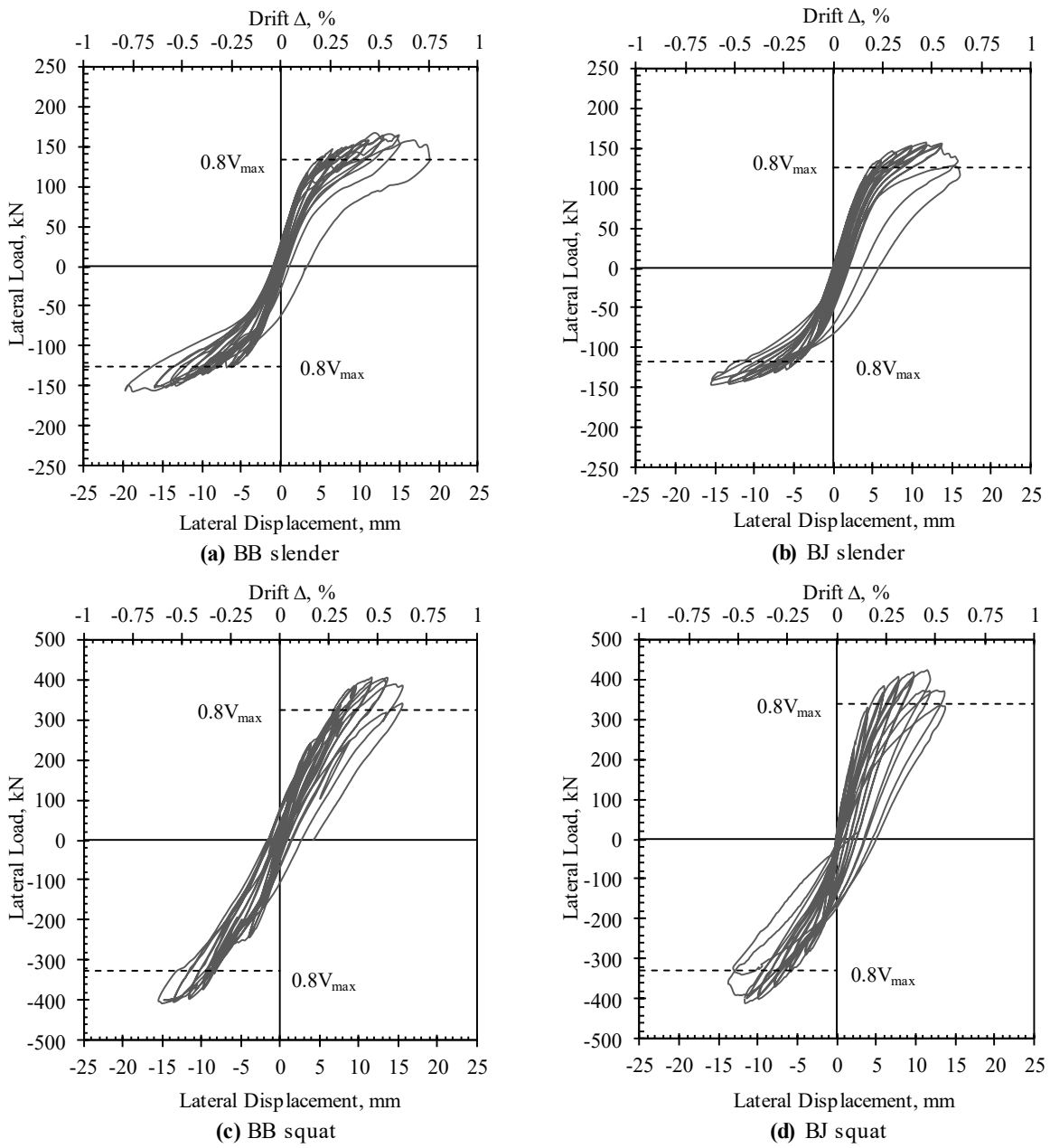

Figure 3.10 Load-Displacement Hysteresis Loop Diagram

After experiencing the first diagonal cracks, the hysteretic response exhibited wider cycles for both walls indicating that more energy was dissipated due to the occurrence of more new cracks or widening of the existing cracks. As shown in Table 3.4, both walls attained nearly equal peak lateral load regardless of the horizontal reinforcement type and different shear reinforcement ratio with only 6% difference in lateral maximum capacity. This finding was also observed by Tomaževič and Lutman (1988). Tomaževič and Lutman (1988) tested slender walls (H/L=2.3) implementing three horizontal reinforcement ratios; 0.5% for steel

bars and 0.14% and 0.28% for wire reinforcement. They found that all walls attained nearly equal peak lateral load with an average difference of 4%. After reaching the peak lateral load in the push loading direction, no drop in the shear strength of the slender walls was observed in the subsequent cycles until the last cycle, where a sudden drop occurred. This plateau of peak load corresponded to the dominant flexural behaviour experienced by the slender walls, as observed also by Calderón et al. (2020) when they tested slender PG wall (H/L=2.23).

3.3.1.2 Squat walls

These walls had roughly equal amounts of horizontal reinforcement of 0.04% and 0.05% for BB squat and BJ squat walls, respectively. Similar to slender walls, both squat walls exhibited linear-elastic behaviour prior to the appearance of the first crack. Narrow cycles and a roughly symmetric response with low dissipated energy characterized this behaviour. At the strut formation stage, both squat walls had the first diagonal crack throughout the wall panel. BJ squat wall was slightly stronger than the BB squat wall (11% difference).

Following the first diagonal crack, both walls began to show wider cycles, indicating that more energy was dissipated as a result of the occurrence of more new cracks or the expansion of existing cracks. Both walls attained nearly equal peak lateral load (2% difference), as observed in Table 3.4. This is in line with the findings by Baenziger and Porter (2011), Stathis et al. (2018), and Calderón et al. (2021a). Similar to BB squat and BJ squat walls, those authors employed equal horizontal reinforcement and an aspect ratio close to one. Following the peak lateral load, the shear strength started to degrade, as shown in Figure 3.10. This deterioration was relatively gradual in both walls.

3.3.1.3 Discussion

Overall, the tested walls showed a relatively narrow hysteretic response compared to the other tested walls found in the literature. This may be attributed to the reinforcement details that were designed for non-seismic applications. For instance, anchorage and vertical reinforcement were not detailed following the seismic provisions and guidelines. The tested walls reinforced with bond beam had anchorage detailing of 90 degrees and walls reinforced with bed-joint had no special detailing such as the closed stirrups around the vertical reinforcement (Rizaee 2015). In the current study, the design of walls targeted the economic

factor over the seismic performance since these walls are applicable to the Canadian Prairie region. In addition, the lower vertical reinforcement to horizontal reinforcement ratio (ρ_v/ρ_h) employed in the tested walls may cause this phenomenon as observed by Nolph and ElGawady (2012).

Furthermore, an asymmetry is observed in the hysteretic response of the tested walls. This may be attributed to many factors; first, the reinforcement detailing of these walls was non-seismic. Second, the nature of inconsistency inherited in the PG walls compared to the FG walls (Voon 2007) directed the push loading direction to dominate the response over the pull direction regarding the crack width and residual displacements. Finally, applying high axial load plays a significant role in producing such a response due to the brittleness behaviour, as observed by Hoque (2013) and Rizaee (2015).

The backbone curves superimposed for all walls are presented in Figure 3.11. For slender walls, there is a fairly similar shape despite having different horizontal reinforcement ratios. This is attributed to the flexural behaviour experienced by both walls. This is reflected in approximately equal lateral loads and their associated displacements at the different milestones, according to Table 3.4, particularly in the push loading direction. In squat walls where the shear behaviour controls the wall behaviour, BB squat wall was less stiff than BJ squat wall before the peak load state. This is observed by the damage progressions of both walls, where the BB squat wall experienced more cracks than the BJ squat wall before the peak load state. This could be explained due to the distributed reinforcement of bed-joint, which controls the development of the crack's growth (Schultz et al. 1998; Calderon et al. 2021a). Regarding the aspect ratio, it is confirmed experimentally that the peak strength of PG walls is increased by decreasing the aspect ratio, as observed by many studies (Matsumura, 1988; Fattal, 1993; Voon and Ingham, 2006; Hamedzadeh, 2013, Ramírez et al., 2016). On the other hand, the horizontal reinforcement type (bond beam or bed-joint reinforcement) was observed to have a negligible effect on the peak strength of PG walls when similar reinforcement ratios are used, both square and slender walls. In addition, there was no significant effect of aspect ratio and horizontal reinforcement type on the deformation capacity.

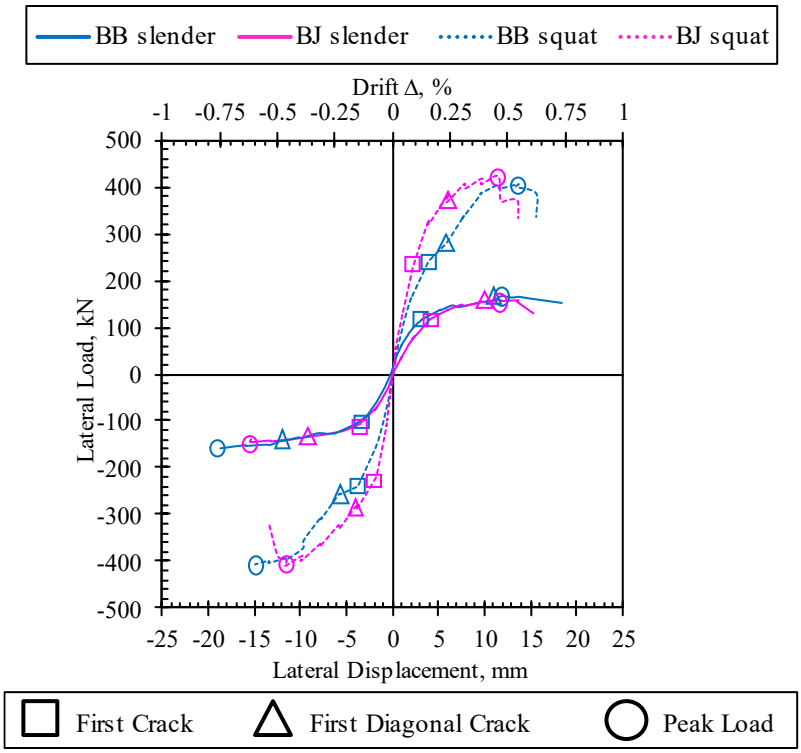

Figure 3.11 Comparison of backbone curve in both loading directions

3.3.3. Energy Dissipation

Energy dissipation indicates how much the system withstands the applied loads without significant damage. The dissipated energy is the area enclosed by the hysteric loop in one complete cycle, as shown in Figure 3.12. Therefore, this energy was evaluated as a summation of the two repetitive cycles for each displacement level until reaching the peak lateral load because some walls experienced sudden deterioration of strength, leading to brittle failure after reaching the peak load.

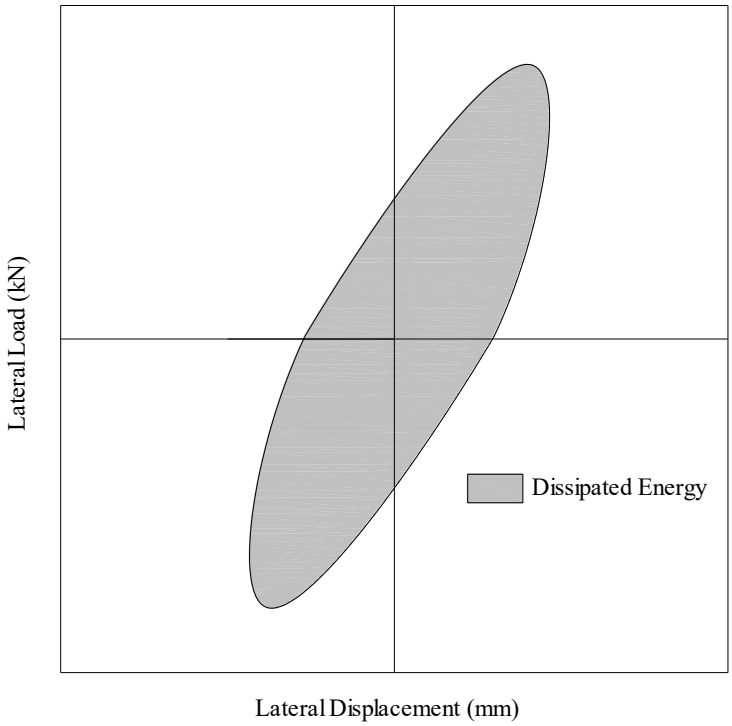

Figure 3.12 Computation of dissipated energy in one completed cycle

Figure 3.13 shows the development of the dissipated energy with respect to the drift ratio and how the variation of the aspect ratio and horizontal reinforcement types affect this parameter. Generally, walls with a lower aspect ratio show a higher amount of energy than those with a higher aspect ratio. This finding was agreed with (Ramírez et al. 2016), implying that walls with lower aspect ratio experienced a wide range of damage even during the first imposed displacement levels. Basically, walls reinforced with horizontal reinforcement attain higher resistance and dissipated energy than the un-reinforced ones (Tomaževič 1999; Haach et al. 2010). Slender walls either reinforced by bond beam or bed-joint reinforcement presented similar levels of dissipated energy. On the other hand, BJ squat wall showed higher dissipation of energy than BB squat wall by 45%. This demonstrated the viability of bed-joint reinforcement to control the cracks development by forcing new cracks to initiate and limit the growth of existing cracks. Finally, it is noted that, walls with a lower aspect ratio started showing higher increments of dissipated energy from an approximately drift ratio of 0.15%. At this drift ratio, either visible cracks were observed or a significant change in the stiffness occurred. This implies that the horizontal reinforcement started contributing to the wall system.

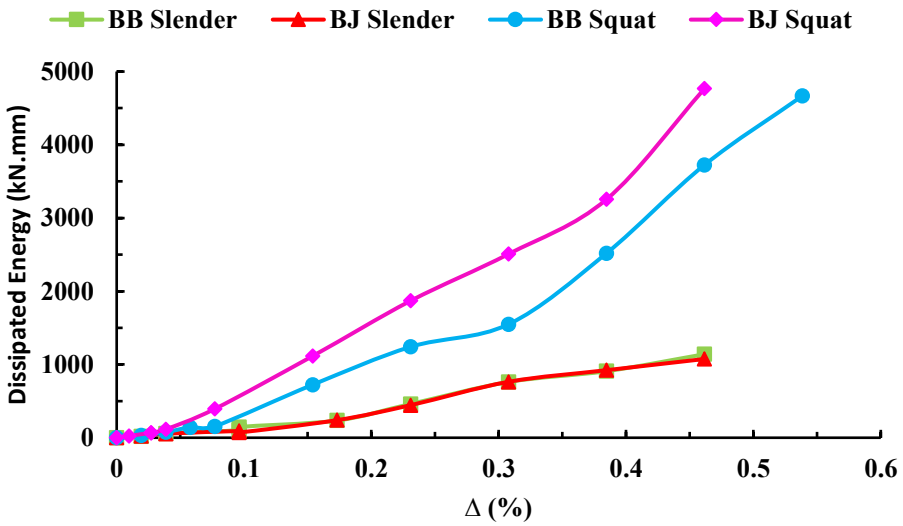

Figure 3.13 Dissipated energy of all tested walls

3.3.4. Displacement Ductility

Ductility is the parameter that demonstrates the capacity of the wall to resist repeated lateral load reversals without substantial degradation of strength or can be defined as a measure of the wall's capacity to withstand deformations beyond the yield limit without losing resistance to such loads. To simplify ductility estimation, the idealization of the experimental load-displacement envelope of the in-plane cyclic test as a bilinear envelope has been suggested by most of the literature. There are several approaches to estimating ductility using the idealized bilinear envelope in the literature. However, there is no matching between them (Shedid et al. 2008). In this study, we adopted one approach that has been followed by Calderón et al. (2020). This approach estimated the ductility as a ratio of maximum displacement (δ_{max}) associated with the maximum lateral load recorded during the test and yield displacement of the idealized envelope (δ_y), as shown in Figure 3.14. The yielding displacement (δ_y) was calculated to ensure that the idealized curve contains the same amount of energy as the experimental envelope curve (E_{env}) up to the point where the maximum load is reached. This approach neglected the post-peak stage due to the large variability and undesirable damage state exhibited by PG walls in the post-peak stage (Calderón et al. 2020).

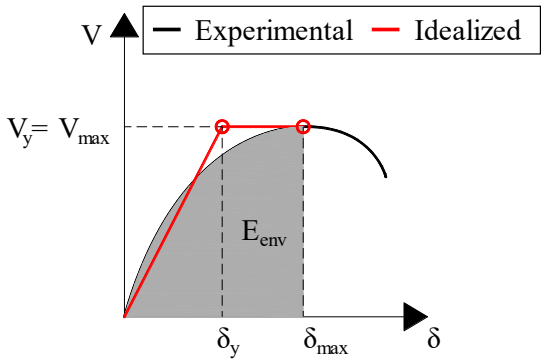

Figure 3.14 Idealization of the envelope curve adapted from Calderón et al. (2020)

Table 3.5 presents the parameters of the idealized envelopes and the ductility values of the tested walls. In addition, Fig. 3.15(a) compares the ductility values calculated in both load directions and on average. It is noted that the ductility values of all walls ranged between 1.73 (BB squat wall in the pull loading direction) and 2.67 (BJ slender wall in the pull loading direction). Slender walls obtained comparable ductility values due to the dominant flexural behavior for both walls. On the other hand, squat walls that failed in diagonal shear showed that squat walls reinforced with bed-joint had higher ductility by more than 16%.

For seismic design, ductility reduction factors (Rd) for short period structures such as reinforced masonry structures can be estimated using Eq. (1), as proposed by Paulay and Priestly (1992). The calculated values are depicted in Fig. 3.15(b) and listed in Table 3.5. The Rd values ranged between 1.57 and 2.08. It is observed that the Rd values followed the same trend as the ductility values due to the nature of Eq. (1). Based on SFRS Ductility-Related Force Modification Factors provided by National Building code of Canada, NBCC (2020) for masonry structures detailed and designed according to CSA S304 (2014), it is noted that the obtained Rd values lie within the conventional shear walls (Rd=1.5) and the moderately ductile shear walls (Rd=2.0).

$$R_d = \sqrt{2\mu_d - 1} \qquad (1)$$

All in all, despite the non-agreement in one approach to computing the ductility, it can be utilized as an indication of the capacity of the wall system to properly respond to seismic movements of the whole structure. However, there is an urgent need to propose a unified approach to ductility calculation.

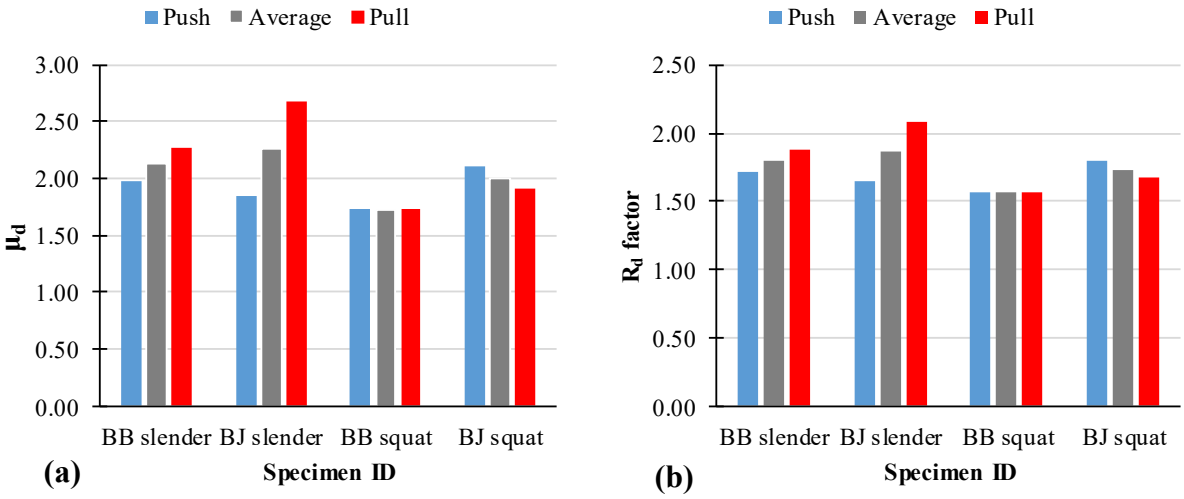

Figure 3.15 (a) Displacement ductility and (b) ductility reduction factor for low period structures

Table 3.5 Parameters of idealized envelopes, ductility, and R factors

Specimen ID	Load Direction	δ_y (mm)	δ_{Vmax} (mm)	V_{max} (kN)	μ_d	$\overline{\mu_d}$	R	$\overline{R}$
BB slender	Push	6.2	12.3	166	1.98	2.13	1.72	1.8
	Pull	8.6	19.5	157	2.28		1.89	
BJ slender	Push	6.6	12.2	157	1.85	2.26	1.64	1.86
	Pull	6.0	16	146	2.67		2.08	
BB squat	Push	8.2	14.2	404	1.74	1.73	1.57	1.57
	Pull	9.0	15.6	407	1.73		1.57	
BJ squat	Push	5.6	11.9	422	2.11	2.01	1.79	1.74
	Pull	6.3	12.1	410	1.91		1.68	

3.3.5. Comments of Current Findings with Previous Research

This sub-section compares the impact of reinforcement configuration, particularly horizontal reinforcement type (bond beam and bed joint reinforcement), on test outputs such as peak strength, energy dissipation, displacement ductility, and crack pattern, with those reported in the literature. Specifically, those comparative studies on the performance of bond beam vs bed-joint reinforcement of PG walls (Table 3.6). By examining these factors, we can gain insight into the effectiveness of different reinforcement strategies and their potential impact on the overall performance of the structure.

The literature indicates that the use of different types of horizontal reinforcement did not have a significant impact on peak strength when equal aspect ratios were employed, which is consistent with the findings of this study. However, the results of this study, as well as those of Tomaževič and Lutman (1988), Baenziger and Porter (2011), Hoque (2013), Bolhassani et al. (2016b), Stathis et al. (2018), and Calderón et al. (2021a), demonstrate that bed-joint reinforcement is a superior option for enhancing the energy dissipation and displacement ductility of PG walls. This finding is consistent across a wide range of design parameters, as shown in Table 6. Similarly, the literature indicates that bed-joint reinforcement is more effective than bond beam reinforcement in controlling crack patterns, as it forces new cracks to distribute throughout the wall panel and limits the growth of existing cracks, thereby improving wall integrity, particularly in the post-peak stage. This is consistent with the findings of the current research, which demonstrated an improvement in crack width with the use of bed-joint reinforcement, as compared to bond beam solution. Hoque (2013) is the only study listed in Table 6 that does not report a clear advantage of bed-joint reinforcement in controlling crack patterns where she found that the cracking pattern was more distributed over the surface of the specimens containing a bond beam, while cracks concentrated into a large X-pattern in specimens containing bed-joint reinforcement.

Based on the extensive literature survey, bed-joint reinforcement has emerged as a reliable and effective option for horizontal reinforcement of PG walls. This conclusion is supported by studies that had a wide range of variables, including wall geometry, compressive strength of masonry, axial stress, vertical and horizontal reinforcement ratios, and masonry typology. Therefore, it can be concluded that bed-joint reinforcement is a viable option for enhancing the performance and structural integrity of PG walls.

Table 3.6 Summary of previous studies on the performance of bond beam vs bed-joint reinforcement of PG walls (Design Parameters)

Study	Tomaževič and Lutman (1988)	Yancey and Scribner (1989)	Schultz (1996) and Schultz et al. (1998)	Baenziger and Porter (2011)	Hoque (2013)	Bolhassani et al. (2016b)	Stathis et al. (2018)	Schultz and Johnson (2019)	Calderón et al. (2021a)	Current Study
Country	Slovenia	USA	USA	USA	Canada	USA	Canada	USA	Chile	Canada
Aspect Ratio, h/l (Unitless)	1.25, 2.30	1.17	1.0, 0.7, 0.5	0.93, 0.62	1.0	1.0	1.0	0.67	0.86	1.86, 1.00
Height, h (mm)	760, 1405	1422	1422	2642	1800	3860	1800	4267.2	2270	2600
Length, l (mm)	610	1219	1422, 2032, 2845	2845, 4267	1800	3860	1800	6500	2640	1400, 2600
Thickness, t (mm)	100	194	195	194	190	200	190	190	140	190
Vertical reinforcement, ρ_v (%)	0.26, 0.52	0	[0.20-0.41]	[0.14-0.25]	0.13	0.07	0.13	[0.04-0.05]	0.34	0.09
Bond Beam reinforcement, ρ_h (%)	0	[0-0.22]	[0.05-0.12]	[0.05-0.11]	[0-0.17]	[0.07-0.08]	0.09	[0.03-0.06]	[0.06-0.1]	0.04, 0.09
Bed-joint reinforcement, ρ_h (%)	[0-0.5]	[0-0.06]	[0.06-0.11]	[0-0.18]	[0-0.03]	0.03	[0.06-0.09]	0.05	[0.03-0.1]	0.05
Gross axial stress, σ (MPa)	0.98	0.74	[0.45-0.48]	0	[1.20-1.26]	[0.06-0.08]	N/A	0.05	0.5	1.9
Compressive strength, f'_m (MPa)	9.5, 10.7	N/A	[12-14]	13.9, 19.8	16.6	16.8, 18.4	N/A	17.3, 23.1	9.67	20.5

3.4 In-plane Strength of PG Walls Prediction

This section compares the results of the tested walls' peak lateral load with the in-plane strength prediction equations found in North American codes (CSA S304 and TMS 402). Since the slender walls failed in flexure and the squat walls failed in diagonal shear, flexural and shear strength prediction is discussed separately in two sub-sections.

3.4.1. Flexural Strength Prediction

The flexural strength of PG masonry walls can be predicted by various simple formulae found in the literature, such as Cardenas and Magura's (1973) equation. Although these equations are straightforward to implement, they have some conditions that restrict their use for all design scenarios. The general flexural analysis method offers the flexibility of predicting the flexural capacity of any number and distribution of reinforcement layers. This method is based on the plane section assumption as well as the compatibility and equilibrium equations. The neutral axis (c) of the cross-section of the wall is located using an iterative process by varying c until $N=C_m+C_s-T_s$, where N is the axial load, C_m is the internal compression forces coming from masonry, C_s is the total internal compression forces coming from the steel and T_s is the total internal tension forces coming from the steel. The equations used to find C_m, C_s, and T_s are described in Eq. (2), Eq. (3), and Eq. (4), respectively.

$$C_m = \alpha_1 f'_m \beta_1 c b \tag{2}$$

$$C_s = A_s \left(\varepsilon_m \left(\frac{c-d'}{c} \right) \right) E_s \leq A_s f_{yv} \tag{3}$$

$$T_s = A_s \left(\varepsilon_m \left(\frac{d-c}{c} \right) \right) E_s \leq A_s f_{yv} \tag{4}$$

Figure 3.16 shows the slender wall cross-section, the strains' distribution, and the internal forces of masonry and vertical steel. After locating the neutral axis (c), the ultimate flexural capacity (M_u) is determined by summing the moments of the internal forces about the extreme compression fiber of the cross-section as described in Eq. (5). Finally the shear load associated with the ultimate flexural moment (V_f) is determined by dividing the moment (M_u) to the wall height (h).

$$M_u = T_{s1}d_1 + N\frac{L}{2} - C_{s1}d_2 - C_m\frac{a}{2} \quad (5)$$

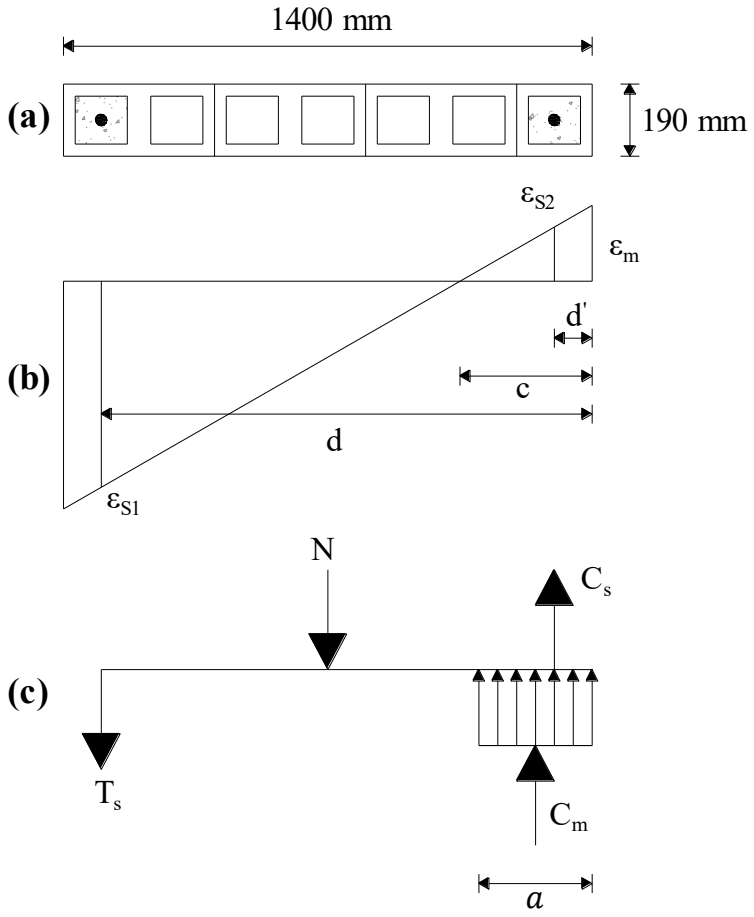

Figure 3.16 General Flexural Analysis; (a) cross-section of the slender wall, (b) strains distribution, and (c) internal forces distribution

Table 3.7 presents the results of flexural strength prediction for the slender walls. A satisfactory prediction is achieved by comparing the resulting flexural capacity with the maximum peak strength resulting in the slender walls. This could explain why the in-plane flexural capacity of PG walls can be predicted with high accuracy in contrast to the in-plane shear strength described in the next sub-section, as observed previously by Shing et al. (1990) and Haach et al. (2010).

Table 3.7 Performance of the flexural strength prediction method

Model	BB slender			BJ slender		
	$V_{exp.}^*$ (kN)	V_f (kN)	$V_{exp.}/V_f$	$V_{exp.}^*$ (kN)	V_f (kN)	$V_{exp.}/V_f$
General Flexural Analysis	166	166	1.00	157	166	0.95

**Maximum experimental peak load recorded*

3.4.2. Shear Strength Prediction

PG masonry shear walls may fail in shear in three distinct modes; diagonal shear, crushing of compressive strut, and sliding shear. However, PG walls may experience mixed shear failure modes besides the flexural failure mode (Dhanasekar, 2011; Haach et al. 2011; Oan, 2013). Aside from diagonal shear and crushing of compressive strut, sliding shear is not common in PG walls where a typical amount of vertical reinforcement and axial load can prevent such failure (Oan 2013; Rizaee 2015). Therefore, the in-plane shear strength prediction, considering the diagonal shear and its upper limit applied to avoid crushing of compressive strut, is investigated. There are several research- and code-based equations used to predict the in-plane shear strength found in the literature. This study considers prediction equations found in North American codes (CSA S304 and TMS 406) and one of the latest research-based equations (Izquierdo 2021). Both code-based equations have many similarities in terms of the masonry, axial stress, and horizontal reinforcement contributions as well as excluding the contribution of vertical reinforcement and mortar strength (Dillon 2015; Izquierdo 2021). In addition, both code-based equations impose an upper limit to prevent the crushing of compressive strut, which relies on the compressive strength of masonry. Table 3.8 describes these equations in terms of design parameter contribution (masonry, axial stress, and horizontal reinforcement) and their upper limit. The nomenclature for the equations listed below is expanded in the LIST OF SYMBOLS AND ABBREVIATIONS.

Table 3.8 In-plane shear strength code-based equations

Equation	In-plane shear strength contribution			
	Masonry (V_m)	**Axial Stress (V_p)**	**Horizontal Reinforcement (V_{sh})**	**Upper Limit, V_r (kN)**
CSA S304-14 (2014)	$0.16\left(2 - \frac{M_f}{V_f d_v}\right)\sqrt{f'_m}\ t\ d_v\gamma_g$	$0.25\mathrm{P}\gamma_g$	$0.6A_{h,bar}f_{yh}\frac{d_v}{s_h}$	$\leq 0.4\sqrt{f'_m}\,td_v\gamma_g$
TMS 402/602-16 (2016)	$0.083\left(4.0 - 1.75\frac{M}{V\mathrm{l}}\right)\sqrt{f'_m}A_{net}\gamma_{g,\mathrm{US}}$	$0.25P\gamma_{g,\mathrm{US}}$	$0.5\left(\frac{A_{h,bar}f_{yh}\mathrm{l}}{A_{nv}s_h}\right)A_{net}\gamma_{g,\mathrm{US}}$	$\leq 0.33\sqrt{f'_m}A_{net}\gamma_{g,US}$

Table 3.9 presents the results of in-plane shear strength prediction for the squat walls. Except for Izquierdo's (2021) equation, TMS without upper limit equation had the best prediction, and TMS with upper limit equation had the worst prediction. It should be noted that TMS w/UL controls the prediction of the squat walls due to the high conservative limit imposed by TMS 406 to avoid the extreme brittle failure of the compressive strut. In contrast, the squat walls were experimentally failed in diagonal shear, which pointed out that even a wall that is predicted to fail with strut failure can fail by diagonal tension shear. In general, when compressive strut failure occurs is still relativity unknown (Bentz et al. 2006).

VC-RS4 model developed by Izquierdo (2021), which is described in Equation (6), surpassed the prediction ability of the code-based equations. VA-RS4 is the more practical equation due to the non-inclusion of mortar strength in contrast to the other models developed by Izquierdo (2021). The models by Izquierdo, interestingly, do not include a term for horizontal reinforcement but include vertical reinforcement. The nomenclature of the below equation is described in the LIST OF SYMBOLS AND ABBREVIATIONS.

$$0.0538\mathrm{L} + 4.83f'_{mg} + 0.245P + 0.067A_{vf} - 0.0553\,s_{v,ave} \quad (6)$$

Regarding the CSA equation, it successfully predicted the dominant failure mode (diagonal shear). However, its strength prediction was conservative. To better understand the contribution of each parameter towards the in-plane shear strength of both code-based equations, Table 3.10 compares the parameters' contributions of both equations.

Table 3.9 Performance of the shear strength prediction method

Equation	BB squat			BJ squat		
	$V_{exp.}$*** (kN)	V_n (kN)	$V_{exp.}/V_n$	V_{exp}***. (kN)	V_n (kN)	$V_{exp.}/V_n$
CSA w/UL*	407	312	1.30	422	327	1.29
CSA wo/UL**	407	312	1.30	422	327	1.29

* *w/UL means with upper limit*
***wo/UL means without upper limit*
*** *Maximum experimental peak load recorded*

Table 3.10 Contribution of equation's parameters

Equation	BB squat				BJ squat			
	Masonry (kN)	Axial Stress (kN)	H.Reinf.* (kN)	UL** (kN)	Masonry. (kN)	Axial Stress (kN)	H.Reinf.* (kN)	UL** (kN)
CSA S304	140	118	54	350	140	118	68	350
TMS 406	153	182	42	271	153	182	54	271

* *Horizontal reinforcement*
***Upper limit*

According to Table 3.10, there is no significant difference (9%) in the masonry contribution between both equations. On the other hand, there is an increasing contribution of the axial load of the TMS 406 equation by 54%, which is reflected in the horizontal reinforcement contribution, where the CSA S304 equation has an increase of 27%. With regards to the upper limit, there is an increase of 29% of the CSA S304 limit over the TMS 406 limit. This is explained why TMS 406 predicts a crushing in the compressive strut. It could be observed that there is a visible discrepancy in the axial load contribution, horizontal reinforcement contribution, and the upper limit between both code-based equations, which highlights the need to reconsider the contribution of the different design parameters or add new design parameters to the revised equations as concluded by Dillon (2015) and Izquierdo (2021).

Overall, the performance of CSA and TMS equations cannot be assessed using only two wall specimens. However, it provides insights and considers a first step as more experimental walls

will be tested. In addition to the experimental dataset, using reliable macro-based or micro-based numerical models could be a vital tool to allow the experimental results to be expanded to a wider variety of design variables, which facilitates understanding the contribution of each design parameter toward the shear strength of PG walls. Consequently, suggested modifications can be proposed to such equations to improve the accuracy and precision of their prediction of the in-plane strength of PG walls.

3.5 Summary and Conclusions

The experimental investigation involved four full-scale PG masonry shear walls that were subjected to a combination of reversal cyclic lateral load and constant vertical load. The design and construction of the tested specimens incorporated practical design details and actual practice construction. The effect of the variable design parameters (aspect ratio and horizontal reinforcement type) on the response of PG walls against cyclic loading was investigated using hysteretic response, damage progression, and shear strength. Additionally, the prediction of the in-plane strength (flexural and shear strength) of the tested walls was obtained and compared to the experimental results. There was no apparent effect of the horizontal reinforcement type on the peak strength, both types are equally effective when provided according to the engineering rules in the standards. However, the aspect ratio had a significant effect. The BB slender wall showed less damage distribution than the BJ slender wall, while the BB squat wall had three times the average crack's width compared to the BJ squat wall due to the distribution of bed-joint reinforcement along the wall height. Bed-joint reinforcement demonstrated to be superior in controlling cracks' width in walls that failed in shear, specifically after reaching the peak load, while the presence of grout in bond beams prevented the cracks from distributing evenly throughout the wall surface, particularly in the middle of the diagonal path of the wall. The general flexural analysis accurately predicted the peak lateral load of the slender walls, indicating that the flexural behaviour of PG walls can be predicted with no complexity in contrast to the shear behaviour. Examination of CSA and TMS equations against the experimental results of squat walls revealed that Izquierdo's (2021) model was better in predicting the shear strength. In addition, a high difference in the contribution of the axial load, horizontal reinforcement, and upper limit was observed when comparing CSA and TMS equations. This inconsistency of CSA and TMS equations points

out the necessity of revising the contribution of each parameter in the current code-based equations and considering updating the current design parameters coefficients and/or adding new design parameters to improve the accuracy and the precisions of the revised equations in the next version of the masonry standard codes.

Overall, it was found that the expected behavior of the tested walls designed in areas with low seismic risk areas following the Canadian standard was flexure for slender walls and shear for squat walls, which was demonstrated experimentally in this study. Regarding the shear-dominated walls (squat walls), experimental results showed that bed-joint reinforcement had better crack width control, energy dissipation and ductility than bond beam reinforcement since the bond beam had 90 degrees anchorage detailing, not 180 degrees where literature showed the superiority of 180 degrees anchorage detailing in terms of ductility, strength degradation, and shear failure mode. Consequently, bed-joint reinforcement demonstrated to be a viable option as a shear reinforcement for PG walls in areas with low seismic hazard risk where economical factor prevailed.

4. ANALYSIS MODELS

Partially Grouted Masonry Shear Walls: Analysis Models using Macro-Modelling Approach

Amr Ba Rahim [a], Clayton Pettit [a], Carlos 'Lobo' Cruz Noguez [a], and Yong Li[a]

[a] *Department of Civil and Environmental Engineering, University of Alberta, 9211-116 Street, Edmonton, Alberta T6G 1H9, Canada*

Abstract (359)

Partially Grouted (PG) masonry shear walls are widely utilized in North America as a lateral force resisting system, due to their economic viability and practicality by grouting only cells containing reinforcing steel, while the remaining cells remain hollow. The in-plane lateral behaviour of PG walls is characterized by a complex interplay and nonlinear relationships between the diverse materials utilized in the assemblage, including masonry block, mortar, grout, and reinforcing steel, as well as the discontinuities created by the voids in the ungrouted cells. To better comprehend and characterize the in-plane response of PG walls, finite element (FE) methods have been employed based on micro- and macro-modeling formulations. Micro-modeling involves the separate definition of each material present in the masonry assemblage, along with the interfaces between them. This approach, though accurate, is both time-consuming and computationally intensive. Hence, more efficient analysis models, such as macro-modeling, which entails treating the masonry assemblage as a region with averaged properties, are preferred. In this paper, a macro-modeling approach is presented, aimed at investigating the in-plane shear behaviour of PG walls using FE software that implements the modified compression field theory, originally developed for reinforced-concrete members. The validity of a FE macro-modeling approach is established through the validation of nine PG walls, experimentally tested from the literature, covering a wide range of design parameters, including compressive strength, aspect ratio, axial stress, and reinforcement ratio. The model was found to satisfactorily simulate the response of the experimental walls up to the peak strength. The validation process also highlighted the importance of reporting joint shear strength in the literature, which was found to have a significant impact on the model results. The study also revealed that by increasing the vertical reinforcement and axial stress, it is possible to change the failure mode from flexural or mixed shear-flexure to diagonal shear failure. Additionally, the accuracy of wall models generated using the developed model was examined, revealing that the general flexural analysis method was able to predict the flexural

strength accurately. However, the CSA S304 equation was found to be overly conservative at higher compressive strength levels and inconsistent in its estimation of the contribution of horizontal reinforcement.

4.1 Introduction

The development of safe and economical in-plane design methods for PG walls is important, since they are cost-effective and practical to build in non-seismic zones. The finite element method (FEM) is a robust numerical tool to simulate the response of PG walls in recent decades through two modelling approaches: macro-modelling, preferred for studying the global response of whole buildings or large structural systems, and micro-modelling, suited for studying the local response of smaller structural systems or components.

Macro-modeling represents masonry as a homogeneous composite material, where the constitutive relationships for units, mortar, and unit-mortar interface are averaged in a homogeneous continuum (Lourenço 2002). Its application allows estimating the global structural response in terms of maximum resistance, displacement ductility and force-displacement relationship.

Seif ElDin (2016), Hung (2018), and Bolaños (2020) employed the macro-modeling approach to develop 2D analysis models for PG walls subjected to cyclic loads using the VecTor2 software. Hung (2018) found that the "Joint Shear Strength Ratio," which is the ratio between the shear strength of the joints and the maximum compressive strength of the masonry, was found to have the most notable impact on the predicted response after conducting various parametric studies. Bolaños (2020) revealed that the numerical model was able to accurately capture the elastic stiffness for all the simulated walls. As a result, Seif ElDin (2016), Hung (2018), and Bolaños (2020) showed that the macro-modeling was a viable approach for understanding the behaviour of PG walls.

Micro-modelling consists of discretizing the masonry in a detailed or simplified way, explicitly modelling all (or the majority) of the constituent materials and interfaces in masonry units, mortar joints, grout, and the discontinuities between units and mortar joints (Lourenço et al. 1995). The behaviour of each discretized component is represented by a different constitutive law. The use of micro-modelling makes it possible to capture local failure mechanisms and obtain the response of an individual component or a part of it in terms of the local stresses and strains.

Haach et al. (2011), Arnau et al. (2015), and Calderón et al. (2017) used a micro-modelling approach to simulate the response of PG walls against cyclic loading using the DIANA FEA software. While Haach et al. (2011) used a simplified micro-modelling approach, Arnau et al. (2015) and Calderón et al. (2017) used a detailed micro-modelling approach. They all reported that the results of their developed models had a satisfactory correlation with the experimental results in terms of strength and displacement. The models also were shown to be able to predict the cracking patterns observed experimentally.

To sum up, the use of the finite-element method in the development of numerical models has been successful in capturing important structural response aspects of masonry elements. Micro-modelling offers a detailed understanding of local response mechanisms, such as cracking at mortar joints and through blocks, but it is a computationally intensive and time-consuming approach. On the other hand, macro-modelling provides a faster and more cost-effective way of capturing the global response of wall structures, making it ideal for conducting extensive parametric analyses needed to develop design equations.

The literature review shows that macro-modelling has the potential to accurately capture the peak strength and to conduct parametric studies (Seif ElDin 2016; Medeiros et al. 2020). However, the simulation ability of macro-models is limited by certain factors, such as the joint shear strength ratio (JSSR). According to Hung (2018), the JSSR, which represents the ratio of shear strength at joints (c) to compressive strength of masonry (f'_m), significantly impacts the peak load and corresponding displacement of PG walls as shown in Figure 4.1.

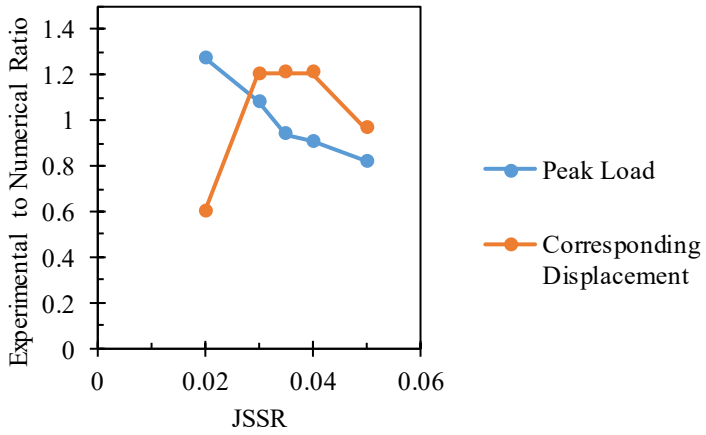

Figure 4.1 Sensitivity curve of varying JSSR adapted from Hung (2018)

As the JSSR is a crucial aspect in defining any macro-model, one option is to use equations such as TMS 402 [Eq. (1)] to calculate it.

$$V_{nm} = \left[4.0 - 1.75\left(\frac{M_u}{V_u d_v}\right)\right] A_{nv}\sqrt{f'_m} \quad (1)$$

where V_{nm} is the shear strength of mortar joint, $\frac{M_u}{V_u}$ is the ratio of ultimate moment demand to ultimate shear demand, d_v is effective depth for shear calculations need not taken as less than $0.8l_w$ for walls, A_{nv} is net shear area, and f'_m is the compressive strength of ungrouted masonry. This option was adopted by Medeiros et al. (2020). An alternative approach is to estimate the value of JSSR through a best-fit comparison of the numerical and experimental results. This approach was adopted by Elmeligy et al. (2021) in light of the insufficient experimental data available. In this paper, experimental studies that reported the Joint Shear Strength Ratio (JSSR) were selected for validating the developed FE model to increase the reliability of the validation process. Furthermore, the triplet test used to determine the JSSR is presented, as well as its significance, by calibrating the JSSR of one wall from a study that did not report this ratio.

This paper presents the development and validation of a finite element (FE) macro model for masonry walls. The developed model's ability is evaluated against various experimental results. After validating the developed model, numerical investigation is conducted to study the influence of vertical reinforcement and axial load on changing the failure mode. Finally, the accuracy of the general flexural analysis method for walls that failed in flexure and the shear strength equation of CSA S304 for walls that failed in diagonal shear are assessed using numerical walls generated from the developed model.

4.2 Analysis Models

The nonlinear finite element analysis program VecTor2 (VecTor Analysis Group 2019) was used to develop analysis models for partially grouted masonry walls. VecTor2 implements the modified compression field theory (MCFT) formulation proposed by Vecchio and Collins (1986) for reinforced concrete and the disturbed stress field model (DSFM) proposed by Facconi (2012) for masonry. VecTor2 allows for the simulation of the monotonic response of masonry materials (Facconi 2012; Facconi et al. 2013). Masonry is a material made of

masonry units and mortar joints. Similarly to the method used to analyze cracked concrete, the smeared crack approach, when analyzing large masonry structures, the masonry can be represented as a continuum material with average properties, where joint failures spread across a single finite element (Wong et al. 2013).

This section describes the materials models used to develop the FE model as well as the model definition in terms of boundary conditions, loading applications, and elements. Finally, the importance of JSSR is discussed, and an experimental setup to determine the JSSR (joint shear strength ratio) through triplet test is presented.

4.2.1. Materials Models

The mechanical behaviour of the materials in the numerical model was represented using material models for masonry and reinforcing steel available in the VecTor2 program. The input data for these models was obtained from materials characterization tests, which provided the mechanical properties of the materials. The material models chosen for the analysis models were the result of extensive fit tests, ensuring a reasonable match between numerical and experimental results. The material models used to simulate the behaviour of masonry and steel reinforcement are summarized in Table 4.1. A complete description of the selected material models is found in Wong et al. (2013) and more in-depth for masonry materials in Facconi et al. (2013).

Table 4.1 Materials Models for numerical simulation

Material	Behaviour	Model
Masonry	Compressive strength (pre-maximum resistance)	Hoshikuma et al.,1997
	Compressive strength (maximum post-resistance)	Masonry (Facconi)
	Compression softening	Masonry (Laurenco)
	Tensile stiffening	Modified Bentz, 2003
	Tensile softening	Nonlinear (Hordijk)
	Crack slip calculation	Masonry I
Reinforcement	Stress-Strain response	Ductile (trilinear relationship)
	Dowel action	Tassios (Crack Slip)
	Buckling	Akkaya 2012 (Modified Dhakal-Maekawa)

4.2.1.1. Materials models for masonry

Pauley and Priestley (1992) found that the compressive behaviour of masonry can be effectively represented by concrete models. The Hoshikuma et al. (1997) model and Masonry model proposed by Facconi (2013) were utilized to define the compressive behaviour of masonry. The first model captures the ascending branch of the constitutive relationship up to the masonry compressive strength (f'_m). The second model depicts the descending branch in a bilinear manner (as seen in Figure 4.12). Wong et al. (2013) recommended the Hoshikuma et al. (1997) model for masonry as it allows independent definition of the compressive strength (f'_m), peak strain (ε_o), and initial elastic modules (E_c). It's important to note that Masonry model was adapted for masonry materials based on Priestley and Elder's (1983) modified Kent-Park model. To account for compression softening (the reduction of compressive strength (f'_m) and peak strain (ε_o) due to transverse cracking), softening in compression was modeled using Laurenco and Rots' (1997) Masonry model.

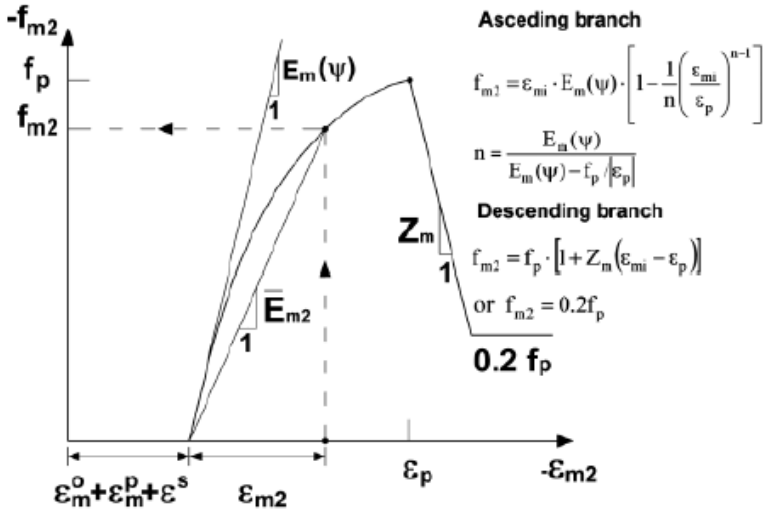

Figure 4.2 Compression model for masonry adapted from Facconi et al. (2013)

To describe the tensile behaviour of masonry, two material models were considered. The initial behaviour, up to the tensile strength (f_t) level, was represented by an elastic linear model, while Hordijk's (1992) model was utilized to represent the behaviour after reaching its maximum strength. This latter model was validated by Wong et al. (2013) for use in masonry. Figure 4.3 illustrates the constitutive relationship adopted for this model. Additionally, tension

stiffening was taken into account by using the default model of Modified Bentz et al. (2006), as recommended by Wong et al. (2013).

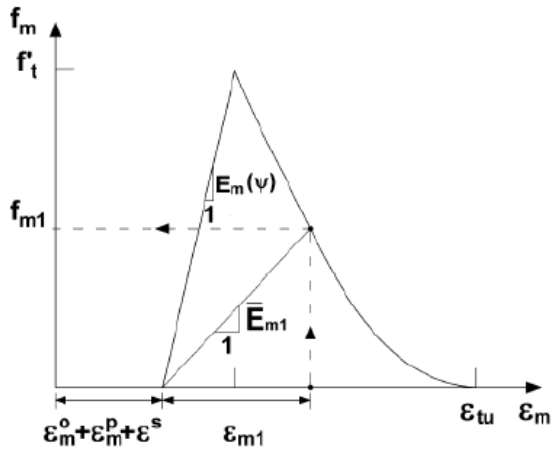

Figure 4.3 Tension model for masonry adapted from Facconi et al. (2013)

In order to consider the effect of shear slippage of mortar joints on the overall response of masonry, the VecTor2 program implemented a model called Masonry I. This model employs a constitutive elastoplastic relationship between the local shear at joints V_j and shear strain γ^s_j, where δ_j^s represents the shear slip and t_j denotes the thickness of the joint (as depicted in Figure 4.4). The linear-elastic branch of the model has a slope corresponding to the masonry shear stiffness G_{mj}. This model is based on the Mohr-Coulomb yield criterion.

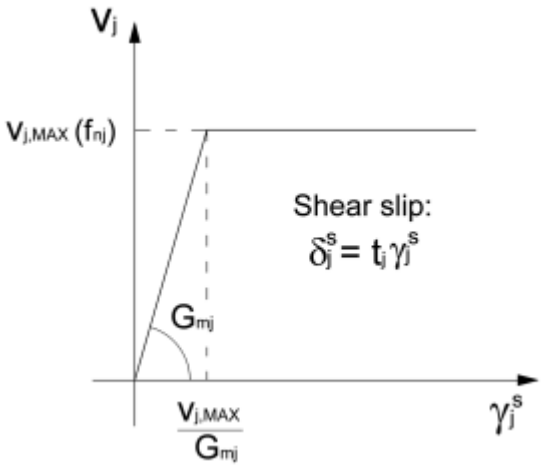

Figure 4.4 Shear stress-strain response for masonry joints adapted from Facconi et al. (2013)

4.2.1.2. Materials models for reinforcement

The stress-strain relationship of the vertical and horizontal reinforcement was represented using the Elastic-Hardening (Trilinear) model. This model depicts the initial linear-elastic response, followed by a yield plateau, and then a linear strain-hardening phase until failure. This model accurately captures the behaviour of steel reinforcement under monotonic loading, as demonstrated in Figure 4.5. As shown in Figure 4.5, yield strength (F_y), ultimate strength (F_u), elastic modulus (E_s), strain hardening strain (ε_{sh}), and ultimate strain (ε_u) can be calibrated through tension tests conducted on the vertical and horizontal reinforcement specimens.

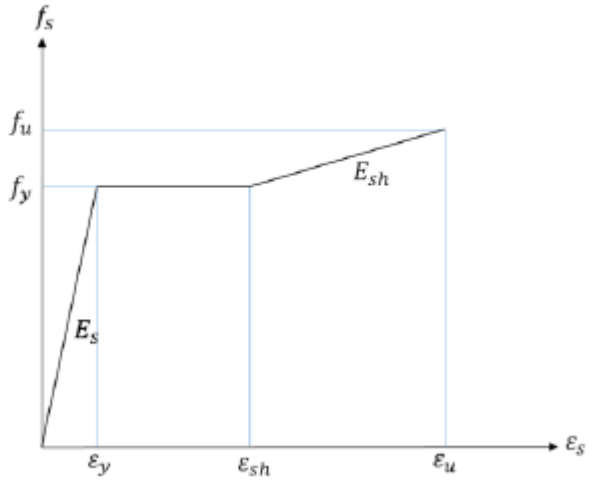

Figure 4.5 Trilinear stress-strain response for steel reinforcement

The shear resistance provided by steel reinforcement that crosses cracks, known as dowel action, was estimated using the Tassios model. This model assumes that the reinforcement behaves like a beam and the surrounding masonry functions as an elastic foundation. The relationship between the shear force per dowel action (V_{du}) and the shear slip along the crack (δ_s) is defined by a linear elastic, perfectly plastic behaviour, as depicted in Figure 4.6. It's worth mentioning that this model is the default model in VecTor2. The buckling of the reinforcement was considered using the modified Dhakal-Maekawa model proposed by

Akkaya et al. (2013), which was recommended by VecTor2. This model performed better than the original model, as reported by Akkaya et al. (2013). Finally, it is assumed that the reinforcement is perfectly bonded throughout its entire length.

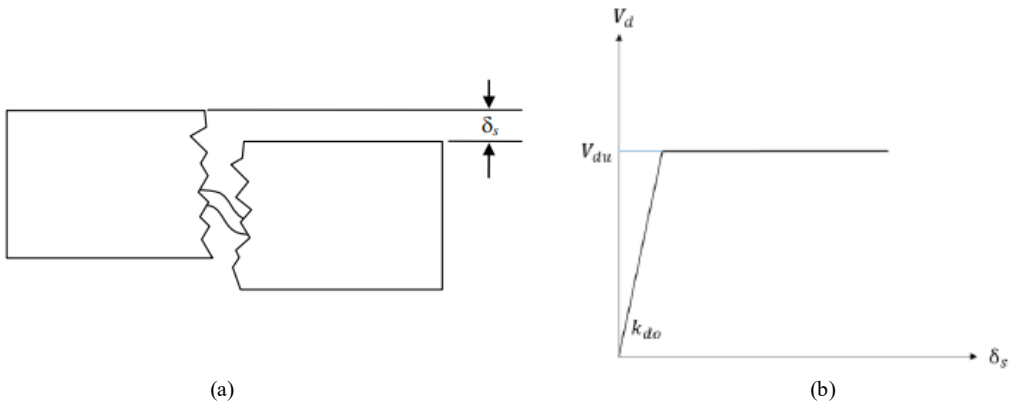

Figure 4.6 (a) Dowel action mechanism (Wong et al. 2013), (b) shear force vs shear slip relationship

4.2.2. Model Definition and Discretization

The developed model comprised of four-node plane stress elements, rectangular in shape, to represent both the ungrouted and grouted masonry, and two-node truss-bar discrete elements to simulate the horizontal and vertical reinforcement. The dimensions of the rectangular elements were set at 100x100mm, which enabled modeling the steel reinforcement in a discrete manner due to the spacing of concrete block cells and joints. The use of square elements and a rationally refined mesh has been shown to improve the accuracy of the model (Medeiros et al. 2020). The only difference between the ungrouted and grouted elements was the thickness, with the grouted elements having a thickness equal to the full width of the wall and the ungrouted elements having a thickness equal to the unit block's face shell thicknesses.

The boundary conditions of the developed model were defined by restricting the nodes either at the bottom or both the bottom and top of the wall model. In the case of single curvature (cantilevered) conditions, the bottom nodes were restricted in the x and y directions with pinned supports. Meanwhile, double curvature boundary conditions were simulated by restricting nodes with the same pinned supports at both the bottom and top of the wall model. The loading beams used in the literature were made of reinforced concrete, reinforced

masonry, or steel. In the developed model, the loading beams were heavily reinforced in both directions to maintain an elastic behaviour during loading.

With respect to loading conditions, the application of sequential loads can either be force-based or displacement-based, as described by Tomaževič et al. (1996). VecTor2 offers the option to specify force-based loading through the application of nodal loads, or displacement-based loading through support displacements. The vertical loads were applied to each node at the top of the loading beam, accurately simulating the distributed experimental vertical loads on the wall. To ensure a balanced distribution of lateral loads to the wall, the lateral loads were applied to the central node of the loading beam.

Figure 4.7 presents a demonstration of the modeling of two walls, one reinforced horizontally using bond beams and the other using bed-joint reinforcement. These walls are based on the experimental study presented in Chapter 3. As shown in Figure 4.7, three rectangular elements were utilized, one for ungrouted masonry without reinforcement, one for grouted masonry with reinforcement laid inside it and grout filling the cores, and the last for reinforced concrete serving as a loading beam. Meanwhile, three truss-bar elements were employed for the representation of vertical reinforcement, bond beams, and bed-joint reinforcement. Finally, the wall is subjected to both vertical and lateral loads, as indicated in Figure 4.7.

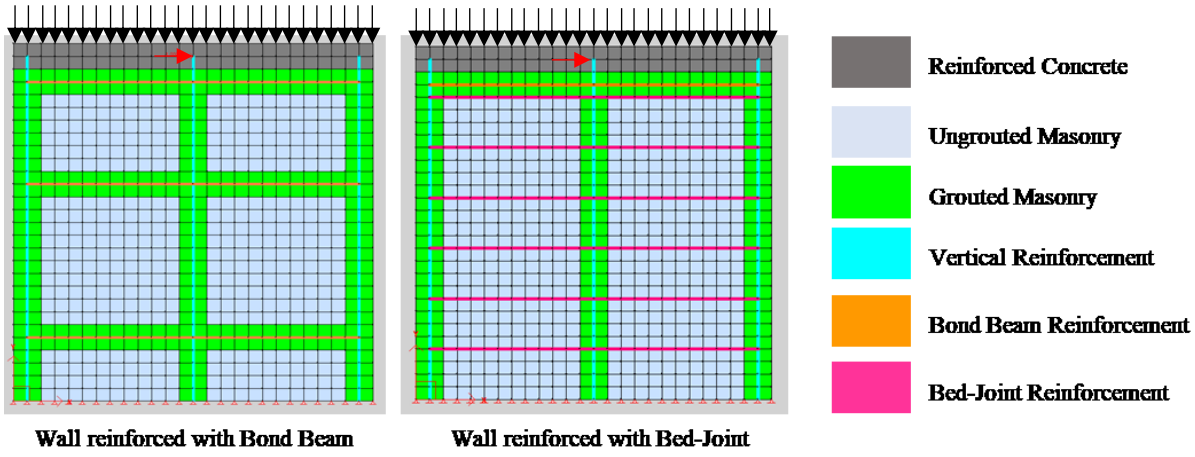

Figure 4.7 Developed Model of squat wall presented in Chapter 3

4.2.3. Definition of Joint Shear Strength Ratio (JSSR)

The accuracy of macro-models using VecTor2, as found by Hung (2018), is highly influenced by the joint shear strength ratio (JSSR), which is the ratio between the shear strength of

masonry joints (c) and the compressive strength of masonry (f'_m). The JSSR describes the shear behaviour through mortar-block interface along with vertical loads. In other words the relationship between mortar shear strength and masonry compressive strength as shown in Figure 4.8. To establish an experimental value for JSSR, shear tests on triplets were conducted following the EN1052-3 (2002) standard, using North American masonry typology (concrete hollow blocks with mortared joints). A total of five normal pre-compression levels were applied, with values of 0 MPa, 1.0 MPa, 1.5 MPa, 2.0 MPa, and 2.5 MPa.

A total of 15 triplets were fabricated, with three triplets corresponding to each pre-compression level. The triplets were constructed by stacking three ungrouted units with 10mm mortar joints. Each block unit measured 390x190x190mm in dimension. The experimental setup is shown in Figure 4.9(a). This test configuration has been adopted by several researchers to study the shear bond properties of mortar joints, as noted in the works of Haach (2009), Sandoval and Arnau (2016), and Bolaños (2020).

To apply the horizontal and vertical loads, two separate actuator systems were utilized. Four horizontal jacks were employed to maintain the average pre-compression level at a constant value, while a vertical jack was utilized to impose shear displacements until the failure of the mortar joints occurred. The specifics of the loading and instrumentation are depicted in Figure 4.9(b).

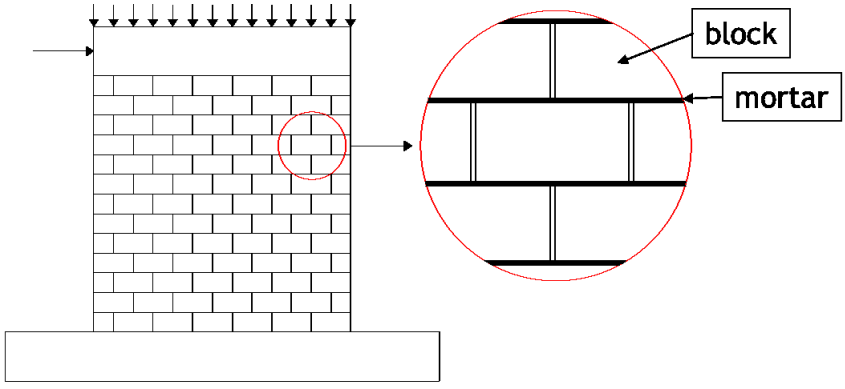

Figure 4.8 Relationship through the interface between mortar and masonry block

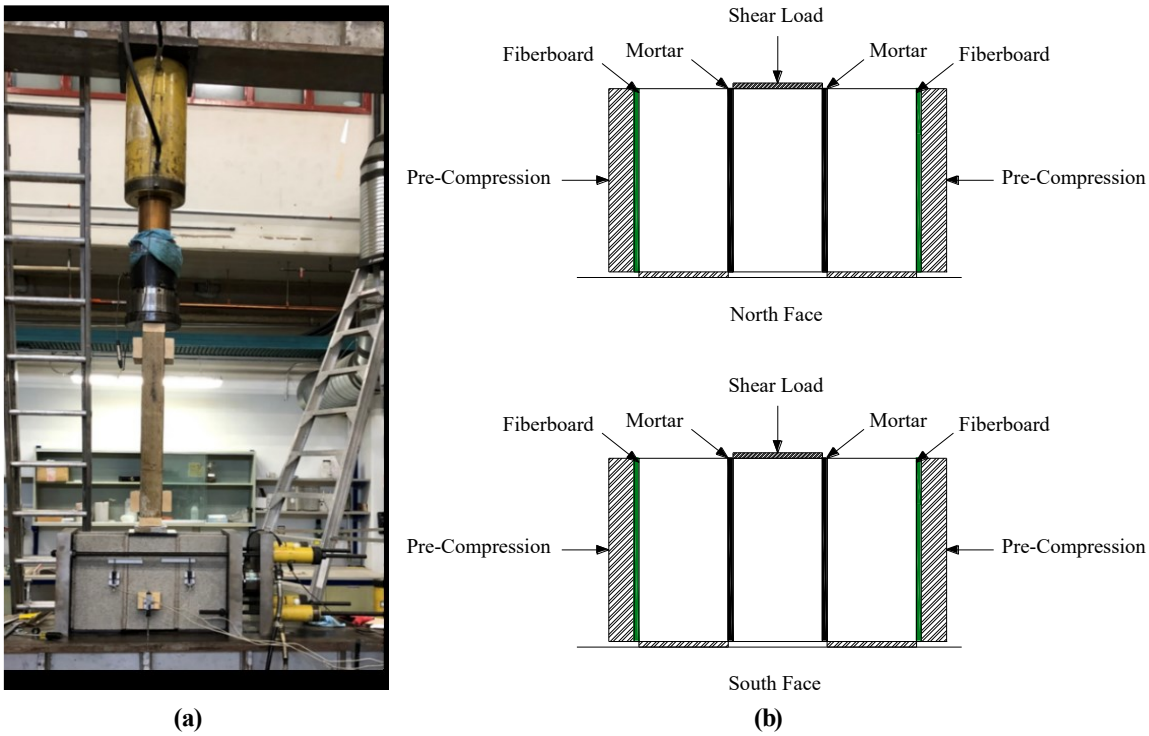

Figure 4.9 Triplet Test: (a) test setup and (b) Loadings and Instrumentation layout

The relationships between shear bond stress and global shear displacement were obtained for various levels of normal pre-compression (as shown in Figure 4.10a). In tests where pre-compression was applied, the results showed three distinct stages of behaviour: an elastic-linear regime, a period of softening beyond the maximum strength, and a plateau strength until the end of the test. In the case where no pre-compression was applied, the initial stiffness was lower compared to the other tests. The maximum average shear bond strength values (τ) obtained were 0.13 MPa, 1.20 MPa, 1.63 MPa, 2.02 MPa, and 2.68 MPa for normal pre-compression levels of 0.0 MPa, 1.0 MPa, 1.5 MPa, 2.0 MPa, and 2.5 MPa, respectively.

Using the Mohr-Coulomb frictional law ($\tau = c + \tan(\theta).\sigma$), the failure behaviour of the mortar joints was described through a linear regression relationship between maximum shear bond stresses (τ) and normal pre-compression stresses (σ) as shown in Figure 4.10b. From this relationship, the initial cohesion parameter (c) and initial internal friction angle (θ) were found to be c = 0.148 MPa and $\theta = 44.7^{\circ}$($\tan\theta = 0.989$), respectively. A linear regression produced a coefficient of determination $R^2 = 0.98$.

The specimens showed distinct damage patterns in terms of failure mode depending on the level of pre-compression used (Figure 4.12). These damage patterns were compared with the typical failure types in EN1052-3 (2002) (Figure 4.11). Shear failure was observed either in the unit/mortar bond area, on one or divided between two unit faces, or shear failure just in the mortar, as seen in Figure 4.12. It was found that the resulting failure types were approximately identical with those recommended in the standard code.

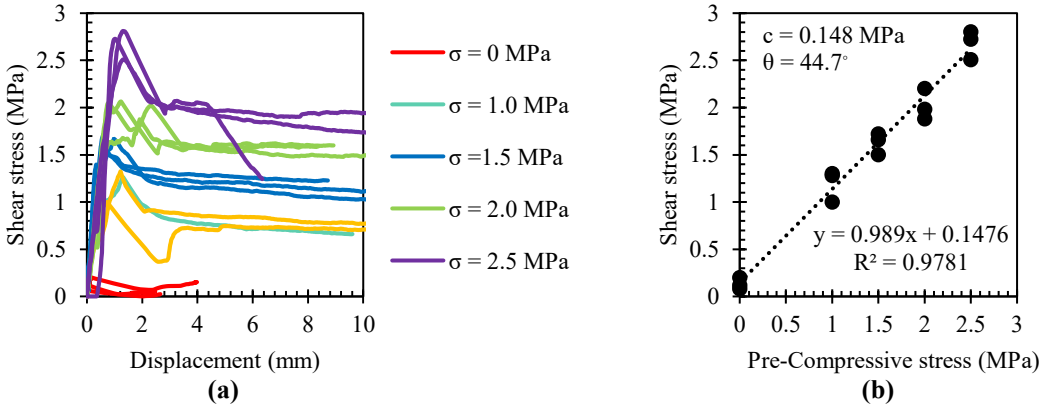

Figure 4.10 (a) Shear bond stress vs shear displacement diagram for different levels of pre-compression, (b) Relationship between maximum shear bond stress vs. pre-compressive stress

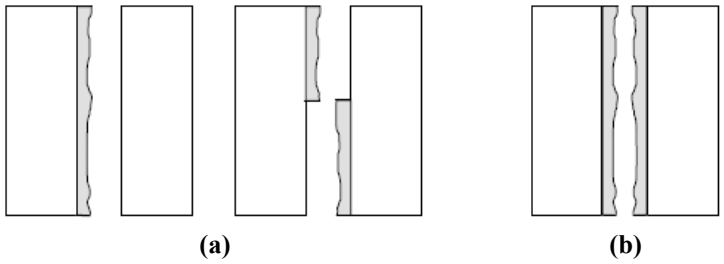

Figure 4.11 (a) Shear failure in the unit/mortar bond area either on one or divided between two units and (b) Shear failure only in the mortar (EN1052-3 2002)

Figure 4.12 Failure modes observed in triplet tests

4.3 Validation

This section describes the experimental walls selected for validation, and then the developed model's performance is assessed. Finally, the influence of JSSR (joint shear strength ratio) on simulating the global response of PG walls in terms of peak strength, corresponding displacement, and initial stiffness was described.

4.3.1. Description of Validated Walls

Numerous studies on the experimental behaviour of shear-critical reinforced masonry walls suffer from a lack of complete description of the material properties, leading to a greater dependence on assumptions and rough estimates when modelling such walls (Al-Ahdal et al. 2022). In order to validate the developed model, nine PG walls were selected from the literature, representing four studies that provided sufficient material properties. The selected walls are noteworthy for covering a wide range of design parameters and incorporating both horizontal reinforcement types (bond beam and bed-joint), which enhances the credibility of the finite element (FE) model. The material properties of these walls are summarized in Table 4.2. For additional information on the selected walls, please refer to the following studies (Haach et al. 2010, Ramírez et al. 2016, Calderón et al. 2021a, Chapter 3).

The geometry of the walls was varied, with height-to-length ratios (H/L) ranging from 1.86 to 0.44, resulting in five different aspect ratios, as seen in Table 4.2. These aspect ratios represent the variation found in the aspect ratios of 205 experimental walls documented by Izquierdo (2021). All the walls were built with full-scale blocks, except for the N150-B1 wall (Haach et al. 2010), which used half-scale blocks. Additionally, all the walls had a running bond masonry pattern. The individual properties of the block units, mortar, and grout were ignored, as the developed model adopts a macro-model approach, considering only the properties of the masonry assemblage (masonry prism).

When it comes to masonry assemblage properties, most literature sources do not provide the tensile strength (f_t). To address this, the default value of ($f_t = 0.33\sqrt{f'_m}$) suggested by Wong et al. (2013), has been adopted, where f'_m is the masonry compressive strength. Similarly, unless otherwise reported, the initial elastic modules ($E_c = 3320\sqrt{f'_m} + 6900$) and strain at the peak stress ($\varepsilon_o = 1.8 + 0.0075 f'_m$) have been calculated. It's important to properly define the

total slip strain and average crack spacing, as they are dependent on head and bed joint spacing (Sadeghian and Vecchio 2018), and should be reported as specified in the literature. Table 4.3 lists the properties of ungrouted and grouted masonry for the masonry assemblage. Notably, all the studies considered for validation in this work reported the experimental value of the joint shear strength ratio (JSSR).

Three out of the nine walls were reinforced horizontally with a bond beam, while the others were reinforced horizontally with bed-joint reinforcement, as illustrated in Table 4.2. Bond beam reinforcement consists of horizontal steel bars placed at the centre of a masonry course, which is then filled with grout. Bed-joint reinforcement consists of a ladder- or truss-type steel reinforcement that is embedded in the horizontal mortar joints. It is worth noting that the horizontal reinforcement ratios for all validated walls represent the full range of the 205 experimental walls in the database, as reported by Izquierdo (2021).

Similar to the horizontal reinforcement, all validated walls in this study feature vertical reinforcement ratios that are within the range reported in Izquierdo's (2021) database of 205 experimental walls. Steel rebar were used as the vertical reinforcement in all of the walls, with the exception of the N150-B1 wall (Haach et al. 2010) which utilized prefabricated trussed reinforcement. To ensure proper bonding between the masonry and reinforcement, all the hollow cells housing the vertical reinforcement were filled with grout.

In terms of the material properties for both horizontal and vertical reinforcement, the yield strength (F_y), ultimate strength (F_u), elastic modulus (E_s), strain hardening strain (ε_{sh}), and ultimate strain (ε_u) were obtained from the studies. Where information was lacking, the default values suggested by Wong et al. (2013) (F_u=1.5F_y, E_s=200000 MPa, ε_{sh}=0.005, and ε_u=0.15) from the VecTor2 model were utilized. The properties of both the horizontal and vertical reinforcement are summarized in Table 4.4.

All of the validated walls were designed with a cantilever-like boundary condition. Reinforced concrete beams were added at the top and bottom of the tested walls, serving as loading beams and base supports, respectively. The loading beams ensured proper anchorage of the vertical reinforcement and distributed the applied vertical and lateral loads evenly.

All validated walls were subjected to a combination of constant vertical loads and cyclic lateral loads in their loading protocol. The aim of the loading setups, while not identical for each wall, was to ensure an even distribution of the applied loads from the loading beam to the wall panel. It's noteworthy that the variation of the applied axial loads, as shown in Table 4.2, falls within the range of the database reported by Izquierdo (2021). The lateral loads were applied in a reversed cyclic manner for all validated walls. The forced-controlled protocol was adopted for applying the vertical loads, while the displacement-controlled protocol was adopted for applying the lateral loads. The testing sequence was almost identical for all validated walls, with the vertical loads being applied first until reaching the target value, then kept constant during the test. The lateral loads were then applied in a reversed mode until the tested wall failed.

The failure modes of the validated walls were primarily diagonal shear failure, with exceptions being the BJ slender wall (Chapter 3) and N150-B1 wall (Haach et al. 2010) , which experienced mixed shear-flexure failure, and the BB slender wall (Chapter 3), which experienced flexure failure. The diagonal shear failure was indicated by diagonal cracking in both directions, yielding of the horizontal reinforcement, and no yielding of the vertical reinforcement. In the case of mixed shear-flexure failure, the walls first showed diagonal cracking, which was then followed by yielding or crushing at the bottom corner of the wall when lateral loads increased. The flexure failure was indicated by yielding of the vertical reinforcement without diagonal cracking.

Table 4.2 Details of the validated experimental walls

Wall ID	Aspect Ratio	Height	Length	Reinforcement Ratio		Gross Axial Stress	Masonry Comp. Strength	**JSSR[3]**	**FM[4]**
				Vertical	Horizontal				
	Unitless	mm	mm	(%)	(%)	MPa	MPa		
BB slender (Chapter 3)[1]	1.86	2600	1400	0.09	0.09	1.9	20.5	0.0074	**F**
BJ slender (Chapter 3)[2]	1.86	2600	1400	0.09	0.05	1.9	20.5	0.0074	**M**
BB squat (Chapter 3)[1]	1.00	2600	2600	0.09	0.04	1.9	20.5	0.0074	**S**
BJ squat (Chapter 3)[2]	1.00	2600	2600	0.09	0.05	1.9	20.5	0.0074	**S**
BBRW (Calderón et al. 2021a)[1]	0.86	2270	2640	0.41	0.085	0.5	9.67	0.05	**S**
BJRW (Calderón et al. 2021a)[2]	0.86	2270	2640	0.41	0.087	0.5	9.67	0.05	**S**
N150-B1 (Haach et al. 2010)[2]	0.67	800	1206	0.098	0.094	1.3	5.95	0.071	**M**
Wall M5 (Ramírez et al. 2016)[2]	0.44	1400	2590	0.18	0.04	0.56	5.54	0.05	**S**
Wall M6 (Ramírez et al. 2016)[2]	0.44	1400	2590	0.18	0.08	0.56	5.54	0.05	**S**

1 Horizontally reinforced with bond beam
2 Horizontally reinforced with bed-joint
3 JSSR=**J**oint **S**hear **S**trength **R**atio
4 FM=Failure Mode, **F**=Flexure, **M**=Mixed Shear-Flexure, and **S**=Diagonal Shear

Table 4.3 Ungrouted vs Grouted masonry materials properties for the experimental walls

Wall ID	Ungrouted masonry				Grouted masonry			
	f'm (MPa)	ft (MPa)	Ec (MPa)	ε_o (me)	f'm (MPa)	ft (MPa)	Ec (MPa)	ε_o (me)
BB slender (Chapter 3)[1]	22	1.55[3]	6619	3.05	16.4	1.34[3]	20067	3.2
BJ slender (Chapter 3)[2]	22	1.55[3]	6619	3.05	16.4	1.34[3]	20067	3.2
BB squat (Chapter 3)[1]	22	1.55[3]	6619	3.05	16.4	1.34[3]	20067	3.2
BJ squat (Chapter 3)[2]	22	1.55[3]	6619	3.05	16.4	1.34[3]	20067	3.2
BBRW (Calderón et al. 2021a)[1]	23	1.58[3]	14671	1.97[3]	23	1.58[3]	14671	1.97[3]
BJRW (Calderón et al. 2021a)[2]	23	1.58[3]	14671	1.97[3]	23	1.58[3]	14671	1.97[3]
N150-B1 (Haach et al. 2010)[2]	18.6	1.42[3]	10500	1.94[3]	-	-	-	-
Wall M5 (Ramírez et al. 2016)[2]	14.3	0.85	10115	1.28	31.7	2.87	25464	2.04
Wall M6 (Ramírez et al. 2016)[2]	14.3	0.85	10115	1.28	31.7	2.87	25464	2.04

1 Horizontally reinforced with bond beam
2 Horizontally reinforced with bed-joint
3 VecTor2 default value

Table 4.4 Horizontal and vertical reinforcement properties for the experimental walls

Wall ID	Horizontal reinforcement					Vertical reinforcement				
	F_y (MPa)	F_u (MPa)	E_s (MPa)	ε_{sh} (me)	ε_u (me)	F_y (MPa)	F_u (MPa)	E_s (MPa)	ε_{sh} (me)	ε_u (me)
BB slender (Chapter 3)[1]	521	643	208989	4.4	148	455	679	188960	4.2	159
BJ slender (Chapter 3)[2]	617	642	339408	4.8	19.5	455	679	188960	4.2	159
BB squat (Chapter 3)[1]	521	643	208989	4.4	148	455	679	188960	4.2	159
BJ squat (Chapter 3)[2]	617	642	339408	4.8	19.5	455	679	188960	4.2	159
BBRW (Calderón et al. 2021a)[1]	395	506	207600	1.9	265	521	769	196100	2.7	154
BJRW (Calderón et al. 2021a)[2]	645	667	206000	3.1	31	521	769	196100	2.7	154
N150-B1 (Haach et al. 2010)[2]	580	700	196000	3	20	580	700	196000	3	20
Wall M5 (Ramírez et al. 2016)[2]	531	664	183048	2.9	11.2	427	630	208174	4.5	12.6
Wall M6 (Ramírez et al. 2016)[2]	531	664	183048	2.9	11.2	427	630	208174	4.5	12.6

1 Horizontally reinforced with bond beam
2 Horizontally reinforced with bed-joint
3 VecTor2 default value

4.3.2. Validation Results

The accuracy of the developed model was evaluated by comparing the monotonic load-displacement responses obtained from the simulations with the experimental results (as shown in Figure 4.13). Vector2 does not currently have a hysteretic model for masonry materials, so a full cyclic analysis could not be performed. However, previous studies (Calderón et al. 2017; Bolaños 2020; Calderón et al. 2021b) have demonstrated that the calculated monotonic responses provide a good approximation of the cyclic response of shear-critical specimens in terms of peak load, corresponding displacement, and initial stiffness.

To determine the validity of the analysis model developed in this study, parameters such as initial stiffness, maximum resistance, and its associated displacement were also quantified and

compared to their counterpart experimental results, as illustrated in Table 4.5. Here the initial stiffness was calculated based on the guidelines proposed by Park (1988) as implemented by Tolou-kian and Cruz-Noguez (2022). According to Park (1988), the initial stiffness is calculated based on the equivalent yield model. If F_u is the peak strength, then the initial stiffness is defined as the slope of the ascending part of the idealized backbone curve when it crosses the measured backbone curve at strength of 0.75 F_u.

Table 4.5 Results of FE model validation

Wall ID	Peak load			Displacement[1]			Initial stiffness		
	Exp.	Num.	Exp. / Num.	Exp.	Num.	Exp. / Num.	Exp.	Num.	Exp. / Num.
	kN	kN	Unitless	mm	mm	Unitless	kN/mm	kN/mm	Unitless
BB slender (Chapter 3)[1]	166	160	1.04	15.9	14.8	1.07	39.6	40	0.99
BJ slender (Chapter 3)[2]	157	152	1.03	14.1	17.7	0.80	30.7	30.4	1.00
BB squat (Chapter 3)[1]	407	397	1.03	14.9	10.9	1.37	51.8	66.2	0.78
BJ squat (Chapter 3)[2]	422	376	1.12	12	12.2	0.98	84.4	76	1.11
BBRW (Calderón et al. 2021a)[1]	388	412	0.94	10.1	13.7	0.74	49.3	58.8	0.84
BJRW (Calderón et al. 2021a)[2]	388	397	0.98	13.3	13.3	1.00	52.8	50.4	1.05
N150-B1 (Haach et al. 2010)[2]	93	95	0.98	4.2	3.9	1.08	54.7	55.9	0.98
Wall M5 (Ramírez et al. 2016)[2]	316	330	0.96	3.1	2.19	1.42	210.7	240	0.88
Wall M6 (Ramírez et al. 2016)[2]	330	367	0.90	2.7	3.1	0.87	275	305.8	0.90
Average			1.00			1.04			0.95
Maximum			1.12			1.42			1.11
Minimum			0.90			0.74			0.78
Range			0.22			0.68			0.33
Stdv.			0.065			0.234			0.105

1 Displacement at peak load
2 Horizontally reinforced with bond beam
3 Horizontally reinforced with bed-joint

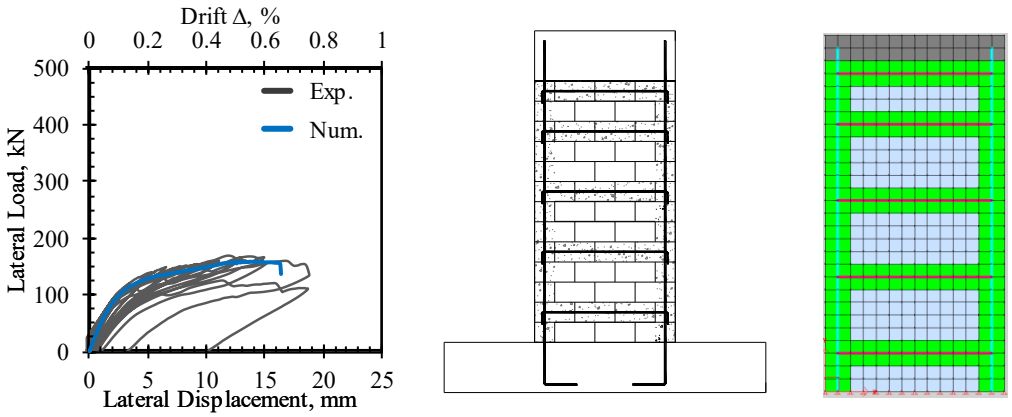

(a) BB slender (Chapter 3)

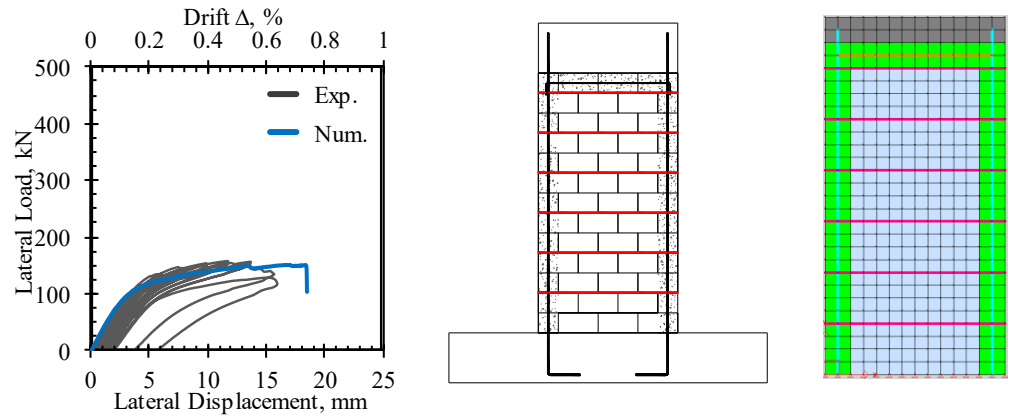

(b) BJ slender (Chapter 3)

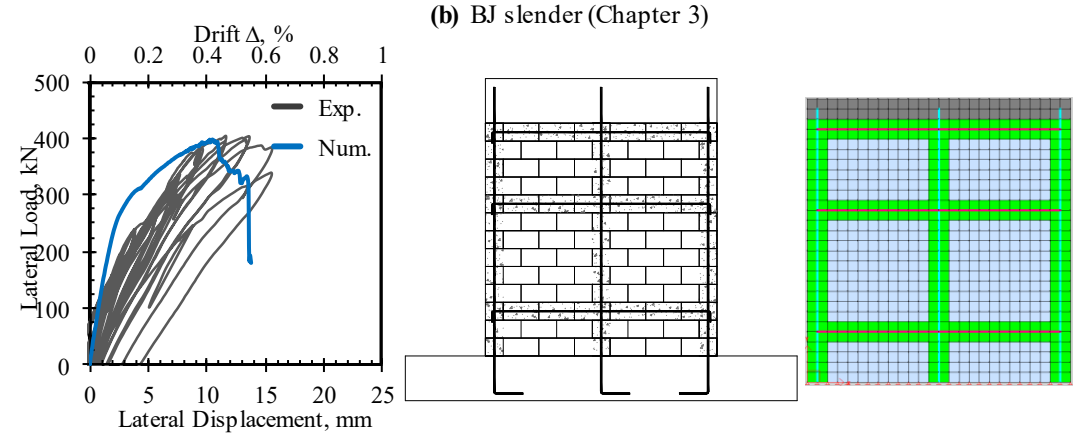

(c) BB squat (Chapter 3)

Figure 4.13 Comparison of force-displacement response between the numerical model and experimental walls

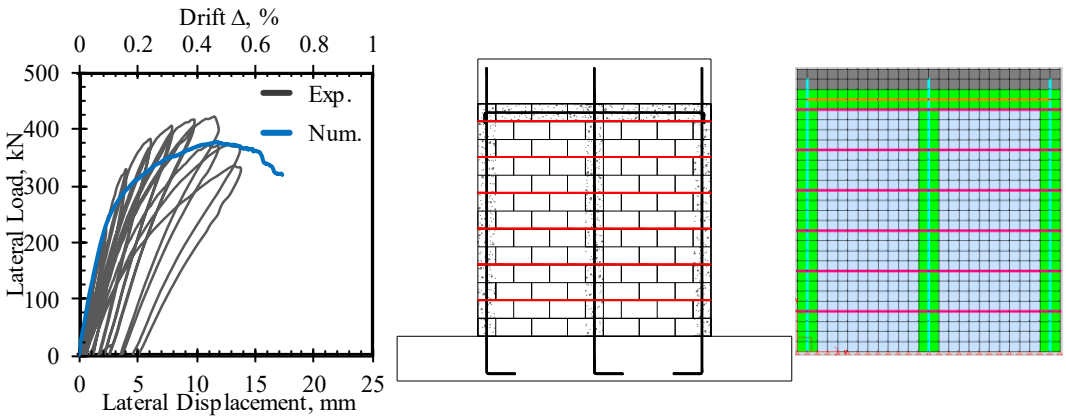

(d) BJ squat (Chapter 3)

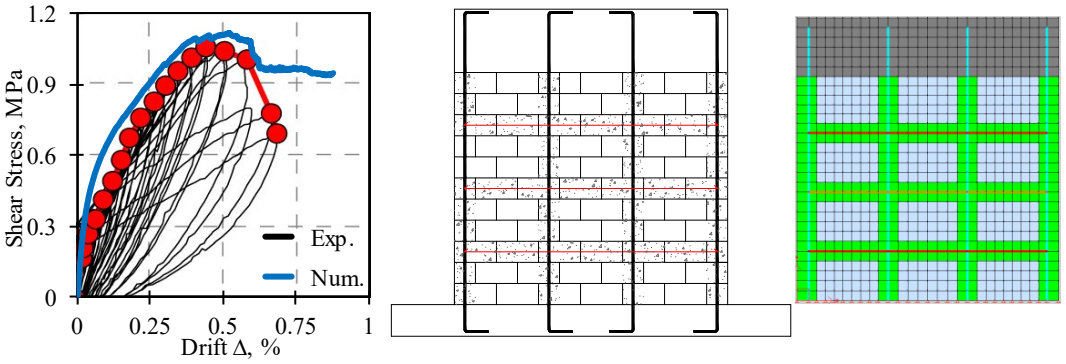

(e) BBRW (Calderón et al. 2021a)

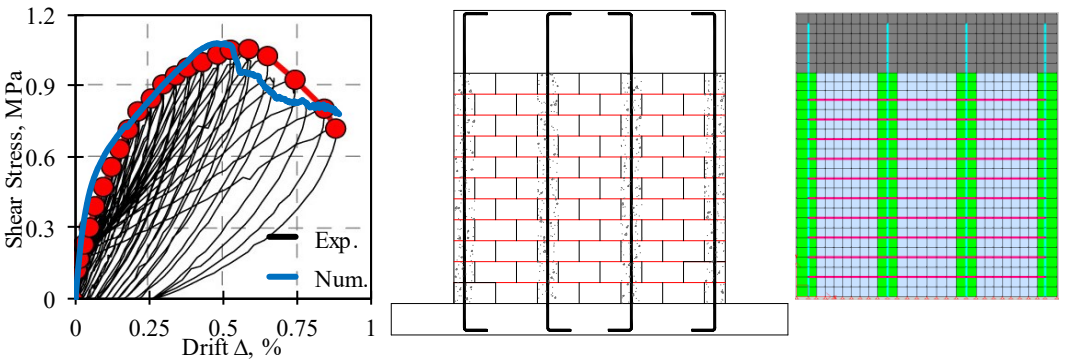

(f) BJRW (Calderón et al. 2021a)

Figure 4.13 Comparison of force-displacement response between the numerical model and experimental walls (Continued)

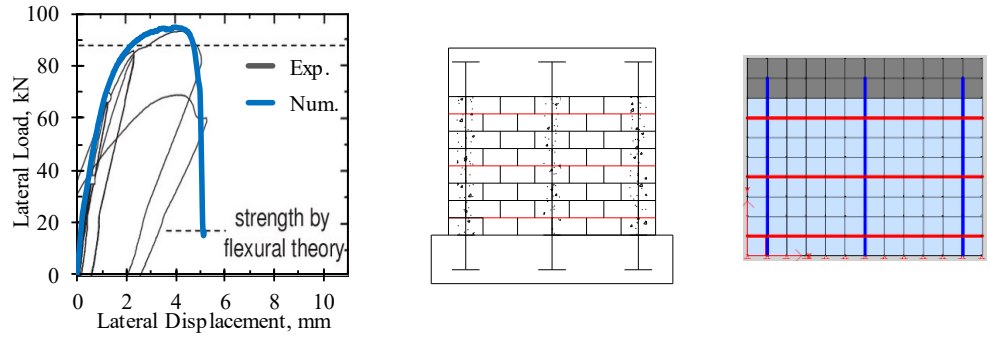

(g) N150-B1 (Haach et al. 2010)

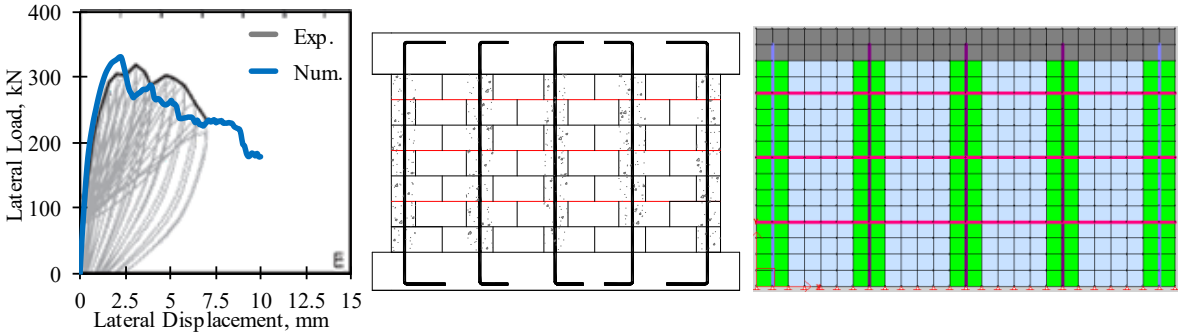

(h) Wall M5 (Ramírez et al. 2016)

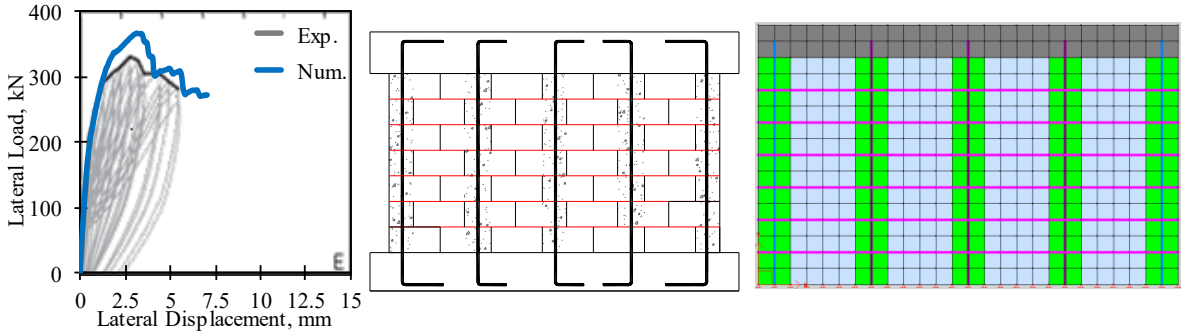

(i) Wall M6 (Ramírez et al. 2016)

Figure 4.13 Comparison of force-displacement response between the numerical model and experimental walls (Continued)

Figure 4.13 shows that the monotonic response calculated with the model reasonably approximates the linear and non-linear behaviour of the walls obtained experimentally. The initial elastic stiffness and its degradation were consistent with that described by the experimental curves. The post-peak branch was not captured well in most cases. This is in line with findings by Minaie (2009), Medeiros et al. (2020), and Elmeligy et al. (2021), where Elmeligy et al. (2021) pointed out that the brittleness and high anisotropy of the ungroted portion of PG walls caused inconsistent prediction of the post-peak region in contrast to FG walls. According to Table 4.5, the model was capable of predicting the peak load for all walls

with great accuracy, where the maximum and minimum ratio between the experimental and numerical (Exp. /Num.) were 1.12 and 0.90, respectively, and the average was 1.00 with low standard deviation. Similarly to the peak load, the initial stiffness was predicted with an acceptable average, range, standard deviation of the Exp. /Num. ratio of 0.95, 0.33, and 0.105, respectively. This good agreement was also noticed in comparing the numerical load-displacement response and its experimental counterpart as shown in Figure 4.13. Regarding the displacement at the peak load, the average of Exp. /Num. ratio of 1.04 showed that the numerical model reasonably matched the experimental result. However, the range between the maximum and minimum and the standard deviation of the ratio Exp. /Num. revealed that there was considerable variability between the numerical and experimental results. Compared to predicting the peak load, Calderón et al. (2021b) attributed the inconsistency of predicting the displacement at peak load to the anticipated experimental variability of testing identical PG walls, where their conclusion was based on the experimental results by Arnau et al. (2015) and Araya-letelier et al. (2019).

The developed model was able to accurately predict the cracking pattern at the peak load, as demonstrated in Figures 4.14 to 4.17. Figure 4.14 shows that the model correctly captured the flexural failure, indicated by the yielding of the vertical reinforcement in the tension zone (represented by the green colour). Similarly, the mixed shear-flexure failure mode was accurately predicted, as seen in Figure 4.15, where the model captured the diagonal cracks and the yielding of the vertical reinforcement in the tension zone (represented by the green colour). Finally, Figures 4.16 and 4.17 show that the model effectively captured the diagonal shear failure, characterized by diagonal cracks from the upper corner to the toe in the compression zone and the yielding of the horizontal reinforcement (either bond beam or bed-joint reinforcement) within the path of the cracks (represented by the green colour).

According to the comparison of numerical and experimental primary results, the numerical model is capable of reproducing the PG walls response under combined vertical and lateral loads with variable design parameters, indicating that the developed model can be used to analyze wall models with variables not experimentally tested.

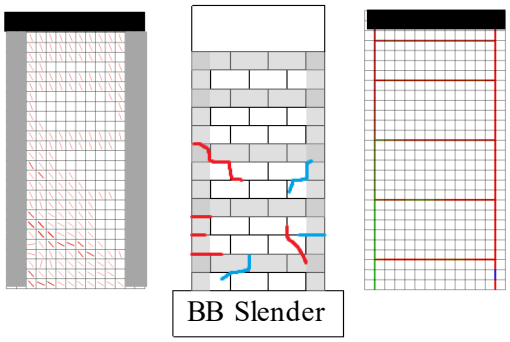

Figure 4.14 (a) numerical, (b) experimental cracking pattern at the peak load, and (c) average reinforcement steel stresses at the peak load for BB slender wall (Chapter 3) failed in flexure

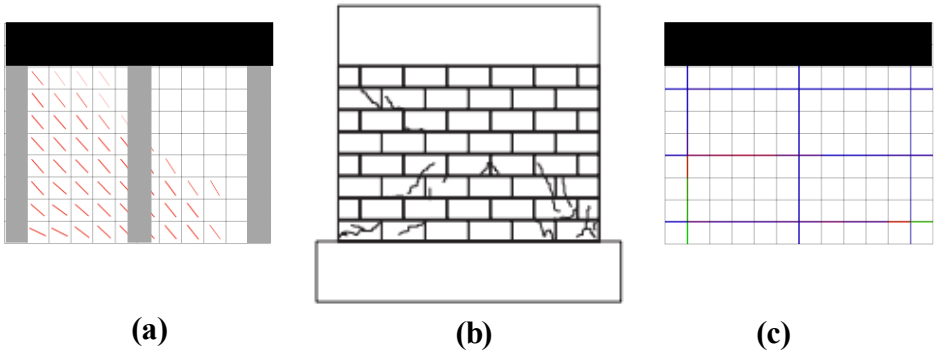

Figure 4.15 (a) numerical, (b) experimental cracking pattern at the peak load, and (c) average reinforcement steel stresses at the peak load for N150-B1 (Haach et al. 2010) failed in mixed shear-flexure

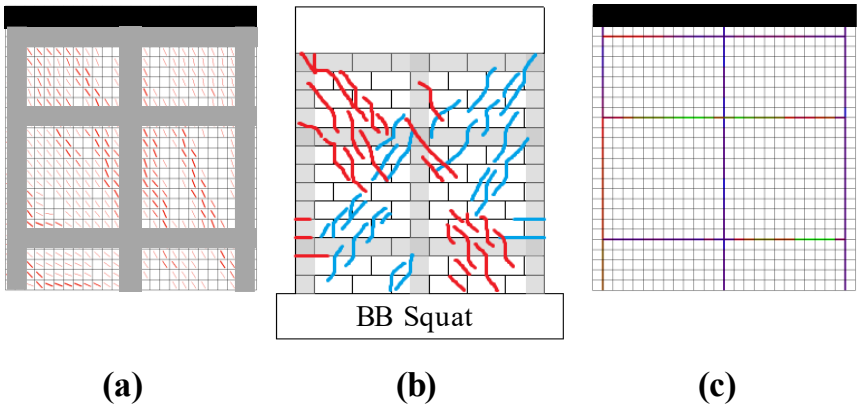

Figure 4.16 (a) numerical, (b) experimental cracking pattern at the peak load, and (c) average reinforcement steel stresses at the peak load for BB squat wall (Chapter 3) failed in diagonal shear

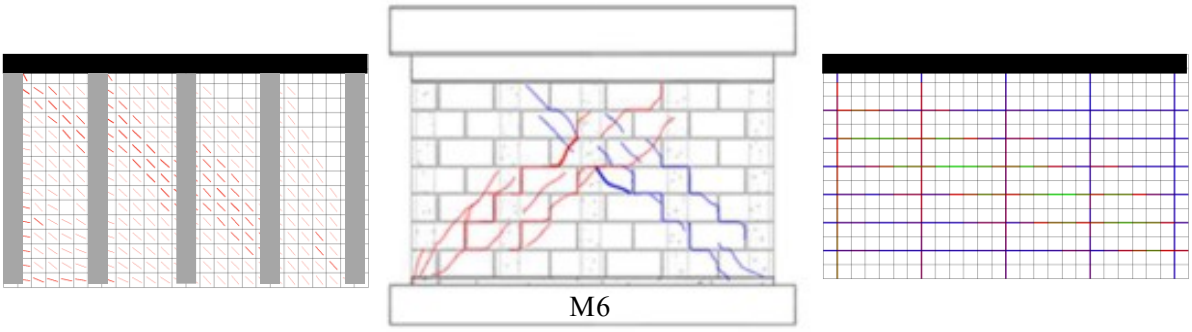

Figure 4.17 (a) numerical, (b) experimental cracking pattern at the peak load, and (c) average reinforcement steel stresses at the peak load for M6 wall (Ramírez et. al.2016) failed in diagonal shear

4.3.3. Influence of the Joint Shear Strength Ratio (JSSR) on Predicting the PG Wall Response

The PG 127-48I wall, tested by Elmapruk et al. (2020) and failed in diagonal shear, was chosen to demonstrate the impact of JSSR on peak strength. The calibration process involved adjusting the JSSR in VecTor2 while keeping other parameters constant until a reasonable agreement with experimental results was achieved. As shown in Figure 4.18(a), the load-drift response is significantly influenced by the change in JSSR. The sensitivity curve in Figure 4.18(b) indicated that the optimal value of JSSR is 0.035, where the initial stiffness, peak load, and corresponding displacement were aligned with the experimental results.

This calibration process highlights the significance of reporting JSSR in experimental studies when validating FE models without relying on calibration. As a result, the JSSR value reported in the selected experimental studies was incorporated into the FE model validation, as listed in Table 4.2.

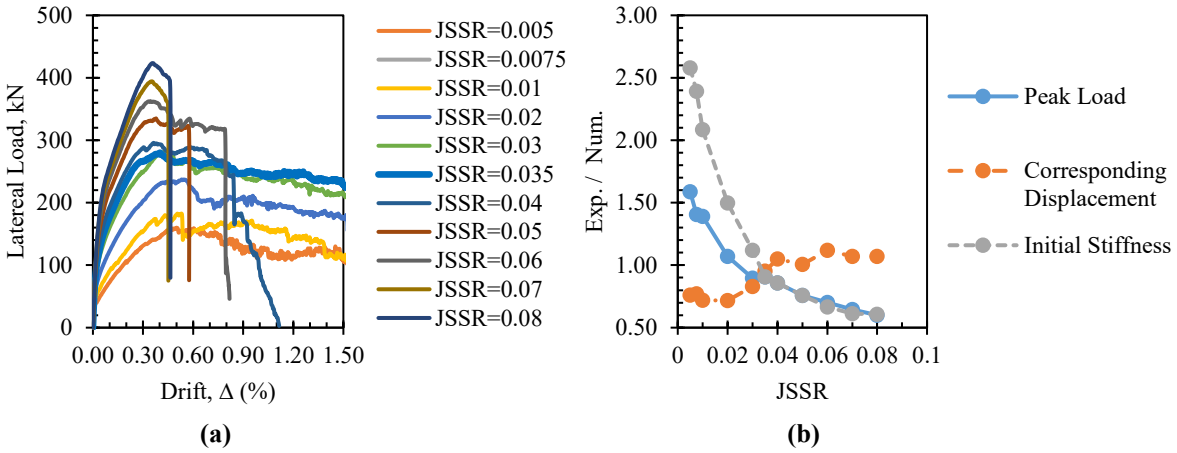

Figure 4.18 Calibration process (a) Load-Drift relationship and (b) sensitivity curve of varying JSSR

4.4 Numerical Investigation on the Failure Mode Prediction

As mentioned in the previous section, six out of nine of the validated walls failed in a diagonal shear. The remaining three walls failed in flexure or mixed shear-flexure. All the validated walls that failed in diagonal shear had an aspect ratio of 1 or less. On the other hand, the walls failed in flexure or mixed shear-flexure were having a high aspect ratio of 1.86, except N150-B1 wall (Haach et al. 2010) which had an aspect ratio of 0.68.

This section aimed to investigate the prediction of failure mode in partially grouted masonry walls. The investigation was conducted using the developed FE model, which analyzed the effect of two key parameters, vertical reinforcement and axial loads, on the failure mode. For the purpose of the study, wall models with a high aspect ratio (H/L=1.86) were selected, as they were deemed to be more susceptible to flexural failure due to their high aspect ratio.

4.4.1. Influence of Vertical Reinforcement

The role of vertical reinforcement in a masonry shear wall is comparable to the reinforcement at the top and bottom of a beam. It serves primarily to counter the axial compressive and tensile forces that arise at the ends of the wall due to the moment caused by the eccentric application of axial and lateral forces. In other words, the main function of vertical reinforcement, particularly boundary vertical reinforcing bars, is to increase the flexural capacity in PG walls. Therefore, elevating the amount of the vertical reinforcement was one option used by several authors to ensure the experimental walls to be shear-critical (Calderón

et al. 2021b). On the other hand, vertical reinforcement is thought to contribute to PG wall shear capacity by vertical confinement and dowel action (Dillon 2015).

The developed model was used to examine the impact of vertical reinforcement on the prediction of failure mode in partially grouted masonry walls. For this study, BB slender and BJ slender walls were selected from Chapter 3 research and a parametrical analysis was carried out by varying the amount of vertical reinforcement while keeping other parameters constant to solely assess the influence of vertical reinforcement on the failure mode prediction. The vertical reinforcement ratio, ρv, was varied in the range of [0.02-0.44] % based on gross area.

The numerical analysis showed that an increase in vertical reinforcement can change the failure mode from flexural or mixed shear-flexure to diagonal shear failure. The results indicated that BJ slender walls need $\rho_v > 0.09\%$ to change the dominant failure mode, while BB slender walls require $\rho_v > 0.22\%$, as demonstrated in Figure 4.19. This difference is attributed to the amount of horizontal reinforcement, as BB slender walls have almost double the amount of horizontal reinforcement compared to BJ slender walls, as indicated in Table 4.2. It is observed that this relationship of the horizontal reinforcement ratio between the two walls was reflected in the amount of the vertical reinforcement ratio limit needed to change the dominant failure mode. Figure 4.20 displays the cracking pattern and reinforcement stress contour for walls with a vertical reinforcement ratio above the limits stated above ($\rho_v > 0.22\%$ for BB slender wall and $\rho_v > 0.09\%$ for BJ slender wall). It is clearly visible that both walls failed in diagonal shear, indicated by the presence of diagonal cracks, yielding of the

horizontal reinforcement, and non-yielding of the vertical reinforcement. It is noteworthy that the yielding is indicated by the green colour in Figure 4.20(b).

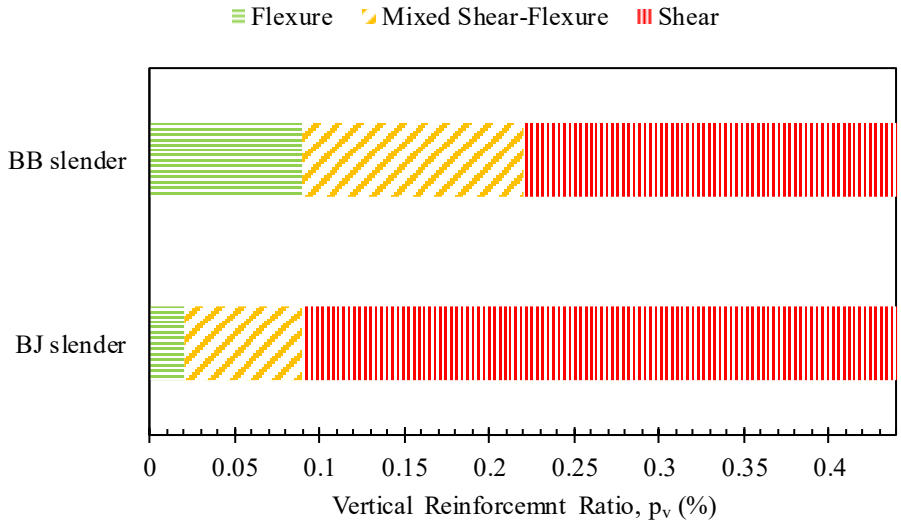

Figure 4.19 Influence of vertical reinforcement ratio on predicting the failure mode for BB slender and BJ slender walls

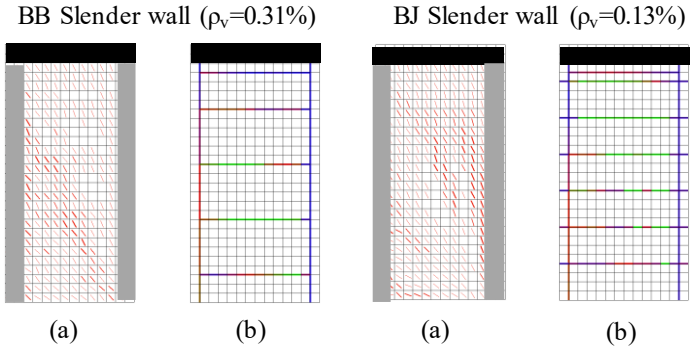

Figure 4.20 (a) numerical cracking pattern at the peak load, and (b) average reinforcement steel stresses at the peak load for BB slender and BJ slender walls

4.4.2. Influence of Axial Loads

A masonry shear wall in a building is responsible for resisting both lateral and vertical loads, including the gravity loads from the upper stories. The level of axial load that a wall is subjected to varies depending on its location within the building, and this parameter has a significant impact on the wall's behaviour under lateral loads. Multiple studies have shown that increasing the axial load leads to an increase in the ultimate shear resistance of PG shear walls (Matsumura 1988; Voon and Ingham 2006; Haach 2009; Ramírez et al. 2016). Additionally, adding axial load is known to cause a change in the failure mode from flexure

or mixed shear-flexure to brittle diagonal shear, as confirmed by Shing et al. (1989), Voon and Ingham (2006), da Porto et al. (2009), and Dillon (2015).

The developed model was utilized to investigate the effect of axial load on the prediction of failure mode, represented by the ratio of axial stress to compressive strength (σ/f'_m). BB slender and BJ slender walls were picked from Chapter 3 study to conduct a parametrical analysis where the σ/f'_m ratio was altered while keeping other parameters constant, in order to determine the impact of axial load on the failure mode prediction of partially grouted masonry walls. The range of variation for the σ/f'_m ratio was [5-20] %.

The numerical analysis revealed that increasing axial load can transform the failure mode from flexural or mixed shear-flexure to diagonal shear failure. The results showed that BJ slender walls need a σ/f'_m ratio greater than 10% to shift the dominant failure mode, while BB slender walls require a ratio of more than 15%, as shown in Figure 4.21. This difference in σ/f'_m requirements is attributed to the fact that the BB slender wall had a higher horizontal reinforcement ratio (ρ_h of BB slender wall approximately equals $2\rho_h$ of BJ slender wall), resulting in a higher shear capacity. Figure 4.22 displays the cracking pattern and reinforcement stress distribution for walls with an σ/f'_m ratio exceeding the aforementioned limits ($\sigma/f'm > 15\%$ for BB slender wall, and $\sigma/f'm > 10\%$ for BJ slender wall). It is evident that both walls failed in diagonal shear, indicated by the presence of diagonal cracks, yielding of the horizontal reinforcement, and non-yielding of the vertical reinforcement. The green colour in Figure 4.22(b) indicates yielding.

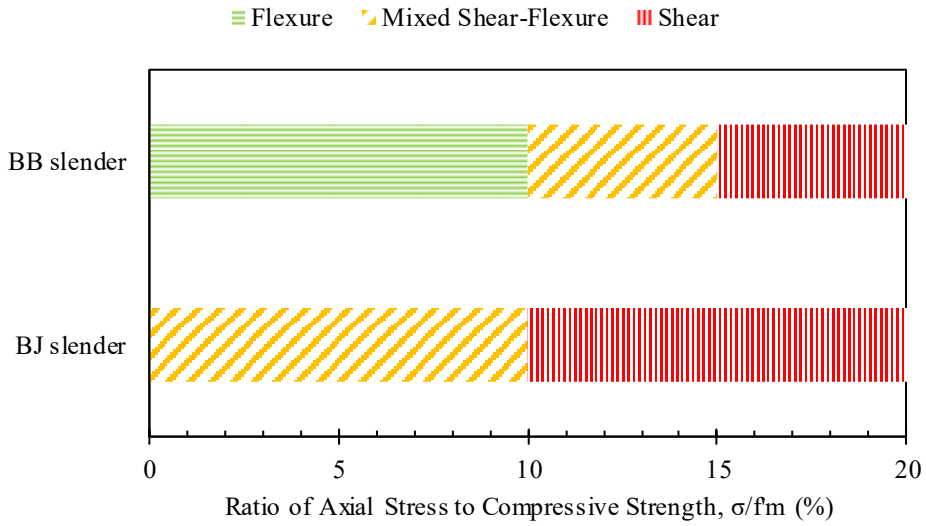

Figure 4.21 Influence of axial load on predicting the failure mode for BB slender and BJ slender walls

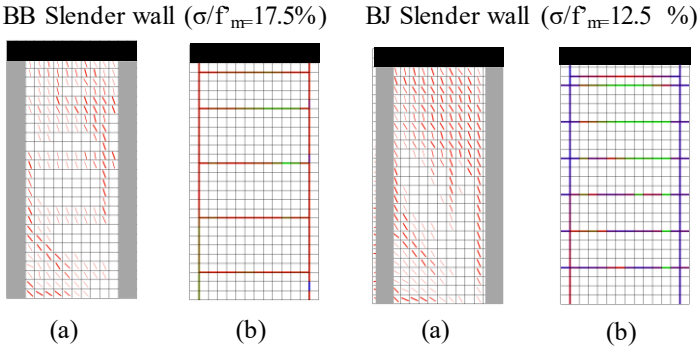

Figure 4.22 (a) numerical cracking pattern at the peak load, and (b) average reinforcement steel stresses at the peak load for BB slender and BJ slender walls

4.5 Estimation of In-Plane Strength

Building masonry walls that are safe and economical requires a reasonable degree of accuracy of the in-plane strength estimation. In this matter, predicting flexural strength is relatively simple and requires less validation (Haach et al. 2010). However, the existing code-based equations used to estimate the diagonal shear strength of PG walls may be incorrect or overly conservative, leading to in inconsistent strength estimations. For instance, Izquierdo (2021) found that the estimation of CSA S304 equation was inconsistent in terms of high standard of deviation.

In this section, the goal was to examine the accuracy of estimating the flexural strength through the general flexural analysis method and the diagonal shear strength through the CSA

S304 equation. To achieve this, multiple variants of BB slender wall (Chapter 3) that failed in flexure, and BB squat wall (Chapter 3) that failed in diagonal shear were utilized. The wall models were varied by adjusting the compressive strength or the horizontal reinforcement ratio, while keeping all other parameters constant, with the exception of elevating the vertical reinforcement ratio of the BB squat wall to ensure failure in diagonal shear.

4.5.1. Estimation of Flexural Strength

The general flexural analysis method offers a versatile solution for predicting the flexural capacity of walls with varying numbers and distributions of reinforcement layers. This method is based on the plane section assumption and compatibility and equilibrium equations. To locate the neutral axis (c) of the wall cross-section, an iterative process is used by adjusting c until $N=C_m+C_s-T_s$, where N represents the axial load, C_m represents the internal compression forces from the masonry, C_s represents the total internal compression forces from the steel, and T_s represents the total internal tension forces from the steel. The equations for calculating C_m, C_s, and T_s are described in Eq. (2), Eq. (3), and Eq. (4) respectively. The explanation of the symbols used in the equations can be found in the Notation section.

$$C_m = \alpha_1 f'_m \beta_1 c b \tag{2}$$

$$C_s = A_s \left(\varepsilon_m \left(\frac{c-d'}{c} \right) \right) E_s \leq A_s f_{yv} \tag{3}$$

$$T_s = A_s \left(\varepsilon_m \left(\frac{d-c}{c} \right) \right) E_s \leq A_s f_{yv} \tag{4}$$

Once the neutral axis (c) has been determined, the ultimate flexural capacity (M_u) is calculated by adding up the internal forces' moments around the outermost compression fiber of the cross-section, as outlined in Eq. (5). Finally, the shear load related to the ultimate flexural moment (V_f) is found by dividing the moment (M_u) by the wall height (h).

$$M_u = T_{s1} d_1 + N \frac{L}{2} - C_{s1} d_2 - C_m \frac{a}{2} \tag{5}$$

Figure 4.23 shows the comparison between the observed peak load of BB slender wall models that failed in flexure and the predicted peak load using the general flexural analysis method. A satisfactory prediction of flexural strength was achieved for all BB slender wall models.

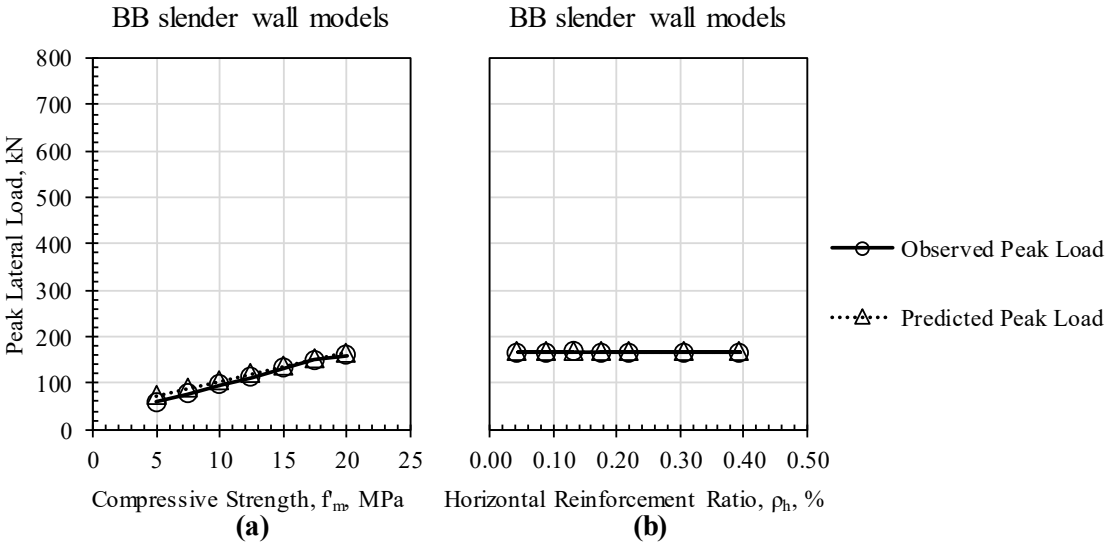

Figure 4.23 Performance of general flexural analysis method on estimating flexural strength of BB slender wall models with varying (a) compressive strength, f'_m and (b) horizontal reinforcement ratio, ρ_h

4.5.2. **Estimation of Diagonal Shear Strength**

The Canadian code (CSA S304-14 2014) provides an equation for predicting the in-plane shear strength of masonry walls, which can be found in clause 10.10.2.1 and is presented here as Eq. (6). The equation consists of two parts: the left part predicts the diagonal shear capacity while the right part serves as an upper limit to prevent crushing of the compressive strut. The symbols used in the equation are explained in the Notation section.

$$\left(0.16\left(2-\frac{M_f}{V_f d_v}\right)\sqrt{f'_m}\,td_v+0.25\mathrm{P}\right)\gamma_g+0.6A_{h,bar}f_{yh}\frac{d_v}{s_h}\quad\leq 0.4\sqrt{f'_m}\,td_v\gamma_g \tag{6}$$

Figure 4.24 compares the observed peak load of the BB squat wall models, which failed in diagonal shear, with the predicted peak load using the CSA S304 equation [left part of Eq. (6)]. It was observed that the CSA S304 equation predictions were conservative at higher levels of compressive strength. Regarding the variation of the horizontal reinforcement ratio, the comparison revealed inconsistent estimations, where the predictions were overly conservative at lower horizontal reinforcement ratios and not conservative at higher ratios. This is consistent with the findings of Hassanli et al. (2014) and Dillon (2015), who noted that most shear strength equations, including the CSA S304 equation, were inconsistent in their contribution of horizontal reinforcement. Thus, a parametric study is needed to understand the

contribution of horizontal reinforcement and other parameters in the CSA S304 equation in order to suggest revisions for the next edition of the code.

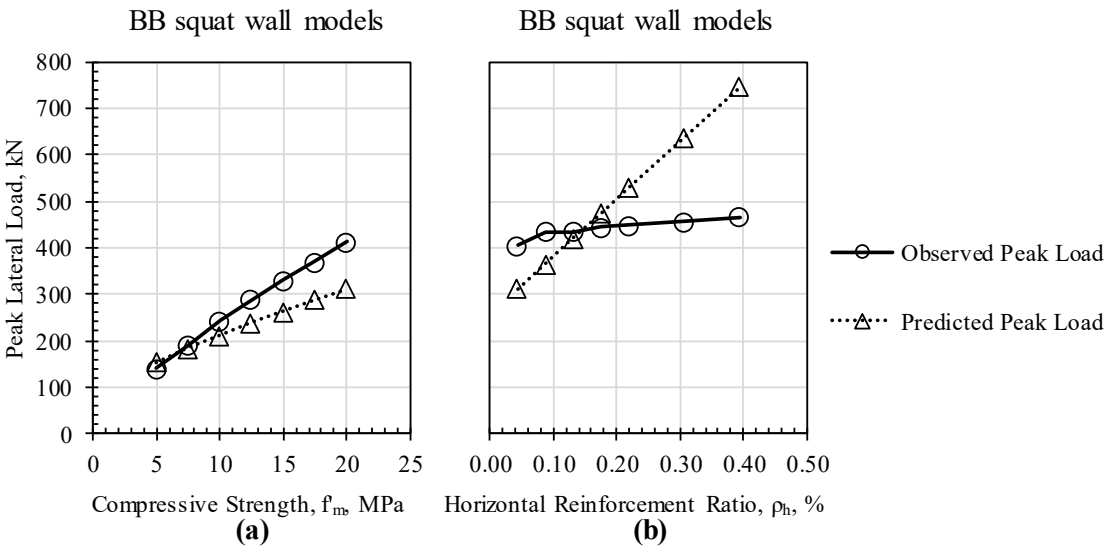

Figure 4.24 Performance of CSA S304 equation on estimating diagonal shear strength of BB squat wall models with varying (a) compressive strength, f'_m and (b) horizontal reinforcement ratio, ρ_h

4.6 Conclusions

This paper presented the development of the FE macro-model and then evaluated the developed model against 9 PG walls from various experimental studies. After that, the effect of vertical reinforcement and axial load on altering the failure mode was analyzed numerically. The predictive ability of the general flexural analysis method for walls that fail due to flexure and the shear strength equation of CSA S304 for walls that fail in diagonal shear were evaluated using numerical walls generated from the developed model. As a result of all the above, we can draw the following conclusions:

- The defined model showed a reasonable agreement with experimental results in terms of the linear and non-linear response of the load-displacement relationship up to the peak load. The peak load was accurately predicted with an average of 1.00 between the experimental and numerical results. This developed model had the advantage of being validated with several walls from different sources and having variable design parameters, which in turn strengthened the credibility of the model to conduct a reliable parametric study.
- The validation process revealed that reporting the experimental value of JSSR is crucial, as all validated walls had reported their experimental JSSR values. The significance of JSSR in predicting the general response of PG walls was further demonstrated by conducting a parametric analysis on an experimental wall that did not report the JSSR value.
- The validated developed model was used to investigate the effect of vertical reinforcement and axial loads on failure mode prediction for BB slender and BJ walls. The investigation found that increasing vertical reinforcement can change the failure mode from flexural or mixed shear-flexure to diagonal shear failure. The results indicated that BJ slender wall models need a vertical reinforcement ratio (ρ_v) greater than 0.09% to change the dominant failure mode, while BB slender wall models require a ρ_v greater than 0.22%. The study also found that increasing axial load can transform the failure mode from flexural or mixed shear-flexure to diagonal shear failure. The results showed that BJ slender wall models need a ratio of axial stress to

compressive strength (σ/f'_m) greater than 10% to shift the dominant failure mode, while BB slender wall models require a ratio of more than 15%.

- This paper also aimed to examine the accuracy of estimating the flexural strength and the diagonal shear strength of wall models generated from the developed model. The general flexural analysis method was used to estimate the flexural strength for wall models failed in flexure, and the CSA S304 equation was used to estimate the diagonal shear strength for wall models failed in diagonal shear. The results showed that the general flexural analysis method was able to accurately predict the flexural strength of the BB slender wall models. On the other hand, the CSA S304 equation was found to be conservative at higher levels of compressive strength and inconsistent in its estimation of the contribution of horizontal reinforcement for BB squat wall models. This study concludes that a parametric study is needed to understand the contribution of different parameters in the CSA S304 equation and suggest revisions for the next edition of the code.

5. PARAMETRIC STUDY

Shear Strength of Partially Grouted Masonry Shear Walls: Parametric Study

Amr Ba Rahim [a], Clayton Pettit [a], Carlos 'Lobo' Cruz Noguez [a], and Yong Li[a]

[a] *Department of Civil and Environmental Engineering, University of Alberta, 9211-116 Street, Edmonton, Alberta T6G 1H9, Canada*

Abstract (328)

Numerous efforts have been made to study the shear strength of partially grouted (PG) concrete masonry shear walls against in-plane loads. PG masonry is a cost-effective option as a lateral-load resisting system in areas with low seismicity, as it does not require as much material and labour as fully grouted (FG). Unfortunately, Experimental studies that address the behaviour of PG shear walls are scarce, and the amount of data is limited due to the inherent experimental constraints associated with full-scale testing and inconsistencies related to how the data is reported. For instance, there were 301 PG walls experimentally tested found in the literature. After synthetization and scrutinization of 292 PG walls, Izquierdo (2021) reduced them to 205 PG walls. The finite-element (FE) method offers an alternative to understand and characterize the in-plane response of PG walls, studying data that is numerically created. In this study, the development of an FE macro-model for PG walls using off-the-shelf element and material formulations is presented and later validated with experimental results obtained from the literature. The walls used in the validation process aimed to cover a range of parameters representative of typical design scenarios. A parametric analysis is conducted to study the effect of design parameters (horizontal reinforcement type, aspect ratio, compressive strength of masonry, level of axial stress, and horizontal and vertical reinforcement ratio) on the shear strength of PG shear walls. The results show that the compressive strength of masonry and axial stress had a substantial effect on the peak shear strength. On the other hand, the amount of horizontal and vertical reinforcement had no significant effect on the peak load. Based on the parametric analysis results, an attempt to improve the predictive ability of the CSA S304 equation was made by conducting a regression analysis on a total of 442 experimental and numerical walls that failed in a diagonal shear.

The precision and accuracy of the CSA S304 equation were increased by 59 percent and 99 percent, respectively.

5.1 Introduction

In areas with low seismicity, partially grouted (PG) masonry shear walls are a common choice for lateral force-resisting systems in masonry construction. In PG masonry, only the block cells that contain reinforcement are grouted, while in fully grouted (FG) masonry, all cells are grouted, regardless of whether they contain reinforcement or not. However, despite their practicality, PG masonry walls has not been extensively researched, which tends to focus more on FG masonry walls due to their widespread use in applications with moderate to high seismicity, where their improved ductility, strength, and stiffness are advantageous.

The shear response of FG walls under in-plane loading is better understood than that of PG walls, as the behaviour of FG masonry resembles that of reinforced concrete (RC). For instance, theories to predict normal and shear stresses for RC such as the Modified Compression Field Theory, advanced by Vecchio and Collins (1986) have been successfully adapted for FG masonry (Banting 2012; Seif ElDin 2016). In contrast, the shear behaviour of PG walls under in-plane lateral loading is complex and not yet fully characterized due to the non-linear interaction of the wall system components (unit block, grouted and ungrouted cells, mortar, grout, and reinforcing steel).

To better understand the in-plane shear behaviour of PG walls, research has employed both experimental and numerical methods. While experimental testing provides the most desirable data for analysis, experimental, financial, and time constraints have hindered research on PG shear wall behaviour. A total of merely 301 experimentally tested PG walls were collected from literature. A comprehensive synthesization and scrutinization process was conducted by Dillon (2015), Hung (2018), and Izquierdo (2021), a process which aims to minimize the variation between the studies and remove the inconsistencies across various research datasets. After synthesization and scrutinization, Izquierdo (2021) reduced the available complete dataset of 292 to 205 PG walls by only including walls that have the variables that are commonly found in the existing code- and research-based equations.

Numerical tools provide an effective alternative to overcome the limitations associated with experimental investigations. The finite element (FE) method has been widely used to simulate the structural behaviour of masonry over the last few decades. FE applications in structural

engineering can be broadly categorized into two modeling approaches: micro- and macro-modeling. While the micro-modeling technique can capture response mechanisms at the local level, such as cracking processes at the mortar joints and through the blocks, it is computationally expensive and time-consuming (Lourenço et al. 1995). In contrast, macro-modeling allows for capturing the global response of wall structures in a relatively shorter time and at a reduced cost (Lourenço 2002). This approach may be particularly suitable for conducting an extensive parametric analysis required to enhance the precision and accuracy of current design equations.

In recent years, several parametric studies have been conducted to investigate the behaviour of masonry walls using either micro- or macro-modeling approaches after validating finite element (FE) models. Notably, researchers such as Maleki (2008), Haach et al. (2011), Minaie et al. (2014), Seif ElDin (2016), Medeiros et al. (2020), and Calderón et al. (2021b) have contributed to this body of knowledge.

Maleki (2008) studied the effect of vertical (ρ_v) and horizontal (ρ_h) reinforcement ratios as well as the level of axial stress (σ_g) on the PG masonry walls response. Maleki (2008) developed a FE program where an orthotropic rotating smeared crack model was adopted for masonry and the reinforcement was represented by a separate overlaid element connected to the masonry element at each node. Maleki's (2008) study implemented five axial stress levels ranging from 0 to 1.5MPa (based on gross area). Besides it altered the failure mode from flexural to shear, Maleki (2008) found that peak load increased with increasing the axial stress. Three different ratios for vertical reinforcement were adopted (ρ_v = 0.09, 0.18, and 0.27%), where Maleki (2008) observed that increasing the amount of vertical reinforcement increased the peak load by changing the failure mode from flexure to shear. The horizontal reinforcement (bond beam) ratio was reported to have no effect on the peak load when employing three ratios (ρ_h = 0.025, 0.05, and 0.1%).

Haach et al. (2011) conducted an extensive parametric study investigating the effect of axial stress (σ_g), aspect ratio (H/L), boundary conditions, and vertical (ρ_v) and/or horizontal (ρ_h) reinforcement ratio on the performance of unreinforced and reinforced masonry walls. Haach et al. (2011) employed a simplified micro-modelling approach to reproduce the monotonic envelops of force-displacement response of PG walls tested at reversible cyclic mode using a

2D numerical model. The model proposed by Lourenço and Rots (1997) for the monotonic simulation of masonry structures was implemented. Haach et al. (2011) found that the horizontal reinforcement (joint reinforcement) had a modest effect on the peak load of cantilevered walls because of dominant flexural behaviour and hence the reinforcement activated after the peak load except in walls with very low aspect ratios. This conclusion was drawn after implementing four ratios (ρ_h = 0, 0.03, 0.05, and 0.08%) with the interaction of five aspect ratios (H/L = 2.33, 1.4, 1.00, 0.78, and 0.64) and five levels of axial stress as a function of compressive strength of masonry (σ_g/f'_m= 0, 0.1, 0.2, 0.4, and 0.6). Similar to horizontal reinforcement, Haach et al. (2011) used four ratios of internal vertical reinforcement. It was reported that the vertical reinforcement effect is dependent on the dominant behaviour of the wall. While it had a significant effect on the lateral capacity of flexural-dominated walls, it had a low impact on shear-dominated walls.

Minaie et al. (2014) used a nonlinear 3D detailed micro-modelling approach using ABAQUS software package to investigate the effect of the out-of-plane drift on the in-plane response of cantilevered PG walls by employing aspect ratio (H/L), axial stress (σ_g), and out-of-plane displacement as the variable parameters in the parametric study. Minaie et al. (2014) implemented three aspect ratios (H/L = 4, 2, 1.34), three levels of axial stress (σ_g = 0.34, 0.69, 1.03MPa), and eight magnitudes of out-of-plane drifts, generating 72 wall models. The adopted range of aspect ratios and axial stress variables was within the range commonly found in low-rise masonry buildings. Minaie et al. (2014) observed that the axial stress and aspect ratio had directly and inversely proportional effects on increasing the effect of the out-of-plane displacement on increasing the in-plane capacity of PG walls.

Seif ElDin (2016) utilized a macro-modelling approach only to analyze the FG walls, where he simulated nine FG walls that had been experimentally tested in the study. Seif ElDin (2016) found a good agreement between the numerical model and the experimental results. After validating, Seif ElDin (2016) expanded the study of FG walls by conducting a parametric study where aspect ratio (H/L), level of axial stress (σ_g), and horizontal reinforcement (deformed bars) spacing were selected as the variables to study parametrically their influence on the in-plane response of FG walls. Seif ElDin (2016) generated eight wall models by employing two aspect ratios (H/L = 1 and 2), two levels of axial stress (σ_g = 0 and 1MPa), and

two values of horizontal reinforcement spacing (200 and 400mm). Similar to Haach et al. (2011), Seif ElDin (2016) noted a negligible effect of horizontal reinforcement in a wall with a higher aspect ratio since it was flexurally-dominated. On the other hand, horizontal reinforcement had a minor effect on the shear strength of a wall with a lower aspect ratio. In addition, Seif ElDin (2016) found that the lateral load capacity increased due to either increasing the axial stress or decreasing the aspect ratio.

Medeiros et al. (2020) adopted a macro-modelling approach to simulate the response of PG walls subjected to in-plane loads using VecTor2 software package. The validated model was utilized to conduct a parametric study of PG walls with openings to study the effect of ungrouted (f'_{mug}) and grouted (f'_{mg}) masonry compressive strength, mortar shear strength, vertical reinforcement ratio (ρ_v) and spacing, horizontal reinforcement (bond beam) ratio (ρ_h) and spacing, axial stress (σ_g), aspect ratio (H/L), and opening size on the lateral capacity and its corresponding displacement as well as the initial stiffness of such walls. A wide range of variables was adopted in the study to cover most of the design scenarios possibilities. Different levels of influence were found in this parametric study. While ungrouted/grouted masonry compressive strength, mortar shear strength, vertical reinforcement ratio, and aspect ratio had a significant effect on the peak load, axial stress had a modest effect. On the other hand, horizontal reinforcement ratio, vertical and horizontal reinforcement spacing, and opening size had negligible effects. Medeiros et al. (2020) noted that the aspect ratio was the only parameter with an inverse correlation with the peak load.

Recently, Calderón et al. (2021b) generated 16 PG wall models made of clay brick and reinforced horizontally by bed-joint reinforcement to conduct a parametric study using a detailed micro-modeling approach. The studied parameters were four aspect ratios (H/L=0.55, 0.99, and 1.35), four levels of axial stress as a function of masonry compressive strength (σ_g/f'_m=2.5, 5, 7.5, and 10%), two horizontal reinforcement (joint reinforcement) ratios (ρ_h = 0.081, 0.16%). Calderón et al. (2021b) observed that the peak load did not significantly impact by increasing the horizontal reinforcement ratio. In addition, it was observed that aspect ratio and axial stress were inversely and directly related to increasing the peak load, respectively.

An analysis of the literature shows that there is a need to conduct a parametric study that covers both types of horizontal reinforcement types (bond beam and bed-joint reinforcement)

and investigate their effect with the interaction of variable aspect ratios, reinforcement ratios, levels of axial stress, and masonry compressive strength to understand better the in-plane response of PG walls made of concrete blocks in one single study. The variability of the parameters in the parametric study should be within the upper and lower bounds found in design scenarios found in typical buildings and within the ranges recommended in the masonry standards to have rational outcomes (Minaie 2009). Izquierdo (2021) performed an extensive database assembly of 205 PG experimental walls illustrating the variables' distribution and identifying the range of the variables studied. For this purpose, the variable parameters selected in this study to cover the range reported in Izquierdo's (2021) study as well as the masonry code standards; CSA S304 (2014) and TMS 402 (2016). As a result, 1074 wall models were generated.

This paper presents the development of a finite element macro model and its validation against multiple experimental results found in the literature. The validated model was then used to conduct a parametric study on 541 wall models that failed numerically in diagonal shear, investigating the impact of independent variables on the peak shear strength of PG walls. Finally, a regression analysis was performed on a selection of 195 experimental walls and 247 wall models to enhance the accuracy and precision of the CSA S304 equation used for predicting the diagonal shear capacity of PG walls.

5.2 PG Masonry Walls Behaviour against In-Plane Loads

Several studies have been conducted to study the in-plane shear behaviour of PG walls by varying the design parameters such as aspect ratio, axial stress, strength of masonry materials, boundary conditions, and reinforcement detailing (El-Dakhakhni and Ashour 2017). All studies concluded that the behaviour of PG walls against in-plane loads is complex, particularly those walls that failed in a diagonal shear. This may be attributed to the interaction of different materials that constitute this wall system (block unit, mortar, grout, and reinforcing bar). The diagonal shear failure can be characterized by diagonal cracks and yielding of horizontal (shear) reinforcement (Haach et al. 2012). On the other hand, sliding shear failure can be avoided by utilizing appropriate mortar quality, along with typical axial loads and suitable amounts of vertical reinforcement (Oan, 2013; Rizaee, 2015).

Chapter 3 described the cyclic test of four full-scale partially grouted walls to investigate the influence of horizontal reinforcement type and aspect ratio on their behaviour. The study found that the type of horizontal reinforcement had a negligible effect on the peak load, while the peak strength decreased with increasing aspect ratio. Bed-joint reinforcement was observed to control the crack width in walls that failed in diagonal shear due to the even distribution of reinforcement along the wall height. In contrast, bond beam reinforcement did not show this effect. Additionally, the use of CSA and TMS equations to predict the diagonal shear of the tested shear-critical squat walls led to inconsistencies in the axial stress and horizontal reinforcement contribution.

Regarding the performance of the code-based shear strength equations, Izquierdo (2021) found that the CSA S304 equation is more conservative than the TMS 406 (Figure 5.1) and has a higher level of data dispersion (standard deviation) by 78% when examining these equations on 205 walls found in the literature. To improve the accuracy of the developed models, Izquierdo (2021) included the mortar strength contribution and excluded the horizontal reinforcement contribution, which is in contrast to most of the code- and research-based equations. For instance, one model of Izquierdo's (2021) models is described in Eq. (1) as follows.

$$-0.0205\mathrm{H} + 0.0337\mathrm{L} + 6f_{mortar} + 0.0917A_{vi} + 0.289\mathrm{P} \quad (1)$$

where H, L, f_{mortar}, A_{vi}, and P are the wall height, wall width, compressive strength of mortar, area of interior vertical reinforcement, and axial load, respectively. Izquierdo (2021) found that the developed models surpassed the performance of the existing code- and research-based equations.

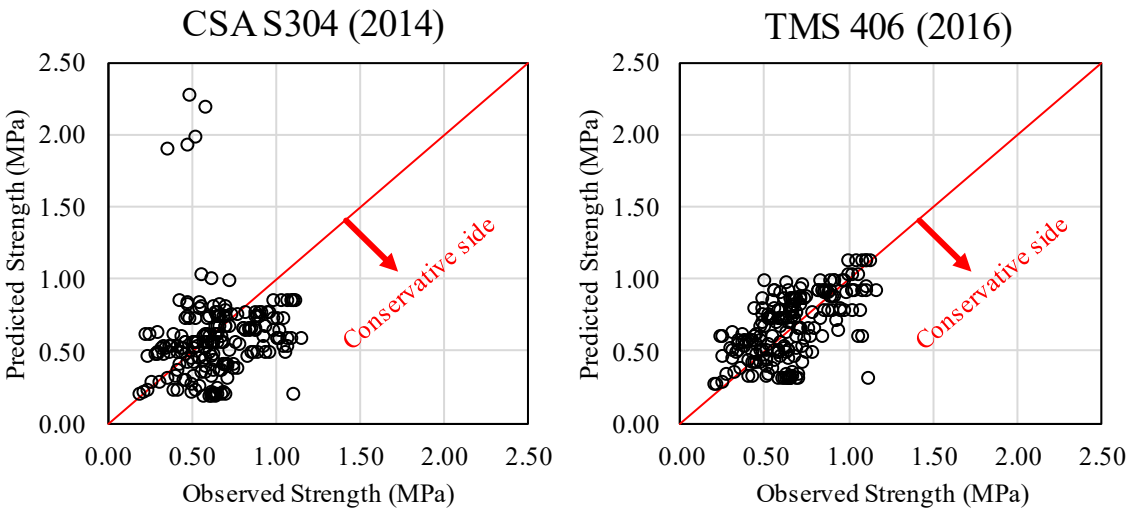

Figure 5.1 Performance of CSA S304 (2014) and TMS 406 (2016) diagonal shear strength equation adapted from Izquierdo (2021)

Overall, developing reliable FE models to generate numerical walls beside the experimental walls found in the literature is an important step to update the current coefficients of the design parameters contributions in the North American design codes, particularly diagonal shear strength equations of PG walls (El-Dakhakhni and Ashour 2017). Consequently, more safer and accurate prediction equation for the cost-effective solution in masonry construction can be achieved.

The literature review revealed that the macro-modeling approach is a viable method for capturing the peak strength and facilitating extensive parametric analyses, as demonstrated by previous studies (Seif ElDin 2016; Medeiros et al. 2020). However, this approach has certain limitations that can hinder its simulation capabilities, such as the joint shear strength ratio (JSSR). According to Hung (2018), the JSSR, which is the ratio of joint shear strength (c) to masonry compressive strength (f'_m), can have a significant impact on the shear response of PG walls.

5.3 FE Models

5.3.1. Model Development

The nonlinear finite element analysis program VecTor2 (VecTor Analysis Group 2019) was utilized in this study. This program employs the modified compression field theory (MCFT) formulation proposed by Vecchio and Collins (1986) for reinforced concrete and the disturbed stress field model (DSFM) proposed by Facconi (2012) for masonry. It is capable of simulating the monotonic response of masonry materials (Facconi 2012; Facconi et al. 2013). In addition, this program can model masonry as a continuum with average properties, where joint failures spread over a single element for sufficiently large masonry structures (Wong et al. 2013). As a result, this program can consider both the overall performance of the composite material on an average level and the specific response of the mortar joints to shear slip (Sadeghian and Vecchio 2018).

The FE models of PG walls were developed using rectangular plane stress elements for the ungrouted and grouted masonry and trussed elements for the horizontal and vertical steel reinforcement. The dimensions of the plane stress elements were selected to be (100x100mm). This meshing size permits to simulate the reinforcement in a discrete fashion. Besides that, the square elements and the rationally refined mesh enhance the model's accuracy (Medeiros et al. 2020). The difference between the ungrouted and grouted elements lies in the thickness. While grouted elements were considered the full width of the wall, ungrouted elements were taken as the full face shell thickness of the unit block. The boundary conditions were defined by restricting the bottom nodes in the x and y directions with pinned supports in the case of single curvature (cantilevered) conditions while restricting both bottom and top nodes when the boundary conditions are double curvature. The developed model was analyzed by applying vertical loads to each node at the top of the loading beam, which accurately simulated the distributed experimental vertical loads on the wall. In addition, lateral loads were applied at the central node of the loading beam to ensure a balanced distribution of lateral loads to the wall. It is important to mention that VecTor2 allows the user to apply force-based loading by specifying nodal loads or displacement-based loading through support displacements.

The material behavioural models provided in VecTor2 were used to represent the mechanical behaviour of masonry and reinforcing steel in the developed model. The input data for these models were obtained from materials characterization tests, which supplied the mechanical properties of the materials. The material models selected for the analysis were chosen after extensive fit tests, which ensured a reasonable match between the numerical and experimental results. Table 5.1 summarizes the material models employed to simulate the behaviour of masonry and steel reinforcement. For a more detailed explanation of the developed model, refer to Chapter 4.

Table 5.1 Materials Models for the developed model

Material	Behaviour	Model
Masonry	Compressive strength (pre-maximum resistance)	Hoshikuma et al.,1997
	Compressive strength (maximum post-resistance)	Masonry (Facconi)
	Compression softening	Masonry (Laurenco)
	Tensile stiffening	Modified Bentz, 2003
	Tensile softening	Nonlinear (Hordijk)
	Crack slip calculation	Masonry I
Reinforcement	Stress-Strain response	Ductile (trilinear relationship)
	Dowel action	Tassios (Crack Slip)
	Buckling	Akkaya 2012 (Modified Dhakal-Maekawa)

5.3.2. Model Verification

The accuracy of the developed FE model in capturing the global response of PG walls was validated against nine PG walls from four studies (Haach et al. 2010, Ramírez et al. 2016, Calderón et al. 2021a, Chapter 3). These selected walls cover a broad range of design parameters and include horizontal reinforcement types (bond beam and bed-joint), which enhances the credibility of the FE model. The material properties of these walls are presented in Table 5.2. For further details on defining these walls in the developed model, please refer to Chapter 4.

Table 5.2 Materials Properties of the experimental walls

Wall ID	Aspect Ratio	Height	Length	Reinforcement Ratio		Gross Axial Stress	Masonry Comp. Strength	JSSR[3]	FM[4]
				Vertical	Horizontal				
	Unitless	mm	mm	(%)	(%)	MPa	MPa		
BB slender (Chapter 3)[1]	1.86	2600	1400	0.09	0.09	1.9	20.5	0.0074	**F**
BJ slender (Chapter 3)[2]	1.86	2600	1400	0.09	0.05	1.9	20.5	0.0074	**M**
BB squat (Chapter 3)[1]	1.00	2600	2600	0.09	0.04	1.9	20.5	0.0074	**S**
BJ squat (Chapter 3)[2]	1.00	2600	2600	0.09	0.05	1.9	20.5	0.0074	**S**
BBRW (Calderón et al. 2021a)[1]	0.86	2270	2640	0.41	0.085	0.5	9.67	0.05	**S**
BJRW (Calderón et al. 2021a)[2]	0.86	2270	2640	0.41	0.087	0.5	9.67	0.05	**S**
N150-B1 (Haach et al. 2010)[2]	0.67	800	1206	0.098	0.094	1.3	5.95	0.071	**M**
Wall M5 (Ramírez et al. 2016)[2]	0.44	1400	2590	0.18	0.04	0.56	5.54	0.05	**S**
Wall M6 (Ramírez et al. 2016)[2]	0.44	1400	2590	0.18	0.08	0.56	5.54	0.05	**S**

1 Horizontally reinforced with bond beam
2 Horizontally reinforced with bed-joint
3 JSSR=**J**oint **S**hear **S**trength **R**atio
4 FM=Failure Mode, **F**=Flexure, **M**=Mixed Shear-Flexure, and **S**=Diagonal Shear

Sample of validation results in terms of force-displacement response, cracking pattern, and average reinforcement stresses' contour for BB slender wall (Chapter 3) and M6 wall (Ramírez et al. 2016) are shown in Figures 5.2 and 5.3, respectively. For complete results, please refer to Chapter 4. In the pre-peak branch, the monotonic response calculated with the model was found to reasonably approximate the walls' linear and non-linear behaviour obtained experimentally. The initial elastic stiffness and its degradation were consistent with those described by the experimental curves, but the post-peak branch was not captured well in most cases. The developed model accurately predicted the cracking pattern at the peak load. Figure 5.2 shows that the model captured the flexural failure of the BB slender wall, represented by the yielding of vertical reinforcement in the tension zone (indicated by the green colour). Similarly, the developed model captured the diagonal shear failure of the M6 wall, characterized by diagonal cracks from the upper corner to the toe in the compression zone and the yielding of horizontal reinforcement within the path of the diagonal cracks (indicated by the green colour), as shown in Figure 5.3.

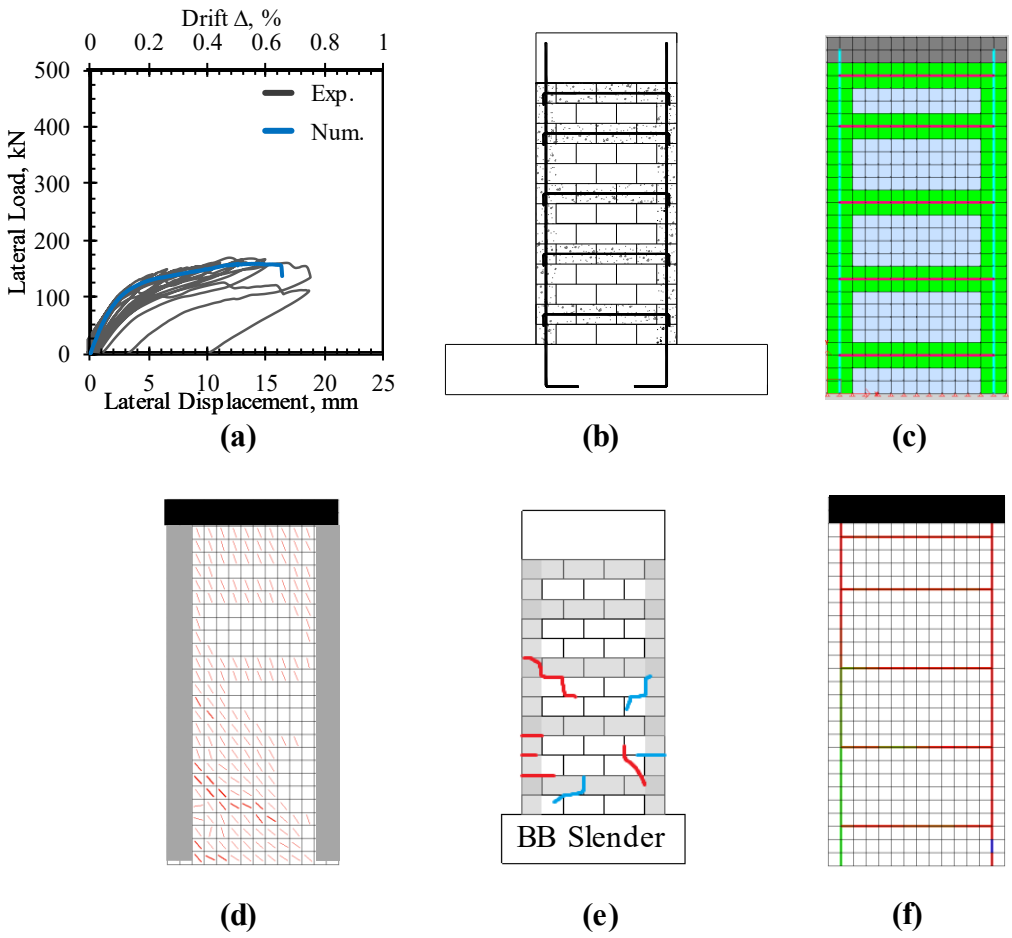

Figure 5.2 Validation results; (a) Comparison of force-displacement response between the numerical model and experimental walls, (b) Experimental wall, (c) Numerical wall, (d) Numerical cracking pattern at the peak load, (e) experimental cracking pattern at the peak load, and (f) average reinforcement steel stresses at the peak load for BB slender wall (Chapter 3) failed in flexure

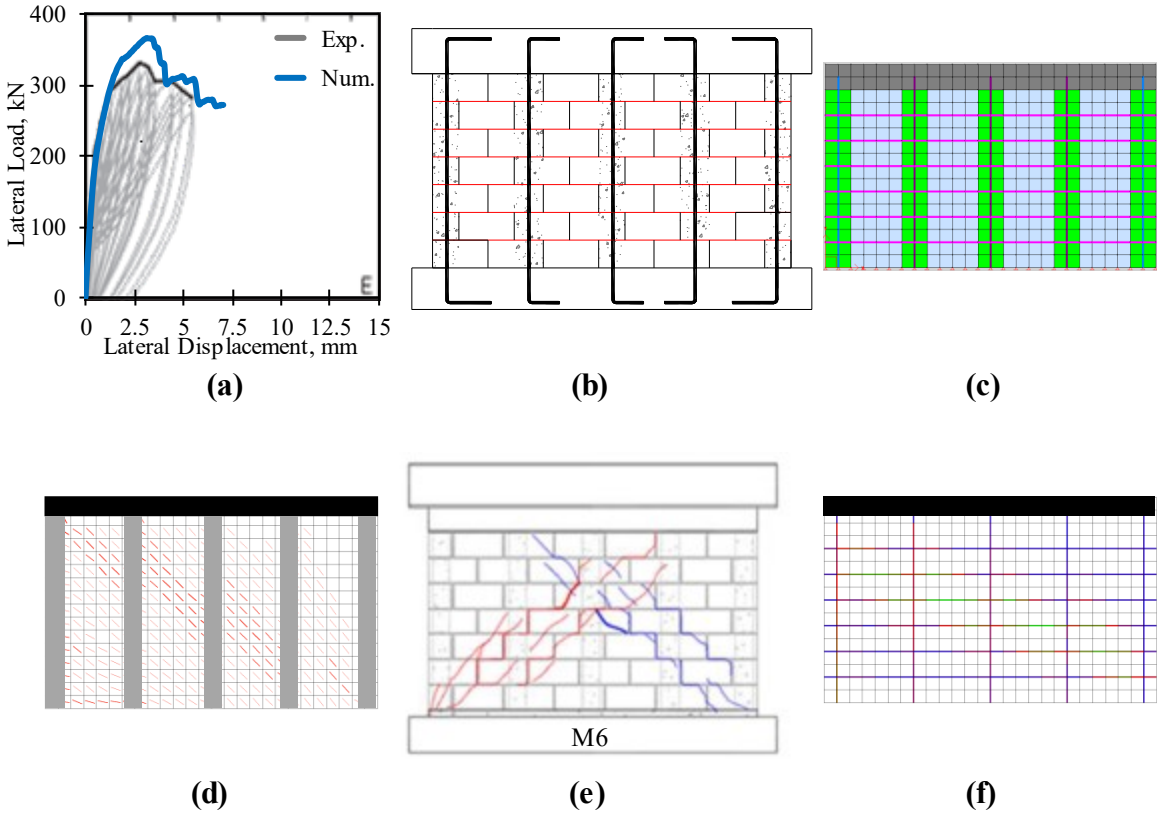

Figure 5.3 Validation results; (a) Comparison of force-displacement response between the numerical model and experimental walls, (b) Experimental wall, (c) Numerical wall, (d) Numerical cracking pattern at the peak load, (e) experimental cracking pattern at the peak load, and (f) average reinforcement steel stresses at the peak load for M6 wall (Ramírez et al. 2016) failed in diagonal shear

In addition, the initial stiffness, maximum resistance, and corresponding displacement were used to verify the accuracy of the developed model. Table 5.3 presents a comparison between the numerical and experimental results. The initial stiffness was calculated using the guidelines proposed by Park (1988), as implemented by Tolou-kian and Cruz-Noguez (2022). According to Park (1988), the initial stiffness is obtained based on the equivalent yield model, where if F_u is the peak strength, the initial stiffness is defined as the slope of the ascending portion of the idealized backbone curve at the point where it intersects the measured backbone curve at a strength of 0.75 F_u.

Table 5.3 Results of FE model validation

Wall ID	Peak load			Displacement[1]			Initial stiffness		
	Exp.	Num.	Exp. / Num.	Exp.	Num.	Exp. / Num.	Exp.	Num.	Exp. / Num.
	kN	kN	Unitless	mm	mm	Unitless	kN/mm	kN/mm	Unitless
BB slender (Chapter 3)[1]	166	160	1.04	15.9	14.8	1.07	39.6	40	0.99
BJ slender (Chapter 3)[2]	157	152	1.03	14.1	17.7	0.80	30.7	30.4	1.00
BB squat (Chapter 3)[1]	407	397	1.03	14.9	10.9	1.37	51.8	66.2	0.78
BJ squat (Chapter 3)[2]	422	376	1.12	12	12.2	0.98	84.4	76	1.11
BBRW (Calderón et al. 2021a)[1]	388	412	0.94	10.1	13.7	0.74	49.3	58.8	0.84
BJRW (Calderón et al. 2021a)[2]	388	397	0.98	13.3	13.3	1.00	52.8	50.4	1.05
N150-B1 (Haach et al. 2010)[2]	93	95	0.98	4.2	3.9	1.08	54.7	55.9	0.98
Wall M5 (Ramírez et al. 2016)[2]	316	330	0.96	3.1	2.19	1.42	210.7	240	0.88
Wall M6 (Ramírez et al. 2016)[2]	330	367	0.90	2.7	3.1	0.87	275	305.8	0.90
Average			1.00			1.04			0.95
Maximum			1.12			1.42			1.11
Minimum			0.90			0.74			0.78
Stdv.			0.065			0.234			0.105

1 Displacement at peak load
2 Horizontally reinforced with bond beam
3 Horizontally reinforced with bed-joint

Table 5.3 demonstrates that the developed model accurately predicted the peak load for all the walls considered, with an average experimental-to-numerical ratio (Exp. / Num.) of 1.00 and a standard deviation of 0.065. The initial stiffness was also reasonably predicted, with an average Exp. / Num. ratio of 0.95 and a standard deviation of 0.105. Although the average Exp. / Num. ratio of 1.04 for the displacement at the peak load indicates reasonable agreement, the standard deviation of the ratio reveals significant variability between the numerical and experimental results. Calderón et al. (2021b) explained that the variation in the experimental results of identical PG walls could be the reason for the inconsistency in predicting the displacement at peak load, a conclusion drawn based on the results reported by Arnau et al. (2015) and Araya-letelier et al. (2019).

The comparison of the numerical and experimental results shows that the developed model accurately replicates the response of PG walls subjected to combined vertical and lateral loads with varying design parameters. This finding suggests that the model is suitable for conducting a parametric study, which could include variables ranges with different combinations that have not been experimentally investigated.

5.4 Parametric Study

5.4.1. Criteria for Selecting Parameters Variables

Following model validation, a parametric study was undertaken to investigate the in-plane response of PG walls under combined axial and lateral loads, while considering the effects of various design parameters. The study included six independent variables: the type of horizontal reinforcement, aspect ratio, compressive strength of the masonry, axial stress, and horizontal and vertical reinforcement ratios. The fixed parameters were wall height, thickness, boundary conditions (cantilevered fashion), reinforcement properties, and loading protocol. This study investigated the effects of the independent parameters on the peak shear strength (the so-called dependent parameter). Table 5.4 describes the selected variables of independent parameters. The values chosen for the independent variable parameters cover a wide range of data from 205 experimental walls documented by Izquierdo (2021), as illustrated in Figure 5.4. This range of independent parameters produces 1068 wall models (534 wall models with bond beam and 534 wall models with bed-joint). The description of the generated wall models is found in Appendix B.

Table 5.4 Range of independent design parameters

Independent Parameter	Variable Range
Horizontal reinforcement type	Bond beam and Bed-joint
Aspect ratio, H/L	0.42, 1.00, and 1.86
Masonry compressive strength, f'_m	[5-20]MPa
Axial stress to masonry compressive strength ratio, σ/f'_m	5, 10, and 15%
Bond beam reinforcement ratio, ρ_h	[0.04-0.52]%
Bed-joint reinforcement ratio, ρ_h	[0.04-0.40]%
Vertical reinforcement ratio, ρ_v	[0.04-0.75]%

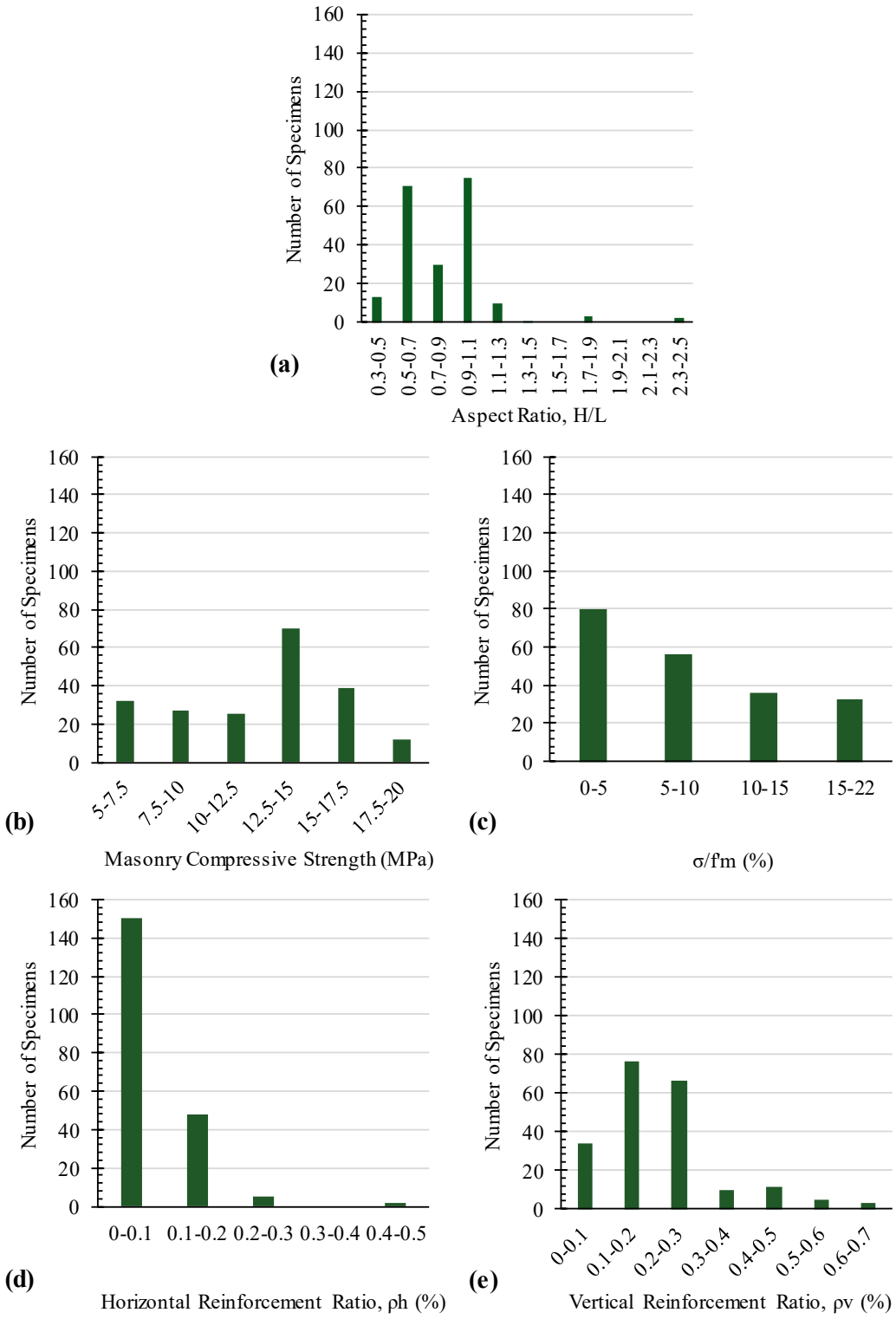

Figure 5.4 Distribution of (a) aspect ratio, (b) masonry compressive strength, (c) axial stress to masonry compressive strength ratio, (d) horizontal reinforcement ratio, and (e) vertical reinforcement ratio adapted from Izquierdo (2021)

5.4.2. Results and Discussion

After conducting a numerical analysis of 1068 wall models, it was found that 541 of them failed numerically due to diagonal shear. In Figure 5.5 below, the diagonal shear failure mode is contrasted with the flexure failure mode, where flexure failure (Figure 5.5(a)) is evidenced by horizontal cracks at the bottom and yielding of the vertical reinforcement (indicated by the green colour). However, by increasing the vertical reinforcement ratio of the same wall model, the failure mode can be shifted to diagonal shear (Figure 5.5(b)), which is identified by diagonal cracks and yielding of the horizontal reinforcement at the peak load (indicated by the green colour). Consequently, the wall models identified by the failure mode of diagonal shear were investigated parametrically to evaluate the effect of independent parameters on the peak strength.

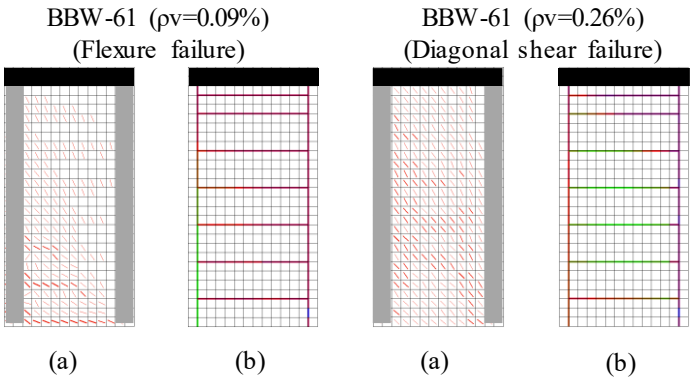

Figure 5.5 (a) numerical cracking pattern at the peak load, and (b) average reinforcement steel stresses at the peak load for BBW-61 with ρ_v=0.09% and BBW-61 with ρ_v=0.26%, respectively

5.4.2.1 Effect of masonry compressive strength and axial stress

The dependent peak load due to the variation of the compressive strength of masonry with variable H/L and σ/f'_m ratios for wall models reinforced with either bond beam or bed-joint reinforcement are shown in Figures 5.6(a) and 5.6(b), respectively. For illustration purposes, Figure 5.6 shows results corresponding to wall models in which the horizontal and vertical reinforcement ratios are 0.04% and 0.22%, respectively. Results for other ratios show similar trends. As a reference, the predictions of the Canadian standard for masonry structures CSA S304 (2014) equation for diagonal shear capacity are presented alongside the numerical results.

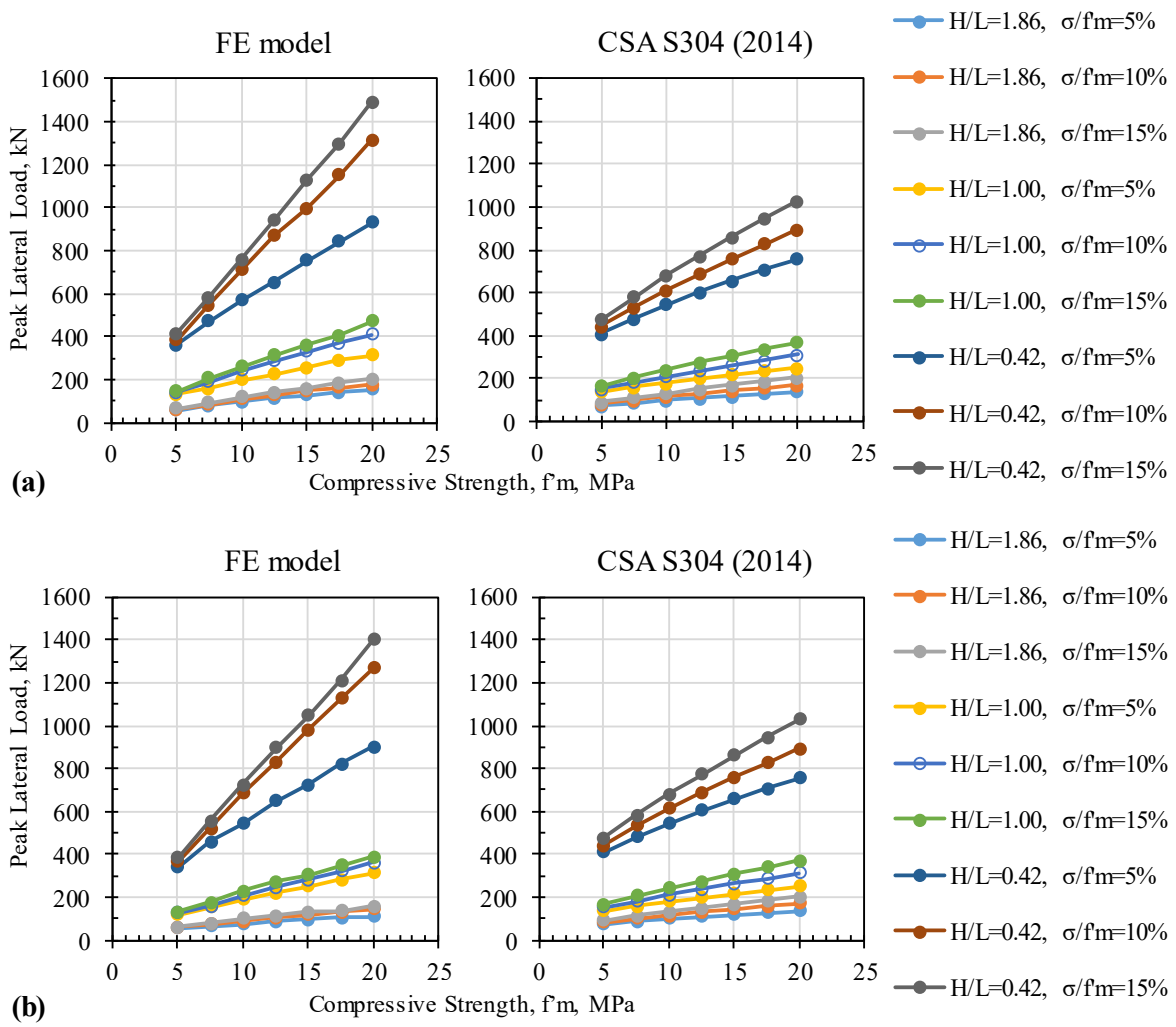

Figure 5.6 Effect of masonry compressive strength and axial stress on peak lateral load for (a) walls with bond beam and (b) walls with bed-joint where vertical and horizontal reinforcement ratio of 0.22% and 0.04%, respectively

According to Figure 5.6, the peak load generally exhibited an approximately linear trend with increasing compressive strength for both horizontal reinforcement types and for all H/L and σ/f'_m ratios. This finding aligns with experimental results reported by Meli et al. (1968), Matsumura (1988), and Shing et al. (1990). Furthermore, the trend of increasing peak lateral load was more pronounced in walls with lower aspect ratios than in walls with higher aspect ratios. This observation could be attributed to the dominant behaviour discrepancy between walls with lower and higher aspect ratios in terms of failure mode (shear or flexure), as reported by da Porto et al. (2009). Squat walls generally have a higher moment capacity due

to the deeper moment arm compared to slender walls where shear failure is more likely to occur. Consequently, increasing the compressive strength will increase the strength of compressive strut, which is responsible for the shear strength. Conversely, slender walls are vulnerable to failure in flexure, where increasing the compressive strength will not significantly contribute to the shear strength of such walls.

The effect of horizontal reinforcement type on the peak load was found to be insignificant across all compressive strength levels (5-20 MPa) and aspect ratios. This result is consistent with experimental findings by Tomaževič and Lutman (1988), Schultz (1996), Schultz et al. (1998), and Calderón et al. (2021a), who investigated walls with aspect ratios of 0.5, 1.0, and 2.3, all of which failed in diagonal shear and exhibited similar peak loads regardless of the horizontal reinforcement type or quantity.

Regarding the axial stress, it was noticed that the peak load is directly proportional to increasing the axial stress for both horizontal reinforcement types and all aspect ratios. This is in line with what has been reported by Drysdale and Hamid (2005), Voon and Ingham (2008), Haach (2009), Vasconcelos and Lourenço (2009), and Oan (2013). Similar to the effect of masonry compressive strength, the effect of axial stress on squat walls ($H/L \leq 1$) was more pronounced in contrast to slender walls. This was attributed to the governing failure mode (da Porto et al. 2009). As pointed out by Haach et al. (2011) and Dillon (2015), walls with no or little axial load are inclined to be flexurally-dominated and with increasing the axial stress, the moment capacity increases leading to facilitate the development of shear failure. In addition, the horizontal reinforcement type did not have a substantial effect on the peak load at all levels of axial stress and for all aspect ratios.

Figure 5.6 shows that the CSA S304-2014 equation underestimates the contribution of masonry compressive strength and axial stress, which is more visible with a lower aspect ratio and higher compressive strength and axial stress.

The analysis model also showed that there is a threshold to the increase in peak strength due to axial stress, as depicted in Figure 5.7. Beyond this threshold, the peak lateral load decreased due to a shift in failure mode to compression failure. This finding is consistent with the work

of Page (1989), as demonstrated in Figure 5.8. It was observed that this behaviour is applicable to both types of horizontal reinforcement.

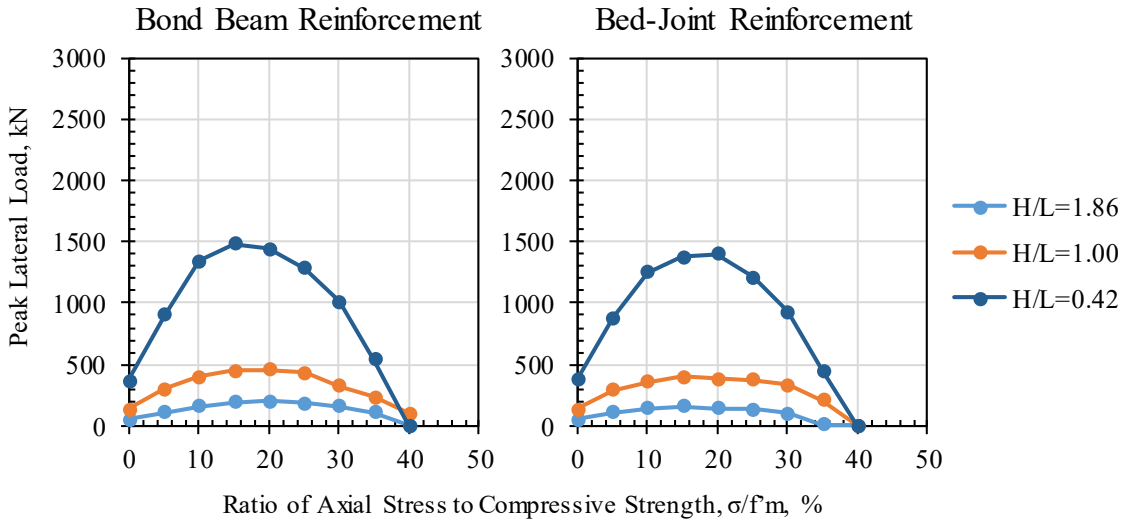

Figure 5.7 Interaction diagram between the peak lateral load and axial stress

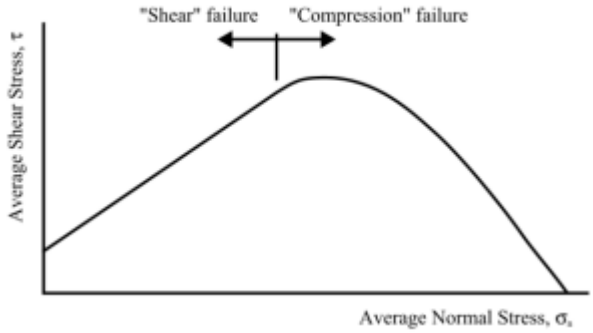

Figure 5.8 Relationship between average shear stress and average normal stress (adapted from Page 1989)

5.4.2.2 Effect of horizontal and vertical reinforcement ratio

Figures 5.9(a) and 5.9(b) depict the dependent peak load resulting from the variation of horizontal reinforcement ratio with different H/L and vertical reinforcement ratios for walls reinforced with either bond beam or bed-joint reinforcement, respectively. The wall models considered in Figure 5.9 have a masonry compressive strength of 20MPa and σ/f'_m ratio of 10%, selected for illustrative purposes. The variation in peak load results for different compressive strengths and axial stresses follow a similar trend as the displayed ones. The predictions of CSA S304 (2014) for diagonal shear capacity are also provided as a reference.

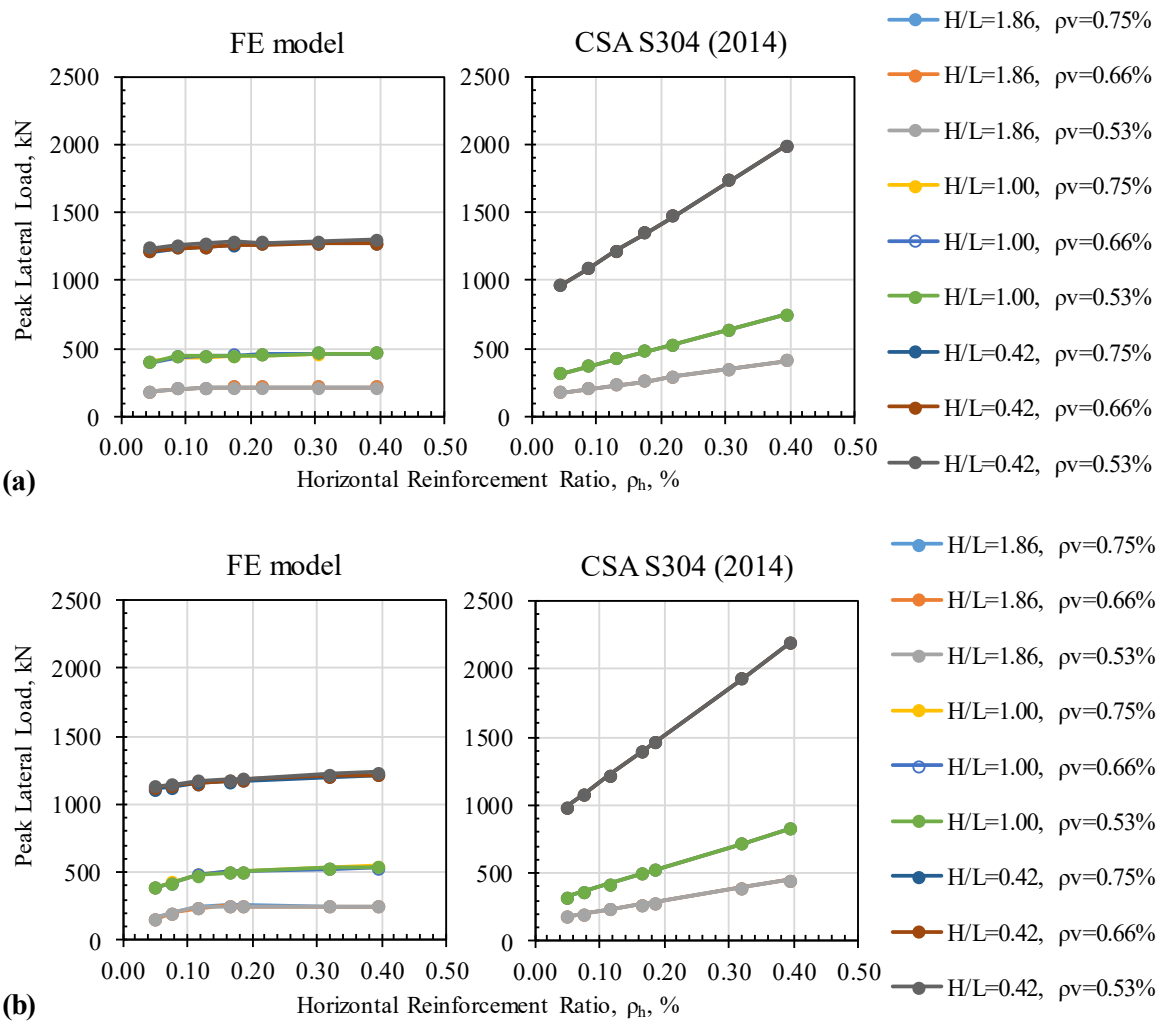

Figure 5.9 Effect of horizontal and vertical reinforcement ratio on peak lateral load for (a) walls with bond beam and (b) walls with bed-joint where masonry compressive strength and σ/f'_m ratio of 20 MPa and 10%, respectively

Figure 5.9 shows that increasing the horizontal reinforcement ratio did not significantly influence the peak shear strength for all H/L ratios and vertical reinforcement ratios, regardless of whether the wall was reinforced with bond beam or bed-joint (less than 10% increase). This finding is consistent with the observations of Maleki (2008) and Medeiros et al. (2020). While Maleki (2008) studied walls with an aspect ratio (H/L) of 1 and employed three horizontal reinforcement ratios (ρ_h) of 0.025, 0.05, and 0.1%, Medeiros et al. (2020) studied walls with aspect ratios (H/L) of 1.63, 1.24, 0.84, and 0.45 and used horizontal reinforcement ratios (ρ_h) of 0.048, 0.105, and 0.19%. All authors agreed that there is no significant change in the peak load due to the variation of the horizontal reinforcement ratio. Hassanli et al. (2014) provided

a plausible explanation for this phenomenon, suggesting that in highly reinforced walls, steel does not yield, and peak strength is determined by the development of major cracks that the force cannot pass through. As a result, shear strength does not improve as horizontal reinforcement is added beyond a certain limit. Based on that, Hassanli et al. (2014) and Dillon (2015) concluded that most shear strength equations, including CSA S304 (2014), overestimate the contribution of horizontal reinforcement. This overestimation is evident in the CSA S304 equation, as shown in Figure 5.9 for both horizontal reinforcement types. With respect to the horizontal reinforcement type, there was no substantial effect on the peak load at all horizontal and vertical reinforcement ratios. Similarly, the vertical reinforcement ratio did not add any significant contribution to the peak strength for wall models that failed predominantly in diagonal shear.

5.5 Approach to Improve the Accuracy of the CSA S304 Equation

Recent studies have shown that the design expressions in the CSA S304 standard used to predict the in-plane shear strength of PG walls may not be accurate or conservative for certain design scenarios (Haider 2007; Minaie et al. 2010; Nolph and ElGawady 2012; Hassanli and Elgawady 2013; Hassanli et al. 2014; Janaraj and Dhanasekar 2016; Izquierdo 2021; Izquierdo et al. 2022). The parametric study conducted in this study found that the prediction of the CSA S304 equation underestimated the contribution of compressive strength of masonry and axial stress while overestimating the contribution of horizontal reinforcement ratio. These findings highlight the need to reconsider the contributions of the current CSA S304 equation.

This study aims to improve the predictive accuracy of the CSA equation by updating its coefficients for different terms. The CSA S304 equation is used to calculate the unfactored in-plane shear resistance, as shown in Eq. (2). The left part of the equation is used to predict the diagonal shear capacity, while the right part is an upper limit to prevent the crushing of the compressive strut. The nomenclature used in this equation is expanded in the Notation list section.

$$\left(0.16\left(2-\frac{M_f}{V_f d_v}\right)\sqrt{f'_m}\,td_v+0.25\mathrm{P}\right)\gamma_g+0.6A_{h,bar}f_{yh}\frac{d_v}{s_h}\quad\leq 0.4\sqrt{f'_m}\,td_v\gamma_g \tag{2}$$

5.5.1. Database

In order to develop an analytical model for predicting the resistance of masonry walls, it is essential to consider the failure mode, as pointed out by Haach et al. (2011). Therefore, for this study, 195 experimental PG walls that failed in diagonal shear were selected from the literature (see Appendix C). Moreover, 247 PG wall models that were expected to fail in pure diagonal shear, as determined using the current CSA S304 equation (see Appendix D), were also included. Wall models that failed or were expected to fail due to flexure, mixed flexure-shear, or crushing of the compressive strut were excluded. It should be noted that the numerical walls developed in this study did not capture the post-peak response correctly in most cases, as previously mentioned. As a result, a total of 442 experimental and numerical walls were the database in this study.

To validate the updated coefficients of the CSA S304 equation [left part of Eq. (2)], 10% of the experimental and numerical walls were randomly set aside to be used later in examining the performance of the proposed equation and comparing it to the current one.

5.5.2. Regression Analysis

After performing a stepwise regression analysis on a dataset of 442 PG walls, including both experimental and numerical walls, an equation is proposed to predict the diagonal shear strength of PG walls. This equation is intended to resemble the parameters of CSA S304 [left part of Eq. (2)] and is presented in Eq. (3).

$$\left(0.20799\left(2-\frac{M_f}{V_f d_v}\right)\sqrt{f'_m}\,td_v+0.4694\mathrm{P}\right)\gamma_g+0.0608A_{h,bar}f_{yh}\frac{d_v}{s_h} \tag{3}$$

Compared to the original CSA S304 equation [left part of Eq. (2)], our proposed equation [Eq. (3)] shows a 30% increase in the contribution of masonry compressive strength and an 88% increase in axial stress contribution. This finding is consistent with the observations made in Section 5.4.2.1 when comparing the FE models and CSA S304 prediction results. Additionally, the contribution of horizontal reinforcement in Eq. (3) is reduced by a factor of ten when compared to Eq. (2). This highlights the need to reevaluate the horizontal reinforcement contribution, as previously discussed in Section 5.4.2.2, in light of the coefficient of 0.6 for this parameter in the current CSA S304 equation [left part of Eq. (2)].

5.5.3. Evaluation of the Predictive Power of the Proposed Equation

Various statistical measures, including Root Mean Squared Error (RMSE), Mean prediction Error (ME), mean, standard deviation, minimum, maximum, 5th percentile, and 95th percentile of the ratio of observed strength to the predicted strength (V_o/V_n), were used to assess the performance of the proposed equation [Eq. (3)], compared to the current CSA S304 equation [left part of Eq. (2)].

Root Mean Squared Error (RMSE) is a variance indicator expressing the precision of the prediction equation (Sheiner and Beal 1981). As the RMSE value is closer to zero, the error is lower. Mean prediction Error (ME) is a measure of bias, indicating the degree of accuracy of the prediction equation. ME value can be either positive or negative where the biased equation will have too positive or too negative ME value. If the fitted values tend to underestimate the observed values, the ME value is positive. A negative ME value, on the other hand, implies that the fitted values typically overestimate the observed values. A value of V_o/V_n of one indicates the ideal situation, where the equation predicts shear strength perfectly. A value of V_o/V_n greater than one indicates that the equation underpredicts the shear strength (conservative predictions), while a value less than one indicates that the equation overpredicts the shear strength (unconservative predictions). The 5th and 95th percentile are the lower and upper limits of 95% of the selected walls (total of 442 PG walls).

The performance of the proposed coefficients to the CSA S304 equation against the current equation is presented in Table 5.5 and depicted in Figure 5.10.

Table 5.5 Statistical performance of the diagonal shear capacity prediction

Model	RMSE	ME	V_o/V_n					
	(kN)	(kN)	Average	Std. dev.	Min.	Max.	5th	95th
Proposed Equation	72	0	1.08	0.391	0.59	4.31	0.75	1.82
CSA S304 (2014)	174	46	1.22	0.534	0.19	5.61	0.69	2.03

The results revealed that the proposed equation [Eq. (3)] performed significantly better than the current CSA S304 equation [left part of Eq. (2)] in terms of RMSE by 59% and ME by 99%. Both equations were on the conservative (safe) prediction side according to the average V_o/V_n value. However, the proposed equation was less conservative by 12%. Also, the higher

standard deviation that the current CSA S304 equation is commonly known for was reduced considerably by 27% when using the proposed equation. While the minimum of V_o/V_n was increased three times, the maximum of V_o/V_n was reduced by 23% when the proposed equation was used. This was reflected in the lower limit (5^{th} percentile) and upper limit (95^{th} percentile). As a result, all the predictions of the proposed equation were closer to the ideal V_o/V_n value of 1.

According to Figure 5.10, the proposed equation showed that the majority of the data points (239 out of 442 walls) were around the ideal scenario (V_o/V_n =1) by ±10%. In other words, the V_o/V_n value of 239 walls was in the range of [0.9-1.1]. Conversely, the current CSA S304 equation had limited data points (142 out of 442 walls). In addition, the proposed equation showed almost non-conservative (overestimated) predictions in contrast to the current equation. Experimental and numerical walls corresponding to ten percent of the database, selected randomly and not used in the training phase of the proposed equation, were used to examine the predictive ability of the model, as shown in Figure 5.11. It is seen that the proposed equation had a better performance compared to the current equation in the Canadian masonry standard.

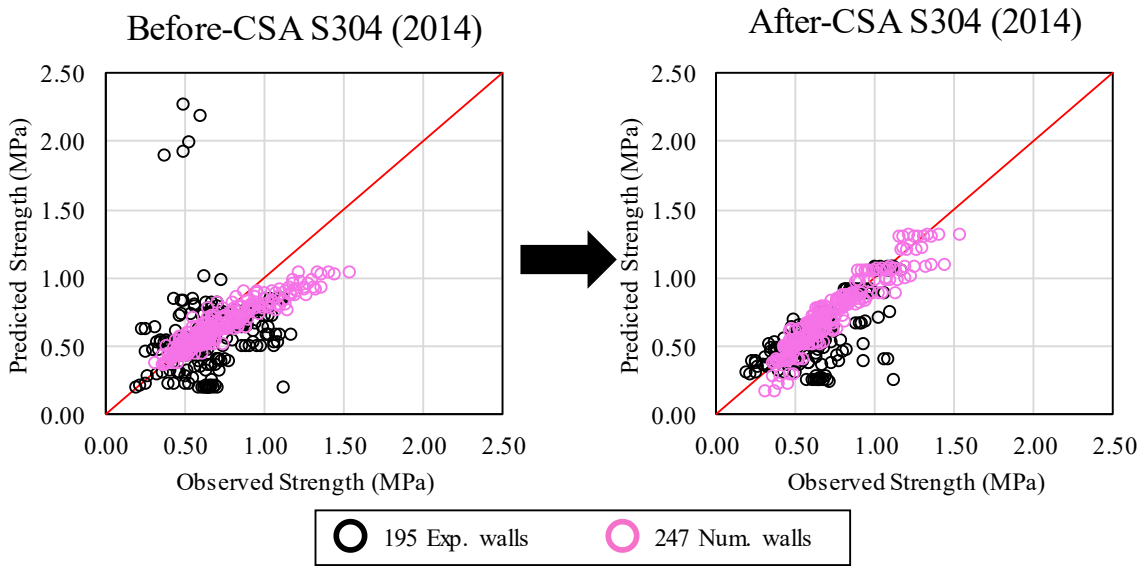

Figure 5.10 Performance of proposed coefficients of CSA S304 equation on 442 experimental and numerical walls

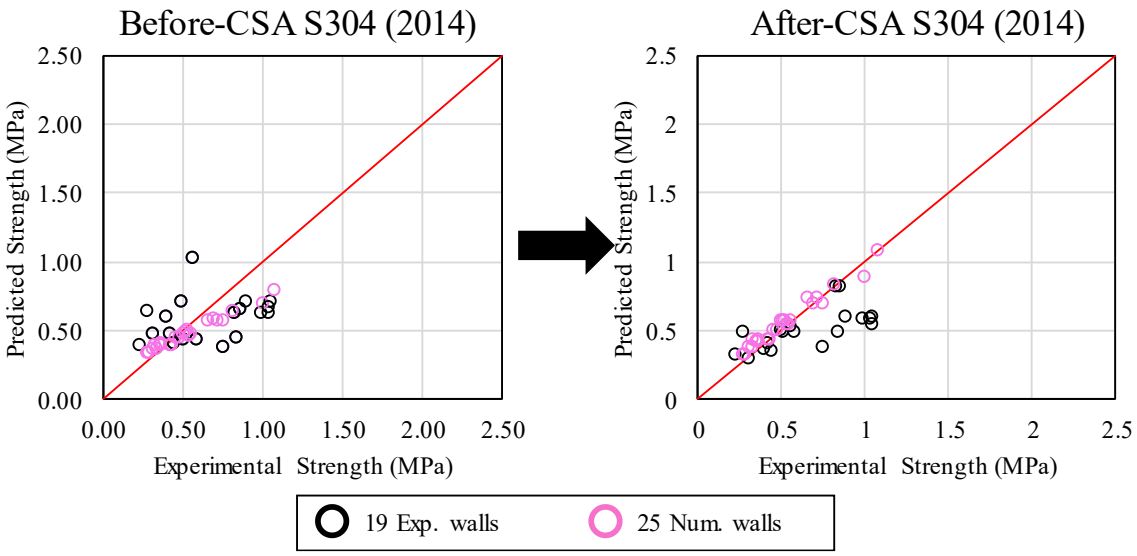

Figure 5.11 Validation results of the proposed coefficients of the current CSA S304 equation

5.6 Conclusions

This paper introduced the description of the FE macro-model and tested the model's accuracy against 9 PG walls sourced from different experimental studies. Furthermore, the study explored the maximum strength of PG walls by conducting a parametric study to determine how design parameters, commonly used in research-based and code-based equations, impacted their strength. This study analyzed 541 wall models that failed numerically in diagonal shear. From the findings, an approach to improve the precision of the existing CSA S304 equation that calculates diagonal in-plane shear strength was proposed. Consequently, the conclusions drawn from this paper are as follows:

- The developed FE macro-model was found to be in reasonable agreement with experimental results for both linear and non-linear responses of the load-displacement relationship up to the peak load. The model accurately predicted the peak load with an average error of 1.00 between the numerical and experimental results. One of the major advantages of this model is its validation with several walls from different sources with varying design parameters. This validation greatly strengthened the credibility of the developed model, allowing for conducting a reliable parametric study.

- The results of the parametric study showed that the compressive strength of masonry and axial stress are crucial factors that impact the shear strength of PG walls. The study found that even small changes in these parameters can have a significant effect on the shear strength of the wall models. This highlights the importance of accurately determining the contribution of compressive strength of masonry and axial stress when designing PG walls.
- There was no considerable effect of the variable amount of the horizontal and vertical reinforcement on the peak load. In particular, the negligible effect of the horizontal reinforcement amount on the shear strength raised concern about its contribution to current shear strength equations, including the CSA S304 equation.
- The stepwise regression analysis of 442 experimental and numerical walls identified coefficients that can significantly improve the precision and accuracy of the CSA S304 equation. The suggested coefficients improved the equation's precision by 59% as measured by RMSE and accuracy by 99% as measured by ME, based on the results. Moreover, the data dispersion around the average (standard deviation) was reduced by 27%, indicating a more reliable and consistent estimation of the diagonal in-plane shear strength of PG walls.

6. CONCLUSIONS AND RECOMMENDATIONS

6.1 Summary

6.1.1. Experimental Study

This part of the study described the experimental investigation of four full-scale PG masonry shear walls subjected to a combination of reversal cyclic lateral load and constant vertical load. Practical design details and actual practice construction were incorporated into the design and construction of the tested specimens. Hysteretic response, damage progression, peak strength, energy dissipation, and displacement ductility were utilized to investigate the effect of the variable design parameters considered in this study (aspect ratio and horizontal reinforcement type) on the resposne of PG walls against cyclic loading. In addition, shear strength expressions found in the North American codes equations were used to predict the shear strength of the tested walls that failed in shear and then validate their predictive ability against the experimental results. On the other hand, the general flexural analysis method was used to predict the flexural strength of walls that failed in flexure.

6.1.2. Analytical Study

This part of the study presented the definition of the FE macro-model and then evaluated the defined model against 9 PG walls from various experimental studies. After that, the shear strength of PG walls was investigated using a parametric study to see how the design parameters used in the majority of code- and research-based equations affect this strength. Based on the results of the parametric study on 541 wall models failed in diagonal shear, an approach was suggested to improve the accuracy of the current CSA S304 equation used to calculate the diagonal in-plane shear strength.

6.2 Conclusions

6.2.1. Experimental Study

From the experimental study, the following conclusions can be drawn:

- There is no apparent effect of the horizontal reinforcement type on the peak strength. Both are equally effective in providing peak strength when they are provided according to the engineering rules in the standards. However, the aspect ratio had a significant effect.
- Slender wall with bond beams showed less damage distribution than the slender wall with bed-joint reinforcement – this is because of the comparatively higher horizontal reinforcement provided and the excessive grouting. On the other hand, the squat wall with bond beams had three times the average crack's width than the squat wall with bed-joint reinforcement at the post peak load state due to the distribution of bed-joint reinforcement along the wall height.
- Bed-joint reinforcement demonstrated to be superior in controlling cracks' width in walls that failed in shear, specifically after reaching the peak load. On the other hand, the presence of grout in bond beams prevented the cracks from distributing evenly throughout the wall surface, particularly in the middle of the diagonal path of the wall.
- The study revealed that bed-joint reinforcement was a more effective option for enhancing the energy dissipation and displacement ductility of squat walls that have failed in diagonal shear. Specifically, it was found that the squat wall reinforced with bed-joint reinforcement showed a 45% increase in energy dissipation and a 16% increase in displacement ductility, compared to the squat wall reinforced with a bond beam. However, the horizontal reinforcement type did not have a significant impact on the energy dissipation or displacement ductility of slender walls, which were dominated by flexural behavior.
- The general flexural analysis accurately predicts the peak lateral load of the slender walls, which confirms that the flexural behaviour of PG walls can be comprehended with no complexity in contrast to the shear behaviour.
- Examination of CSA and TMS equations against the experimental results of squat walls revealed that Izquierdo's (2021) model was better at predicting shear strength.

In addition, a high difference in the contribution of the axial load, horizontal reinforcement, and upper limit was observed when comparing CSA and TMS equations. This inconsistency of CSA and TMS equations points out the necessity of revising the contribution of each parameter in the current equations and/or considering adding new parameters to improve the accuracy and the precisions of the revised equations in the next version of the masonry standard codes.

6.2.2. Analytical Study

As a result of all the above, we can draw the following conclusions:

- The developed model showed a reasonable agreement with experimental results in terms of the linear and non-linear response of the load-displacement relationship up to the peak load. The peak load was accurately predicted with an average of 1.00 between the experimental and numerical results. This developed model had the advantage of being validated with several walls from different sources and having variable design parameters, which in turn strengthened the credibility of the model to conduct a reliable parametric study.
- The validation process revealed that reporting the experimental value of JSSR (Joint Shear Strength Ratio) is crucial, as all validated walls had reported their experimental JSSR values. The significance of JSSR in predicting the general response of PG walls was further demonstrated by conducting a parametric analysis on an experimental wall that did not report the JSSR value.
- The validated developed model was used to investigate the effect of vertical reinforcement and axial loads on failure mode prediction for BB slender and BJ walls. The investigation found that increasing vertical reinforcement can change the failure mode from flexural or mixed shear-flexure to diagonal shear failure. The results indicated that BJ slender wall models need a vertical reinforcement ratio (ρ_v) greater than 0.09% to change the dominant failure mode, while BB slender wall models require a ρ_v greater than 0.22%. The study also found that increasing axial load can transform the failure mode from flexural or mixed shear-flexure to diagonal shear failure. The results showed that BJ slender wall models need a ratio of axial stress to

compressive strength (σ/f'_m) greater than 10% to shift the dominant failure mode, while BB slender wall models require a ratio of more than 15%.

- The validated developed mode also aimed to examine the accuracy of estimating the flexural strength and the diagonal shear strength of wall models generated from the developed model. The general flexural analysis method was used to estimate the flexural strength for wall models failed in flexure, and the CSA S304 equation was used to estimate the diagonal shear strength for wall models failed in diagonal shear. The results showed that the general flexural analysis method was able to accurately predict the flexural strength of the BB slender wall models. On the other hand, the CSA S304 equation was found to be conservative at higher levels of compressive strength and inconsistent in its estimation of the contribution of horizontal reinforcement for BB squat wall models. This study concludes that a parametric study is needed to understand the contribution of different parameters in the CSA S304 equation and suggest revisions for the next edition of the code.
- The results of the parametric study showed that the compressive strength of masonry and axial stress are crucial factors that impact the shear strength of PG walls. The study found that even small changes in these parameters can have a significant effect on the shear strength of the wall models. This highlights the importance of accurately determining the contribution of compressive strength of masonry and axial stress when designing PG walls.
- There was no considerable effect of the variable amount of the horizontal and vertical reinforcement on the peak load. In particular, the negligible effect of the horizontal reinforcement amount on the shear strength raised concern about its contribution to current shear strength equations, including the CSA S304 equation.
- The stepwise regression analysis of 442 experimental and numerical walls identified coefficients that can significantly improve the precision and accuracy of the CSA S304 equation. The suggested coefficients improved the equation's precision by 59% and accuracy by 99%, based on the results. Moreover, the data dispersion around the average was reduced by 27%, indicating a more reliable and consistent estimation of the diagonal in-plane shear strength of PG walls.

6.3 Recommendations and Future Research

Recommendations and suggestions have arisen on the research deck which some of them are listed as recommended future works.

6.3.1. Experimental Study

- Adding full-scale testing of slender walls (H/L=1.86) by decreasing the horizontal reinforcement ratio i.e. violating the standard code regulations. As a result, a complete conclusion on the slender wall response when it is a shear-dominated.
- Adding full-scale testing of walls having either vertical reinforcement or horizontal reinforcement to isolate the influence of the reinforcement contribution to the peak load.
- Comparing the effect of different boundary conditions (single curvature vs double curvature) on the PG walls behaviour is needed to be studied experimentally.
- Introducing smart strengthening materials to the PG walls and then conducting some testing to evaluate the improvement of the cyclic behaviour of such wall systems.

6.3.2. Analytical Study

- A universal definition of design parameters in all code- and research-based equations is recommended for implementation during the shear strength calculation so that consistent predictions can be determined by all interested researchers and practice engineers.
- More data points are suggested to add to the current database since it was found that the more data we train any proposed equation, the more precise and accurate equation we get.
- A distinction between PG and FG walls is suggested to be mandatory in masonry standard codes.
- The parametric analysis revealed the necessity to reconsider the current design parameters found in the CSA S304 equation used to calculate the diagonal shear strength.

- It is recommended to examine adding new or removing design parameters in the diagonal shear strength in a reasonable way for the purpose of developing the most precise and accurate predictive equation.

REFERENCES

Aguilar, V., Sandoval, C., Adam, J. M., Garzón-Roca, J., and Valdebenito, G. (2016). "Prediction of the shear strength of reinforced masonry walls using a large experimental database and artificial neural networks." *Structure and Infrastructure Engineering*, 12(12), 1661–1674.

Ahmadi, F., Hernández, J., Sherman, J., Kapoi, C., Klingner, R. E., and McLean, D. I. (2014). "Seismic performance of cantilever-reinforced concrete masonry shear walls." J. Struct. Eng., 10.1061/(ASCE)ST .1943-541X.0000941, 04014051.

Akkaya, Y., Guner, S. and Vecchio, F. J., (2013). "Modeling hysteretic response of reinforcing bars including buckling in reinforced concrete members"

Al-Ahdal, A., Aly, N., and Galal, K. (2022). "Simplified analytical models for partially grouted reinforced masonry shear walls." *Engineering Structures*, Elsevier Ltd, 252(December 2021), 113643.

Araya-letelier, G., Calderón, S., Sandoval, C., Sanhueza, M., and Murcia-delso, J. (2019). "Fragility functions for partially-grouted masonry shear walls with bed-joint reinforcement." *Engineering Structures*, Elsevier, 191(January), 206–218.

Arnau, O., Sandoval, C., and Murià-Vila, D. (2015). "Determination and validation of input parameters for detailed micro-modelling of partially grouted reinforced masonry walls." *Proceedings of the Tenth Pacific Conference on Earthquake Engineering*, Sydney, Australia, (110).

ASTM A615. (2014). *Standard Specification for Deformed and Plain Carbon-Steel Bars for Concrete Reinforcement*. ASTM.

ASTM A951. (2000). *Standard Specification for Masonry Joint Reinforcement*.

Baenziger, G., and Porter, M. L. (2011). "Joint reinforcement for masonry shear walls." *11th North American Masonry Conference*, Minneapolis, MN, USA.

Banting, B. (2013). "Seismic Performance Quantification of Concrete Block Masonry Structural Walls with Confined Boundary Elements and Development of the Normal Strain- adjusted Shear Strength Expression (NSSSE)." McMaster University ©.

Banting, B. R., and El-Dakhakhni, W. W. (2012). “Force- and Displacement-Based Seismic Performance Parameters for Reinforced Masonry Structural Walls with Boundary Elements.” *Journal of Structural Engineering*, 138(12), 1477–1491.

Banting, B. R., and El-Dakhakhni, W. W. (2014). “Seismic Performance Quantification of Reinforced Masonry Structural Walls with Boundary Elements.” *Journal of Structural Engineering*, 140(5).

Bentz, E. C., Vecchio, F. J., and Collins, M. P. (2006). “Simplified Modified Compression Field Theory for Calculating Shear Strength of Reinforced Concrete Elements.” ACI Structural Journal, 103(4), 614–624.

Bolaños, P. AR. (2020) “Analisis De Fragilidad Sismica De Edificaciones De Albañileria Armada.” Pontificia Universidad Catolica De Chile Escuela De Ingenieria.

Bolhassani, M., Hamid, A. A., Johnson, C., and Schultz, A. E. (2016a). “Shear strength expression for partially grouted masonry walls.” *Engineering Structures*, Elsevier Ltd, 127, 475–494.

Bolhassani, M., Hamid, A., and Moon, F. (2016b). “Enhancement of lateral in-plane capacity of partially grouted concrete masonry shear walls.” *Engineering Structures*, Elsevier Ltd, 108, 59–76.

BS EN 1052-1:1999. (1999). *Methods of test for masonry Ð Part 1: Determination of compressive strength*. *European Committee for standardization*, BSI.

Calderón, S., Sandoval, C., and Arnau, O. (2017). “Shear response of partially-grouted reinforced masonry walls with a central opening: Testing and detailed micro-modelling.” *Materials and Design*, Elsevier Ltd, 118, 122–137.

Calderón, S., Vargas, L., Sandoval, C., and Araya-Letelier, G. (2020). “Behavior of Partially Grouted Concrete Masonry Walls under Quasi-Static Cyclic Lateral Loading.” Materials, 13(10), 2424.

Calderón, S., Sandoval, C., Araya-Letelier, G., Inzunza, E., and Milani, G. (2021a). “Quasi-static testing of concrete masonry shear walls with different horizontal reinforcement schemes.” *Journal of Building Engineering*, 38(June 2021), 102201.

Calderón, S., Sandoval, C., Milani, G., and Arnau, O. (2021b). “Detailed micro-modeling of

partially grouted reinforced masonry shear walls : extended validation and parametric study." *Archives of Civil and Mechanical Engineering*, Springer London, 21(3), 1–24.

Cardenas, A. E., and Magura, D. D. (1973). "Strength of High-Rise Shear Walls-Rectangular Cross Section, Response of Multistory Concrete Structures to Lateral Forces." ACI STRUCTURAL JOURNAL, SP-36, 119–150.

Clough, R. W., and Penzien, J. (2003). *Dynamics of structures*. *Computers & Structures, Inc.*

CSA A23.1:19. (2019). Concrete materials and methods of concrete construction/Test methods and standard practices for concrete. CSA Group.

CSA S304-14. (2014). Design of masonry structures. CSA Group.

CSA 165-14. (2014). *CSA Standards on concrete masonry units*. CSA Group.

CSA A179-14. (2014). *Mortar and grout for unit masonry*. CSA Group.

Da Porto, F., Mosele, F. and Modena, C., 2009. Reinforced Clay Masonry Walls Under Shear Compression Loads: Experimental Behaviour. Proceedings, 11th Canadian Masonry Symposium, Toronto, Canada, pp. 39-48.

Dastfan, M., and Driver, R. G. (2015). "Large scale test of a modular steel plate shear wall with partially encased composite columns." *Journal of Structural Engineering*, 2(142).

Dhanasekar, M. (2011). "Shear in Reinforced and Unreinforced Masonry: Response, Design and Construction." *Procedia Engineering*, Elsevier B.V., 14, 2069–2076.

Dillon, P. (2015). "Shear Strength Prediction Methods for Grouted Masonry Shear Walls." Brigham Young University.

Dillon, P., and Fonseca, F. S. (2017). "Uncertainty in partially grouted masonry shear strength predictions." *13th Canadian Masonry Symposium*, Halifax.

Drysdale, R. G., and Hamid, A. A. (2005). *Masonry Structures Behaviour and Design*. Canada Masonry Design Centre, Mississauga, Ontario.

Elmapruk, J., ElGawady, M. A., and Hassanli, R. (2020). "Experimental and Analytical Study on the Shear-Strength of Partially Grouted Masonry Walls." *Journal of Structural Engineering*, 146(8), 04020147.

Elmeligy, O., Aly, N., and Galal, K. (2021). “Sensitivity analysis of the numerical simulations of partially grouted reinforced masonry shear walls.” *Engineering Structures*, Elsevier Ltd, 245(August), 112876.

EN 1052-3. (2002). *Methods of Test for Masonry Part3: Determination of Initial Shear Strength*. CEN.

Facconi, L. (2012). “Fiber Reinforced Concrete and Mortar for Enhanced Structural Universita ’ Degli Studi Di Brescia Luca Facconi Fiber Reinforced Concrete And Mortar For Enhanced Structural Elements And Structural Repair Of.” Universita’ Degli Studi Di Brescia.

Facconi, L., Plizzari, G., and Vecchio, F. (2013). “Disturbed stress field model for unreinforced masonry.” *Journal of Structural Engineering*, 140(4), 1–11.

Fattal, S. G. (1993). "The effect of critical parameters on the behavior of partially-grouted masonry shear walls under lateral loads". (NISTIR 5116), National Institute of Standards and Technology.

FEMA 461. (2007). *Interim Testing Protocols for Determining the Seismic Performance Characteristics of Structural and Nonstructural Components*. Redwood City, California.

Griffiths, D. (1994). “Stiffness matrix of the four-node quadrilateral element in closed form.” *International Journal for Numerical Methods in Engineering*, 37, 1027–1038.

Haach, V. G. (2009). “Development of a design method for reinforced masonry subjected to in-plane loading based on experimental and numerical analysis.” University of Minho.

Haach, V. G., Vasconcelos, G., and Lourenço, P. B. (2010). “Experimental Analysis of Reinforced Concrete Block Masonry Walls Subjected to In-Plane Cyclic Loading.” *Journal of Structural Engineering*, 136(4), 452–462.

Haach, V. G., Vasconcelos, G., and Lourenço, P. B. (2011). “Parametrical study of masonry walls subjected to in-plane loading through numerical modeling.” *Engineering Structures*, Elsevier Ltd, 33(4), 1377–1389.

Haider, W. (2007). “Inplane Response of Wide Spaced Reinforced Masonry Shear Walls.” Central Queensland University Australia.

Hamedzadeh, A. (2013). On the shear strength of partially grouted concrete masonry. [Master's thesis, University of Calgary]. http://dx.doi.org/10.11575/PRISM/27195.

Hassanli, R., and Elgawady, M. A. (2013). "The accuracy of in-plane shear strength of PGM walls in different international standards." *12th Canadian Masonry Symposium*, Vancouver, British Columbia, Canada.

Hassanli, R., Elgawady, M. A., and Mills, J. E. (2014). "An Evaluation of Design Code Expressions for Estimating in-plane Shear Strength of Partially Grouted Masonry Walls." *Australian Journal of Structural Engineering*, Vol 15 No, 299–320.

Hatzinikolas, M., Korany, Y., and Brzev, S. (2015). *Masonry Design FOR ENGINEERS AND ARCHITECTS*. Canadian Masonry Publications, Edmonton, Alberta.

Hidalgo, P., and Luders, C. (1986). "Shear strength of reinforced masonry walls under earthquake excitation." *Proc., 3rd U.S. National Conf. on Earthquake Engineering*, Earthquake Engineering Research Institute, Oakland, CA, 1335–1346.

Hoque, N. (2013). "In-Plane Cyclic Testing of Reinforced Concrete Masonry Walls to Assess the Effect of Varying Reinforcement Anchorage and Boundary Conditions." University of Calgary.

Hordijk, D. A. (1992). Tensile and tensile fatigue behaviour of concrete; experiments, modelling and analyses. *Heron, 37*(1).

Hoshikuma, J., Kawashima, K., Nagaya, K. and Taylor, A.W., 1997. "Stress-Strain Model for Confined Reinforced Concrete in Bridge Piers", ASCE Journal of Structural Engineering, Vol. 123, No. 5, pp. 624-633.

Hung, J. R. (2018). "Artificial Neural Network Model for Analysis of In-Plane Shear Strength of Partially Grouted Masonry Shear Walls." *Master Thesis*, University of Alberta.

International Masonry Institute. (2011). "Masonry Detailing Series." <www.imiweb.org>.

Izquierdo, K. (2021). "Statistical Prediction Methods for the In-Plane Shear Strength of Partially Grouted Masonry Walls." University of Alberta.

Janaraj, T. (2014). "Studies on the In-Plane Shear Response of Confined Masonry Shear Walls." Queensland University of Technology.

Janaraj, T., and Dhanasekar, M. (2016). “Studies on the existing in-plane shear equations of partially grouted reinforced masonry.” *Australian Journal of Structural Engineering*, Taylor & Francis, 17(3), 180–187.

Kaminsono, T. et al., 1988. Experimental Study on Seismic Performance of Reinforced Masonry Walls. Proceedings, 9th World Conference of Earthquake Engineering, Tokyo, Japan, pp. 109- 114.

Kasparik, T., Tait, M. J., and El-Dakhakhni, W. W. (2014). “Seismic performance assessment of partially grouted, nominally reinforced concrete-masonry structural walls using shake table testing.” Journal of Performance of Constructed Facilities, 28(2), 216–227.

Long, L. M. (2006). “Behaviour of Half-scale Reinforced Concrete Masonry Shear Walls.” McMaster University.

Lourenço, P., Rots, J., and Blaauwendraad, J. (1995). “Two approaches for the analysis of masonry structures: micro and macro-modeling.” *Heron (Delft)*.

Lourenço, P. B. (2002). “Computations on historic masonry structures.” *Progress in Structural Engineering and Materials*, 4(3), 301–319.

Mahmood, T., Gheni, A. A., and ElGawady, M. (2021). “In-Plane Seismic Behavior of Special Reinforced Fully Grouted Masonry Shear Walls Subjected to High Axial Loads.” *14th Canadian Masonry Symposium*, Montreal, Canada.

Maleki, M. (2008). “Behaviour of partially grouted masonry shear walls under cyclic reversed loading.” McMaster University.

Matsumura, A. (1988). “Shear strength of reinforced masonry walls.” 9th Worrld Conference of Earthquake Engineering.

Mayes, R. L., Omote, Y., and Clough, R. W. (1976). *Cyclic shear tests on masonry piers, Volume 1: Test Results*. *Rep. No. UCB/EERC-76-8, Earthquake Engineering Research Center, Univ. of California, Berkeley, CA*.

Medeiros, K. A. S., Chavez, K. H., Fonseca, F. S., Parsekian, G. A., and Shrive, N. G. (2020). “Parametric study of multi-story, perforated, partially grouted masonry walls subjected to in-plane cyclic actions.” *Canadian Journal of Civil Engineering*, 1055(August 2020),

1046–1055.

Medeiros, K. A. S., Parsekian, G. A., Shrive, N. G., and Fonseca, F. S. (2022). “Shear load capacity prediction of unperforated and perforated partially grouted masonry walls.” *Engineering Structures*, Elsevier Ltd, 256(December 2021), 113927.

Meli, R., Wolff, A. Z., and Esteve, L. (1968). “Comportamiento de muros de mampostería hueca ante carga lateral alternada.” *Revista ingeniera*, 38(3), 371–390.

Minaie, E. (2009). “Behavior and vulnerability of reinforced masonry shear walls.” Drexel University.

Minaie, E., Mota, M., Moon, F. L., and Hamid, A. A. (2010). “In-Plane Behavior of Partially Grouted Reinforced Concrete Masonry Shear Walls.” *Journal of Structural Engineering*, 136(9), 1089–1097.

Minaie, E., Moon, F. L., and Hamid, A. A. (2014). “Nonlinear finite element modeling of reinforced masonry shear walls for bidirectional loading response.” *Finite Elements in Analysis and Design*, Elsevier, 84, 44–53.

Mobeen, S. S. (2002). “Cyclic Tests of Shear Walls Confined with Double Head Studs.” University of Alberta.

Moghimi, H. (2013). “Steel Plate Shear Walls for Low and Moderate Seismic Regions and Industrial Plants Structural Engineering Department of Civil and Environmental Engineering.” University of Alberta.

NBCC. (2022). “National Building Code of Canada: 2020.” National Research Council of Canada.

Nolph, S. (2010). “In-Plane Shear Performance of partially Grouted Masonry Shear Walls.” Washington State University.

Nolph, S. M., and ElGawady, M. A. (2012). “Static Cyclic Response of Partially Grouted Masonry Shear Walls.” *Journal of Structural Engineering*, 138(7), 864–879.

Nonis, C., Niezrecki, C., Yu, T., Ahmed, S., Su, C., and Schmidt, T. (2013). “Structural Health Monitoring of Bridges using Digital Image Correlation Structural Health Monitoring of Bridges using Digital Image Correlation.” *The International Society for Optical*

Engineering, San Diego, CA, United States.

Oan, A. F. (2013). Diagonal shear of partially grouted concrete masonry panels. [Doctoral dissertation, University of Calgary].

Park, R. (1988). "Ductility Evaluation from Laboratory and Analytical Testing." *Ninth World Conf. Earthq. Eng.*, Tokyo-Kyoto, Japan, 605–616.

Paulay, T., and Priestly, M. J. N. (1992). Seismic Design of Reinforced Concrete and Masonry Buildings. John Wiley & Sons, Inc., Hoboken, NJ, USA.

Ramírez, P., Sandoval, C., and Almazán, J. L. (2016). "Experimental study on in-plane cyclic response of partially grouted reinforced concrete masonry shear walls." *Engineering Structures*, 126, 598–617.

Rizaee, S. (2015). Assessing bond beam horizontal reinforcement efficacy with different end anchorage conditions in concrete block masonry shear walls. [Master's thesis, University of Calgary].

Rizaee, S., Lissel, S., and Shrive, N. G. (2021). "The effect of the amount, distribution, and end anchorage conditions of bond beam reinforcement on the behaviour of concrete masonry shear walls." *Canadian Science Publishing*, 1600(November 2020), 1583–1600.

Sadeghian, V., and Vecchio, F. J. (2018). "The Modified Compression Field Theory: Then and Now." *SP-328: Shear in Structural Concrete*, American Concrete Institute, 1–20.

Sandoval C, Arnau O. (2017). "Experimental characterization and detailed micro-modeling of multi-perforated clay brick masonry structural response." Mater Struct., 50:34

Sandoval, C., Calderón, S., and Almazán, J. L. (2018). "Experimental cyclic response assessment of partially grouted reinforced clay brick masonry walls." *Bulletin of Earthquake Engineering*, 16(7), 3127–3152.

Sarhat, S. R., and Sherwood, E. G. (2015). "he Size Effect in Reinforced Masonry." 12th North American Masonry Conference, Denver, Colorado May 17 – 20, 2015.

Schultz, A. E. (1994). "NIST Research Program on the Seismic Resistance of Partially-

Grouted Masonry Shear Walls (NISTIR 5481)."

Schultz, A. E. (1996). "Seismic performance of partially-grouted masonry shear walls." *Proceedings of Eleventh World Conference on Earthquake Engineering*, Sociedad Mexicana de Ingeniería Sísmica, Mexico.

Schultz, A. E., Hutchinson, R. S., and Cheok, G. C. (1998). "Seismic performance of masonry walls with bed joint reinforcement." *Structural Engineers World Congress*, Elseviwe Science Ltd.

Schultz, A. E., and Johnson, C. A. (2019). "Seismic Resistance Mechanisms in Partially Grouted Shear Walls with New Design Details." *Proceedings of the Thirteenth North American Masonry Conference*, TMS, Salt Lake City, UT, USA, 1274–1286.

Seif ElDin, H. M. (2016). "In-Plane Shear Behaviour of Fully Grouted Reinforced Masonry Shear Walls." Concordia University.

Seif ElDin, H. M. S., & Galal, K. (2018). Effect of reinforcement anchorage end detail and spacing on seismic performance of masonry shear walls. Engineering Structures, 157, 268-279.

Shedid, M. T., Drysdale, R. G., and El-Dakhakhni, W. W. (2008). "Behavior of Fully Grouted Reinforced Concrete Masonry Shear Walls Failing in Flexure: Experimental Results." Journal of Structural Engineering, 134(11), 1754–1767.

Sheiner, L. B., and Beal, S. L. (1981). "Some suggestions for measuring predictive performance." *Journal of Pharmacokinetics and Biopharmaceutics*, 9(4), 503–512.

Shing, P. B., Noland, J. L., Klamerus, E., and Spaeh, H. (1989). "Inelastic Behavior of Concrete Masonry Shear Walls." *Journal of Structural Engineering*, 115(9), 2204–2225.

Shing, P. B., Schuller, M., and Hoskere, V. S. (1990). "In-Plane Resistance of Reinforced Masonry Shear Walls." *Journal of Structural Engineering*, 116(3), 619–640.

Stathis, O., Fischer, O., and Lissel, S. L. (2018). "Effects of horizontal reinforcement distribution on in-plane performance and post-peak behaviour of masonry shear walls." 10th Australian Masonry Conference, SYDNEY AUSTRALIA, 467–478.

Sveinsson, B. I., McNiven, H. D., and Sucuoglu, H. (1985). Cyclic loading tests of masonry

single piers - Volume 4: Additional tests with height to width ratio of 1. University of California.

TMS 402. (2016). *Building Code Requirements and Specification for Masonry Structures*. *The Masonry Society*.

Tolou-kian, M. J., and Cruz-noguez, C. (2022). "Performance design of reinforced concrete shear walls detailed with self-centering reinforcement." *Engineering Structures*, Elsevier Ltd, 252(December 2021), 113533.

Tomaževič, M., and Lutman, M. (1988). "Seismic resistance of reinforced masonry walls." *Proceedings of Ninth World Conference on Earthquake Engineering*, Tokyo-Kyoto, Japan, 97–102.

Tomaževič, M., and Velechovsky, T. (1992). "Some aspects of testing small-scale masonry building models on simple earthquake simulators." *Earthquake Engineering & Structural Dynamics*, 21(11), 945–963.

Tomaževič, M., Lutman, M., and Petković, L. (1996). "Seismic Behavior of Masonry Walls: Experimental Simulation." *Journal of Structural Engineering*, 122(9), 1040–1047.

Tomaževič, M. (1999). Earthquake resistant design of masonry buildings. Advances in Indian Earthquake Engineering and Seismology: Contributions in Honour of Jai Krishna, Imperial College Press.

Vasconcelos, G., and Lourenço, P. B. (2009). "In-Plane Experimental Behavior of Stone Masonry Walls under Cyclic Loading." *Journal of Structural Engineering*, 135(10), 1269–1277.

Vecchio, F. J., and Collins, M. P. (1986). "Modified Compression-Field Theory for Reinforced Concrete Elements Subjected To Shear." *Journal of the American Concrete Institute*, 83(2), 219–231.

Vecchio, F. J. (2000). "Disturbed stress field model for reinforced concrete: Formulation." *Journal of structural engineering New York, N.Y.*

Vecchio, F. J. (2001). "Disturbed stress field model for reinforced concrete: implementation." *Journal of structural engineering New York, N.Y.*

VecTor Analysis Group. (2019). “VecTor2-software-release 4.3.” University of Toronto.

Voon, K. C., and Ingham, J. M. (2006). "Experimental in-plane shear strength investigation of reinforced concrete masonry walls". Journal of Structural Engineering, 132(3), 400–408. https://doi.org/10.1061/(ASCE)0733-9445(2006)132:3(400)

Voon, K. C. (2007). “In-plane Seismic Design of Concrete Masonry Structures.” The University of Auckland.

Voon, K. C., and Ingham, J. M. (2007). “Design Expression for the In-Plane Shear Strength of Reinforced Concrete Masonry.” *Journal of Structural Engineering*, 133(5), 706–713.

Voon, K. C., and Ingham, J. M. (2008). “Experimental In-Plane Strength Investigation of Reinforced Concrete Masonry Walls with Openings.” *Journal of Structural Engineering*, 134(5), 758–768.

Wierzbicki, J. C. (2010). “Behaviour of Reduced-Scale Fully-Grouted Concrete Block Shear Walls.” McMaster University.

Wong, P. S., Vecchio, F. J., and Trommels, H. (2013). *VECTOR2 & FORMWORKS USER’S MANUAL*. University of Toronto, Toronto, ON.

Yancey, C. W. C., and Scribner, C. F. (1989). *Influence of horizontal reinforcement on shear resistance of concrete block masonry walls (NISTIR 4202)*. Gaithersburg, MD, USA.

Zhou, C., and Vecchio, F. J. (2006). “Closed-Form Stiffness Matrix for the Four-Node Quadrilateral Element with a Fully Populated Material Stiffness.” *Journal of Engineering Mechanics*, 1392–1395.

Zohrehheydariha, J., Das, S., and Banting, B. (2017). “Behaviour of Stack Pattern Masonry Beams.” *13th Canadian Masonry Symposium*, Canada Masonry Design Centre, Halifax, Canada.

APPENDIX A: MATERIALS CHARACTERIZATION, AND FULL-SCALE TESTING DESCRIPTION

A.1. Material Characterization

As we know masonry wall is a composite structure consists of different materials having its own properties. Therefore, a clear description of these properties is presented in order to have a better understanding of the structural behaviour of the masonry wall specimens. This description often needs to perform supplementary tests to extract some properties which are highlighted hereafter.

A.1.1. Compressive Test for Standard Blocks

Five samples of 20cm-hollow concrete masonry units CMUs were tested according to CSA 165-14 (2014) to obtain the uniaxial compressive strength. The dimensions of the sample is shown in Figure A.1. Samples were tested between two plates of steel with 50 mm of thickness to ensure an even distribution of vertical loads and avoid flexural effects of the steel plate. Tests were carried out under displacement control by means of a vertical LVDT connected to the actuator at a rate of 5 μ_m/s. Results revealed that the compressive strength of masonry block unit is 19 MPa. Table A.1 shows the results of the compressive test for standard block.

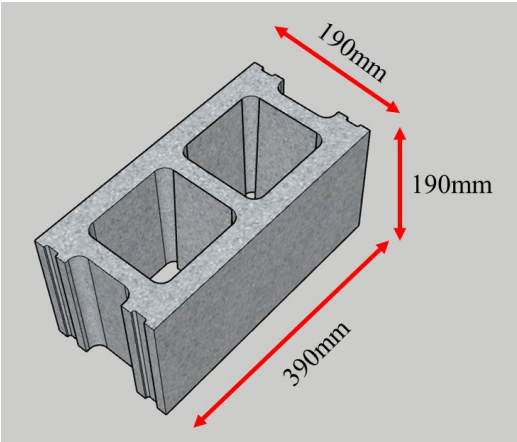

Figure A.1 Dimensions of Standard Block

Table A.1 Results of compressive test for CMU

Specimen	Peak Axial Load (kN)	Compressive Strength (MPa)
1	518	21
2	428	17
3	478	19
4	475	19
5	467	19
Average		19

A.1.2. Compressive Test for Mortar Cubes

The type-S mortar used for masonry joints was tested according to CSA A179-14 (2014). Six 50 mm mortar cubes were sampled from the same batch, used to build the wall panels. The dimensions of the sample is shown in Figure A.2. This test is used to obtain the compressive strength of mortar. Results revealed that the compressive strength of mortar is 14.8 MPa. Table A.2 shows the results of the compressive test for mortar cubes.

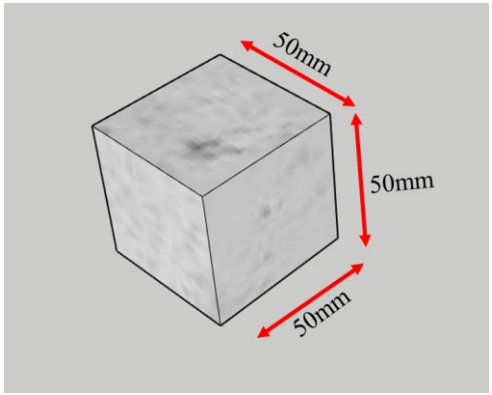

Figure A.2 Dimensions of Mortar cubes

Table A.2 Results of compressive test for mortar cubes

Specimen	Peak Axial Load (kN)	Compressive Strength (MPa)
1	45	18
2	30	11
3	40	16
4	31	12
5	38	15
6	44	17
Average		14.8

A.1.3. Compressive Test for Grout Cylinders

The grout used to fill the vertical cells where vertical rebars placed and the bond beams were tested according to CSA A179-14 (2014). Five cylinders of grout were taken from the same mix, used to build the wall panels. The dimensions of the sample is shown in Figure A.3. This test is used to obtain the compressive strength of grout. Results revealed that the compressive strength of grout is 30.6 MPa. Table A.3 shows the results of the compressive test for grout cylinders.

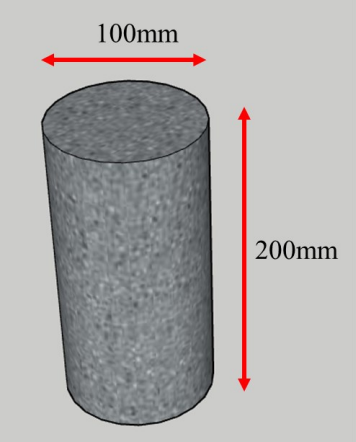

Figure A.3 Dimensions of Grout cylinders

Table A.3 Results of compressive test for grout cylinders

Specimen	Peak Axial Load (kN)	Compressive Strength (MPa)
1	250	31
2	268	33
3	244	30
4	264	33
5	216	27
6	250	31
Average		30.6

A.1.4. Reinforcement

Two reinforcement were used in this experimental program; Grade 400 steel rebars and the Standard: 9 Gauge Side Rods x 9 Gauge Cross Rods with 3.7mm diameter.

Grade 400 steel rebars of 10M (11.3 mm) and 15M (16.2 mm) were used to reinforce the wall panels horizontally and vertically, respectively. Rebar tension test were carried out on 3 samples of 15M and 3 samples of 10M as shown in Figure A.4. The average yield strength of three 10M and three 15M bars were 521 MPa and 455 MPa, respectively. Tables A.4 and A.5 show the results of the rebar tension test of 10M and 15M, respectively.

Figure A.4 Rebar tension test

Table A.4 Steel rebar properties of 10M

Specimen	Yield Strength (MPa)	Elastic Modulus (MPa)	Ultimate Strength (MPa)	Ultimate Strain (m/m)x10^{-3}
1	527	208871	646	90
2	517	211916	641	141
3	520	206180	643	213
Average	521	208989	643	148

Table A.5 Steel rebar properties of 15M

Specimen	Yield Strength (MPa)	Elastic Modulus (MPa)	Ultimate Strength (MPa)	Ultimate Strain (m/m)x10^{-3}
1	456	193016	676	240
2	456	180335	678	131
3	452	193529	684	105
Average	455	188960	679	159

The Standard: 9 Gauge Side Rods x 9 Gauge Cross Rods with 3.7mm diameter, used as a bed-joint reinforcement, were tested to obtain the yield strength. Rebar tension test were carried out on 4 samples. Tension tests were made on individual wires cut from the finished product and tested either across or between the welds. The average yield strength was 617 MPa. Table A.6 shows the results of the tension test of bed-joint reinforcement.

Table A.6 Bed-joint reinforcement properties

Specimen	Yield Strength (MPa)	Elastic Modulus (MPa)	Ultimate Strength (MPa)	Ultimate Strain (m/m)x10^{-3}
1	639	384774	659	18
2	617	341432	648	19
3	601	340413	609	19
4	610	291014	652	22
Average	617	339408	642	19.5

A.1.5. Compressive Test for Masonry (Prism test)

Response of masonry walls subjected to pure compression force is needed for numerical analysis and obtaining the applied axial load for the full-scale cyclic test. Therefore, six 5-course prisms, where three of them were un-grouted while the others were grouted, were built (Figure A.5) and then were tested under uniaxial compression force to get the compressive strength of the masonry according to CSA S304-14 (2014) and BS EN 1052-1:1999 (1999). Results revealed that the average un-grouted and grouted compressive strengths were 22.0 MPa and 16.4 MPa, respectively. Consequently, the weighted masonry compressive strength was 20.5MPa. Tables A.7 and A.8 show the results of the compressive test for ungrouted and grouted prisms, respectively.

Figure A.5 Construction of prisms

Table A.7 Results of compressive test for ungrouted prism

Specimen	Peak Axial Load (kN)	Compressive Strength (MPa)
1	1300	25
2	913	18
3	1231	24
Average		22

Table A.8 Results of compressive test for grouted prism

Specimen	Peak Axial Load (kN)	Compressive Strength (MPa)
1	2104	14
2	2904	19
3	2452	16
Average		16.4

A.2. Full-scale Testing Description

The literature research reveals that most experimental investigations lack vital features in their wall specimens and testing equipment. These include consistent scaling, design details that are representative of the actual masonry construction and complied to the standard codes, boundary conditions that resembles the realistic shear walls, implementing loading system that alleviates most of the limitations found in the literature, and well documented reports of the test results and the material properties.

This sub-section describes the full-scale testing regarding wall specimens design and construction, test setup, boundary conditions, instrumentation, and loading procedure.

A.2.1. Wall Specimens Design

A.2.1.1. Wall Specimen Dimensions

This study includes the testing of four full-scale wall specimens. Each specimen is comprised of three parts – a cap-beam, a wall panel, and a foundation. The cap-beams and the foundations were designed to remain in an elastic range and provide proper boundary conditions to the wall panels (Figure A.6). As observed from the figure, two aspect ratios of the specimens (wall height to wall length) H/L were implemented – 1.86 and 1.00 for slender and squat walls, respectively. Each aspect ratio has two walls distinguished by the horizontal reinforcement

type (Bond beam or Bed-joint reinforcement). The wall specimens dimensions are depicted in Fig. A.6. The current study investigates the shear strength response of PG walls having different horizontal reinforcement types with variable aspect ratios.

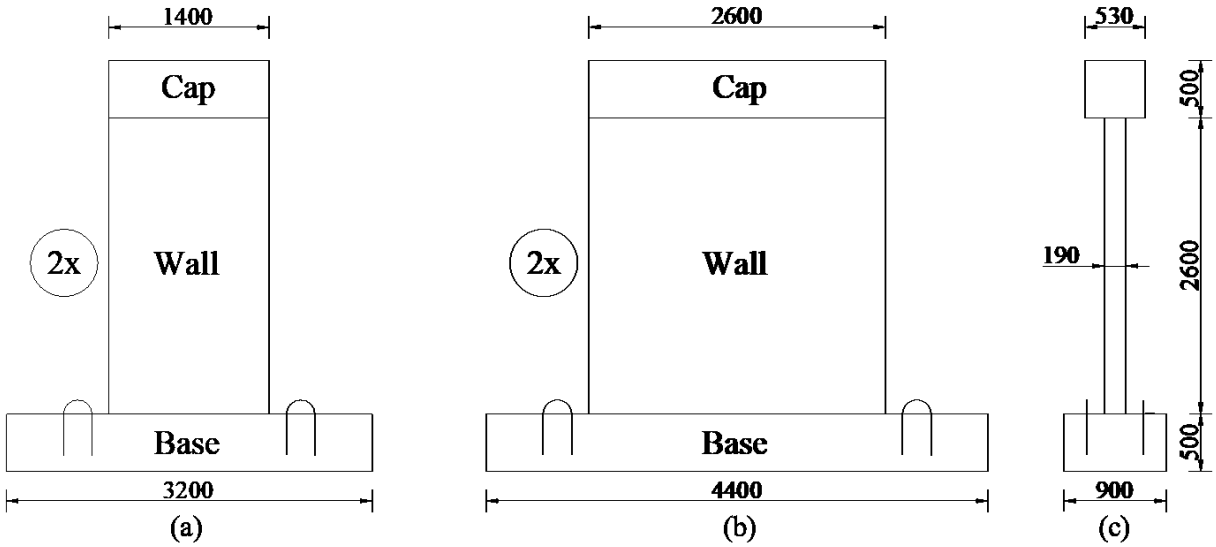

Figure A.6 Geometry of the test specimens (a) Slender wall, (b) squat wall, (c) cross-section

A.2.1.2. Design Criteria

All the test specimens were designed to meet the North American codes (CSA S304 2014) and (TMS 402/602 2016) provisions for reinforced walls subjected to combined axial and in-plane lateral loads. The design approach is to meet the minimum reinforcement ratios and maximum spacing for both vertical and horizontal reinforcement wherever possible. This approach is matching with the realistic design and the actual construction practice when it comes to designing and building reinforced PG walls for non-seismic purposes.

The following sections present design provisions for shear walls, per CSA S304 (2014) and TMS 402/602 (2016) codes in terms of horizontal and vertical reinforcement, check for the axial load, and check for the flexural and shear strength. It is worth noting that all the design calculations were made using nominal strength i.e. reduction resistance factors for masonry and steel (φ_m and φ_s) are not used.

CSA S304-14 (2014)

Provisions for reinforced walls design are found in chapter ten of CSA S304-14 (2014). Section 10 and 15 of this chapter deal with shear design requirements in terms of diagonal shear, sliding shear, and minimum spacing requirements. As the current project investigates the in-plane shear response of PG walls, the selection of the design parameters was to ensure that the test specimens would not fail in pure flexural but in diagonal shear or mixed shear-flexure mode without compromising the adopted design approach of meeting the minimum reinforcement ratios.

These provisions can be described briefly as follows.

I. Vertical Reinforcement

For reinforced walls designed to withstand axial compression and bending, the minimum area for each rebar used in vertical reinforcement shall be 0.00125 A_g where A_g is the gross cross-sectional area of wall, mm^2, but if the spacing is more than 4 times the wall thickness, t, the minimum area of each vertical rebar is 0.00125 (4 t x t) as per clause 10.15.1.1. Clause 10.15.1.2 requires that the minimum vertical reinforcement used to resist the flexural tensile stresses shall be continuous over the height of the loadbearing wall, 2400 mm as a maximum spacing, placed at each side of the movement joints, and placed at corners, intersections, and end of walls.

Maximum vertical reinforcement ratio shall be 2% of the gross cross-sectional area of the wall as per clause 10.15.2 and the maximum size of deformed reinforcement shall be 25M as per Clause 12.1.2.

II. Horizontal Reinforcement

For reinforced walls designed to resist the in-plane shear loads, horizontal reinforcement shall be continuous along the wall length, spaced not more than the lesser of 2400 mm or 0.5 l_w for bond beams, and 600 mm for joint reinforcement, and provided at the top of the wall and where the wall is connected to the roof and floor assemblies as per clause 10.15.1.4. Maximum horizontal reinforcement ratio shall be 2% of the gross cross-sectional area of the wall as per clause 10.15.2. Clause 10.15.3 states that wire reinforcement placed in the mortar

joints may be considered as horizontal reinforcement where it is continuous and spliced according to Clause 12.

Maximum size of deformed reinforcement shall be 25M for bond beam as per Clause 12.1.2. For joint reinforcement, the diameter shall be between 3.0 mm and not more than one-half the mortar joint thickness or 5.0 mm, whichever is less as per Clause 12.1.4.

Clause 12.4.11.2 requires the shear reinforcement of 15M and smaller bars to be anchored around longitudinal bar by a standard hook as per CSA A23.1.

III. Check for Axial Load

Clause 10.4.1 limits the factored axial load resistance P_r, of compression member by not greater than, $P_r = 0.8(0.85\ \phi_m f'_m A_e)$ (A.1)

Where:

P_r = factored axial load resistance (kN)

ϕ_m = resistance factor for masonry = 0.6

f'_m = compressive strength of masonry normal to the bed joint (MPa)

A_e = effective cross-sectional area of masonry (mm^2)

IV. Check for Flexural and Shear Strength

Shear walls shall be designed in a way that their resisting factored moment at the critical section, where first yielding happens, is greater than the factored demand. The moment capacity can be found either via Cardenas and Magura (1973) equation or general flexural analysis method. The latter method is quite complicated by hand, in particular of PG walls case. Cardenas and Magura (1973) equations can be applied in condition of distributed reinforcement. It was adapted for masonry design by Anderson and Brzev (2009). These equations are given by:

$$M_r = 0.5\phi_s f_y A_s l_w \left(1 + \frac{P_f}{\phi_s f_y A_s}\right)\left(1 - \frac{c}{l_w}\right) \quad \text{(A.2)}$$

$$\omega = \frac{\phi_s f_y A_s}{\phi_m f'_m l_w t} \quad \text{(A.3)}$$

$$\alpha = \frac{P_f}{\phi_m f'_m l_w t} \quad \text{(A.4)}$$

$$\frac{c}{l_w} = \frac{\omega+\alpha}{2\omega+0.68} \quad \text{(A.5)}$$

Where:

ϕ_s = resistance factor for reinforcemnt = 0.85

f_y = yield strength of reinforcement (MPa)

l_w = wall length (mm)

P_f = factored axial load (kN)

A_s = total vertical reinforcemnt area (kN) for non-siesmic design purposes

= area of vertical reinforcemnt subjected to tension for seismic design purposes

c = distance from extreme compression fibre to the neutral axis (mm)

f'_m = compressive strength of masonry normal to bed joint (MPa)

t = wall thickness (mm)

ϕ_m = resistance factor for masonry = 0.6

The in-plane shear resistance of reinforced wall is determined using Clauses 10.10.2.1 and 10.10.2.3 which is explained previously in detail in Section 3.4.2. In additon, sliding shear capacity can be found using the equation in Clause 10.10.5.1. This equation is given by:

$$V_r = \phi_m \mu C \quad \text{(A.6)}$$

Where

ϕ_m = resistance factor for masonry = 0.6

μ = 1.0 for a masonry-to-masonry or masonry-to-roughened-concrete sliding plane

= 0.7 for a masonry-to-smooth-concrete or masonry-to-bare-steel sliding plane

C = compressive force in the masonry acting normal to the sliding plane, normally taken as P_d plus the factored tensile force at yield of the vertical dowels crossing the sliding plane, $\phi_s A_s f_y$ (Figure A.7)

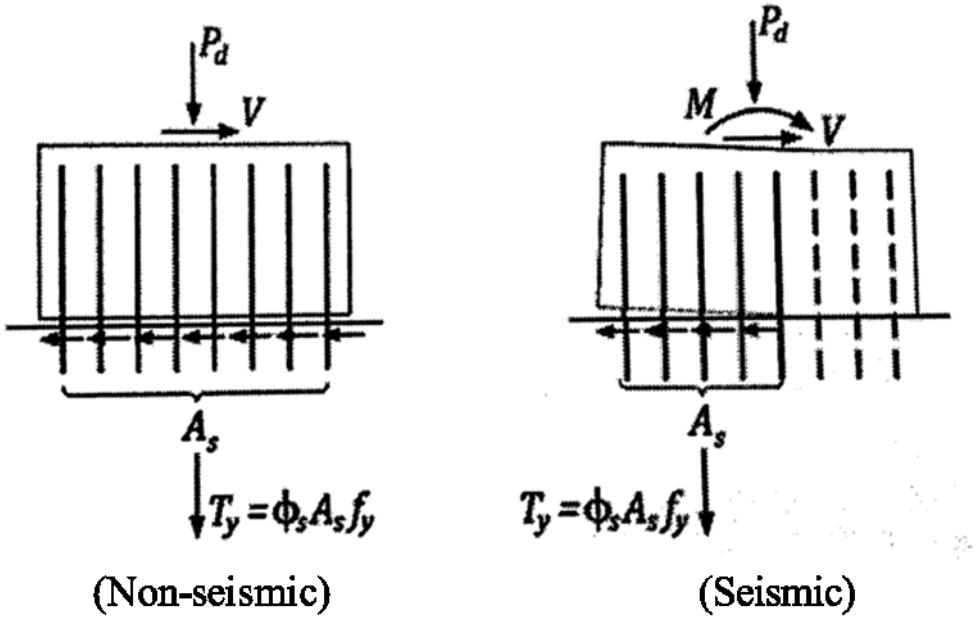

Figure A.7 In-plane sliding shear resistance mechanism (Anderson and Brzev 2009)

TMS 402/602-16 (2016)

Provisions for reinforced walls design are found in chapter nine of TMS 402/602-16 (2016). Section 3 of this chapter deals with reinforced masonry in terms of flexural and axial strength, in-plane shear strength, shear-friction strength, and reinforcement requirements. As the current project investigates the in-plane shear response of PG walls, the selection of the design

parameters was to ensure that the test specimens will not fail in pure flexural but in diagonal shear or mixed shear-flexure mode without compromising the adopted design approach of meeting the minimum reinforcement ratios.

These provisions can be described briefly as follows.

I. Vertical Reinforcement

For reinforced walls, the vertical rebar diameter shall not be larger than 29 mm and the area of the reinforcing bars placed in a cell or in a course of hollow unit construction shall not exceed 4% of the cell area as per Clause 9.3.3.1(a). The maximum area of flexural tensile reinforcement for reinforced walls having $M_u / (V_u d_v) \geq 1$ shall not exceed the area required to maintain the axial equilibrium under the conditions listed in Clause 9.3.3.2.1.

Clause 9.3.6.2 states that the vertical reinforcement required to resist in-plane loads shall be provided perpendicular to the shear reinforcement and shall be at least one-third of the shear reinforcement area. In addition, this reinforcement shall be uniformly distributed and shall not exceed 2440 mm spacing.

II. Horizontal Reinforcement

For bond beam reinforcement, the maximum diameter of rebar shall not be larger than 29 mm as per Clause 9.3.3.1(a). On the other hand, Clause 9.3.3.1 (b) limits using the joint reinforcement to be at least 4.8 mm diameter. The latter limit is to provide sufficient strain capacity to avoid rupture according to the commentary of TMS 402/602-16 (2016).

Joint reinforcement used as shear reinforcement shall consist of at least two 4.8 mm diameter longitudinal wires located within a bed joint and placed over the masonry unit face shells. The maximum spacing of joint reinforcement used as shear reinforcement shall not exceed 406 mm for Seismic Design Categories (SDC) A and B and shall not exceed 203 mm in PG walls for SDC C, D, and F as per Clause 9.3.3.4.

SDC is the design earthquake spectral response acceleration at short periods, S_{DC} (ASCE/SEI 7-16 2016). This is equivalent to S(T) in NBC (2015). Seismic category A corresponds to buildings in areas where expected ground shaking will be minor with good Soils such as Rock.

Seismic Category B corresponds to buildings of Occupancy Groups I, II and III where expected ground shaking will be moderate with stratified soils such as dense soil and soft rock. Seismic Category C corresponds to buildings of Occupancy Groups IV where expected ground shaking will be moderate and buildings of occupancy categories I, II, and III where more severe ground shaking will occur. Seismic Category D corresponds to buildings and structures in areas expected to experience severe and destructive ground shaking but not located close to a major fault. Sites with poor soils such as soft soils are a good example. Seismic Category E corresponds to buildings of Occupancy Groups I, II and III in areas near major active faults. Soil or rock is of no consequence i.e. they are not essential in withstanding the severe event. Seismic Design Category F corresponds to buildings of Occupancy Groups IV areas near major active faults. Soil or rock is of no consequence.

Occupancy Groups can be illustrated in Table A.

Table A.9 Occupancy categories classification and their importance factors (Tables 1.5-1 and 11.5-1) ASCE 7-10

Occupancy Category	Examples	Notes	Importance Factors
I	• Agricultural facilities • Minor storage facilities	Low hazard to human life	1.0
II	• Residential homes	Structures not listed in Categories I, III and IV	1.0
III	• Daycare facilities with a capacity > 150 • Elementary or secondary school with a capacity > 250 • Hospitals	Substantial hazard to human life	1.25
IV	• Fire, ambulance and police stations	Essential facilities	1.5

III. Check for Axial Load

Clause 9.3.4.1.1 limits the nominal axial compressive strength P_n, by not greater than,

$$P_n = 0.8\left[0.8f'_m(A_n - A_{st}) + f_y A_{st}\right]\left[1 - \left(\frac{h}{140r}\right)^2\right] \quad \text{(A.7)}$$

Where:

P_n = nominal axial strength (N)

f'_m = specified compressive strength of concrete masonry (MPa)

A_n = net cross-sectional area of the wall (mm^2)

A_{st} = total area of vertical reinforcement (mm^2)

f_y = specified yield strength of steel for reinforcement (MPa)

h = effective height of wall (mm)

r = radius of gyration (mm)

IV. Check for Flexural and Shear Strength

Shear walls shall be designed to resist in-plane loads. In order to achieve this scope, flexural, shear, and shear-friction strength shall be satisfied as per Clause 9.3.6. Regarding flexural strength, Cardenas and Magura (1973) equations can be used to calculate the nominal flexural strength. This equation is explained in detail in CSA S304-14 (2014) Section. Another method of flexural strength calculation is to use the assumption of an equivalent rectangular stress block i.e. strain-compatibility analysis as recommended in commentary of Clause 9.3.4.1.1.

The nominal in-plane shear strength of reinforced wall is determined using Clause 9.3.4.1.2 which is explained previously in detail in section 2.3.4. In addition, shear-friction strength can be calculated using the equations found in Clause 9.3.6.5. The nominal shear-friction strength V_{nf} , at a horizontal interface is give by:

For $\frac{M_u}{V_u d_v} \leq 0.5$

$$V_{nf} = \mu\left(A_{sp} f_y + P_u\right) \geq 0 \qquad \text{(A.8)}$$

For $\frac{M_u}{V_u d_v} \geq 1.0$

$$V_{nf} = 0.42 f'_m A_{nc} \quad \text{(A.9)}$$

Where

M_u = strength level moment (N.mm)

V_u = strength level shear load (N)

d_v = actual depth of a member in direction of shear considered (mm)

V_{nf} = nominal shear-friction strength (N)

μ = coefficient of friction

= 1.0 for masonry on concrete with unfinished surafce and finished surface that has been intenionally roughned

= 0.7 for all other sitautions

A_{sp} = cross-sectional area of reinforcement within the net shear area, perpendicular to and crossing the horizontal shear plane (mm^2)

f_y = specified yield strength of steel for reinforcement (MPa)

P_u = strength level axial load (N)

f'_m = specified compressive strength of concrete masonry (MPa)

A_{nc} = net cross-sectional area between the neutral axis of bending and the fiber of maximum compressive strain calculated at the nominal moment capacity of the section (mm^2)

Where $\frac{M_u}{V_u d_v}$ is between 0.5 and 1.0, the shear-friction strength can be determined by linear interpolation of the two above equations. The reinforcement A_{sp} in equation (A.8) should be adequately anchored above and below the horizontal shear plane to develop the required yield strength of the reinforcement. The axial load, P_u can be negative in case of a tension force. The reinforcement A_{nc} can be calculated using flexural analysis i.e. strain-compatibility analysis.

A.2.1.3. Design of Slender Wall with BB Reinforcement

The slender wall with BB (Bond Beam) reinforcement was a conventional shear wall designed for non-seismic purposes. The wall panel was 2600 mm high, 1400 mm length, and 190 mm thickness. The wall specimen had an aspect ratio (H/L) of 1.86. This aspect ratio considered as a slender wall for in-plane shear loads design as specified in Clause 10.10.2.2 (CSA S304-14 2014). This clause specified the walls with low-aspect ratio (H/L <1) as squat shear walls which implied that the walls with high aspect ratio (H/L>1) were considered as slender shear walls. It is worthily noting that this aspect ratio does not relate to the slenderness ratio (kh/t) used for the out-of-plane design. In addition, this high aspect ratio is rarely implemented in the tested walls in the literature (Izquierdo 2021). This may be attributed that these walls are expected to fail in flexure which is out of their scope.

I. Vertical Reinforcement

For vertical reinforcement, a reinforcement ratio of 0.09% (based on area of each bar divided by the grout spacing and wall thickness) was provided using two rebars of 15M with spacing of 1200 mm. Using 15M rebar is the minimum area of the vertical rebar area when the spacing is more than 4 times the wall thickness (1200 mm > 4*190 mm) as per Clause 10.15.1.1. These rebars were placed at each corner of the wall continuously from the wall base into the capping beam. The vertical reinforcement layout (Figure A.8) satisfied the minimum and maximum reinforcement ratios, spacing, and details clauses in CSA S304-14 (2014) and TMS 402/602-16 (2016).

II. Horizontal Reinforcement

For horizontal reinforcement, a reinforcement ratio of 0.09% (based on area of each bar divided by the vertical spacing and wall thickness) was provided using five bond beams with vertical spacing of 600 mm where each bond beam has a single 10M rebar. The vertical spacing is complied with Clause 10.15.1.4(b) where the spacing shall not exceed the lesser of 2400 mm or 0.5lw. The horizontal rebars were placed starting with $s_h/2$ spacing from the bottom and then placing the first rebar where s_h is the vertical spacing. After that, going up with the specified spacing and the last rebar was placed at the top (Figure A.8). These rebars were anchored with 90º hook into the boundary vertical end cell as per CSA A23.1.

The horizontal reinforcement layout (Figure A.8) satisfied the minimum and maximum reinforcement ratios, spacing, and details clauses in CSA S304-14 (2014) and TMS 402/602-16 (2016).

III. Check for axial load

The check for the maximum nominal axial load resistance was obtained to be 1927 kN as per Clause 10.4.1(CSA S304-14 2014) and 1953 kN as per Clause 9.3.4.1.1(TMS 402/602-16 2016).

IV. Check for the Flexural and Shear Strength

The probable nominal shear associated with flexural capacity was calculated to be 156 kN and 166 kN using Cardenas and Magura (1973) equation and general flexural analysis method, respectively. The expected nominal shear associated with diagonal shear capacity was obtained to be 192 kN and 155 kN using Clauses 10.10.2.3, 10.10.2.3 (CSA S304-14 2014) and Clause 9.3.4.1.2 (TMS 402/602-16 2016) equations used to calculate the in-plane shear resistance of reinforced wall, respectively. The expected nominal sliding shear capacity was calculated to be 489 kN and 660 kN using Clause 10.10.5.1(CSA S304-14 2014) and Clause 9.3.6.5 (TMS 402/602-16 2016) equations used to calculate the in-plane shear resistance of reinforced wall, respectively.

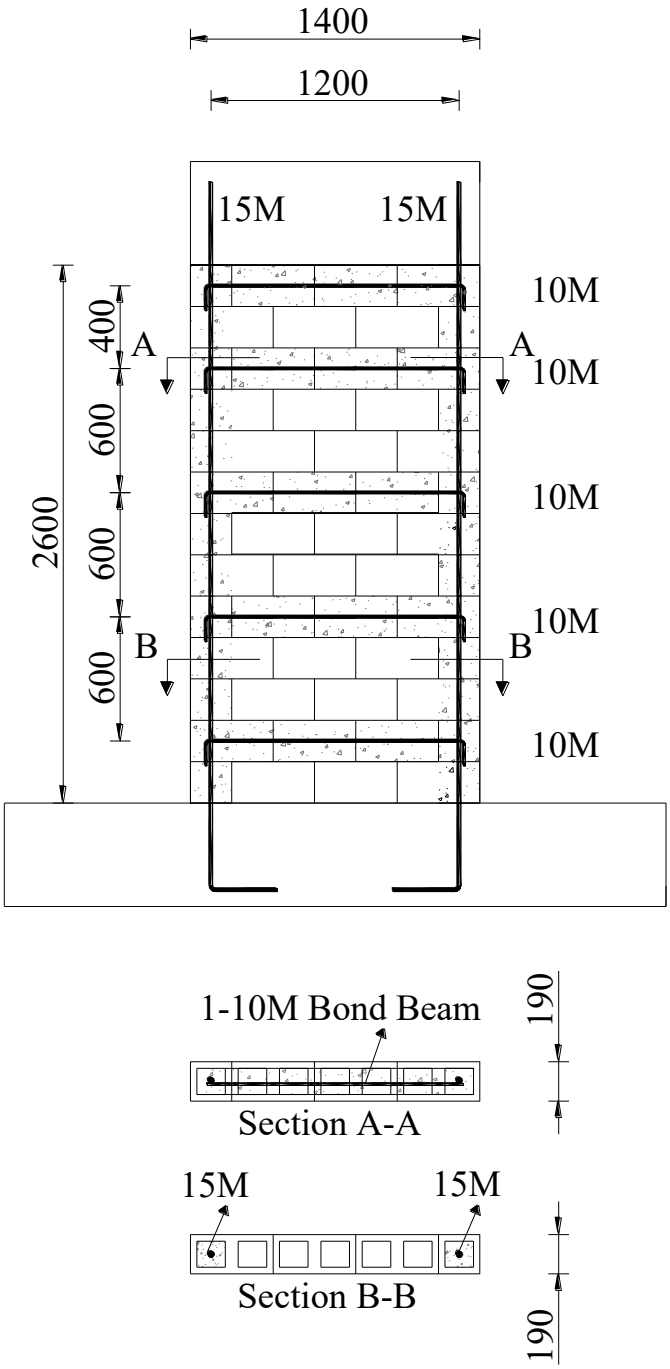

Figure A.8 Reinforcement layout of the slender wall with BB reinforcement

It is concluded that both the flexural and in-plane shear capacity were very close, which implied that this wall would have a mixed shear-flexure failure (Haach et al. 2013). Most of the literature found to use a high vertical reinforcement ratio to ensure that the wall will fail in shear by increasing the flexural capacity (Ramírez et al. 2016), but increasing the vertical reinforcement may also increase the shear strength (Shing et al. 1989). On the other hand, the

actual construction practice adopts much lower reinforcement ratios, which our primary objective is to replicate the realistic design details found in the masonry construction industry. This is where design and research deviate. If a specific failure mode is intended to obtain, then increasing the vertical reinforcement ratio is implemented. However, increasing the vertical reinforcement ratio was found not to significantly alter the failure mode to pure shear failure due to the high aspect ratio and the maximum reinforcement regulations in the standard codes.

A.2.1.4. Design of Slender Wall with BJ Reinforcement

The slender wall with BJ (Bed-Joint) reinforcement was a conventional shear wall designed for non-seismic purposes. The wall panel was 2600 mm high, 1400 mm length, and 190 mm thickness. The wall specimen had an aspect ratio (H/L) of 1.86. This aspect ratio considered as a slender wall for in-plane shear loads design as specified in Clause 10.10.2.2 (CSA S304-14 2014).

I. Vertical Reinforcement

For vertical reinforcement, a reinforcement ratio of 0.09% (based on area of each bar divided by the grout spacing and wall thickness) was provided using two rebars of 15M with spacing of 1200 mm. Using 15M rebar is the minimum area of the vertical rebar area when the spacing is more than 4 times the wall thickness (1200 mm > 4*190 mm) as per Clause 10.15.1.1. These rebars were placed at each corner of the wall continuously from the wall base into the capping beam. The vertical reinforcement layout (Figure A.9) satisfied the minimum and maximum reinforcement ratios, spacing, and details clauses in CSA S304-14 (2014) and TMS 402/602-16 (2016).

II. Horizontal Reinforcement

For horizontal reinforcement, a reinforcement ratio of 0.05% (based on area of each bar divided by the vertical spacing and wall thickness) was provided using ladder-type reinforcement of 3.7mm diameter with vertical spacing of 400 mm (every other course). The vertical spacing is complied with Clause 10.15.1.4(b) where the spacing shall not exceed 600mm for joint reinforcement. TMS 402/602-16 (2016) considers this spacing as the maximum spacing required for joint reinforcement in areas with no-or low-seismic hazard as

per Clause 9.3.3.4. In addition, a bond beam with single 10M was placed at the top of the wall panel, following Clause 10.15.1.4 (d) in CSA S304-14 (2014) (Figure A.9). It should be noted that TMS 402/602-16 (2016) limits the minimum size of joint reinforcement as 4.8 mm in contrast to CSA S304-14 (2014) which limits the size to be at least 3mm. Joint reinforcement (Ladder-type) is available in the market in two common sizes; 3.7 mm and 4.8 mm.

The horizontal reinforcement layout (Figure A.9) satisfied the minimum and maximum reinforcement ratios, spacing, and details clauses in CSA S304-14 (2014) and TMS 402/602-16 (2016).

III. Check for Axial load

The check for the maximum nominal axial load resistance was obtained to be 1927 kN as per Clause 10.4.1(CSA S304-14 2014) and 1953 kN as per Clause 9.3.4.1.1(TMS 402/602-16 2016). These checks were similar to the slender wall with BB reinforcement since they both have similar parameters in terms of vertical reinforcement, wall geometry, and compressive strength of masonry.

IV. Check for Flexural and Shear Strength

The probable nominal shear associated with flexural capacity was calculated to be 156 kN and 166 kN using Cardenas and Magura (1973) equation and general flexural analysis method, respectively. The expected nominal shear associated with diagonal shear capacity was obtained to be 178 kN and 155 kN using Clauses 10.10.2.3, 10.10.2.3 (CSA S304-14 2014) and Clause 9.3.4.1.2 (TMS 402/602-16 2016) equations used to calculate the in-plane shear resistance of reinforced wall, respectively. The expected nominal sliding shear capacity was calculated to be 489 kN and 660 kN using Clause 10.10.5.1(CSA S304-14 2014) and Clause 9.3.6.5 (TMS 402/602-16 2016) equations used to calculate the in-plane shear resistance of reinforced wall, respectively.

It is found that both the flexural and in-plane shear capacity were very close, which implied that this wall would have a mixed shear-flexure failure (Haach et al. 2013).

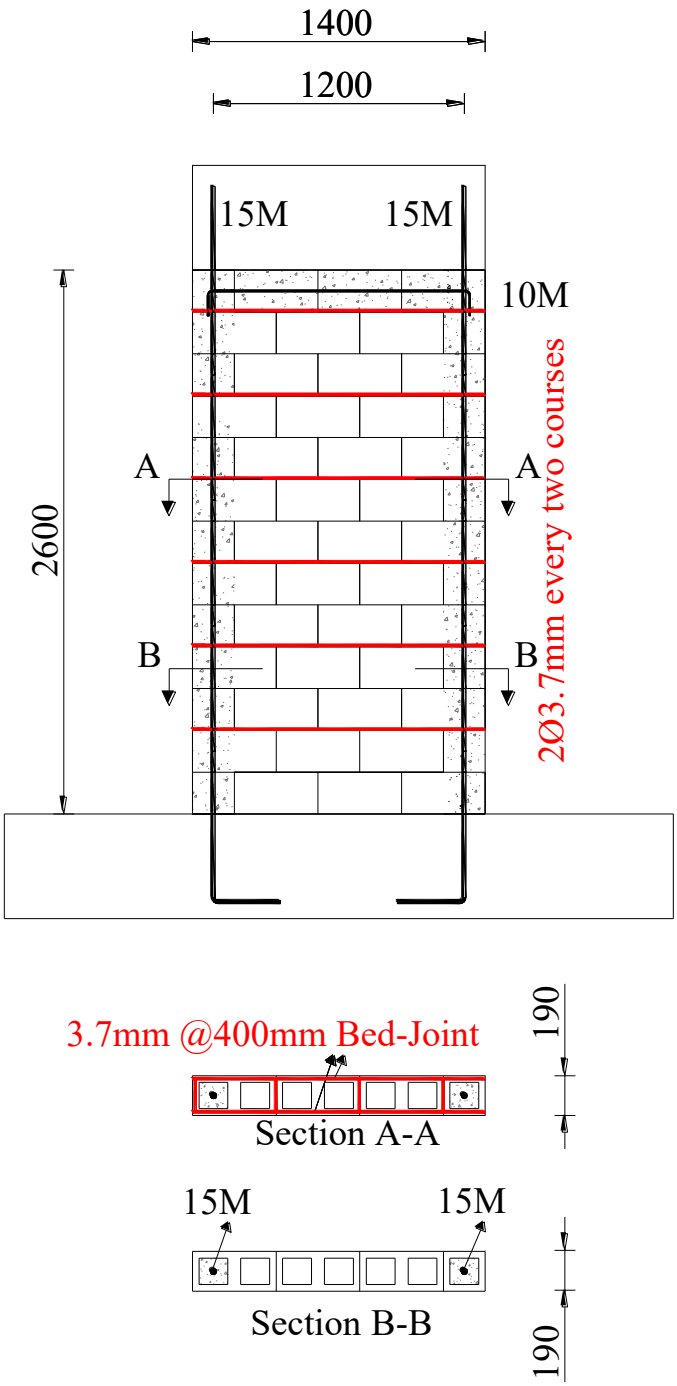

Figure A.9 Reinforcement layout of the slender wall with BJ reinforcement

A.2.1.5. Design of Squat Wall with BB Reinforcement

The squat wall with BB (Bond Beam) reinforcement was a conventional shear wall designed for non-seismic purposes. The wall panel was 2600 mm high, 2600 mm length, and 190 mm thickness. The wall specimen had an aspect ratio (H/L) of 1.00. This aspect ratio considered as a squat wall for in-plane shear loads design as specified in Clause 10.10.2.2 (CSA S304-14 2014). Even though this clause considers aspect ratio of H/L<1 as a squat wall without including H/L=1, this wall will be considered as a squat wall to distinguish it from the slender wall with H/L=1.86.

I. Vertical Reinforcement

For vertical reinforcement, a reinforcement ratio of 0.09% (based on area of each bar divided by the grout spacing and wall thickness) was provided using three rebars of 15M with spacing of 1200 mm. Using 15M rebar is the minimum area of the vertical rebar area when the spacing is more than 4 times the wall thickness (1200 mm > 4*190 mm) as per Clause 10.15.1.1. These rebars were placed at each corner and the middle of the wall continuously from the wall base into the capping beam. It is worthy nothing that the maximum spacing of the vertical reinforcement is 2400 mm and 2440 mm as per CSA S304-14 (2014) and TMS 402/602-16 (2016), respectively. However, the spacing of 1200 mm was adopted to make the vertical reinforcement ratio consistent throughout all the tested walls since it is considered as a fixed parameter in this study.

The vertical reinforcement layout (Figure A.10) satisfied the minimum and maximum reinforcement ratios, spacing, and details clauses in CSA S304-14 (2014) and TMS 402/602-16 (2016)

II. Horizontal Reinforcement

For horizontal reinforcement, a reinforcement ratio of 0.04% (based on area of each bar divided by the vertical spacing and wall thickness) was provided using three bond beams with vertical spacing of 1200 mm where each bond beam has a single 10M rebar. The vertical spacing is complied with Clause 10.15.1.4(b) where the spacing shall not exceed the lesser of 2400 mm or 0.5lw. The horizontal rebars were placed starting with sh/2 spacing from the

bottom and then placing the first rebar where s_h is the vertical spacing. After that, going up with the specified spacing and the last rebar was placed at the top (Figure A.10). These rebars were anchored with 90º hook into the boundary vertical end cell as per CSA A23.1.

The horizontal reinforcement layout (Figure A.10) satisfied the minimum and maximum reinforcement ratios, spacing, and details clauses in CSA S304-14 (2014) and TMS 402/602-16 (2016).

III. Check for Axial load

The check for the maximum nominal axial load resistance was obtained to be 3385 kN as per Clause 10.4.1(CSA S304-14 2014) and 3394 kN as per Clause 9.3.4.1.1(TMS 402/602-16 2016).

IV. Check for Flexural and Shear Strength

The probable nominal shear associated with flexural capacity was calculated to be 520 kN and 554 kN using Cardenas and Magura (1973) equation and general flexural analysis method, respectively. The expected nominal shear associated with diagonal shear capacity was obtained to be 312 kN and 271 kN using Clauses 10.10.2.3, 10.10.2.3 (CSA S304-14 2014) and Clause 9.3.4.1.2 (TMS 402/602-16 2016) equations used to calculate the in-plane shear resistance of reinforced wall, respectively. The expected nominal sliding shear capacity was calculated to be 872 kN and 1317 kN using Clause 10.10.5.1(CSA S304-14 2014) and Clause 9.3.6.5 (TMS 402/602-16 2016) equations used to calculate the in-plane shear resistance of reinforced wall, respectively.

It is found that the diagonal shear capacity was less than the flexural capacity and the sliding shear capacity which implied that the failure mode would be in-plane shear.

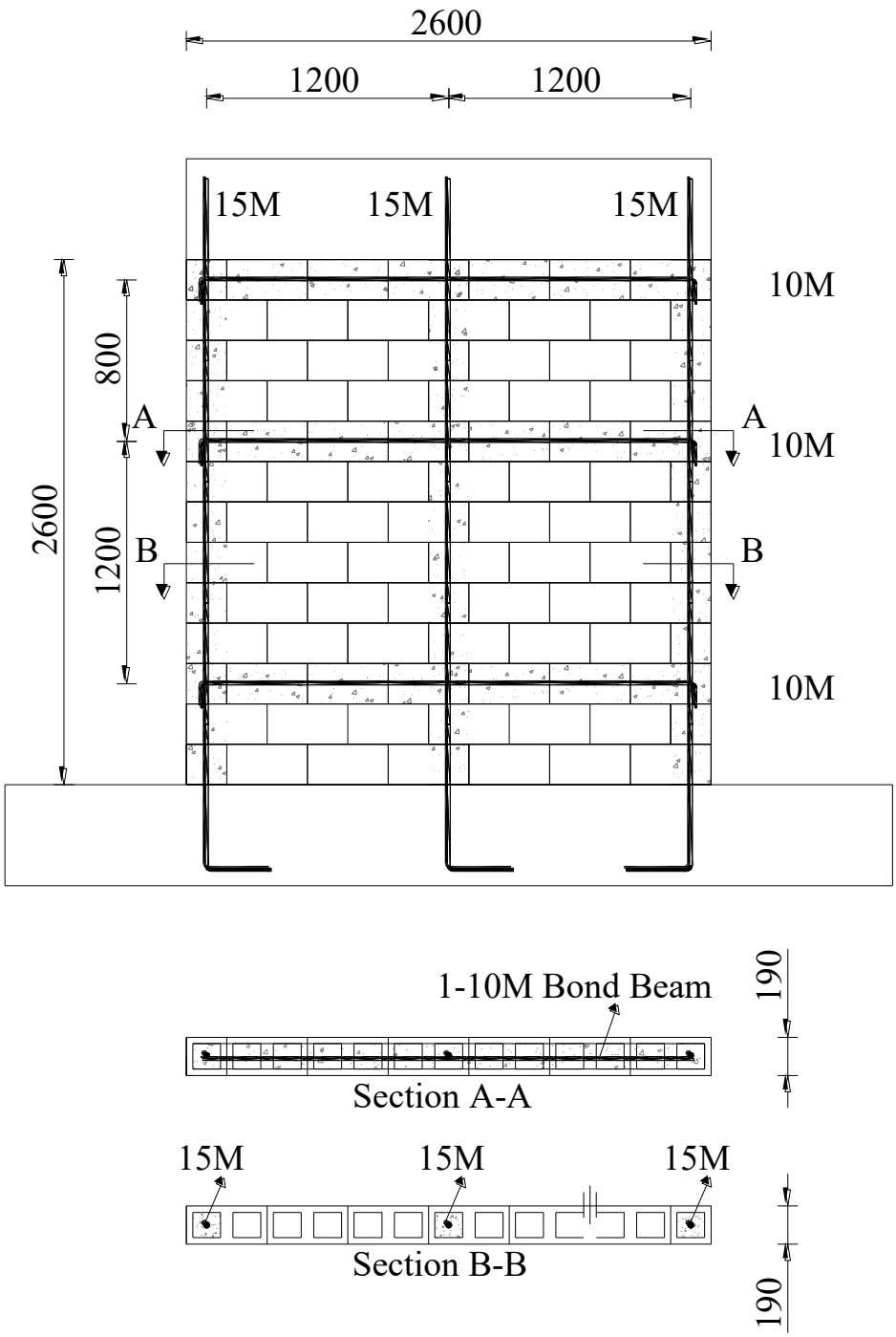

Figure A.10 Reinforcement layout of the squat wall with BB reinforcement

A.2.1.6. Design of Squat Wall with BJ Reinforcement

The squat wall with BJ (Bed-joint) reinforcement was a conventional shear wall designed for non-seismic purposes. The wall panel was 2600 mm high, 2600 mm length, and 190 mm thickness. The wall specimen had an aspect ratio (H/L) of 1.00. This aspect ratio considered as a squat wall for in-plane shear loads design as specified in Clause 10.10.2.2 (CSA S304-14 2014). Even though this clause considers aspect ratio of H/L<1 as a squat wall without including H/L=1, this wall will be considered as a squat wall to distinguish it from the slender wall with H/L=1.86.

I. Vertical Reinforcement

For vertical reinforcement, a reinforcement ratio of 0.09% (based on area of each bar divided by the grout spacing and wall thickness) was provided using three rebars of 15M with spacing of 1200 mm. Using 15M rebar is the minimum area of the vertical rebar area when the spacing is more than 4 times the wall thickness (1200 mm > 4*190 mm) as per Clause 10.15.1.1. These rebars were placed at each corner and the middle of the wall continuously from the wall base into the capping beam. It is worthy nothing that the maximum spacing of the vertical reinforcement is 2400 mm and 2440 mm as per CSA S304-14 (2014) and TMS 402/602-16 (2016), respectively. However, the spacing of 1200 mm was adopted to make the vertical reinforcement ratio consistent throughout all the tested walls since it is considered as a fixed parameter in this study.

The vertical reinforcement layout (Figure A.11) satisfied the minimum and maximum reinforcement ratios, spacing, and details clauses in CSA S304-14 (2014) and TMS 402/602-16 (2016)

II. Horizontal Reinforcement

For horizontal reinforcement, a reinforcement ratio of 0.05% (based on area of each bar divided by the vertical spacing and wall thickness) was provided using ladder-type reinforcement of 3.7mm diameter with vertical spacing of 400 mm (every other course). The vertical spacing is complied with Clause 10.15.1.4(b) where the spacing shall not exceed 600mm for joint reinforcement. TMS 402/602-16 (2016) considers this spacing as the

maximum spacing required for joint reinforcement in areas with no-or low-seismic hazard as per Clause 9.3.3.4. In addition, a bond beam with single 10M was placed at the top of the wall panel, following Clause 10.15.1.4 (d) in CSA S304-14 (2014) (Figure A.11). It should be noted that TMS 402/602-16 (2016) limits the minimum size of joint reinforcement as 4.8 mm in contrast to CSA S304-14 (2014) which limits the size to be at least 3mm. Joint reinforcement (Ladder-type) is available in the market in two common sizes; 3.7 mm and 4.8 mm.

The horizontal reinforcement layout (Figure A.11) satisfied the minimum and maximum reinforcement ratios, spacing, and details clauses in CSA S304-14 (2014) and TMS 402/602-16 (2016).

III. Check for Axial load

The check for the maximum nominal axial load resistance was obtained to be 3385 kN as per Clause 10.4.1(CSA S304-14 2014) and 3394 kN as per Clause 9.3.4.1.1(TMS 402/602-16 2016). These checks were similar to the squat wall with BB reinforcement since they both have similar parameters in terms of vertical reinforcement, wall geometry, and compressive strength of masonry.

IV. Check for Flexural and Shear Strength

The probable nominal shear associated with flexural capacity was calculated to be 520 kN and 554 kN using Cardenas and Magura (1973) equation and general flexural analysis method, respectively. The expected nominal shear associated with diagonal shear capacity was obtained to be 327 kN and 271 kN using Clauses 10.10.2.3, 10.10.2.3 (CSA S304-14 2014) and Clause 9.3.4.1.2 (TMS 402/602-16 2016) equations used to calculate the in-plane shear resistance of reinforced wall, respectively. The expected nominal sliding shear capacity was calculated to be 872 kN and 1317 kN using Clause 10.10.5.1(CSA S304-14 2014) and Clause 9.3.6.5 (TMS 402/602-16 2016) equations used to calculate the in-plane shear resistance of reinforced wall, respectively.

It is found that the diagonal shear capacity was less than the flexural capacity and the sliding shear capacity which implied that the failure mode would be in-plane shear.

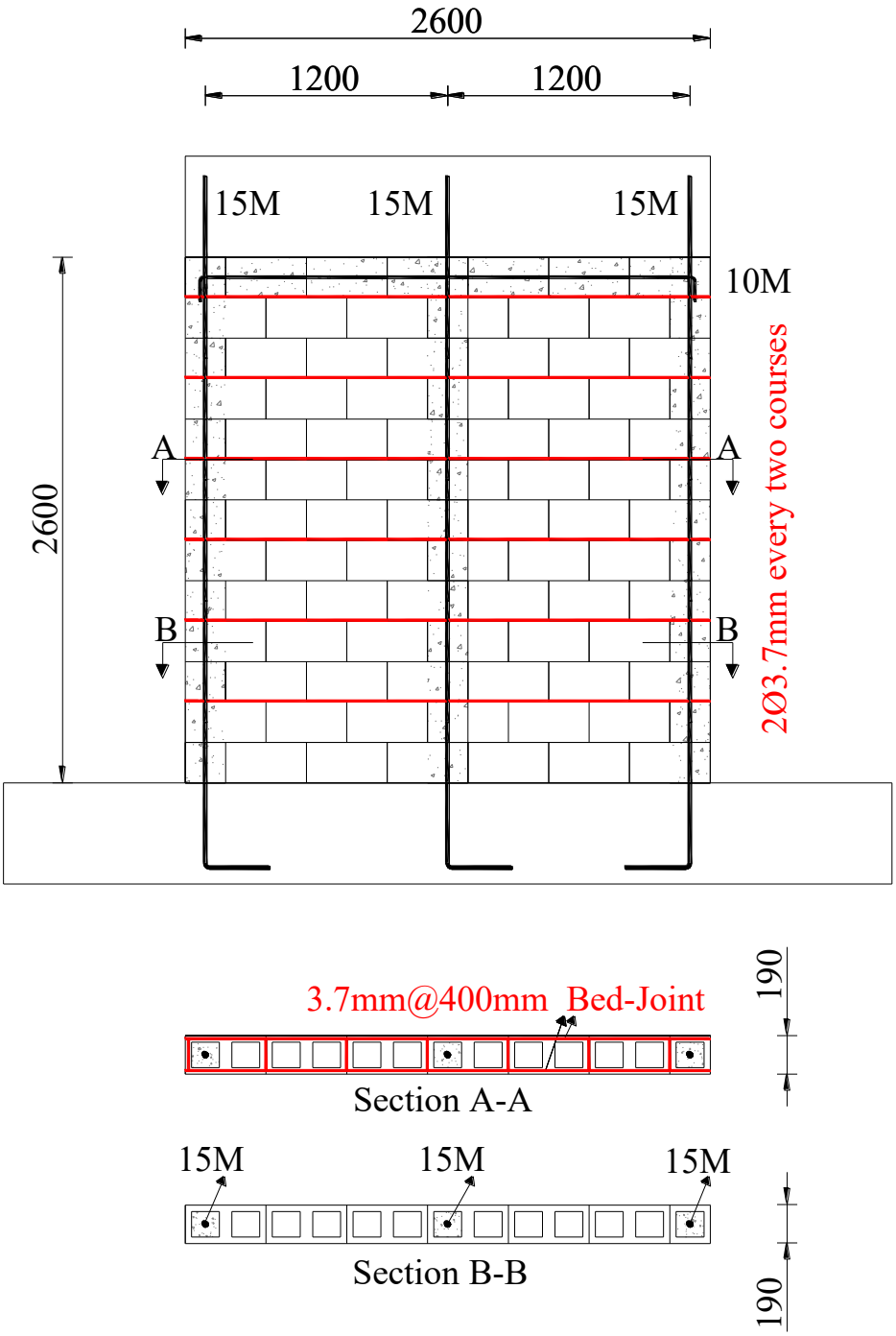

Figure A.11 Reinforcement layout of the squat wall with BJ reinforcement

A.2.1.7. Design Summary

Table A.11 summarizes the design details of the walls planned to be tested under cyclic loading condition. According to this table, two design variables (aspect ratio and horizontal reinforcement type) were implanted in these studies while other parameters remained unchanged on all the test specimens. It is noted that the horizontal reinforcement ratios of all the tested walls were approximately equal except that of slender wall with BB reinforcement. This is because of the Clause 10.15.1.4(b) which limits the maximum spacing to be the lesser of 2400 mm or $0.5l_w$ (CSA S304-14 2014). Vertical reinforcement was provided using 15M rebar at 1200 mm spacing following the standard codes and the actual practice found in the masonry industry (Hatzinikolas et al. 2015).

Table A.10 Design details of specimens

	Specimen ID	Specimen Dimensions			Aspect Ratio	Vertical Reinforcement		Horizontal Reinforcement		Axial Load
		h mm	l mm	t mm	h/l	Vertical layout	ρ_v (%)	Horizontal layout	ρ_h (%)	σ / f'_m (%)
Slender walls	Slender-BB	2600	1400	190	1.86	15M@1200	0.09	10M@600	0.09	15
	Slender-BJ	2600	1400	190	1.86	15M@1200	0.09	3.7mm@400 + 1-10M	0.05	15
Squat walls	Squat-BB	2600	2600	190	1.00	15M@1200	0.09	10M@1200	0.04	15
	Squat-BJ	2600	2600	190	1.00	15M@1200	0.09	3.7mm@400 + 1-10M	0.05	15

The failure mode of the slender walls were expected to be mixed shear-flexure mode while the squat walls were expected to be diagonal shear. Flexural failure is likely to occur in reinforced walls with aspect ratio of one and higher and moderate level of axial stress (σ / f'_m <10%) (Brzef and Anderson 2018). Our scope is to ensure that all the tested walls to fail in a diagonal shear without compromising the design standards restrictions and the realistic details in the actual construction. Pumping the vertical reinforcement may not have that significant effect on increasing the flexural capacity due the aspect ratio and the maximum size and ratio of the vertical reinforcement as per CSA S304-14 (2014) and TMS 402/602-16 (2016). On the other hand, increasing the axial load may lead to alter the flexural failure mode to diagonal shear (Takashi et al. 1986; Shing et al. 1990; Voon and Ingham 2006; da Porto et al. 2009). This may be attributed to the additional compression provided by the axial load that aids in resisting the overturning moment and hence increasing the flexural capacity which promotes

the failure mode shift. As a result, a high axial load level was adopted in this study in terms of axial stress to the compressive strength of masonry i.e. $\sigma / f'_m = 15\%$. The axial stress was calculated based on the gross-sectional area while the compressive strength of masonry, f'_m is obtained from the material properties tests (Prism tests). The resulted f'_m is 13.3 and 13.1 MPa for slender and squat walls, respectively. Therefore, 530 kN and 970 kN were applied as the axial load on the slender and the squat walls, respectively. These applied loads were less than the maximum nominal axial loads as per CSA S304-14 (2014) and TMS 402/602-16 (2016).

A.2.2. Wall Specimens Construction

All the tested walls were constructed by professional masons using hollow concrete masonry units CMUs, following running bond approach. The construction process of the test specimens consisted of three stages; (1) construction of reinforced concrete base, (2) Construction of wall panels on the base using CMUs with nominal dimensions (400x200x200) mm, and (3) construction and placing of capping beam on the top of wall panels. 20 cm standard, half standard, and knock out lintel blocks were used to build the walls. Knock out lintel was used throughout the wall height to allow the bond beam reinforcement placement and the grout continuity.

Head and bed joint thickness of approximately 10 mm was implemented where Type S Portland Lime & Sand premixed mortar, which is commonly used at the masonry construction, was used throughout the joints. Core Fill Grout-Coarse was used to fill the vertical cells where vertical reinforcement placed and the bond beams along the whole length. The vertical reinforcement was continuously placed through the test specimen height without lab splice where it hooked to the base using 90º hook and to the capping beam by welding them with cross rebar to ensure a strong connection between the capping beam and the tested wall, as well as a uniform distribution of lateral loads through the whole length of the tested wall. Bed-joint reinforcement in term of ladder-type reinforcement of 3.7 mm diameter was placed on the top of bed joint of the blocks following the reinforcement details previously explained. The masonry walls were cured under laboratory environment control. Figures A.12 and A.13 show the construction process and the test specimens after construction.

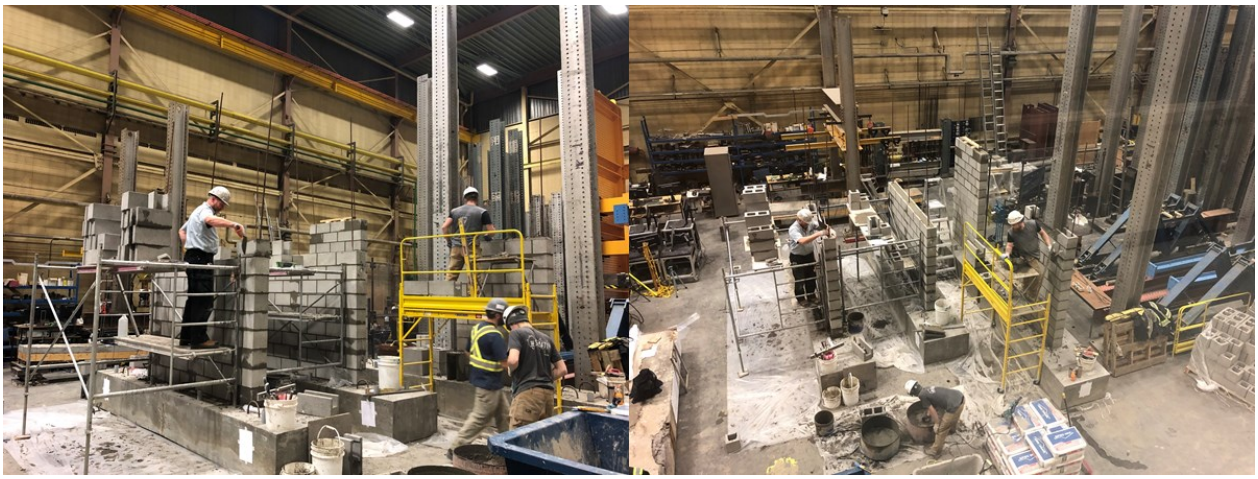

Figure A.12 Tested walls during construction

Figure A.13 Tested walls after construction

A.2.3. Boundary Conditions and Test Setup

The specimens were tested in a cantilevered (fixed-free) fashion (Figure A.14). The bases and capping beams were heavily reinforced concrete blocks to ensure they remain in the elastic zone during the test. For each specimen, the base was bolted to the strong floor of the laboratory via high strength bolts to securely fixed and avoid slippage of the wall specimens. The capping beams provided the required connection to the wall panel to transfer the vertical and lateral loads. As the in-plane response of the specimens was to be studied, the out-of-plane displacements of the walls were restrained, as demonstrated in Figure A.15.

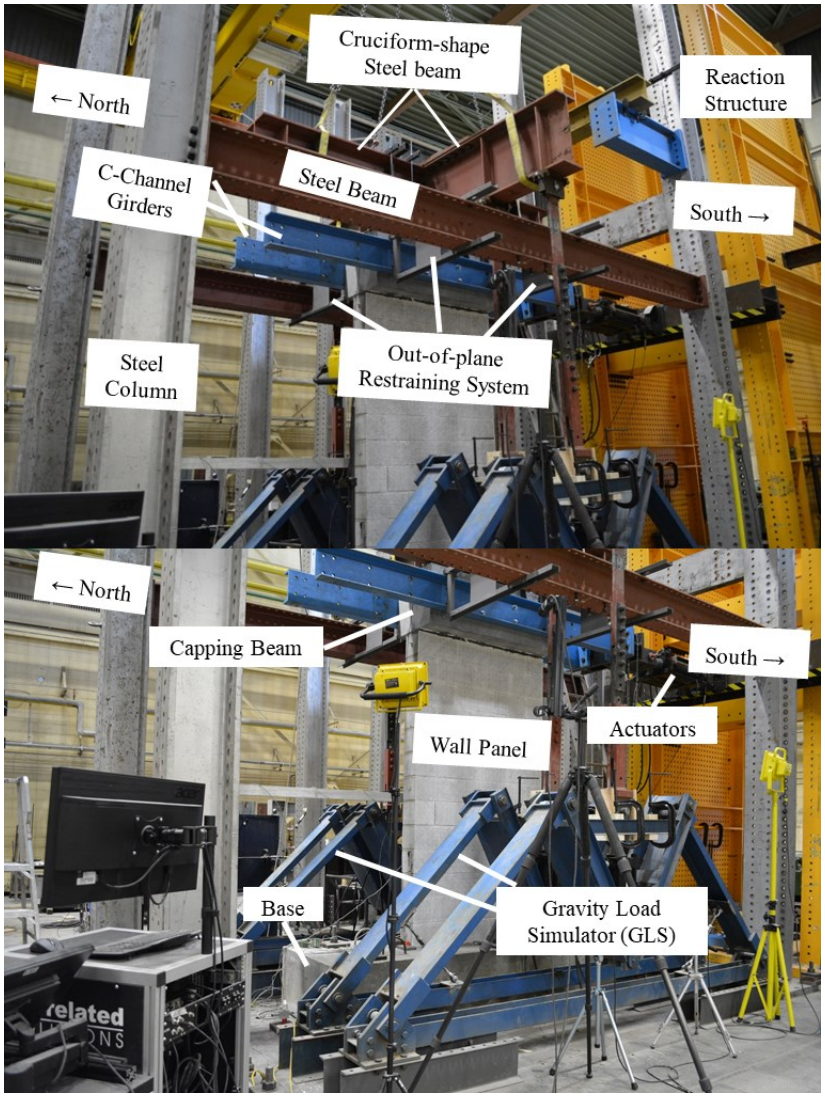

Figure A.14 Test Setup

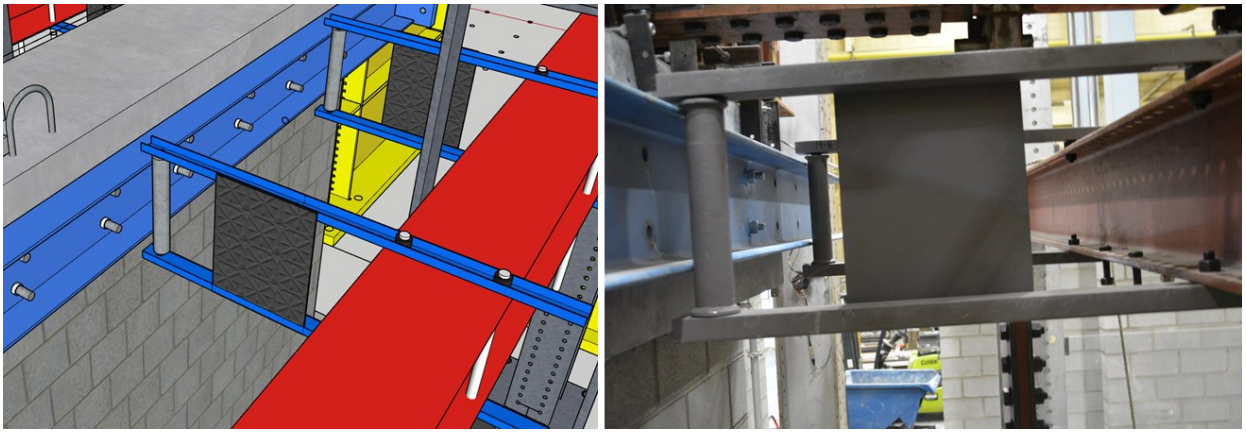

Figure A.15 Out-of-plane restraining system

The top point of each specimen was free to move in the in-plane direction of the wall panel, while the out-of-plane displacements were reduced using the restraining system shown in Figure A.15. As illustrated in the figure, four rectangular steel frames were used to prevent the out-of-plane displacement of the wall specimen, two at each side. These frames were connected at far end to the steel beam of the test frame while touching the capping beam through steel rollers. This restraining system allowed the in-plane deformation of the shear wall through the steel rollers while resisting the out-of-plane displacements.

As Figures A.16 and A.17 show, two actuators were used to apply the pre-defined displacement reversals in each specimen. These double-acting hydraulic jacks of 800kN capacity (Push-Pull) were connected at one end to a rigid reaction structure comprised of steel shear walls, while the other end was connected to the wall panel through two C-channels attached to the capping beam via high-strength rods. This connection allowed even distribution of lateral load transfer to the wall panel.

The vertical loads were applied to the test specimen through four gravity load simulators (GLS) of 350 kN capacity of each one, two at each side of the wall specimen (Figures A.16 and A.17). These GLSs were connected to a cruciform shape beam at the top of the wall panel using tension tie rods. This assembly had an advantage of maintaining a constant axial load throughout the lateral movement of the wall (Mobeen 2002).

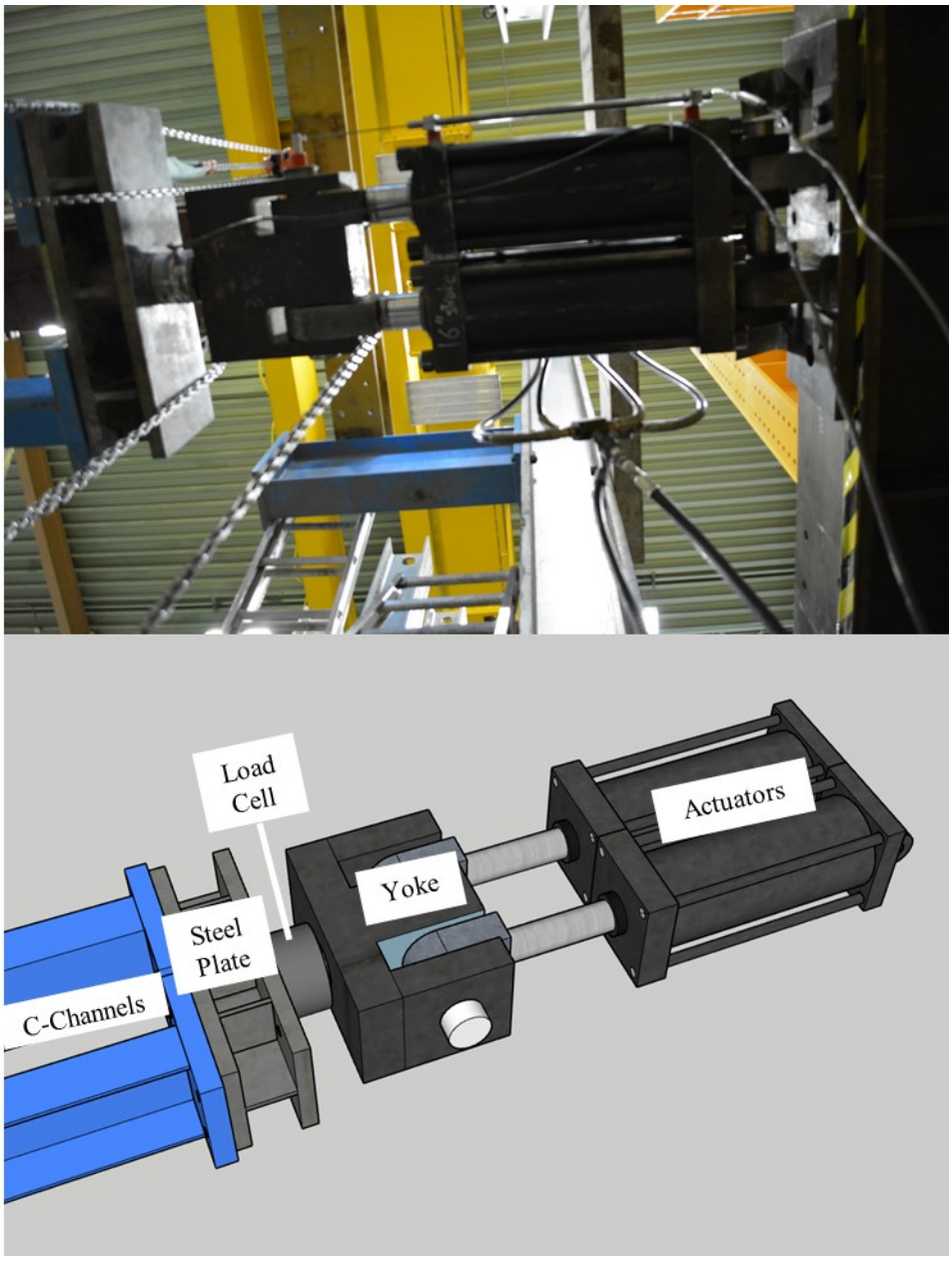

Figure A.16 Lateral load assembly

In summary, this setup was designed to simulate the cyclic loading conditions and comprised from the base system, lateral load assembly, vertical load assembly, and out-of-plane restraining system as shown in Figures A.17, A.18, and A.19.

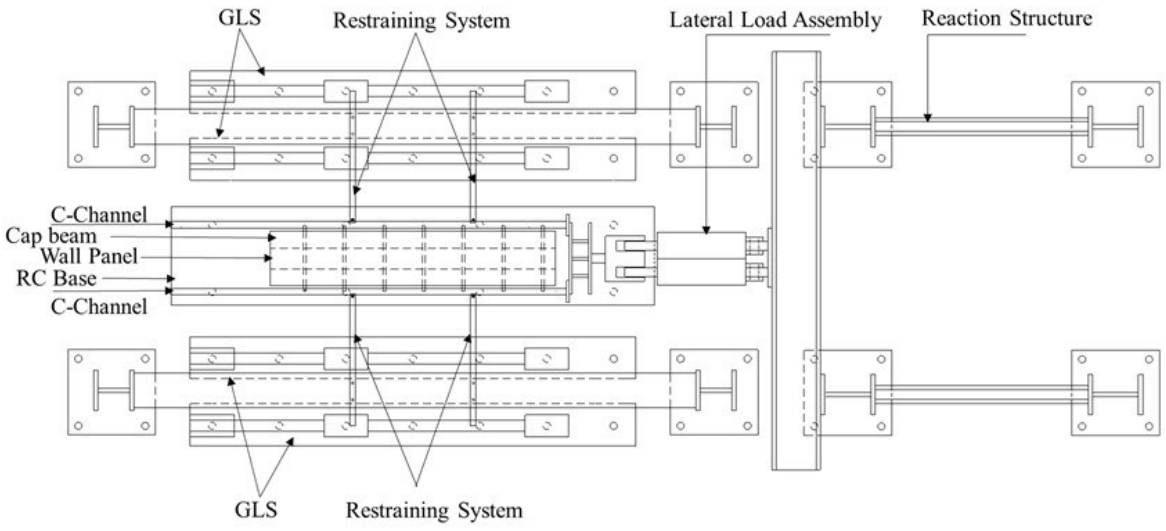

Figure A.17 Plan view of the test setup (Excluding the Cruciform-shape beam for clarity purposes)

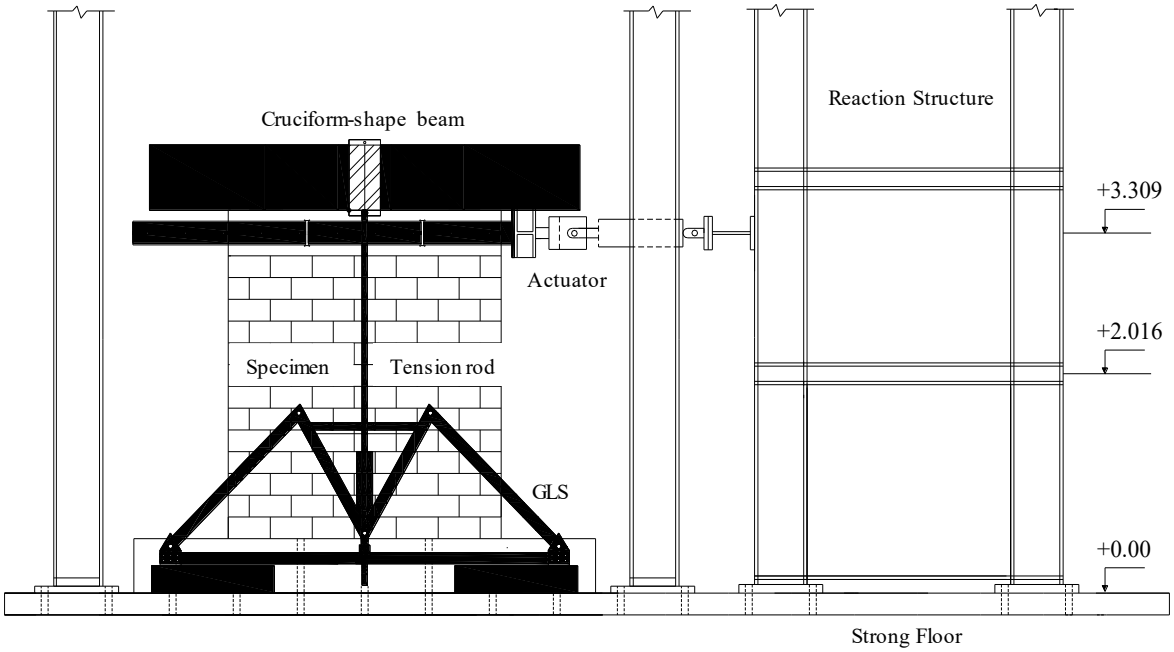

Figure A.18 Side view of the test setup (Excluding the frame beam for clarity purposes)

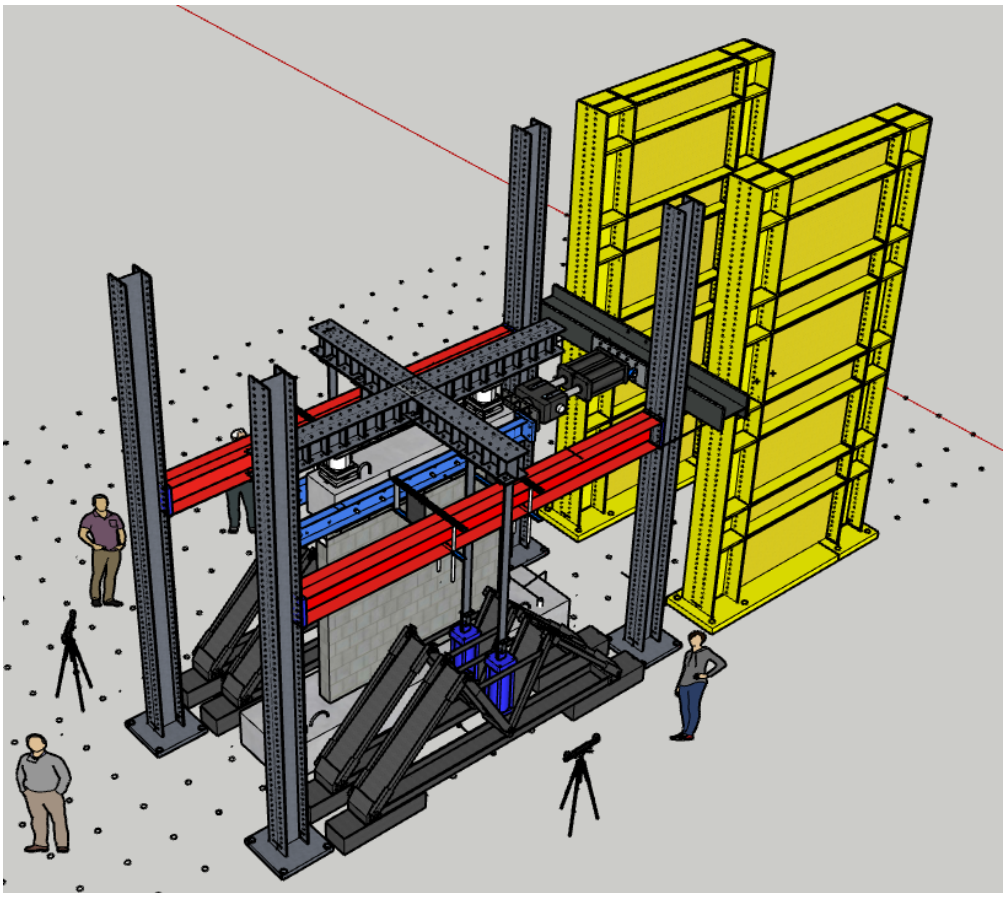

Figure A.19 3D-Model of testing set-up for the full-scale specimens

A.2.4. Instrumentation and Loading Procedure

The instrumentation layout of all test specimens is illustrated in Figure A.20. There were 16 channels to capture and measure the loads and displacements that resulted during the test. These channels comprise load cells, cable transducers, and Linear Variable Differential Transformers (LVDTs). Channels 0 and 1 were used to measure the vertical and lateral loads, respectively. Channels 2, 3, and 4 were used to measure the lateral displacement at the mid-capping beam, top wall panel, and mid-wall panel, respectively. The slip of the wall base and RC base were measured using channels 5 and 6, respectively. Channel pairs of 7&8, 9&10, and 11&12 were used to measure the vertical displacement at two-course height, four-course height, and between base and capping beam, respectively. Channels 13 and 14 were used to measure the diagonal displacement within the whole wall panel. Out-of-plane displacement at the mid-wall panel was registered using channel 15. In addition, several strain gauges (S.Gs) were installed at the vertical and horizontal rebars before construction to measure the strains

of the steel rebars during the cyclic test. These gauges were positioned at various steel rebars locations to capture the cyclic response of the reinforcement as shown in Figure A.21.

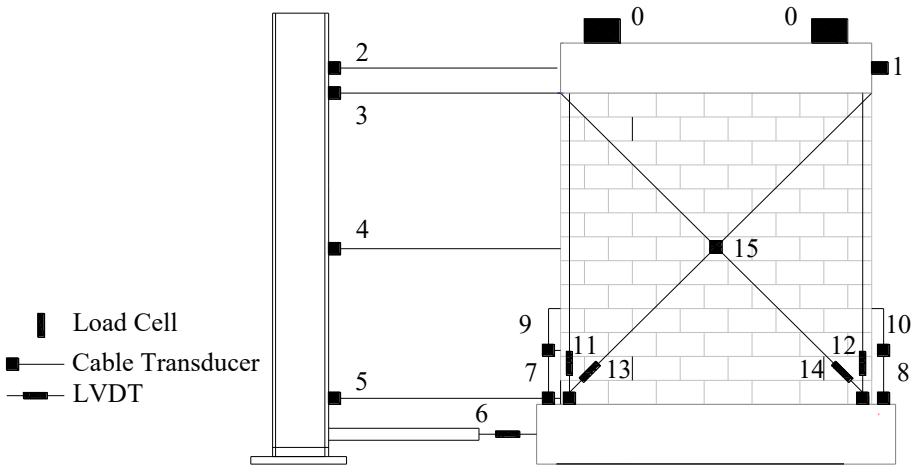

Figure A.20 Instrumentation layout

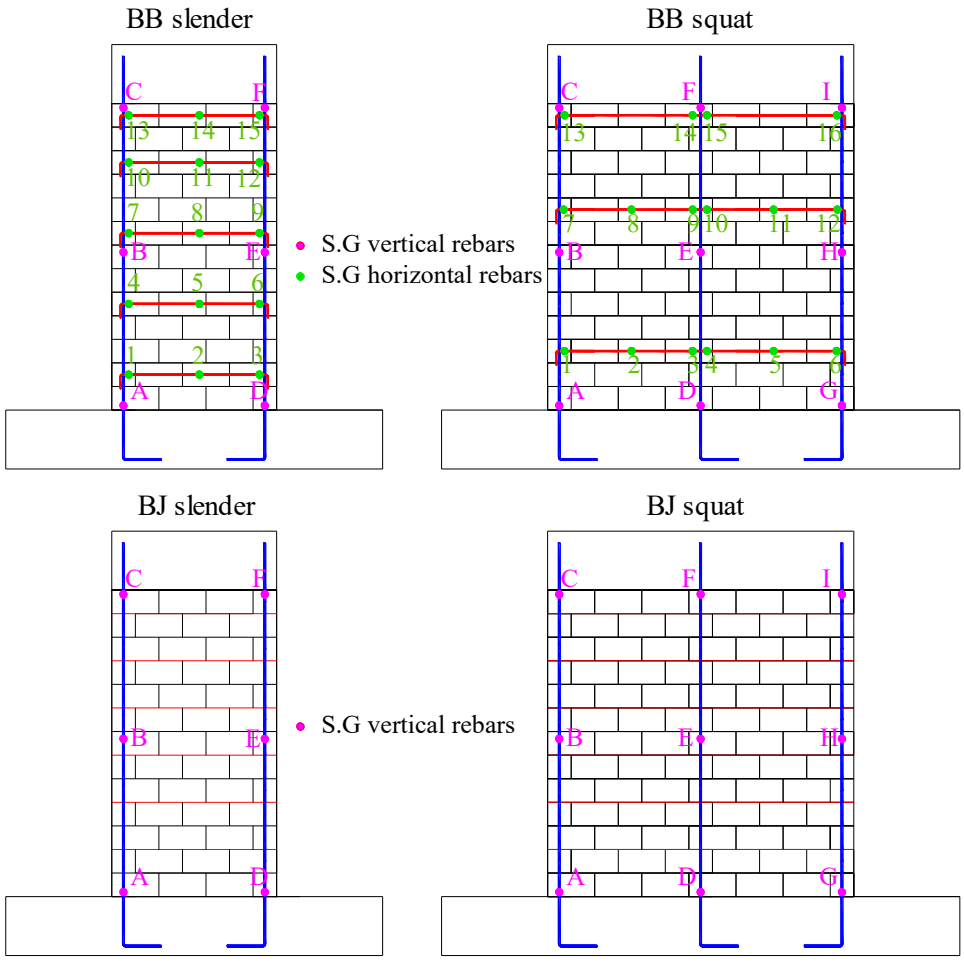

Figure A.21 Location of strain gauges on vertical and horizontal reinforcement

Finally, a Digital Image Correlation (DIC) system was implemented to measure the strains field of the west side of the wall specimen. This innovative system enhanced the ability to capture the strains in different directions, which enabled to identify crack propagation during the tests. The DIC zones layout is illustrated in Figure A.22.

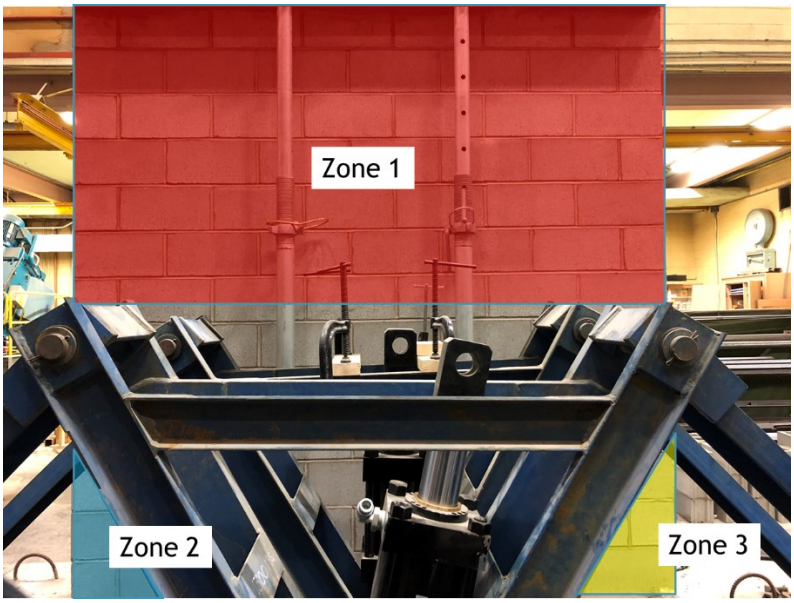

Figure A.21 DIC zones layout

Test specimens were subjected first to vertical loads up to certain limit using load-control protocol and then they were kept constant during the test. This limit depends on the ratio of the axial stress to the compressive strength of masonry unit block ($\sigma/f_{unit\ block}$= 0.1). The total applied vertical loads on the top of the test specimens were 516 kN and 973 kN for wall panels of an aspect ratio of 1.86 and wall panels of an aspect ratio 1.00, respectively. In-plane lateral loads then were applied in a reversal mode (Push then Pull at each displacement level) using a displacement-control protocol, as seen in Figure A.23. Each displacement level was repeated twice so that the stiffness degradation can be captured clearly (FEMA 461 2007). The Loading rate was 6 mm/min at the first displacement levels and then increased to 12 mm/min at latter levels. Finally, the test was stopped when the lateral loads reached 80% of the peak lateral load resulted during the test which defined as a failure point of the test specimen.

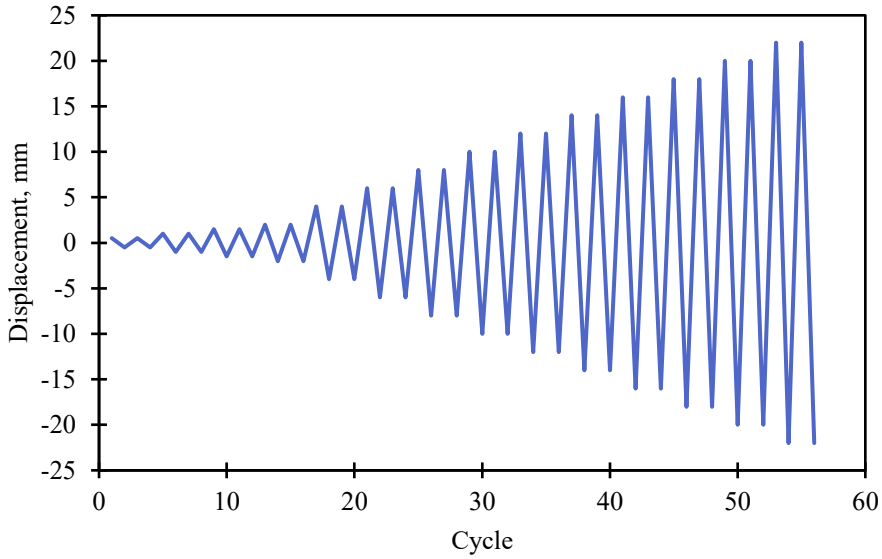

Figure A.22 Loading Protocol

APPENDIX B: DESCRIPTION OF NUMERICAL WALLS PROPERTIES

Wall ID	Aspect ratio H/L	Height H	Length L	Reinforcement ratio		Masonry comp. strength f'_m	Gross Axial stress/Masonry comp. strength, σ/f'_m
				Vertical ρ_v	Horizontal ρ_h		
	(Unitless)	(mm)	(mm)	(%)	(%)	(MPa)	(%)
BBW-1	1.86	2600	1400	0.26	0.13	10	5
BBW-2	1.86	2600	1400	0.26	0.09	10	5
BBW-3	1.86	2600	1400	0.26	0.04	10	5
BBW-4	1.86	2600	1400	0.18	0.13	10	5
BBW-5	1.86	2600	1400	0.18	0.09	10	5
BBW-6	1.86	2600	1400	0.18	0.04	10	5
BBW-7	1.86	2600	1400	0.09	0.13	10	5
BBW-8	1.86	2600	1400	0.09	0.09	10	5
BBW-9	1.86	2600	1400	0.09	0.04	10	5
BBW-10	1.86	2600	1400	0.26	0.13	10	10
BBW-11	1.86	2600	1400	0.26	0.09	10	10
BBW-12	1.86	2600	1400	0.26	0.04	10	10
BBW-13	1.86	2600	1400	0.18	0.13	10	10
BBW-14	1.86	2600	1400	0.18	0.09	10	10
BBW-15	1.86	2600	1400	0.18	0.04	10	10
BBW-16	1.86	2600	1400	0.09	0.13	10	10
BBW-17	1.86	2600	1400	0.09	0.09	10	10
BBW-18	1.86	2600	1400	0.09	0.04	10	10
BBW-19	1.86	2600	1400	0.26	0.13	10	15
BBW-20	1.86	2600	1400	0.26	0.09	10	15
BBW-21	1.86	2600	1400	0.26	0.04	10	15
BBW-22	1.86	2600	1400	0.18	0.13	10	15
BBW-23	1.86	2600	1400	0.18	0.09	10	15
BBW-24	1.86	2600	1400	0.18	0.04	10	15
BBW-25	1.86	2600	1400	0.09	0.13	10	15
BBW-26	1.86	2600	1400	0.09	0.09	10	15
BBW-27	1.86	2600	1400	0.09	0.04	10	15
BBW-28	1.86	2600	1400	0.26	0.13	15	5
BBW-29	1.86	2600	1400	0.26	0.09	15	5
BBW-30	1.86	2600	1400	0.26	0.04	15	5

* **BBW** means **W**alls reinforced with **B**ond **B**eam while **BJW** means **W**alls reinforced with **B**ed **J**oint

Wall ID	Aspect ratio H/L	Height H	Length L	Reinforcement ratio		Masonry comp. strength f'_m	Gross Axial stress/Masonry comp. strength, σ/f'_m
				Vertical ρ_v	Horizontal ρ_h		
	(Unitless)	(mm)	(mm)	(%)	(%)	(MPa)	(%)
BBW-31	1.86	2600	1400	0.18	0.13	15	5
BBW-32	1.86	2600	1400	0.18	0.09	15	5
BBW-33	1.86	2600	1400	0.18	0.04	15	5
BBW-34	1.86	2600	1400	0.09	0.13	15	5
BBW-35	1.86	2600	1400	0.09	0.09	15	5
BBW-36	1.86	2600	1400	0.09	0.04	15	5
BBW-37	1.86	2600	1400	0.26	0.13	15	10
BBW-38	1.86	2600	1400	0.26	0.09	15	10
BBW-39	1.86	2600	1400	0.26	0.04	15	10
BBW-40	1.86	2600	1400	0.18	0.13	15	10
BBW-41	1.86	2600	1400	0.18	0.09	15	10
BBW-42	1.86	2600	1400	0.18	0.04	15	10
BBW-43	1.86	2600	1400	0.09	0.13	15	10
BBW-44	1.86	2600	1400	0.09	0.09	15	10
BBW-45	1.86	2600	1400	0.09	0.04	15	10
BBW-46	1.86	2600	1400	0.26	0.13	15	15
BBW-47	1.86	2600	1400	0.26	0.09	15	15
BBW-48	1.86	2600	1400	0.26	0.04	15	15
BBW-49	1.86	2600	1400	0.18	0.13	15	15
BBW-50	1.86	2600	1400	0.18	0.09	15	15
BBW-51	1.86	2600	1400	0.18	0.04	15	15
BBW-52	1.86	2600	1400	0.09	0.13	15	15
BBW-53	1.86	2600	1400	0.09	0.09	15	15
BBW-54	1.86	2600	1400	0.09	0.04	15	15
BBW-55	1.86	2600	1400	0.26	0.13	20	5
BBW-56	1.86	2600	1400	0.26	0.09	20	5
BBW-57	1.86	2600	1400	0.26	0.04	20	5
BBW-58	1.86	2600	1400	0.18	0.13	20	5
BBW-59	1.86	2600	1400	0.18	0.09	20	5
BBW-60	1.86	2600	1400	0.18	0.04	20	5

* **BBW** means **W**alls reinforced with **B**ond **B**eam while **BJW** means **W**alls reinforced with **B**ed **J**oint

Wall ID	Aspect ratio H/L	Height H	Length L	Reinforcement ratio		Masonry comp. strength f'_m	Gross Axial stress/Masonry comp. strength, σ/f'_m
				Vertical ρ_v	Horizontal ρ_h		
	(Unitless)	(mm)	(mm)	(%)	(%)	(MPa)	(%)
BBW-61	1.86	2600	1400	0.09	0.13	20	5
BBW-62	1.86	2600	1400	0.09	0.09	20	5
BBW-63	1.86	2600	1400	0.09	0.04	20	5
BBW-64	1.86	2600	1400	0.26	0.13	20	10
BBW-65	1.86	2600	1400	0.26	0.09	20	10
BBW-66	1.86	2600	1400	0.26	0.04	20	10
BBW-67	1.86	2600	1400	0.18	0.13	20	10
BBW-68	1.86	2600	1400	0.18	0.09	20	10
BBW-69	1.86	2600	1400	0.18	0.04	20	10
BBW-70	1.86	2600	1400	0.09	0.13	20	10
BBW-71	1.86	2600	1400	0.09	0.09	20	10
BBW-72	1.86	2600	1400	0.09	0.04	20	10
BBW-73	1.86	2600	1400	0.26	0.13	20	15
BBW-74	1.86	2600	1400	0.26	0.09	20	15
BBW-75	1.86	2600	1400	0.26	0.04	20	15
BBW-76	1.86	2600	1400	0.18	0.13	20	15
BBW-77	1.86	2600	1400	0.18	0.09	20	15
BBW-78	1.86	2600	1400	0.18	0.04	20	15
BBW-79	1.86	2600	1400	0.09	0.13	20	15
BBW-80	1.86	2600	1400	0.09	0.09	20	15
BBW-81	1.86	2600	1400	0.09	0.04	20	15
BBW-82	1	2600	2600	0.26	0.13	10	5
BBW-83	1	2600	2600	0.26	0.09	10	5
BBW-84	1	2600	2600	0.26	0.04	10	5
BBW-85	1	2600	2600	0.18	0.13	10	5
BBW-86	1	2600	2600	0.18	0.09	10	5
BBW-87	1	2600	2600	0.18	0.04	10	5
BBW-88	1	2600	2600	0.09	0.13	10	5
BBW-89	1	2600	2600	0.09	0.09	10	5
BBW-90	1	2600	2600	0.09	0.04	10	5

* **BBW** means **W**alls reinforced with **B**ond **B**eam while **BJW** means **W**alls reinforced with **B**ed **J**oint

Wall ID	Aspect ratio H/L	Height H	Length L	Reinforcement ratio		Masonry comp. strength f'_m	Gross Axial stress/Masonry comp. strength, σ/f'_m
				Vertical ρ_v	Horizontal ρ_h		
	(Unitless)	(mm)	(mm)	(%)	(%)	(MPa)	(%)
BBW-91	1	2600	2600	0.26	0.13	10	10
BBW-92	1	2600	2600	0.26	0.09	10	10
BBW-93	1	2600	2600	0.26	0.04	10	10
BBW-94	1	2600	2600	0.18	0.13	10	10
BBW-95	1	2600	2600	0.18	0.09	10	10
BBW-96	1	2600	2600	0.18	0.04	10	10
BBW-97	1	2600	2600	0.09	0.13	10	10
BBW-98	1	2600	2600	0.09	0.09	10	10
BBW-99	1	2600	2600	0.09	0.04	10	10
BBW-100	1	2600	2600	0.26	0.13	10	15
BBW-101	1	2600	2600	0.26	0.09	10	15
BBW-102	1	2600	2600	0.26	0.04	10	15
BBW-103	1	2600	2600	0.18	0.13	10	15
BBW-104	1	2600	2600	0.18	0.09	10	15
BBW-105	1	2600	2600	0.18	0.04	10	15
BBW-106	1	2600	2600	0.09	0.13	10	15
BBW-107	1	2600	2600	0.09	0.09	10	15
BBW-108	1	2600	2600	0.09	0.04	10	15
BBW-109	1	2600	2600	0.26	0.13	15	5
BBW-110	1	2600	2600	0.26	0.09	15	5
BBW-111	1	2600	2600	0.26	0.04	15	5
BBW-112	1	2600	2600	0.18	0.13	15	5
BBW-113	1	2600	2600	0.18	0.09	15	5
BBW-114	1	2600	2600	0.18	0.04	15	5
BBW-115	1	2600	2600	0.09	0.13	15	5
BBW-116	1	2600	2600	0.09	0.09	15	5
BBW-117	1	2600	2600	0.09	0.04	15	5
BBW-118	1	2600	2600	0.26	0.13	15	10
BBW-119	1	2600	2600	0.26	0.09	15	10
BBW-120	1	2600	2600	0.26	0.04	15	10

* **BBW** means **W**alls reinforced with **B**ond **B**eam while **BJW** means **W**alls reinforced with **B**ed **J**oint

Wall ID	Aspect ratio H/L	Height H	Length L	Reinforcement ratio		Masonry comp. strength f'_m	Gross Axial stress/Masonry comp. strength, σ/f'_m
				Vertical ρ_v	Horizontal ρ_h		
	(Unitless)	(mm)	(mm)	(%)	(%)	(MPa)	(%)
BBW-121	1	2600	2600	0.18	0.13	15	10
BBW-122	1	2600	2600	0.18	0.09	15	10
BBW-123	1	2600	2600	0.18	0.04	15	10
BBW-124	1	2600	2600	0.09	0.13	15	10
BBW-125	1	2600	2600	0.09	0.09	15	10
BBW-126	1	2600	2600	0.09	0.04	15	10
BBW-127	1	2600	2600	0.26	0.13	15	15
BBW-128	1	2600	2600	0.26	0.09	15	15
BBW-129	1	2600	2600	0.26	0.04	15	15
BBW-130	1	2600	2600	0.18	0.13	15	15
BBW-131	1	2600	2600	0.18	0.09	15	15
BBW-132	1	2600	2600	0.18	0.04	15	15
BBW-133	1	2600	2600	0.09	0.13	15	15
BBW-134	1	2600	2600	0.09	0.09	15	15
BBW-135	1	2600	2600	0.09	0.04	15	15
BBW-136	1	2600	2600	0.26	0.13	20	5
BBW-137	1	2600	2600	0.26	0.09	20	5
BBW-138	1	2600	2600	0.26	0.04	20	5
BBW-139	1	2600	2600	0.18	0.13	20	5
BBW-140	1	2600	2600	0.18	0.09	20	5
BBW-141	1	2600	2600	0.18	0.04	20	5
BBW-142	1	2600	2600	0.09	0.13	20	5
BBW-143	1	2600	2600	0.09	0.09	20	5
BBW-144	1	2600	2600	0.09	0.04	20	5
BBW-145	1	2600	2600	0.26	0.13	20	10
BBW-146	1	2600	2600	0.26	0.09	20	10
BBW-147	1	2600	2600	0.26	0.04	20	10
BBW-148	1	2600	2600	0.18	0.13	20	10
BBW-149	1	2600	2600	0.18	0.09	20	10
BBW-150	1	2600	2600	0.18	0.04	20	10

* **BBW** means **W**alls reinforced with **B**ond **B**eam while **BJW** means **W**alls reinforced with **B**ed **J**oint

Wall ID	Aspect ratio H/L	Height H	Length L	Reinforcement ratio		Masonry comp. strength f'_m	Gross Axial stress/Masonry comp. strength, σ/f'_m
				Vertical ρ_v	Horizontal ρ_h		
	(Unitless)	(mm)	(mm)	(%)	(%)	(MPa)	(%)
BBW-151	1	2600	2600	0.09	0.13	20	10
BBW-152	1	2600	2600	0.09	0.09	20	10
BBW-153	1	2600	2600	0.09	0.04	20	10
BBW-154	1	2600	2600	0.26	0.13	20	15
BBW-155	1	2600	2600	0.26	0.09	20	15
BBW-156	1	2600	2600	0.26	0.04	20	15
BBW-157	1	2600	2600	0.18	0.13	20	15
BBW-158	1	2600	2600	0.18	0.09	20	15
BBW-159	1	2600	2600	0.18	0.04	20	15
BBW-160	1	2600	2600	0.09	0.13	20	15
BBW-161	1	2600	2600	0.09	0.09	20	15
BBW-162	1	2600	2600	0.09	0.04	20	15
BBW-163	0.42	2600	6200	0.26	0.13	10	5
BBW-164	0.42	2600	6200	0.26	0.09	10	5
BBW-165	0.42	2600	6200	0.26	0.04	10	5
BBW-166	0.42	2600	6200	0.18	0.13	10	5
BBW-167	0.42	2600	6200	0.18	0.09	10	5
BBW-168	0.42	2600	6200	0.18	0.04	10	5
BBW-169	0.42	2600	6200	0.09	0.13	10	5
BBW-170	0.42	2600	6200	0.09	0.09	10	5
BBW-171	0.42	2600	6200	0.09	0.04	10	5
BBW-172	0.42	2600	6200	0.26	0.13	10	10
BBW-173	0.42	2600	6200	0.26	0.09	10	10
BBW-174	0.42	2600	6200	0.26	0.04	10	10
BBW-175	0.42	2600	6200	0.18	0.13	10	10
BBW-176	0.42	2600	6200	0.18	0.09	10	10
BBW-177	0.42	2600	6200	0.18	0.04	10	10
BBW-178	0.42	2600	6200	0.09	0.13	10	10
BBW-179	0.42	2600	6200	0.09	0.09	10	10
BBW-180	0.42	2600	6200	0.09	0.04	10	10

* **BBW** means **W**alls reinforced with **B**ond **B**eam while **BJW** means **W**alls reinforced with **B**ed **J**oint

Wall ID	Aspect ratio H/L	Height H	Length L	Reinforcement ratio		Masonry comp. strength f'_m	Gross Axial stress/Masonry comp. strength, σ/f'_m
				Vertical ρ_v	Horizontal ρ_h		
	(Unitless)	(mm)	(mm)	(%)	(%)	(MPa)	(%)
BBW-181	0.42	2600	6200	0.26	0.13	10	15
BBW-182	0.42	2600	6200	0.26	0.09	10	15
BBW-183	0.42	2600	6200	0.26	0.04	10	15
BBW-184	0.42	2600	6200	0.18	0.13	10	15
BBW-185	0.42	2600	6200	0.18	0.09	10	15
BBW-186	0.42	2600	6200	0.18	0.04	10	15
BBW-187	0.42	2600	6200	0.09	0.13	10	15
BBW-188	0.42	2600	6200	0.09	0.09	10	15
BBW-189	0.42	2600	6200	0.09	0.04	10	15
BBW-190	0.42	2600	6200	0.26	0.13	15	5
BBW-191	0.42	2600	6200	0.26	0.09	15	5
BBW-192	0.42	2600	6200	0.26	0.04	15	5
BBW-193	0.42	2600	6200	0.18	0.13	15	5
BBW-194	0.42	2600	6200	0.18	0.09	15	5
BBW-195	0.42	2600	6200	0.18	0.04	15	5
BBW-196	0.42	2600	6200	0.09	0.13	15	5
BBW-197	0.42	2600	6200	0.09	0.09	15	5
BBW-198	0.42	2600	6200	0.09	0.04	15	5
BBW-199	0.42	2600	6200	0.26	0.13	15	10
BBW-200	0.42	2600	6200	0.26	0.09	15	10
BBW-201	0.42	2600	6200	0.26	0.04	15	10
BBW-202	0.42	2600	6200	0.18	0.13	15	10
BBW-203	0.42	2600	6200	0.18	0.09	15	10
BBW-204	0.42	2600	6200	0.18	0.04	15	10
BBW-205	0.42	2600	6200	0.09	0.13	15	10
BBW-206	0.42	2600	6200	0.09	0.09	15	10
BBW-207	0.42	2600	6200	0.09	0.04	15	10
BBW-208	0.42	2600	6200	0.26	0.13	15	15
BBW-209	0.42	2600	6200	0.26	0.09	15	15
BBW-210	0.42	2600	6200	0.26	0.04	15	15

* **BBW** means **W**alls reinforced with **B**ond **B**eam while **BJW** means **W**alls reinforced with **B**ed **J**oint

Wall ID	Aspect ratio H/L	Height H	Length L	Reinforcement ratio		Masonry comp. strength f'_m	Gross Axial stress/Masonry comp. strength, σ/f'_m
				Vertical ρ_v	Horizontal ρ_h		
	(Unitless)	(mm)	(mm)	(%)	(%)	(MPa)	(%)
BBW-211	0.42	2600	6200	0.18	0.13	15	15
BBW-212	0.42	2600	6200	0.18	0.09	15	15
BBW-213	0.42	2600	6200	0.18	0.04	15	15
BBW-214	0.42	2600	6200	0.09	0.13	15	15
BBW-215	0.42	2600	6200	0.09	0.09	15	15
BBW-216	0.42	2600	6200	0.09	0.04	15	15
BBW-217	0.42	2600	6200	0.26	0.13	20	5
BBW-218	0.42	2600	6200	0.26	0.09	20	5
BBW-219	0.42	2600	6200	0.26	0.04	20	5
BBW-220	0.42	2600	6200	0.18	0.13	20	5
BBW-221	0.42	2600	6200	0.18	0.09	20	5
BBW-222	0.42	2600	6200	0.18	0.04	20	5
BBW-223	0.42	2600	6200	0.09	0.13	20	5
BBW-224	0.42	2600	6200	0.09	0.09	20	5
BBW-225	0.42	2600	6200	0.09	0.04	20	5
BBW-226	0.42	2600	6200	0.26	0.13	20	10
BBW-227	0.42	2600	6200	0.26	0.09	20	10
BBW-228	0.42	2600	6200	0.26	0.04	20	10
BBW-229	0.42	2600	6200	0.18	0.13	20	10
BBW-230	0.42	2600	6200	0.18	0.09	20	10
BBW-231	0.42	2600	6200	0.18	0.04	20	10
BBW-232	0.42	2600	6200	0.09	0.13	20	10
BBW-233	0.42	2600	6200	0.09	0.09	20	10
BBW-234	0.42	2600	6200	0.09	0.04	20	10
BBW-235	0.42	2600	6200	0.26	0.13	20	15
BBW-236	0.42	2600	6200	0.26	0.09	20	15
BBW-237	0.42	2600	6200	0.26	0.04	20	15
BBW-238	0.42	2600	6200	0.18	0.13	20	15
BBW-239	0.42	2600	6200	0.18	0.09	20	15
BBW-240	0.42	2600	6200	0.18	0.04	20	15

* **BBW** means **W**alls reinforced with **B**ond **B**eam while **BJW** means **W**alls reinforced with **B**ed **J**oint

Wall ID	Aspect ratio H/L	Height H	Length L	Reinforcement ratio		Masonry comp. strength f'_m	Gross Axial stress/Masonry comp. strength, σ/f'_m
				Vertical ρ_v	Horizontal ρ_h		
	(Unitless)	(mm)	(mm)	(%)	(%)	(MPa)	(%)
BBW-241	0.42	2600	6200	0.09	0.13	20	15
BBW-242	0.42	2600	6200	0.09	0.09	20	15
BBW-243	0.42	2600	6200	0.09	0.04	20	15
BJW-1	1.86	2600	1400	0.26	0.08	10	5
BJW-2	1.86	2600	1400	0.26	0.05	10	5
BJW-3	1.86	2600	1400	0.26	0.04	10	5
BJW-4	1.86	2600	1400	0.18	0.08	10	5
BJW-5	1.86	2600	1400	0.18	0.05	10	5
BJW-6	1.86	2600	1400	0.18	0.04	10	5
BJW-7	1.86	2600	1400	0.09	0.08	10	5
BJW-8	1.86	2600	1400	0.09	0.05	10	5
BJW-9	1.86	2600	1400	0.09	0.04	10	5
BJW-10	1.86	2600	1400	0.26	0.08	10	10
BJW-11	1.86	2600	1400	0.26	0.05	10	10
BJW-12	1.86	2600	1400	0.26	0.04	10	10
BJW-13	1.86	2600	1400	0.18	0.08	10	10
BJW-14	1.86	2600	1400	0.18	0.05	10	10
BJW-15	1.86	2600	1400	0.18	0.04	10	10
BJW-16	1.86	2600	1400	0.09	0.08	10	10
BJW-17	1.86	2600	1400	0.09	0.05	10	10
BJW-18	1.86	2600	1400	0.09	0.04	10	10
BJW-19	1.86	2600	1400	0.26	0.08	10	15
BJW-20	1.86	2600	1400	0.26	0.05	10	15
BJW-21	1.86	2600	1400	0.26	0.04	10	15
BJW-22	1.86	2600	1400	0.18	0.08	10	15
BJW-23	1.86	2600	1400	0.18	0.05	10	15
BJW-24	1.86	2600	1400	0.18	0.04	10	15
BJW-25	1.86	2600	1400	0.09	0.08	10	15
BJW-26	1.86	2600	1400	0.09	0.05	10	15
BJW-27	1.86	2600	1400	0.09	0.04	10	15

* **BBW** means **W**alls reinforced with **B**ond **B**eam while **BJW** means **W**alls reinforced with **B**ed **J**oint

Wall ID	Aspect ratio H/L	Height H	Length L	Reinforcement ratio		Masonry comp. strength f'_m	Gross Axial stress/Masonry comp. strength, σ/f'_m
				Vertical ρ_v	Horizontal ρ_h		
	(Unitless)	(mm)	(mm)	(%)	(%)	(MPa)	(%)
BJW-28	1.86	2600	1400	0.26	0.08	15	5
BJW-29	1.86	2600	1400	0.26	0.05	15	5
BJW-30	1.86	2600	1400	0.26	0.04	15	5
BJW-31	1.86	2600	1400	0.18	0.08	15	5
BJW-32	1.86	2600	1400	0.18	0.05	15	5
BJW-33	1.86	2600	1400	0.18	0.04	15	5
BJW-34	1.86	2600	1400	0.09	0.08	15	5
BJW-35	1.86	2600	1400	0.09	0.05	15	5
BJW-36	1.86	2600	1400	0.09	0.04	15	5
BJW-37	1.86	2600	1400	0.26	0.08	15	10
BJW-38	1.86	2600	1400	0.26	0.05	15	10
BJW-39	1.86	2600	1400	0.26	0.04	15	10
BJW-40	1.86	2600	1400	0.18	0.08	15	10
BJW-41	1.86	2600	1400	0.18	0.05	15	10
BJW-42	1.86	2600	1400	0.18	0.04	15	10
BJW-43	1.86	2600	1400	0.09	0.08	15	10
BJW-44	1.86	2600	1400	0.09	0.05	15	10
BJW-45	1.86	2600	1400	0.09	0.04	15	10
BJW-46	1.86	2600	1400	0.26	0.08	15	15
BJW-47	1.86	2600	1400	0.26	0.05	15	15
BJW-48	1.86	2600	1400	0.26	0.04	15	15
BJW-49	1.86	2600	1400	0.18	0.08	15	15
BJW-50	1.86	2600	1400	0.18	0.05	15	15
BJW-51	1.86	2600	1400	0.18	0.04	15	15
BJW-52	1.86	2600	1400	0.09	0.08	15	15
BJW-53	1.86	2600	1400	0.09	0.05	15	15
BJW-54	1.86	2600	1400	0.09	0.04	15	15
BJW-55	1.86	2600	1400	0.26	0.08	20	5
BJW-56	1.86	2600	1400	0.26	0.05	20	5
BJW-57	1.86	2600	1400	0.26	0.04	20	5

* **BBW** means **W**alls reinforced with **B**ond **B**eam while **BJW** means **W**alls reinforced with **B**ed **J**oint

Wall ID	Aspect ratio H/L	Height H	Length L	Reinforcement ratio		Masonry comp. strength f'_m	Gross Axial stress/Masonry comp. strength, σ/f'_m
				Vertical ρ_v	Horizontal ρ_h		
	(Unitless)	(mm)	(mm)	(%)	(%)	(MPa)	(%)
BJW-58	1.86	2600	1400	0.18	0.08	20	5
BJW-59	1.86	2600	1400	0.18	0.05	20	5
BJW-60	1.86	2600	1400	0.18	0.04	20	5
BJW-61	1.86	2600	1400	0.09	0.08	20	5
BJW-62	1.86	2600	1400	0.09	0.05	20	5
BJW-63	1.86	2600	1400	0.09	0.04	20	5
BJW-64	1.86	2600	1400	0.26	0.08	20	10
BJW-65	1.86	2600	1400	0.26	0.05	20	10
BJW-66	1.86	2600	1400	0.26	0.04	20	10
BJW-67	1.86	2600	1400	0.18	0.08	20	10
BJW-68	1.86	2600	1400	0.18	0.05	20	10
BJW-69	1.86	2600	1400	0.18	0.04	20	10
BJW-70	1.86	2600	1400	0.09	0.08	20	10
BJW-71	1.86	2600	1400	0.09	0.05	20	10
BJW-72	1.86	2600	1400	0.09	0.04	20	10
BJW-73	1.86	2600	1400	0.26	0.08	20	15
BJW-74	1.86	2600	1400	0.26	0.05	20	15
BJW-75	1.86	2600	1400	0.26	0.04	20	15
BJW-76	1.86	2600	1400	0.18	0.08	20	15
BJW-77	1.86	2600	1400	0.18	0.05	20	15
BJW-78	1.86	2600	1400	0.18	0.04	20	15
BJW-79	1.86	2600	1400	0.09	0.08	20	15
BJW-80	1.86	2600	1400	0.09	0.05	20	15
BJW-81	1.86	2600	1400	0.09	0.04	20	15
BJW-82	1	2600	2600	0.26	0.08	10	5
BJW-83	1	2600	2600	0.26	0.05	10	5
BJW-84	1	2600	2600	0.26	0.04	10	5
BJW-85	1	2600	2600	0.18	0.08	10	5
BJW-86	1	2600	2600	0.18	0.05	10	5
BJW-87	1	2600	2600	0.18	0.04	10	5

* **BBW** means **W**alls reinforced with **B**ond **B**eam while **BJW** means **W**alls reinforced with **B**ed **J**oint

Wall ID	Aspect ratio H/L	Height H	Length L	Reinforcement ratio		Masonry comp. strength f'_m	Gross Axial stress/Masonry comp. strength, σ/f'_m
				Vertical ρ_v	Horizontal ρ_h		
	(Unitless)	(mm)	(mm)	(%)	(%)	(MPa)	(%)
BJW-88	1	2600	2600	0.09	0.08	10	5
BJW-89	1	2600	2600	0.09	0.05	10	5
BJW-90	1	2600	2600	0.09	0.04	10	5
BJW-91	1	2600	2600	0.26	0.08	10	10
BJW-92	1	2600	2600	0.26	0.05	10	10
BJW-93	1	2600	2600	0.26	0.04	10	10
BJW-94	1	2600	2600	0.18	0.08	10	10
BJW-95	1	2600	2600	0.18	0.05	10	10
BJW-96	1	2600	2600	0.18	0.04	10	10
BJW-97	1	2600	2600	0.09	0.08	10	10
BJW-98	1	2600	2600	0.09	0.05	10	10
BJW-99	1	2600	2600	0.09	0.04	10	10
BJW-100	1	2600	2600	0.26	0.08	10	15
BJW-101	1	2600	2600	0.26	0.05	10	15
BJW-102	1	2600	2600	0.26	0.04	10	15
BJW-103	1	2600	2600	0.18	0.08	10	15
BJW-104	1	2600	2600	0.18	0.05	10	15
BJW-105	1	2600	2600	0.18	0.04	10	15
BJW-106	1	2600	2600	0.09	0.08	10	15
BJW-107	1	2600	2600	0.09	0.05	10	15
BJW-108	1	2600	2600	0.09	0.04	10	15
BJW-109	1	2600	2600	0.26	0.08	15	5
BJW-110	1	2600	2600	0.26	0.05	15	5
BJW-111	1	2600	2600	0.26	0.04	15	5
BJW-112	1	2600	2600	0.18	0.08	15	5
BJW-113	1	2600	2600	0.18	0.05	15	5
BJW-114	1	2600	2600	0.18	0.04	15	5
BJW-115	1	2600	2600	0.09	0.08	15	5
BJW-116	1	2600	2600	0.09	0.05	15	5
BJW-117	1	2600	2600	0.09	0.04	15	5

* **BBW** means **W**alls reinforced with **B**ond **B**eam while **BJW** means **W**alls reinforced with **B**ed **J**oint

Wall ID	Aspect ratio H/L	Height H	Length L	Reinforcement ratio		Masonry comp. strength f'_m	Gross Axial stress/Masonry comp. strength, σ/f'_m
				Vertical ρ_v	Horizontal ρ_h		
	(Unitless)	(mm)	(mm)	(%)	(%)	(MPa)	(%)
BJW-118	1	2600	2600	0.26	0.08	15	10
BJW-119	1	2600	2600	0.26	0.05	15	10
BJW-120	1	2600	2600	0.26	0.04	15	10
BJW-121	1	2600	2600	0.18	0.08	15	10
BJW-122	1	2600	2600	0.18	0.05	15	10
BJW-123	1	2600	2600	0.18	0.04	15	10
BJW-124	1	2600	2600	0.09	0.08	15	10
BJW-125	1	2600	2600	0.09	0.05	15	10
BJW-126	1	2600	2600	0.09	0.04	15	10
BJW-127	1	2600	2600	0.26	0.08	15	15
BJW-128	1	2600	2600	0.26	0.05	15	15
BJW-129	1	2600	2600	0.26	0.04	15	15
BJW-130	1	2600	2600	0.18	0.08	15	15
BJW-131	1	2600	2600	0.18	0.05	15	15
BJW-132	1	2600	2600	0.18	0.04	15	15
BJW-133	1	2600	2600	0.09	0.08	15	15
BJW-134	1	2600	2600	0.09	0.05	15	15
BJW-135	1	2600	2600	0.09	0.04	15	15
BJW-136	1	2600	2600	0.26	0.08	20	5
BJW-137	1	2600	2600	0.26	0.05	20	5
BJW-138	1	2600	2600	0.26	0.04	20	5
BJW-139	1	2600	2600	0.18	0.08	20	5
BJW-140	1	2600	2600	0.18	0.05	20	5
BJW-141	1	2600	2600	0.18	0.04	20	5
BJW-142	1	2600	2600	0.09	0.08	20	5
BJW-143	1	2600	2600	0.09	0.05	20	5
BJW-144	1	2600	2600	0.09	0.04	20	5
BJW-145	1	2600	2600	0.26	0.08	20	10
BJW-146	1	2600	2600	0.26	0.05	20	10
BJW-147	1	2600	2600	0.26	0.04	20	10

* **BBW** means **W**alls reinforced with **B**ond **B**eam while **BJW** means **W**alls reinforced with **B**ed **J**oint

Wall ID	Aspect ratio H/L	Height H	Length L	Reinforcement ratio		Masonry comp. strength f'_m	Gross Axial stress/Masonry comp. strength, σ/f'_m
				Vertical ρ_v	Horizontal ρ_h		
	(Unitless)	(mm)	(mm)	(%)	(%)	(MPa)	(%)
BJW-148	1	2600	2600	0.18	0.08	20	10
BJW-149	1	2600	2600	0.18	0.05	20	10
BJW-150	1	2600	2600	0.18	0.04	20	10
BJW-151	1	2600	2600	0.09	0.08	20	10
BJW-152	1	2600	2600	0.09	0.05	20	10
BJW-153	1	2600	2600	0.09	0.04	20	10
BJW-154	1	2600	2600	0.26	0.08	20	15
BJW-155	1	2600	2600	0.26	0.05	20	15
BJW-156	1	2600	2600	0.26	0.04	20	15
BJW-157	1	2600	2600	0.18	0.08	20	15
BJW-158	1	2600	2600	0.18	0.05	20	15
BJW-159	1	2600	2600	0.18	0.04	20	15
BJW-160	1	2600	2600	0.09	0.08	20	15
BJW-161	1	2600	2600	0.09	0.05	20	15
BJW-162	1	2600	2600	0.09	0.04	20	15
BJW-163	0.42	2600	6200	0.26	0.08	10	5
BJW-164	0.42	2600	6200	0.26	0.05	10	5
BJW-165	0.42	2600	6200	0.26	0.04	10	5
BJW-166	0.42	2600	6200	0.18	0.08	10	5
BJW-167	0.42	2600	6200	0.18	0.05	10	5
BJW-168	0.42	2600	6200	0.18	0.04	10	5
BJW-169	0.42	2600	6200	0.09	0.08	10	5
BJW-170	0.42	2600	6200	0.09	0.05	10	5
BJW-171	0.42	2600	6200	0.09	0.04	10	5
BJW-172	0.42	2600	6200	0.26	0.08	10	10
BJW-173	0.42	2600	6200	0.26	0.05	10	10
BJW-174	0.42	2600	6200	0.26	0.04	10	10
BJW-175	0.42	2600	6200	0.18	0.08	10	10
BJW-176	0.42	2600	6200	0.18	0.05	10	10
BJW-177	0.42	2600	6200	0.18	0.04	10	10

* **BBW** means **W**alls reinforced with **B**ond **B**eam while **BJW** means **W**alls reinforced with **B**ed **J**oint

Wall ID	Aspect ratio H/L	Height H	Length L	Reinforcement ratio		Masonry comp. strength f'_m	Gross Axial stress/Masonry comp. strength, σ/f'_m
				Vertical ρ_v	Horizontal ρ_h		
	(Unitless)	(mm)	(mm)	(%)	(%)	(MPa)	(%)
BJW-178	0.42	2600	6200	0.09	0.08	10	10
BJW-179	0.42	2600	6200	0.09	0.05	10	10
BJW-180	0.42	2600	6200	0.09	0.04	10	10
BJW-181	0.42	2600	6200	0.26	0.08	10	15
BJW-182	0.42	2600	6200	0.26	0.05	10	15
BJW-183	0.42	2600	6200	0.26	0.04	10	15
BJW-184	0.42	2600	6200	0.18	0.08	10	15
BJW-185	0.42	2600	6200	0.18	0.05	10	15
BJW-186	0.42	2600	6200	0.18	0.04	10	15
BJW-187	0.42	2600	6200	0.09	0.08	10	15
BJW-188	0.42	2600	6200	0.09	0.05	10	15
BJW-189	0.42	2600	6200	0.09	0.04	10	15
BJW-190	0.42	2600	6200	0.26	0.08	15	5
BJW-191	0.42	2600	6200	0.26	0.05	15	5
BJW-192	0.42	2600	6200	0.26	0.04	15	5
BJW-193	0.42	2600	6200	0.18	0.08	15	5
BJW-194	0.42	2600	6200	0.18	0.05	15	5
BJW-195	0.42	2600	6200	0.18	0.04	15	5
BJW-196	0.42	2600	6200	0.09	0.08	15	5
BJW-197	0.42	2600	6200	0.09	0.05	15	5
BJW-198	0.42	2600	6200	0.09	0.04	15	5
BJW-199	0.42	2600	6200	0.26	0.08	15	10
BJW-200	0.42	2600	6200	0.26	0.05	15	10
BJW-201	0.42	2600	6200	0.26	0.04	15	10
BJW-202	0.42	2600	6200	0.18	0.08	15	10
BJW-203	0.42	2600	6200	0.18	0.05	15	10
BJW-204	0.42	2600	6200	0.18	0.04	15	10
BJW-205	0.42	2600	6200	0.09	0.08	15	10
BJW-206	0.42	2600	6200	0.09	0.05	15	10
BJW-207	0.42	2600	6200	0.09	0.04	15	10

* **BBW** means **W**alls reinforced with **B**ond **B**eam while **BJW** means **W**alls reinforced with **B**ed **J**oint

Wall ID	Aspect ratio H/L	Height H	Length L	Reinforcement ratio		Masonry comp. strength f'_m	Gross Axial stress/Masonry comp. strength, σ/f'_m
				Vertical ρ_v	Horizontal ρ_h		
	(Unitless)	(mm)	(mm)	(%)	(%)	(MPa)	(%)
BJW-208	0.42	2600	6200	0.26	0.08	15	15
BJW-209	0.42	2600	6200	0.26	0.05	15	15
BJW-210	0.42	2600	6200	0.26	0.04	15	15
BJW-211	0.42	2600	6200	0.18	0.08	15	15
BJW-212	0.42	2600	6200	0.18	0.05	15	15
BJW-213	0.42	2600	6200	0.18	0.04	15	15
BJW-214	0.42	2600	6200	0.09	0.08	15	15
BJW-215	0.42	2600	6200	0.09	0.05	15	15
BJW-216	0.42	2600	6200	0.09	0.04	15	15
BJW-217	0.42	2600	6200	0.26	0.08	20	5
BJW-218	0.42	2600	6200	0.26	0.05	20	5
BJW-219	0.42	2600	6200	0.26	0.04	20	5
BJW-220	0.42	2600	6200	0.18	0.08	20	5
BJW-221	0.42	2600	6200	0.18	0.05	20	5
BJW-222	0.42	2600	6200	0.18	0.04	20	5
BJW-223	0.42	2600	6200	0.09	0.08	20	5
BJW-224	0.42	2600	6200	0.09	0.05	20	5
BJW-225	0.42	2600	6200	0.09	0.04	20	5
BJW-226	0.42	2600	6200	0.26	0.08	20	10
BJW-227	0.42	2600	6200	0.26	0.05	20	10
BJW-228	0.42	2600	6200	0.26	0.04	20	10
BJW-229	0.42	2600	6200	0.18	0.08	20	10
BJW-230	0.42	2600	6200	0.18	0.05	20	10
BJW-231	0.42	2600	6200	0.18	0.04	20	10
BJW-232	0.42	2600	6200	0.09	0.08	20	10
BJW-233	0.42	2600	6200	0.09	0.05	20	10
BJW-234	0.42	2600	6200	0.09	0.04	20	10
BJW-235	0.42	2600	6200	0.26	0.08	20	15
BJW-236	0.42	2600	6200	0.26	0.05	20	15
BJW-237	0.42	2600	6200	0.26	0.04	20	15

* **BBW** means **W**alls reinforced with **B**ond **B**eam while **BJW** means **W**alls reinforced with **B**ed **J**oint

Wall ID	Aspect ratio H/L	Height H	Length L	Reinforcement ratio		Masonry comp. strength f'_m	Gross Axial stress/Masonry comp. strength, σ/f'_m
				Vertical ρ_v	Horizontal ρ_h		
	(Unitless)	(mm)	(mm)	(%)	(%)	(MPa)	(%)
BJW-238	0.42	2600	6200	0.18	0.08	20	15
BJW-239	0.42	2600	6200	0.18	0.05	20	15
BJW-240	0.42	2600	6200	0.18	0.04	20	15
BJW-241	0.42	2600	6200	0.09	0.08	20	15
BJW-242	0.42	2600	6200	0.09	0.05	20	15
BJW-243	0.42	2600	6200	0.09	0.04	20	15
BBW-9-5	1.86	2600	1400	0.09	0.04	5	5
BBW-18-5	1.86	2600	1400	0.09	0.04	5	10
BBW-27-5	1.86	2600	1400	0.09	0.04	5	15
BBW-9-7.5	1.86	2600	1400	0.09	0.04	7.5	5
BBW-18-7.5	1.86	2600	1400	0.09	0.04	7.5	10
BBW-27-7.5	1.86	2600	1400	0.09	0.04	7.5	15
BBW-9-12	1.86	2600	1400	0.09	0.04	12.5	5
BBW-18-12	1.86	2600	1400	0.09	0.04	12.5	10
BBW-27-12	1.86	2600	1400	0.09	0.04	12.5	15
BBW-9-17.5	1.86	2600	1400	0.09	0.04	17.5	5
BBW-18-17.5	1.86	2600	1400	0.09	0.04	17.5	10
BBW-27-17.5	1.86	2600	1400	0.09	0.04	17.5	15
BBW-90-5	1	2600	2600	0.09	0.04	5	5
BBW-99-5	1	2600	2600	0.09	0.04	5	10
BBW-108-5	1	2600	2600	0.09	0.04	5	15
BBW-90-7.5	1	2600	2600	0.09	0.04	7.5	5
BBW-99-7.5	1	2600	2600	0.09	0.04	7.5	10
BBW-108-7.5	1	2600	2600	0.09	0.04	7.5	15
BBW-90-12.5	1	2600	2600	0.09	0.04	12.5	5
BBW-99-12.5	1	2600	2600	0.09	0.04	12.5	10
BBW-108-12.5	1	2600	2600	0.09	0.04	12.5	15
BBW-90-17.5	1	2600	2600	0.09	0.04	17.5	5
BBW-99-17.5	1	2600	2600	0.09	0.04	17.5	10
BBW-108-17.5	1	2600	2600	0.09	0.04	17.5	15

* **BBW** means **W**alls reinforced with **B**ond **B**eam while **BJW** means **W**alls reinforced with **B**ed **J**oint

Wall ID	Aspect ratio H/L	Height H	Length L	Reinforcement ratio		Masonry comp. strength	Gross Axial stress/Masonry comp. strength,
				Vertical	Horizontal		
				ρ_v	ρ_h	f'_m	σ/f'_m
	(Unitless)	(mm)	(mm)	(%)	(%)	(MPa)	(%)
BBW-171-5	0.42	2600	6200	0.09	0.04	5	5
BBW-180-5	0.42	2600	6200	0.09	0.04	5	10
BBW-189-5	0.42	2600	6200	0.09	0.04	5	15
BBW-171-7.5	0.42	2600	6200	0.09	0.04	7.5	5
BBW-180-7.5	0.42	2600	6200	0.09	0.04	7.5	10
BBW-189-7.5	0.42	2600	6200	0.09	0.04	7.5	15
BBW-171-12.5	0.42	2600	6200	0.09	0.04	12.5	5
BBW-180-12.5	0.42	2600	6200	0.09	0.04	12.5	10
BBW-189-12.5	0.42	2600	6200	0.09	0.04	12.5	15
BBW-171-17.5	0.42	2600	6200	0.09	0.04	17.5	5
BBW-180-17.5	0.42	2600	6200	0.09	0.04	17.5	10
BBW-189-17.5	0.42	2600	6200	0.09	0.04	17.5	15
BJW-9-5	1.86	2600	1400	0.09	0.04	5	5
BJW-18-5	1.86	2600	1400	0.09	0.04	5	10
BJW-27-5	1.86	2600	1400	0.09	0.04	5	15
BJW-9-7.5	1.86	2600	1400	0.09	0.04	7.5	5
BJW-18-7.5	1.86	2600	1400	0.09	0.04	7.5	10
BJW-27-7.5	1.86	2600	1400	0.09	0.04	7.5	15
BJW-9-12.5	1.86	2600	1400	0.09	0.04	12.5	5
BJW-18-12.5	1.86	2600	1400	0.09	0.04	12.5	10
BJW-27-12.5	1.86	2600	1400	0.09	0.04	12.5	15
BJW-9-17.5	1.86	2600	1400	0.09	0.04	17.5	5
BJW-18-17.5	1.86	2600	1400	0.09	0.04	17.5	10
BJW-27-17.5	1.86	2600	1400	0.09	0.04	17.5	15
BJW-90-5	1	2600	2600	0.09	0.04	5	5
BJW-99-5	1	2600	2600	0.09	0.04	5	10
BJW-108-5	1	2600	2600	0.09	0.04	5	15
BJW-90-7.5	1	2600	2600	0.09	0.04	7.5	5
BJW-99-7.5	1	2600	2600	0.09	0.04	7.5	10
BJW-108-7.5	1	2600	2600	0.09	0.04	7.5	15

* **BBW** means **W**alls reinforced with **B**ond **B**eam while **BJW** means **W**alls reinforced with **B**ed **J**oint

Wall ID	Aspect ratio H/L	Height H	Length L	Reinforcement ratio		Masonry comp. strength f'_m	Gross Axial stress/Masonry comp. strength, σ/f'_m
				Vertical ρ_v	Horizontal ρ_h		
	(Unitless)	(mm)	(mm)	(%)	(%)	(MPa)	(%)
BJW-90-12.5	1	2600	2600	0.09	0.04	12.5	5
BJW-99-12.5	1	2600	2600	0.09	0.04	12.5	10
BJW-108-12.5	1	2600	2600	0.09	0.04	12.5	15
BJW-90-17.5	1	2600	2600	0.09	0.04	17.5	5
BJW-99-17.5	1	2600	2600	0.09	0.04	17.5	10
BJW-108-17.5	1	2600	2600	0.09	0.04	17.5	15
BJW-171-5	0.42	2600	6200	0.09	0.04	5	5
BJW-180-5	0.42	2600	6200	0.09	0.04	5	10
BJW-189-5	0.42	2600	6200	0.09	0.04	5	15
BJW-171-7.5	0.42	2600	6200	0.09	0.04	7.5	5
BJW-180-7.5	0.42	2600	6200	0.09	0.04	7.5	10
BJW-189-7.5	0.42	2600	6200	0.09	0.04	7.5	15
BJW-171-12.5	0.42	2600	6200	0.09	0.04	12.5	5
BJW-180-12.5	0.42	2600	6200	0.09	0.04	12.5	10
BJW-189-12.5	0.42	2600	6200	0.09	0.04	12.5	15
BJW-171-17.5	0.42	2600	6200	0.09	0.04	17.5	5
BJW-180-17.5	0.42	2600	6200	0.09	0.04	17.5	10
BJW-189-17.5	0.42	2600	6200	0.09	0.04	17.5	15
BBW-18-5-Xtra	1.86	2600	1400	0.09	0.04	5	20
BBW-18-7.5-Xtra	1.86	2600	1400	0.09	0.04	7.5	20
BBW-18-Xtra	1.86	2600	1400	0.09	0.04	10	20
BBW-18-12-Xtra	1.86	2600	1400	0.09	0.04	12.5	20
BBW-45-Xtra	1.86	2600	1400	0.09	0.04	15	20
BBW-18-17.5-Xtra	1.86	2600	1400	0.09	0.04	17.5	20
BBW-72-Xtra	1.86	2600	1400	0.09	0.04	20	20
BBW-72-Xtra1	1.86	2600	1400	0.09	0.04	20	25
BBW-72-Xtra2	1.86	2600	1400	0.09	0.04	20	30
BBW-72-Xtra3	1.86	2600	1400	0.09	0.04	20	35
BBW-72-Xtra4	1.86	2600	1400	0.09	0.04	20	40
BBW-72-Xtra5	1.86	2600	1400	0.09	0.04	20	0

* **BBW** means **W**alls reinforced with **B**ond **B**eam while **BJW** means **W**alls reinforced with **B**ed **J**oint

Wall ID	Aspect ratio H/L	Height H	Length L	Reinforcement ratio		Masonry comp. strength f'_m	Gross Axial stress/Masonry comp. strength, σ/f'_m
				Vertical ρ_v	Horizontal ρ_h		
	(Unitless)	(mm)	(mm)	(%)	(%)	(MPa)	(%)
BBW-99-5-Xtra	1	2600	2600	0.09	0.04	5	20
BBW-99-7.5-Xtra	1	2600	2600	0.09	0.04	7.5	20
BBW-99-Xtra	1	2600	2600	0.09	0.04	10	20
BBW-99-12.5-Xtra	1	2600	2600	0.09	0.04	12.5	20
BBW-126-Xtra	1	2600	2600	0.09	0.04	15	20
BBW-99-17.5-Xtra	1	2600	2600	0.09	0.04	17.5	20
BBW-153-Xtra	1	2600	2600	0.09	0.04	20	20
BBW-153-Xtra1	1	2600	2600	0.09	0.04	20	25
BBW-153-Xtra2	1	2600	2600	0.09	0.04	20	30
BBW-153-Xtra3	1	2600	2600	0.09	0.04	20	35
BBW-153-Xtra4	1	2600	2600	0.09	0.04	20	40
BBW-153-Xtra5	1	2600	2600	0.09	0.04	20	0
BBW-180-5-Xtra	0.42	2600	6200	0.09	0.04	5	20
BBW-180-7.5-Xtra	0.42	2600	6200	0.09	0.04	7.5	20
BBW-180-Xtra	0.42	2600	6200	0.09	0.04	10	20
BBW-180-12.5-Xtra	0.42	2600	6200	0.09	0.04	12.5	20
BBW-207-Xtra	0.42	2600	6200	0.09	0.04	15	20
BBW-180-17.5-Xtra	0.42	2600	6200	0.09	0.04	17.5	20
BBW-234-Xtra	0.42	2600	6200	0.09	0.04	20	20
BBW-234-Xtra1	0.42	2600	6200	0.09	0.04	20	25
BBW-234-Xtra2	0.42	2600	6200	0.09	0.04	20	30
BBW-234-Xtra3	0.42	2600	6200	0.09	0.04	20	35
BBW-234-Xtra4	0.42	2600	6200	0.09	0.04	20	40
BBW-234-Xtra5	0.42	2600	6200	0.09	0.04	20	0
BJW-18-5-Xtra	1.86	2600	1400	0.09	0.04	5	20
BJW-18-7.5-Xtra	1.86	2600	1400	0.09	0.04	7.5	20
BJW-18-Xtra	1.86	2600	1400	0.09	0.04	10	20
BJW-18-12.5-Xtra	1.86	2600	1400	0.09	0.04	12.5	20
BJW-45-Xtra	1.86	2600	1400	0.09	0.04	15	20
BJW-18-17.5-Xtra	1.86	2600	1400	0.09	0.04	17.5	20

* **BBW** means **W**alls reinforced with **B**ond **B**eam while **BJW** means **W**alls reinforced with **B**ed **J**oint

Wall ID	Aspect ratio H/L	Height H	Length L	Reinforcement ratio		Masonry comp. strength f'_m	Gross Axial stress/Masonry comp. strength, σ/f'_m
				Vertical ρ_v	Horizontal ρ_h		
	(Unitless)	(mm)	(mm)	(%)	(%)	(MPa)	(%)
BJW-72-Xtra	1.86	2600	1400	0.09	0.04	20	20
BJW-72-Xtra1	1.86	2600	1400	0.09	0.04	20	25
BJW-72-Xtra2	1.86	2600	1400	0.09	0.04	20	30
BJW-72-Xtra3	1.86	2600	1400	0.09	0.04	20	35
BJW-72-Xtra4	1.86	2600	1400	0.09	0.04	20	40
BJW-72-Xtra5	1.86	2600	1400	0.09	0.04	20	0
BJW-99-5-Xtra	1	2600	2600	0.09	0.04	5	20
BJW-99-7.5-Xtra	1	2600	2600	0.09	0.04	7.5	20
BJW-99-Xtra	1	2600	2600	0.09	0.04	10	20
BJW-99-12.5-Xtra	1	2600	2600	0.09	0.04	12.5	20
BJW-126-Xtra	1	2600	2600	0.09	0.04	15	20
BJW-99-17.5-Xtra	1	2600	2600	0.09	0.04	17.5	20
BJW-153-Xtra	1	2600	2600	0.09	0.04	20	20
BJW-153-Xtra1	1	2600	2600	0.09	0.04	20	25
BJW-153-Xtra2	1	2600	2600	0.09	0.04	20	30
BJW-153-Xtra3	1	2600	2600	0.09	0.04	20	35
BJW-153-Xtra4	1	2600	2600	0.09	0.04	20	40
BJW-153-Xtra5	1	2600	2600	0.09	0.04	20	0
BJW-180-5-Xtra	0.42	2600	6200	0.09	0.04	5	20
BJW-180-7.5-Xtra	0.42	2600	6200	0.09	0.04	7.5	20
BJW-180-Xtra	0.42	2600	6200	0.09	0.04	10	20
BJW-180-12.5-Xtra	0.42	2600	6200	0.09	0.04	12.5	20
BJW-207-Xtra	0.42	2600	6200	0.09	0.04	15	20
BJW-180-17.5-Xtra	0.42	2600	6200	0.09	0.04	17.5	20
BJW-234-Xtra	0.42	2600	6200	0.09	0.04	20	20
BJW-234-Xtra1	0.42	2600	6200	0.09	0.04	20	25
BJW-234-Xtra2	0.42	2600	6200	0.09	0.04	20	30
BJW-234-Xtra3	0.42	2600	6200	0.09	0.04	20	35
BJW-234-Xtra4	0.42	2600	6200	0.09	0.04	20	40
BJW-234-Xtra5	0.42	2600	6200	0.09	0.04	20	0

* **BBW** means **W**alls reinforced with **B**ond **B**eam while **BJW** means **W**alls reinforced with **B**ed **J**oint

Wall ID	Aspect ratio H/L	Height H	Length L	Reinforcement ratio		Masonry comp. strength f'_m	Gross Axial stress/Masonry comp. strength, σ/f'_m
				Vertical ρ_v	Horizontal ρ_h		
	(Unitless)	(mm)	(mm)	(%)	(%)	(MPa)	(%)
BBW-63-40	1.86	2600	1400	0.09	0.04	40	5
BBW-72-40	1.86	2600	1400	0.09	0.04	40	10
BBW-81-40	1.86	2600	1400	0.09	0.04	40	15
BBW-144-40	1	2600	2600	0.09	0.04	40	5
BBW-153-40	1	2600	2600	0.09	0.04	40	10
BBW-162-40	1	2600	2600	0.09	0.04	40	15
BBW-225-40	0.42	2600	6200	0.09	0.04	40	5
BBW-234-40	0.42	2600	6200	0.09	0.04	40	10
BBW-243-40	0.42	2600	6200	0.09	0.04	40	15
BJW-63-40	1.86	2600	1400	0.09	0.04	40	5
BJW-72-40	1.86	2600	1400	0.09	0.04	40	10
BJW-81-40	1.86	2600	1400	0.09	0.04	40	15
BJW-144-40	1	2600	2600	0.09	0.04	40	5
BJW-153-40	1	2600	2600	0.09	0.04	40	10
BJW-162-40	1	2600	2600	0.09	0.04	40	15
BJW-225-40	0.42	2600	6200	0.09	0.04	40	5
BJW-234-40	0.42	2600	6200	0.09	0.04	40	10
BJW-243-40	0.42	2600	6200	0.09	0.04	40	15
BBW-227-0.04	0.42	2600	6200	0.26	0.04	20	10
BBW-227-0.09	0.42	2600	6200	0.26	0.09	20	10
BBW-227-0.18	0.42	2600	6200	0.26	0.18	20	10
BBW-227-0.26	0.42	2600	6200	0.26	0.26	20	10
BBW-227-0.35	0.42	2600	6200	0.26	0.35	20	10
BBW-227-0.44	0.42	2600	6200	0.26	0.44	20	10
BBW-227-0.53	0.42	2600	6200	0.26	0.53	20	10
BBW-230-0.04	0.42	2600	6200	0.18	0.04	20	10
BBW-230-0.09	0.42	2600	6200	0.18	0.09	20	10
BBW-230-0.18	0.42	2600	6200	0.18	0.18	20	10
BBW-230-0.26	0.42	2600	6200	0.18	0.26	20	10
BBW-230-0.35	0.42	2600	6200	0.18	0.35	20	10

* **BBW** means **W**alls reinforced with **B**ond **B**eam while **BJW** means **W**alls reinforced with **B**ed **J**oint

Wall ID	Aspect ratio H/L	Height H	Length L	Reinforcement ratio		Masonry comp. strength f'_m	Gross Axial stress/Masonry comp. strength, σ/f'_m
				Vertical ρ_v	Horizontal ρ_h		
	(Unitless)	(mm)	(mm)	(%)	(%)	(MPa)	(%)
BBW-230-0.44	0.42	2600	6200	0.18	0.44	20	10
BBW-230-0.53	0.42	2600	6200	0.18	0.53	20	10
BBW-233-0.04	0.42	2600	6200	0.09	0.04	20	10
BBW-233-0.09	0.42	2600	6200	0.09	0.09	20	10
BBW-233-0.18	0.42	2600	6200	0.09	0.18	20	10
BBW-233-0.26	0.42	2600	6200	0.09	0.26	20	10
BBW-233-0.35	0.42	2600	6200	0.09	0.35	20	10
BBW-233-0.44	0.42	2600	6200	0.09	0.44	20	10
BBW-233-0.53	0.42	2600	6200	0.09	0.53	20	10
BBW-146-0.04	1	2600	2600	0.26	0.04	20	10
BBW-146-0.09	1	2600	2600	0.26	0.09	20	10
BBW-146-0.18	1	2600	2600	0.26	0.18	20	10
BBW-146-0.26	1	2600	2600	0.26	0.26	20	10
BBW-146-0.35	1	2600	2600	0.26	0.35	20	10
BBW-146-0.44	1	2600	2600	0.26	0.44	20	10
BBW-146-0.53	1	2600	2600	0.26	0.53	20	10
BBW-149-0.04	1	2600	2600	0.18	0.04	20	10
BBW-149-0.09	1	2600	2600	0.18	0.09	20	10
BBW-149-0.18	1	2600	2600	0.18	0.18	20	10
BBW-149-0.26	1	2600	2600	0.18	0.26	20	10
BBW-149-0.35	1	2600	2600	0.18	0.35	20	10
BBW-149-0.44	1	2600	2600	0.18	0.44	20	10
BBW-149-0.53	1	2600	2600	0.18	0.53	20	10
BBW-152-0.04	1	2600	2600	0.09	0.04	20	10
BBW-152-0.09	1	2600	2600	0.09	0.09	20	10
BBW-152-0.18	1	2600	2600	0.09	0.18	20	10
BBW-152-0.26	1	2600	2600	0.09	0.26	20	10
BBW-152-0.35	1	2600	2600	0.09	0.35	20	10
BBW-152-0.44	1	2600	2600	0.09	0.44	20	10
BBW-152-0.53	1	2600	2600	0.09	0.53	20	10

* **BBW** means **W**alls reinforced with **B**ond **B**eam while **BJW** means **W**alls reinforced with **B**ed **J**oint

Wall ID	Aspect ratio H/L	Height H	Length L	Reinforcement ratio		Masonry comp. strength f'_m	Gross Axial stress/Masonry comp. strength, σ/f'_m
				Vertical ρ_v	Horizontal ρ_h		
	(Unitless)	(mm)	(mm)	(%)	(%)	(MPa)	(%)
BBW-65-0.04	1.86	2600	1400	0.26	0.04	20	10
BBW-65-0.09	1.86	2600	1400	0.26	0.09	20	10
BBW-65-0.18	1.86	2600	1400	0.26	0.18	20	10
BBW-65-0.26	1.86	2600	1400	0.26	0.26	20	10
BBW-65-0.35	1.86	2600	1400	0.26	0.35	20	10
BBW-65-0.44	1.86	2600	1400	0.26	0.44	20	10
BBW-65-0.53	1.86	2600	1400	0.26	0.53	20	10
BBW-68-0.04	1.86	2600	1400	0.18	0.04	20	10
BBW-68-0.09	1.86	2600	1400	0.18	0.09	20	10
BBW-68-0.18	1.86	2600	1400	0.18	0.18	20	10
BBW-68-0.26	1.86	2600	1400	0.18	0.26	20	10
BBW-68-0.35	1.86	2600	1400	0.18	0.35	20	10
BBW-68-0.44	1.86	2600	1400	0.18	0.44	20	10
BBW-68-0.53	1.86	2600	1400	0.18	0.53	20	10
BBW-71-0.04	1.86	2600	1400	0.09	0.04	20	10
BBW-71-0.09	1.86	2600	1400	0.09	0.09	20	10
BBW-71-0.18	1.86	2600	1400	0.09	0.18	20	10
BBW-71-0.26	1.86	2600	1400	0.09	0.26	20	10
BBW-71-0.35	1.86	2600	1400	0.09	0.35	20	10
BBW-71-0.44	1.86	2600	1400	0.09	0.44	20	10
BBW-71-0.53	1.86	2600	1400	0.09	0.53	20	10
BJW-226-0.05	0.42	2600	6200	0.26	0.05	20	10
BJW-226-0.08	0.42	2600	6200	0.26	0.08	20	10
BJW-226-0.12	0.42	2600	6200	0.26	0.12	20	10
BJW-226-0.17	0.42	2600	6200	0.26	0.17	20	10
BJW-226-0.19	0.42	2600	6200	0.26	0.19	20	10
BJW-226-0.32	0.42	2600	6200	0.26	0.32	20	10
BJW-226-0.40	0.42	2600	6200	0.26	0.40	20	10
BJW-229-0.05	0.42	2600	6200	0.18	0.05	20	10
BJW-229-0.08	0.42	2600	6200	0.18	0.08	20	10

* **BBW** means **W**alls reinforced with **B**ond **B**eam while **BJW** means **W**alls reinforced with **B**ed **J**oint

Wall ID	Aspect ratio H/L	Height H	Length L	Reinforcement ratio		Masonry comp. strength f'_m	Gross Axial stress/Masonry comp. strength, σ/f'_m
				Vertical ρ_v	Horizontal ρ_h		
	(Unitless)	(mm)	(mm)	(%)	(%)	(MPa)	(%)
BJW-229-0.12	0.42	2600	6200	0.18	0.12	20	10
BJW-229-0.17	0.42	2600	6200	0.18	0.17	20	10
BJW-229-0.19	0.42	2600	6200	0.18	0.19	20	10
BJW-229-0.32	0.42	2600	6200	0.18	0.32	20	10
BJW-229-0.40	0.42	2600	6200	0.18	0.40	20	10
BJW-232-0.05	0.42	2600	6200	0.09	0.05	20	10
BJW-232-0.08	0.42	2600	6200	0.09	0.08	20	10
BJW-232-0.12	0.42	2600	6200	0.09	0.12	20	10
BJW-232-0.17	0.42	2600	6200	0.09	0.17	20	10
BJW-232-0.19	0.42	2600	6200	0.09	0.19	20	10
BJW-232-0.32	0.42	2600	6200	0.09	0.32	20	10
BJW-232-0.40	0.42	2600	6200	0.09	0.40	20	10
BJW-145-0.05	1	2600	2600	0.26	0.05	20	10
BJW-145-0.08	1	2600	2600	0.26	0.08	20	10
BJW-145-0.12	1	2600	2600	0.26	0.12	20	10
BJW-145-0.17	1	2600	2600	0.26	0.17	20	10
BJW-145-0.19	1	2600	2600	0.26	0.19	20	10
BJW-145-0.32	1	2600	2600	0.26	0.32	20	10
BJW-145-0.40	1	2600	2600	0.26	0.40	20	10
BJW-148-0.05	1	2600	2600	0.18	0.05	20	10
BJW-148-0.08	1	2600	2600	0.18	0.08	20	10
BJW-148-0.12	1	2600	2600	0.18	0.12	20	10
BJW-148-0.17	1	2600	2600	0.18	0.17	20	10
BJW-148-0.19	1	2600	2600	0.18	0.19	20	10
BJW-148-0.32	1	2600	2600	0.18	0.32	20	10
BJW-148-0.40	1	2600	2600	0.18	0.40	20	10
BJW-151-0.05	1	2600	2600	0.09	0.05	20	10
BJW-151-0.08	1	2600	2600	0.09	0.08	20	10
BJW-151-0.12	1	2600	2600	0.09	0.12	20	10
BJW-151-0.17	1	2600	2600	0.09	0.17	20	10

* **BBW** means **W**alls reinforced with **B**ond **B**eam while **BJW** means **W**alls reinforced with **B**ed **J**oint

Wall ID	Aspect ratio H/L	Height H	Length L	Reinforcement ratio		Masonry comp. strength f'_m	Gross Axial stress/Masonry comp. strength, σ/f'_m
				Vertical ρ_v	Horizontal ρ_h		
	(Unitless)	(mm)	(mm)	(%)	(%)	(MPa)	(%)
BJW-151-0.19	1	2600	2600	0.09	0.19	20	10
BJW-151-0.32	1	2600	2600	0.09	0.32	20	10
BJW-151-0.40	1	2600	2600	0.09	0.40	20	10
BJW-64-0.05	1.86	2600	1400	0.26	0.05	20	10
BJW-64-0.08	1.86	2600	1400	0.26	0.08	20	10
BJW-64-0.12	1.86	2600	1400	0.26	0.12	20	10
BJW-64-0.17	1.86	2600	1400	0.26	0.17	20	10
BJW-64-0.19	1.86	2600	1400	0.26	0.19	20	10
BJW-64-0.32	1.86	2600	1400	0.26	0.32	20	10
BJW-64-0.40	1.86	2600	1400	0.26	0.40	20	10
BJW-67-0.05	1.86	2600	1400	0.18	0.05	20	10
BJW-67-0.08	1.86	2600	1400	0.18	0.08	20	10
BJW-67-0.12	1.86	2600	1400	0.18	0.12	20	10
BJW-67-0.17	1.86	2600	1400	0.18	0.17	20	10
BJW-67-0.19	1.86	2600	1400	0.18	0.19	20	10
BJW-67-0.32	1.86	2600	1400	0.18	0.32	20	10
BJW-67-0.40	1.86	2600	1400	0.18	0.40	20	10
BJW-70-0.05	1.86	2600	1400	0.09	0.05	20	10
BJW-70-0.08	1.86	2600	1400	0.09	0.08	20	10
BJW-70-0.12	1.86	2600	1400	0.09	0.12	20	10
BJW-70-0.17	1.86	2600	1400	0.09	0.17	20	10
BJW-70-0.19	1.86	2600	1400	0.09	0.19	20	10
BJW-70-0.32	1.86	2600	1400	0.09	0.32	20	10
BJW-70-0.40	1.86	2600	1400	0.09	0.40	20	10
Xtra-BBW-9-5	1.86	2600	1400	0.22	0.04	5	5
Xtra-BBW-18-5	1.86	2600	1400	0.22	0.04	5	10
Xtra-BBW-27-5	1.86	2600	1400	0.22	0.04	5	15
Xtra-BBW-9-7.5	1.86	2600	1400	0.22	0.04	7.5	5
Xtra-BBW-18-7.5	1.86	2600	1400	0.22	0.04	7.5	10
Xtra-BBW-27-7.5	1.86	2600	1400	0.22	0.04	7.5	15

* **BBW** means **W**alls reinforced with **B**ond **B**eam while **BJW** means **W**alls reinforced with **B**ed **J**oint

Wall ID	Aspect ratio H/L	Height H	Length L	Reinforcement ratio		Masonry comp. strength f'_m	Gross Axial stress/Masonry comp. strength, σ/f'_m
				Vertical ρ_v	Horizontal ρ_h		
	(Unitless)	(mm)	(mm)	(%)	(%)	(MPa)	(%)
Xtra-BBW-9	1.86	2600	1400	0.22	0.04	10	5
Xtra-BBW-18	1.86	2600	1400	0.22	0.04	10	10
Xtra-BBW-27	1.86	2600	1400	0.22	0.04	10	15
Xtra-BBW-9-12	1.86	2600	1400	0.22	0.04	12.5	5
Xtra-BBW-18-12	1.86	2600	1400	0.22	0.04	12.5	10
Xtra-BBW-27-12	1.86	2600	1400	0.22	0.04	12.5	15
Xtra-BBW-36	1.86	2600	1400	0.22	0.04	15	5
Xtra-BBW-45	1.86	2600	1400	0.22	0.04	15	10
Xtra-BBW-54	1.86	2600	1400	0.22	0.04	15	15
Xtra-BBW-9-17.5	1.86	2600	1400	0.22	0.04	17.5	5
Xtra-BBW-18-17.5	1.86	2600	1400	0.22	0.04	17.5	10
Xtra-BBW-27-17.5	1.86	2600	1400	0.22	0.04	17.5	15
Xtra-BBW-63	1.86	2600	1400	0.22	0.04	20	5
Xtra-BBW-72	1.86	2600	1400	0.22	0.04	20	10
Xtra-BBW-81	1.86	2600	1400	0.22	0.04	20	15
Xtra-BBW-90-5	1	2600	2600	0.22	0.04	5	5
Xtra-BBW-99-5	1	2600	2600	0.22	0.04	5	10
Xtra-BBW-108-5	1	2600	2600	0.22	0.04	5	15
Xtra-BBW-90-7.5	1	2600	2600	0.22	0.04	7.5	5
Xtra-BBW-99-7.5	1	2600	2600	0.22	0.04	7.5	10
Xtra-BBW-108-7.5	1	2600	2600	0.22	0.04	7.5	15
Xtra-BBW-90	1	2600	2600	0.22	0.04	10	5
Xtra-BBW-99	1	2600	2600	0.22	0.04	10	10
Xtra-BBW-108	1	2600	2600	0.22	0.04	10	15
Xtra-BBW-90-12.5	1	2600	2600	0.22	0.04	12.5	5
Xtra-BBW-99-12.5	1	2600	2600	0.22	0.04	12.5	10
Xtra-BBW-108-12.5	1	2600	2600	0.22	0.04	12.5	15
Xtra-BBW-117	1	2600	2600	0.22	0.04	15	5
Xtra-BBW-126	1	2600	2600	0.22	0.04	15	10
Xtra-BBW-135	1	2600	2600	0.22	0.04	15	15

* **BBW** means **W**alls reinforced with **B**ond **B**eam while **BJW** means **W**alls reinforced with **B**ed **J**oint

Wall ID	Aspect ratio H/L	Height H	Length L	Reinforcement ratio		Masonry comp. strength f'_m	Gross Axial stress/Masonry comp. strength, σ/f'_m
				Vertical ρ_v	Horizontal ρ_h		
	(Unitless)	(mm)	(mm)	(%)	(%)	(MPa)	(%)
Xtra-BBW-90-17.5	1	2600	2600	0.22	0.04	17.5	5
Xtra-BBW-99-17.5	1	2600	2600	0.22	0.04	17.5	10
Xtra-BBW-108-17.5	1	2600	2600	0.22	0.04	17.5	15
Xtra-BBW-144	1	2600	2600	0.22	0.04	20	5
Xtra-BBW-153	1	2600	2600	0.22	0.04	20	10
Xtra-BBW-162	1	2600	2600	0.22	0.04	20	15
Xtra-BBW-171-5	0.42	2600	6200	0.22	0.04	5	5
Xtra-BBW-180-5	0.42	2600	6200	0.22	0.04	5	10
Xtra-BBW-189-5	0.42	2600	6200	0.22	0.04	5	15
Xtra-BBW-171-7.5	0.42	2600	6200	0.22	0.04	7.5	5
Xtra-BBW-180-7.5	0.42	2600	6200	0.22	0.04	7.5	10
Xtra-BBW-189-7.5	0.42	2600	6200	0.22	0.04	7.5	15
Xtra-BBW-171	0.42	2600	6200	0.22	0.04	10	5
Xtra-BBW-180	0.42	2600	6200	0.22	0.04	10	10
Xtra-BBW-189	0.42	2600	6200	0.22	0.04	10	15
Xtra-BBW-171-12.5	0.42	2600	6200	0.22	0.04	12.5	5
Xtra-BBW-180-12.5	0.42	2600	6200	0.22	0.04	12.5	10
Xtra-BBW-189-12.5	0.42	2600	6200	0.22	0.04	12.5	15
Xtra-BBW-198	0.42	2600	6200	0.22	0.04	15	5
Xtra-BBW-207	0.42	2600	6200	0.22	0.04	15	10
Xtra-BBW-216	0.42	2600	6200	0.22	0.04	15	15
Xtra-BBW-171-17.5	0.42	2600	6200	0.22	0.04	17.5	5
Xtra-BBW-180-17.5	0.42	2600	6200	0.22	0.04	17.5	10
Xtra-BBW-189-17.5	0.42	2600	6200	0.22	0.04	17.5	15
Xtra-BBW-225	0.42	2600	6200	0.22	0.04	20	5
Xtra-BBW-234	0.42	2600	6200	0.22	0.04	20	10
Xtra-BBW-243	0.42	2600	6200	0.22	0.04	20	15
Xtra-BJW-9-5	1.86	2600	1400	0.22	0.04	5	5
Xtra-BJW-18-5	1.86	2600	1400	0.22	0.04	5	10
Xtra-BJW-27-5	1.86	2600	1400	0.22	0.04	5	15

* **BBW** means **W**alls reinforced with **B**ond **B**eam while **BJW** means **W**alls reinforced with **B**ed **J**oint

Wall ID	Aspect ratio H/L	Height H	Length L	Reinforcement ratio		Masonry comp. strength f'_m	Gross Axial stress/Masonry comp. strength, σ/f'_m
				Vertical ρ_v	Horizontal ρ_h		
	(Unitless)	(mm)	(mm)	(%)	(%)	(MPa)	(%)
Xtra-BJW-9-7.5	1.86	2600	1400	0.22	0.04	7.5	5
Xtra-BJW-18-7.5	1.86	2600	1400	0.22	0.04	7.5	10
Xtra-BJW-27-7.5	1.86	2600	1400	0.22	0.04	7.5	15
Xtra-BJW-9	1.86	2600	1400	0.22	0.04	10	5
Xtra-BJW-18	1.86	2600	1400	0.22	0.04	10	10
Xtra-BJW-27	1.86	2600	1400	0.22	0.04	10	15
Xtra-BJW-9-12.5	1.86	2600	1400	0.22	0.04	12.5	5
Xtra-BJW-18-12.5	1.86	2600	1400	0.22	0.04	12.5	10
Xtra-BJW-27-12.5	1.86	2600	1400	0.22	0.04	12.5	15
Xtra-BJW-36	1.86	2600	1400	0.22	0.04	15	5
Xtra-BJW-45	1.86	2600	1400	0.22	0.04	15	10
Xtra-BJW-54	1.86	2600	1400	0.22	0.04	15	15
Xtra-BJW-9-17.5	1.86	2600	1400	0.22	0.04	17.5	5
Xtra-BJW-18-17.5	1.86	2600	1400	0.22	0.04	17.5	10
Xtra-BJW-27-17.5	1.86	2600	1400	0.22	0.04	17.5	15
Xtra-BJW-63	1.86	2600	1400	0.22	0.04	20	5
Xtra-BJW-72	1.86	2600	1400	0.22	0.04	20	10
Xtra-BJW-81	1.86	2600	1400	0.22	0.04	20	15
Xtra-BJW-90-5	1	2600	2600	0.22	0.04	5	5
Xtra-BJW-99-5	1	2600	2600	0.22	0.04	5	10
Xtra-BJW-108-5	1	2600	2600	0.22	0.04	5	15
Xtra-BJW-90-7.5	1	2600	2600	0.22	0.04	7.5	5
Xtra-BJW-99-7.5	1	2600	2600	0.22	0.04	7.5	10
Xtra-BJW-108-7.5	1	2600	2600	0.22	0.04	7.5	15
Xtra-BJW-90	1	2600	2600	0.22	0.04	10	5
Xtra-BJW-99	1	2600	2600	0.22	0.04	10	10
Xtra-BJW-108	1	2600	2600	0.22	0.04	10	15
Xtra-BJW-90-12.5	1	2600	2600	0.22	0.04	12.5	5
Xtra-BJW-99-12.5	1	2600	2600	0.22	0.04	12.5	10
Xtra-BJW-108-12.5	1	2600	2600	0.22	0.04	12.5	15

* **BBW** means **W**alls reinforced with **B**ond **B**eam while **BJW** means **W**alls reinforced with **B**ed **J**oint

Wall ID	Aspect ratio H/L	Height H	Length L	Reinforcement ratio		Masonry comp. strength f'_m	Gross Axial stress/Masonry comp. strength, σ/f'_m
				Vertical ρ_v	Horizontal ρ_h		
	(Unitless)	(mm)	(mm)	(%)	(%)	(MPa)	(%)
Xtra-BJW-117	1	2600	2600	0.22	0.04	15	5
Xtra-BJW-126	1	2600	2600	0.22	0.04	15	10
Xtra-BJW-135	1	2600	2600	0.22	0.04	15	15
Xtra-BJW-90-17.5	1	2600	2600	0.22	0.04	17.5	5
Xtra-BJW-99-17.5	1	2600	2600	0.22	0.04	17.5	10
Xtra-BJW-108-17.5	1	2600	2600	0.22	0.04	17.5	15
Xtra-BJW-144	1	2600	2600	0.22	0.04	20	5
Xtra-BJW-153	1	2600	2600	0.22	0.04	20	10
Xtra-BJW-162	1	2600	2600	0.22	0.04	20	15
Xtra-BJW-171-5	0.42	2600	6200	0.22	0.04	5	5
Xtra-BJW-180-5	0.42	2600	6200	0.22	0.04	5	10
Xtra-BJW-189-5	0.42	2600	6200	0.22	0.04	5	15
Xtra-BJW-171-7.5	0.42	2600	6200	0.22	0.04	7.5	5
Xtra-BJW-180-7.5	0.42	2600	6200	0.22	0.04	7.5	10
Xtra-BJW-189-7.5	0.42	2600	6200	0.22	0.04	7.5	15
Xtra-BJW-171	0.42	2600	6200	0.22	0.04	10	5
Xtra-BJW-180	0.42	2600	6200	0.22	0.04	10	10
Xtra-BJW-189	0.42	2600	6200	0.22	0.04	10	15
Xtra-BJW-171-12.5	0.42	2600	6200	0.22	0.04	12.5	5
Xtra-BJW-180-12.5	0.42	2600	6200	0.22	0.04	12.5	10
Xtra-BJW-189-12.5	0.42	2600	6200	0.22	0.04	12.5	15
Xtra-BJW-198	0.42	2600	6200	0.22	0.04	15	5
Xtra-BJW-207	0.42	2600	6200	0.22	0.04	15	10
Xtra-BJW-216	0.42	2600	6200	0.22	0.04	15	15
Xtra-BJW-171-17.5	0.42	2600	6200	0.22	0.04	17.5	5
Xtra-BJW-180-17.5	0.42	2600	6200	0.22	0.04	17.5	10
Xtra-BJW-189-17.5	0.42	2600	6200	0.22	0.04	17.5	15
Xtra-BJW-225	0.42	2600	6200	0.22	0.04	20	5
Xtra-BJW-234	0.42	2600	6200	0.22	0.04	20	10
Xtra-BJW-243	0.42	2600	6200	0.22	0.04	20	15

* **BBW** means **W**alls reinforced with **B**ond **B**eam while **BJW** means **W**alls reinforced with **B**ed **J**oint

Wall ID	Aspect ratio H/L	Height H	Length L	Reinforcement ratio		Masonry comp. strength f'_m	Gross Axial stress/Masonry comp. strength, σ/f'_m
				Vertical ρ_v	Horizontal ρ_h		
	(Unitless)	(mm)	(mm)	(%)	(%)	(MPa)	(%)
BBW-231-0.04-0.75	0.42	2600	6200	0.75	0.04	20	10
BBW-231-0.09-0.75	0.42	2600	6200	0.75	0.09	20	10
BBW-231-0.13-0.75	0.42	2600	6200	0.75	0.13	20	10
BBW-231-0.18-0.75	0.42	2600	6200	0.75	0.18	20	10
BBW-231-0.22-0.75	0.42	2600	6200	0.75	0.22	20	10
BBW-231-0.31-0.75	0.42	2600	6200	0.75	0.31	20	10
BBW-231-0.39-0.75	0.42	2600	6200	0.75	0.39	20	10
BBW-231-0.04-0.66	0.42	2600	6200	0.66	0.04	20	10
BBW-231-0.09-0.66	0.42	2600	6200	0.66	0.09	20	10
BBW-231-0.13-0.66	0.42	2600	6200	0.66	0.13	20	10
BBW-231-0.18-0.66	0.42	2600	6200	0.66	0.18	20	10
BBW-231-0.22-0.66	0.42	2600	6200	0.66	0.22	20	10
BBW-231-0.31-0.66	0.42	2600	6200	0.66	0.31	20	10
BBW-231-0.39-0.66	0.42	2600	6200	0.66	0.39	20	10
BBW-231-0.04-0.53	0.42	2600	6200	0.53	0.04	20	10
BBW-231-0.09-0.53	0.42	2600	6200	0.53	0.09	20	10
BBW-231-0.13-0.53	0.42	2600	6200	0.53	0.13	20	10
BBW-231-0.18-0.53	0.42	2600	6200	0.53	0.18	20	10
BBW-231-0.22-0.53	0.42	2600	6200	0.53	0.22	20	10
BBW-231-0.31-0.53	0.42	2600	6200	0.53	0.31	20	10
BBW-231-0.39-0.53	0.42	2600	6200	0.53	0.39	20	10
BBW-153-0.04-0.75	1	2600	2600	0.75	0.04	20	10
BBW-153-0.09-0.75	1	2600	2600	0.75	0.09	20	10
BBW-153-0.13-0.75	1	2600	2600	0.75	0.13	20	10
BBW-153-0.18-0.75	1	2600	2600	0.75	0.18	20	10
BBW-153-0.22-0.75	1	2600	2600	0.75	0.22	20	10
BBW-153-0.31-0.75	1	2600	2600	0.75	0.31	20	10
BBW-153-0.39-0.75	1	2600	2600	0.75	0.39	20	10
BBW-153-0.04-0.66	1	2600	2600	0.66	0.04	20	10
BBW-153-0.09-0.66	1	2600	2600	0.66	0.09	20	10

* **BBW** means **W**alls reinforced with **B**ond **B**eam while **BJW** means **W**alls reinforced with **B**ed **J**oint

Wall ID	Aspect ratio H/L	Height H	Length L	Reinforcement ratio		Masonry comp. strength f'_m	Gross Axial stress/Masonry comp. strength, σ/f'_m
				Vertical ρ_v	Horizontal ρ_h		
	(Unitless)	(mm)	(mm)	(%)	(%)	(MPa)	(%)
BBW-153-0.13-0.66	1	2600	2600	0.66	0.13	20	10
BBW-153-0.18-0.66	1	2600	2600	0.66	0.18	20	10
BBW-153-0.22-0.66	1	2600	2600	0.66	0.22	20	10
BBW-153-0.31-0.66	1	2600	2600	0.66	0.31	20	10
BBW-153-0.39-0.66	1	2600	2600	0.66	0.39	20	10
BBW-153-0.04-0.53	1	2600	2600	0.53	0.04	20	10
BBW-153-0.09-0.53	1	2600	2600	0.53	0.09	20	10
BBW-153-0.13-0.53	1	2600	2600	0.53	0.13	20	10
BBW-153-0.18-0.53	1	2600	2600	0.53	0.18	20	10
BBW-153-0.22-0.53	1	2600	2600	0.53	0.22	20	10
BBW-153-0.31-0.53	1	2600	2600	0.53	0.31	20	10
BBW-153-0.39-0.53	1	2600	2600	0.53	0.39	20	10
BBW-69-0.04-0.75	1.86	2600	1400	0.75	0.04	20	10
BBW-69-0.09-0.75	1.86	2600	1400	0.75	0.09	20	10
BBW-69-0.13-0.75	1.86	2600	1400	0.75	0.13	20	10
BBW-69-0.18-0.75	1.86	2600	1400	0.75	0.18	20	10
BBW-69-0.22-0.75	1.86	2600	1400	0.75	0.22	20	10
BBW-69-0.31-0.75	1.86	2600	1400	0.75	0.31	20	10
BBW-69-0.39-0.75	1.86	2600	1400	0.75	0.39	20	10
BBW-69-0.04-0.66	1.86	2600	1400	0.66	0.04	20	10
BBW-69-0.09-0.66	1.86	2600	1400	0.66	0.09	20	10
BBW-69-0.13-0.66	1.86	2600	1400	0.66	0.13	20	10
BBW-69-0.18-0.66	1.86	2600	1400	0.66	0.18	20	10
BBW-69-0.22-0.66	1.86	2600	1400	0.66	0.22	20	10
BBW-69-0.31-0.66	1.86	2600	1400	0.66	0.31	20	10
BBW-69-0.39-0.66	1.86	2600	1400	0.66	0.39	20	10
BBW-69-0.04-0.53	1.86	2600	1400	0.53	0.04	20	10
BBW-69-0.09-0.53	1.86	2600	1400	0.53	0.09	20	10
BBW-69-0.13-0.53	1.86	2600	1400	0.53	0.13	20	10
BBW-69-0.18-0.53	1.86	2600	1400	0.53	0.18	20	10

* **BBW** means **W**alls reinforced with **B**ond **B**eam while **BJW** means **W**alls reinforced with **B**ed **J**oint

Wall ID	Aspect ratio H/L	Height H	Length L	Reinforcement ratio		Masonry comp. strength f'_m	Gross Axial stress/Masonry comp. strength, σ/f'_m
				Vertical ρ_v	Horizontal ρ_h		
	(Unitless)	(mm)	(mm)	(%)	(%)	(MPa)	(%)
BBW-69-0.22-0.53	1.86	2600	1400	0.53	0.22	20	10
BBW-69-0.31-0.53	1.86	2600	1400	0.53	0.31	20	10
BBW-69-0.39-0.53	1.86	2600	1400	0.53	0.39	20	10
BJW-231-0.04-0.75	0.42	2600	6200	0.75	0.05	20	10
BJW-231-0.08-0.75	0.42	2600	6200	0.75	0.08	20	10
BJW-231-0.12-0.75	0.42	2600	6200	0.75	0.12	20	10
BJW-231-0.17-0.75	0.42	2600	6200	0.75	0.17	20	10
BJW-231-0.19-0.75	0.42	2600	6200	0.75	0.19	20	10
BJW-231-0.32-0.75	0.42	2600	6200	0.75	0.32	20	10
BJW-231-0.39-0.75	0.42	2600	6200	0.75	0.40	20	10
BJW-231-0.04-0.66	0.42	2600	6200	0.66	0.05	20	10
BJW-231-0.08-0.66	0.42	2600	6200	0.66	0.08	20	10
BJW-231-0.12-0.66	0.42	2600	6200	0.66	0.12	20	10
BJW-231-0.17-0.66	0.42	2600	6200	0.66	0.17	20	10
BJW-231-0.19-0.66	0.42	2600	6200	0.66	0.19	20	10
BJW-231-0.32-0.66	0.42	2600	6200	0.66	0.32	20	10
BJW-231-0.39-0.66	0.42	2600	6200	0.66	0.40	20	10
BJW-231-0.04-0.53	0.42	2600	6200	0.53	0.05	20	10
BJW-231-0.08-0.53	0.42	2600	6200	0.53	0.08	20	10
BJW-231-0.12-0.53	0.42	2600	6200	0.53	0.12	20	10
BJW-231-0.17-0.53	0.42	2600	6200	0.53	0.17	20	10
BJW-231-0.19-0.53	0.42	2600	6200	0.53	0.19	20	10
BJW-231-0.32-0.53	0.42	2600	6200	0.53	0.32	20	10
BJW-231-0.39-0.53	0.42	2600	6200	0.53	0.40	20	10
BJW-151-0.04-0.75	1	2600	2600	0.75	0.05	20	10
BJW-151-0.08-0.75	1	2600	2600	0.75	0.08	20	10
BJW-151-0.12-0.75	1	2600	2600	0.75	0.12	20	10
BJW-151-0.17-0.75	1	2600	2600	0.75	0.17	20	10
BJW-151-0.19-0.75	1	2600	2600	0.75	0.19	20	10
BJW-151-0.32-0.75	1	2600	2600	0.75	0.32	20	10

* **BBW** means **W**alls reinforced with **B**ond **B**eam while **BJW** means **W**alls reinforced with **B**ed **J**oint

Wall ID	Aspect ratio H/L	Height H	Length L	Reinforcement ratio		Masonry comp. strength f'_m	Gross Axial stress/Masonry comp. strength, σ/f'_m
				Vertical ρ_v	Horizontal ρ_h		
	(Unitless)	(mm)	(mm)	(%)	(%)	(MPa)	(%)
BJW-151-0.39-0.75	1	2600	2600	0.75	0.40	20	10
BJW-151-0.04-0.66	1	2600	2600	0.66	0.05	20	10
BJW-151-0.08-0.66	1	2600	2600	0.66	0.08	20	10
BJW-151-0.12-0.66	1	2600	2600	0.66	0.12	20	10
BJW-151-0.17-0.66	1	2600	2600	0.66	0.17	20	10
BJW-151-0.19-0.66	1	2600	2600	0.66	0.19	20	10
BJW-151-0.32-0.66	1	2600	2600	0.66	0.32	20	10
BJW-151-0.39-0.66	1	2600	2600	0.66	0.40	20	10
BJW-151-0.04-0.53	1	2600	2600	0.53	0.05	20	10
BJW-151-0.08-0.53	1	2600	2600	0.53	0.08	20	10
BJW-151-0.12-0.53	1	2600	2600	0.53	0.12	20	10
BJW-151-0.17-0.53	1	2600	2600	0.53	0.17	20	10
BJW-151-0.19-0.53	1	2600	2600	0.53	0.19	20	10
BJW-151-0.32-0.53	1	2600	2600	0.53	0.32	20	10
BJW-151-0.39-0.53	1	2600	2600	0.53	0.40	20	10
BJW-70-0.04-0.75	1.86	2600	1400	0.75	0.05	20	10
BJW-70-0.08-0.75	1.86	2600	1400	0.75	0.08	20	10
BJW-70-0.12-0.75	1.86	2600	1400	0.75	0.12	20	10
BJW-70-0.17-0.75	1.86	2600	1400	0.75	0.17	20	10
BJW-70-0.19-0.75	1.86	2600	1400	0.75	0.19	20	10
BJW-70-0.32-0.75	1.86	2600	1400	0.75	0.32	20	10
BJW-70-0.39-0.75	1.86	2600	1400	0.75	0.40	20	10
BJW-70-0.04-0.66	1.86	2600	1400	0.66	0.05	20	10
BJW-70-0.08-0.66	1.86	2600	1400	0.66	0.08	20	10
BJW-70-0.12-0.66	1.86	2600	1400	0.66	0.12	20	10
BJW-70-0.17-0.66	1.86	2600	1400	0.66	0.17	20	10
BJW-70-0.19-0.66	1.86	2600	1400	0.66	0.19	20	10
BJW-70-0.32-0.66	1.86	2600	1400	0.66	0.32	20	10
BJW-70-0.39-0.66	1.86	2600	1400	0.66	0.40	20	10
BJW-70-0.04-0.53	1.86	2600	1400	0.53	0.05	20	10

* **BBW** means **W**alls reinforced with **B**ond **B**eam while **BJW** means **W**alls reinforced with **B**ed **J**oint

Wall ID	Aspect ratio H/L	Height H	Length L	Reinforcement ratio		Masonry comp. strength f'_m	Gross Axial stress/Masonry comp. strength, σ/f'_m
				Vertical ρ_v	Horizontal ρ_h		
	(Unitless)	(mm)	(mm)	(%)	(%)	(MPa)	(%)
BJW-70-0.08-0.53	1.86	2600	1400	0.53	0.08	20	10
BJW-70-0.12-0.53	1.86	2600	1400	0.53	0.12	20	10
BJW-70-0.17-0.53	1.86	2600	1400	0.53	0.17	20	10
BJW-70-0.19-0.53	1.86	2600	1400	0.53	0.19	20	10
BJW-70-0.32-0.53	1.86	2600	1400	0.53	0.32	20	10
BJW-70-0.39-0.53	1.86	2600	1400	0.53	0.40	20	10
BBW-72-0.04-0.75	1.86	2600	1400	0.75	0.04	20	10
BBW-72-0.09-0.75	1.86	2600	1400	0.75	0.09	20	10
BBW-72-0.13-0.75	1.86	2600	1400	0.75	0.13	20	10
BBW-72-0.18-0.75	1.86	2600	1400	0.75	0.18	20	10
BBW-72-0.22-0.75	1.86	2600	1400	0.75	0.22	20	10
BBW-72-0.31-0.75	1.86	2600	1400	0.75	0.31	20	10
BBW-72-0.39-0.75	1.86	2600	1400	0.75	0.39	20	10
BBW-72-0.04-0.66	1.86	2600	1400	0.66	0.04	20	10
BBW-72-0.09-0.66	1.86	2600	1400	0.66	0.09	20	10
BBW-72-0.13-0.66	1.86	2600	1400	0.66	0.13	20	10
BBW-72-0.18-0.66	1.86	2600	1400	0.66	0.18	20	10
BBW-72-0.22-0.66	1.86	2600	1400	0.66	0.22	20	10
BBW-72-0.31-0.66	1.86	2600	1400	0.66	0.31	20	10
BBW-72-0.39-0.66	1.86	2600	1400	0.66	0.39	20	10
BBW-72-0.04-0.53	1.86	2600	1400	0.53	0.04	20	10
BBW-72-0.09-0.53	1.86	2600	1400	0.53	0.09	20	10
BBW-72-0.13-0.53	1.86	2600	1400	0.53	0.13	20	10
BBW-72-0.18-0.53	1.86	2600	1400	0.53	0.18	20	10
BBW-72-0.22-0.53	1.86	2600	1400	0.53	0.22	20	10
BBW-72-0.31-0.53	1.86	2600	1400	0.53	0.31	20	10
BBW-72-0.39-0.53	1.86	2600	1400	0.53	0.39	20	10
BJW-232-0.04-0.75	0.42	2600	6200	0.75	0.05	20	10
BJW-232-0.08-0.75	0.42	2600	6200	0.75	0.08	20	10
BJW-232-0.12-0.75	0.42	2600	6200	0.75	0.12	20	10

* **BBW** means **W**alls reinforced with **B**ond **B**eam while **BJW** means **W**alls reinforced with **B**ed **J**oint

Wall ID	Aspect ratio H/L	Height H	Length L	Reinforcement ratio		Masonry comp. strength f'_m	Gross Axial stress/Masonry comp. strength, σ/f'_m
				Vertical ρ_v	Horizontal ρ_h		
	(Unitless)	(mm)	(mm)	(%)	(%)	(MPa)	(%)
BJW-232-0.17-0.75	0.42	2600	6200	0.75	0.17	20	10
BJW-232-0.19-0.75	0.42	2600	6200	0.75	0.19	20	10
BJW-232-0.32-0.75	0.42	2600	6200	0.75	0.32	20	10
BJW-232-0.39-0.75	0.42	2600	6200	0.75	0.40	20	10
BJW-232-0.04-0.66	0.42	2600	6200	0.66	0.05	20	10
BJW-232-0.08-0.66	0.42	2600	6200	0.66	0.08	20	10
BJW-232-0.12-0.66	0.42	2600	6200	0.66	0.12	20	10
BJW-232-0.17-0.66	0.42	2600	6200	0.66	0.17	20	10
BJW-232-0.19-0.66	0.42	2600	6200	0.66	0.19	20	10
BJW-232-0.32-0.66	0.42	2600	6200	0.66	0.32	20	10
BJW-232-0.39-0.66	0.42	2600	6200	0.66	0.40	20	10
BJW-232-0.04-0.53	0.42	2600	6200	0.53	0.05	20	10
BJW-232-0.08-0.53	0.42	2600	6200	0.53	0.08	20	10
BJW-232-0.12-0.53	0.42	2600	6200	0.53	0.12	20	10
BJW-232-0.17-0.53	0.42	2600	6200	0.53	0.17	20	10
BJW-232-0.19-0.53	0.42	2600	6200	0.53	0.19	20	10
BJW-232-0.32-0.53	0.42	2600	6200	0.53	0.32	20	10
BJW-232-0.39-0.53	0.42	2600	6200	0.53	0.40	20	10

* **BBW** means **W**alls reinforced with **B**ond **B**eam while **BJW** means **W**alls reinforced with **B**ed **J**oint

APPENDIX C: DESCRIPTION OF 195 EXPERIMENTAL WALLS PROPERTIES FAILED IN DIAGONAL SHEAR SELECTED FOR REGRESSIONS ANALYSIS

Wall ID	Aspect ratio H/L	Height H	Length L	Reinforcement ratio		Masonry comp. strength f'_m	Gross Axial stress/Masonry comp. strength, σ/f'_m
				Vertical ρ_v	Horizontal ρ_h		
	(Unitless)	(mm)	(mm)	(%)	(%)	(MPa)	(%)
Scrivener (1967)-D2	1.00	2438	2438	0.11	0.00	19	5
Scrivener (1967)-C10	1.00	2438	2438	0.00	0.19	16	4
Scrivener (1967)-C7	1.00	2438	2438	0.11	0.07	16	5
Scrivener (1967)-C8	1.00	2438	2438	0.15	0.04	15	5
Scrivener (1967)-C9	1.00	2438	2438	0.19	0.00	15	5
Scrivener (1967)-D11	1.00	2438	2438	0.19	0.00	19	5
Scrivener (1967)-C3	1.00	2438	2438	0.22	0.00	15	7
Scrivener (1967)-D12	1.00	2438	2438	0.22	0.07	18	8
Scrivener (1967)-D13	1.00	2438	2438	0.28	0.17	18	7
Scrivener (1967)-D14	1.00	2438	2438	0.28	0.23	18	9
Meli et al. (1968)-Muro 309	0.83	2650	3200	0.26	0.01	11	0
Meli et al. (1968)-Muro 310	0.83	2650	3200	0.26	0.01	10	4
Meli et al. (1968)-Muro 311	0.83	2650	3200	0.26	0.01	10	2
Meli et al. (1968)-Muro 312	0.83	2650	3200	0.12	0.01	9	0
Meli et al. (1968)-Muro 313	0.83	2650	3200	0.12	0.01	10	0
Meli et al. (1968)-Muro 314	0.83	2650	3200	0.26	0.00	10	2
Meli et al. (1968)-Muro 315	0.83	2650	3200	0.12	0.00	10	0
Meli et al. (1968)-Muro 316	0.83	2650	3200	0.26	0.01	9	4
Meli et al. (1968)-Muro 317	0.83	2650	3200	0.26	0.01	10	0
Meli et al. (1968)-Muro 318	0.83	2650	3200	0.26	0.01	10	0
Chen et al. (1978)-HCBL-11-5	1.17	1422	1219	0.17	0.07	13	4
Chen et al. (1978)- HCBL-11-8	1.17	1422	1219	0.43	0.00	14	4
Chen et al. (1978)-HCBL-11-10	1.17	1422	1219	0.43	0.15	13	4
Tomaževic & Lutman (1988)-CN-0	1.25	1520	1220	0.26	0.00	10	10
Tomaževic & Lutman (1988)-CN-14	1.25	1520	1220	0.26	0.12	10	10
Tomaževic & Lutman (1988)-CN-28	1.25	1520	1220	0.26	0.22	10	10
Tomaževic & Lutman (1988)-CN-50	1.25	1520	1220	0.26	0.45	10	10
Tomaževic & Lutman (1988)-CV-0	2.30	2810	1220	0.26	0.00	10	10
Tomaževic & Lutman (1988)-DN-0	1.25	1520	1220	0.52	0.00	8	12
Tomaževic & Lutman (1988)-DN-14	1.25	1520	1220	0.52	0.12	8	12

Wall ID	Aspect ratio H/L	Height H	Length L	Reinforcement ratio		Masonry comp. strength f'_m	Gross Axial stress/Masonry comp. strength, σ/f'_m
				Vertical ρ_v	Horizontal ρ_h		
	(Unitless)	(mm)	(mm)	(%)	(%)	(MPa)	(%)
Tomaževic and Lutman (1988)-DN-28	1.25	1520	1220	0.52	0.22	8	12
Tomaževic and Lutman (1988)-DN-50	1.25	1520	1220	0.52	0.45	8	12
Tomaževic and Lutman (1988)-DV-0	2.30	2810	1220	0.52	0.00	8	12
Johal and Anderson (1988)-DM1	1.00	813	813	0.25	0.00	9	0
Johal and Anderson (1988)-DM2	1.00	813	813	0.25	0.00	9	0
Johal and Anderson (1988)-DM3	1.00	813	813	0.25	0.00	10	0
Johal and Anderson (1988)-DM4	1.00	813	813	0.25	0.00	10	0
Johal and Anderson (1988)-DM5	1.00	813	813	0.25	0.00	10	0
Johal and Anderson (1988)-DM6	1.00	813	813	0.25	0.00	10	0
Johal and Anderson (1988)-DP1	1.00	813	813	0.25	0.00	11	0
Johal and Anderson (1988)-DP2	1.00	813	813	0.25	0.00	11	0
Johal and Anderson (1988)-DS1	1.00	813	813	0.25	0.00	10	0
Johal and Anderson (1988)-DS2	1.00	813	813	0.25	0.00	10	0
Johal and Anderson (1988)-DS3	1.00	813	813	0.25	0.00	11	0
Johal and Anderson (1988)-DS4	1.00	813	813	0.25	0.00	11	0
Johal and Anderson (1988)-DS5	1.00	813	813	0.25	0.00	10	0
Johal and Anderson (1988)-DS6	1.00	813	813	0.25	0.00	10	0
Johal and Anderson (1988)-DP3	1.00	813	813	0.25	0.00	9	0
Johal and Anderson (1988)-DP4	1.00	813	813	0.25	0.00	9	0
Ghanem et al (1992)-SWA	0.98	2761	2816	0.12	0.12	15	5
Ghanem et al (1992)-SWB	0.98	2761	2816	0.12	0.13	15	5
Ghanem et al (1993)-SW-2	0.98	2761	2816	0.12	0.13	15	5
Ghanem et al (1993)-SW-3	0.98	2761	2816	0.12	0.13	15	9
Schultz (1996)-1	0.50	1422	2845	0.20	0.05	14	3
Schultz (1996)-3	0.70	1422	2032	0.29	0.05	14	3
Schultz (1996)-5	1.00	1422	1422	0.41	0.05	14	3
Schultz (1996)-7	0.50	1422	2845	0.20	0.12	14	3
Schultz (1996)-9	0.70	1422	2032	0.29	0.12	14	3
Schultz (1996)-11	1.00	1422	1422	0.41	0.12	14	3
Schultz et al. (1998)-2	0.50	1422	2845	0.20	0.06	12	4

Wall ID	Aspect ratio H/L	Height H	Length L	Reinforcement ratio		Masonry comp. strength f'_m	Gross Axial stress/Masonry comp. strength, σ/f'_m
				Vertical ρ_v	Horizontal ρ_h		
	(Unitless)	(mm)	(mm)	(%)	(%)	(MPa)	(%)
Schultz et al. (1998)-4	0.70	1422	2032	0.29	0.06	12	4
Schultz et al. (1998)-6	1.00	1422	1422	0.41	0.06	12	4
Schultz et al. (1998)-8	0.50	1422	2845	0.20	0.11	12	4
Schultz et al. (1998)-10	0.70	1422	2032	0.29	0.11	12	4
Schultz et al. (1998)-12	1.00	1422	1422	0.41	0.11	12	4
Maleki et al. (2009)-Wall #2	1.00	3830	3830	0.18	0.05	19	4
Maleki et al. (2009)-Wall #3	1.00	3830	3830	0.16	0.05	20	4
Maleki et al. (2009)-Wall #4	0.53	2011	3830	0.19	0.05	19	4
Elmapruk (2010)-PG127-48	0.54	1422	2642	0.33	0.07	15	1
Elmapruk (2010)-PG180-48	0.54	1422	2642	0.33	0.10	15	1
Elmapruk (2010)-PG127-32	0.54	1422	2642	0.33	0.07	16	1
Elmapruk (2010)-PG127-24	0.54	1422	2642	0.34	0.07	16	1
Minaie et al. (2010)-MC 2	0.63	2438	3861	0.15	0.12	7	5
Minaie et al. (2010)-PCL 2	0.63	2438	3861	0.15	0.12	9	0
Baenziger & Porter (2011)-A-1 (DR)	0.86	2438	2845	0.25	0.11	17	0
Baenziger & Porter (2011)-A-2 (JR)	0.86	2438	2845	0.25	0.15	14	0
Baenziger & Porter (2011)-A-6 (JRx2)	0.86	2438	2845	0.30	0.24	16	0
Baenziger & Porter (2011)-B-7 (DR)	0.86	2438	2845	0.20	0.11	20	0
Baenziger & Porter (2011)-B-5 (JR)	0.86	2438	2845	0.20	0.15	16	0
Baenziger & Porter (2011)-D-3 (DR)	0.57	2438	4267	0.20	0.11	14	0
Baenziger & Porter (2011)-D-4 (JR)	0.57	2438	4267	0.23	0.15	16	0
Baenziger & Porter (2011)-D-8 (JRx2)	0.57	2438	4267	0.23	0.24	18	0
Nolph et al. (2012)-PG120-48	0.85	2235	2631	0.46	0.07	12	1
Nolph et al. (2012)-PG085-32	0.85	2235	2631	0.45	0.05	12	1
Nolph et al. (2012)-PG085-24	0.85	2235	2631	0.46	0.05	13	1
Oan (2013)-1	0.63	1000	1600	0.00	0.00	13	11
Oan (2013)-2	0.63	1000	1600	0.00	0.00	13	11
Oan (2013)-3	0.63	1000	1600	0.00	0.00	13	11
Oan (2013)-4	0.63	1000	1600	0.00	0.06	13	11
Oan (2013)-5	0.63	1000	1600	0.00	0.06	13	11

Wall ID	Aspect ratio H/L	Height H	Length L	Reinforcement ratio		Masonry comp. strength f'_m	Gross Axial stress/Masonry comp. strength, σ/f'_m
				Vertical ρ_v	Horizontal ρ_h		
	(Unitless)	(mm)	(mm)	(%)	(%)	(MPa)	(%)
Oan (2013)-6	0.63	1000	1600	0.00	0.06	13	11
Oan (2013)-7	0.63	1000	1600	0.00	0.10	13	11
Oan (2013)-8	0.63	1000	1600	0.00	0.10	13	11
Oan (2013)-9	0.63	1000	1600	0.00	0.10	13	11
Oan (2013)-10	0.63	1000	1600	0.26	0.00	13	11
Oan (2013)-11	0.63	1000	1600	0.26	0.00	13	11
Oan (2013)-12	0.63	1000	1600	0.26	0.00	13	11
Oan (2013)-13	0.63	1000	1600	0.26	0.10	13	11
Oan (2013)-14	0.63	1000	1600	0.26	0.10	13	11
Oan (2013)-15	0.63	1000	1600	0.26	0.10	13	11
Oan (2013)-19	0.63	1000	1600	0.00	0.00	13	17
Oan (2013)-20	0.63	1000	1600	0.00	0.00	13	17
Oan (2013)-21	0.63	1000	1600	0.00	0.00	13	17
Oan (2013)-22	0.63	1000	1600	0.00	0.06	13	17
Oan (2013)-23	0.63	1000	1600	0.00	0.06	13	17
Oan (2013)-24	0.63	1000	1600	0.00	0.06	13	17
Oan (2013)-25	0.63	1000	1600	0.00	0.10	13	17
Oan (2013)-26	0.63	1000	1600	0.00	0.10	13	17
Oan (2013)-27	0.63	1000	1600	0.00	0.10	13	17
Oan (2013)-28	0.63	1000	1600	0.26	0.00	13	17
Oan (2013)-29	0.63	1000	1600	0.26	0.00	13	17
Oan (2013)-30	0.63	1000	1600	0.26	0.00	13	17
Oan (2013)-31	0.63	1000	1600	0.26	0.10	13	17
Oan (2013)-32	0.63	1000	1600	0.26	0.10	13	17
Oan (2013)-33	0.63	1000	1600	0.26	0.10	13	17
Oan (2013)-37	0.63	1000	1600	0.00	0.00	13	22
Oan (2013)-38	0.63	1000	1600	0.00	0.00	13	22
Oan (2013)-39	0.63	1000	1600	0.00	0.00	13	22
Oan (2013)-40	0.63	1000	1600	0.00	0.06	13	22
Oan (2013)-41	0.63	1000	1600	0.00	0.06	13	22

Wall ID	Aspect ratio H/L	Height H	Length L	Reinforcement ratio		Masonry comp. strength f'_m	Gross Axial stress/Masonry comp. strength, σ/f'_m
				Vertical ρ_v	Horizontal ρ_h		
	(Unitless)	(mm)	(mm)	(%)	(%)	(MPa)	(%)
Oan (2013)-42	0.63	1000	1600	0.00	0.06	13	22
Oan (2013)-43	0.63	1000	1600	0.00	0.10	13	22
Oan (2013)-44	0.63	1000	1600	0.00	0.10	13	22
Oan (2013)-45	0.63	1000	1600	0.00	0.10	13	22
Oan (2013)-46	0.63	1000	1600	0.26	0.00	13	22
Oan (2013)-47	0.63	1000	1600	0.26	0.00	13	22
Oan (2013)-48	0.63	1000	1600	0.26	0.00	13	22
Oan (2013)-49	0.63	1000	1600	0.26	0.10	13	22
Oan (2013)-50	0.63	1000	1600	0.26	0.10	13	22
Oan (2013)-51	0.63	1000	1600	0.26	0.10	13	22
Oan (2013)-P2-61	0.63	1000	1600	0.00	0.06	14	14
Oan (2013)-P2-62	0.63	1000	1600	0.00	0.06	14	14
Oan (2013)-P2-63	0.63	1000	1600	0.00	0.06	14	14
Oan (2013)-P2-64	0.63	1000	1600	0.00	0.06	14	14
Oan (2013)-P2-65	0.63	1000	1600	0.00	0.06	14	14
Oan (2013)-P2-66	0.63	1000	1600	0.00	0.06	14	14
Hoque (2013)-1A	1.00	1800	1800	0.18	0.12	17	7
Hoque (2013)-1B	1.00	1800	1800	0.18	0.12	17	7
Hoque (2013)-2A	1.00	1800	1800	0.18	0.12	17	8
Hoque (2013)-2B	1.00	1800	1800	0.18	0.12	17	7
Hoque (2013)-3A	1.00	1800	1800	0.18	0.12	17	7
Hoque (2013)-3B	1.00	1800	1800	0.18	0.12	17	7
Hoque (2013)-3C	1.00	1800	1800	0.18	0.12	17	7
Hoque (2013)-4A	1.00	1800	1800	0.18	0.12	17	7
Hoque (2013)-4B	1.00	1800	1800	0.18	0.12	17	7
Hoque (2013)-4C	1.00	1800	1800	0.18	0.12	17	7
Hoque (2013)-5A	1.00	1800	1800	0.18	0.03	17	7
Hoque (2013)-5B	1.00	1800	1800	0.18	0.03	17	7
Hoque (2013)-6A	1.00	1800	1800	0.18	0.03	17	7
Hoque (2013)-6B	1.00	1800	1800	0.18	0.03	17	7

Wall ID	Aspect ratio H/L	Height H	Length L	Reinforcement ratio		Masonry comp. strength f'_m	Gross Axial stress/Masonry comp. strength, σ/f'_m
				Vertical ρ_v	Horizontal ρ_h		
	(Unitless)	(mm)	(mm)	(%)	(%)	(MPa)	(%)
Hoque (2013)-7A	1.00	1800	1800	0.18	0.03	17	7
Hoque (2013)-7B	1.00	1800	1800	0.18	0.03	17	7
Hoque (2013)-8A	1.00	1800	1800	0.18	0.03	17	7
Hoque (2013)-8B	1.00	1800	1800	0.18	0.03	17	7
Hamedzadeh (2013)-1B (Type A)	0.85	2191	2585	0.18	0.00	7	11
Hamedzadeh (2013)-2A (Type A)	0.85	2191	2585	0.18	0.00	7	8
Hamedzadeh (2013)-2B (Type A)	0.85	2191	2585	0.18	0.00	7	9
Hamedzadeh (2013)-3A (Type A)	1.00	2589	2585	0.18	0.09	7	10
Hamedzadeh (2013)-3B (Type A)	1.00	2589	2585	0.18	0.09	7	9
Hamedzadeh (2013)-4A (Type B)	0.52	2589	4973	0.14	0.09	7	12
Hamedzadeh (2013)-4B (Type B)	0.52	2589	4973	0.14	0.09	7	12
Hamedzadeh (2013)-4C (Type B)	0.52	2589	4973	0.14	0.09	7	13
Hamedzadeh (2013)-5A (Type B)	0.52	2589	4973	0.14	0.09	7	11
Hamedzadeh (2013)-5B (Type B)	0.52	2589	4973	0.14	0.09	7	13
Hamedzadeh (2013)-5C (Type B)	0.52	2589	4973	0.14	0.09	7	15
Hamedzadeh (2013)-6A (Type C)	0.32	1593	4973	0.19	0.15	7	21
Hamedzadeh (2013)-6B (Type C)	0.32	1593	4973	0.19	0.15	7	14
Hamedzadeh (2013)-6C (Type C)	0.32	1593	4973	0.19	0.15	7	15
Hamedzadeh (2013)-7A (Type C)	0.32	1593	4973	0.19	0.15	7	19
Hamedzadeh (2013)-7B (Type C)	0.32	1593	4973	0.19	0.15	7	19
Hamedzadeh (2013)-7C (Type C)	0.32	1593	4973	0.19	0.15	7	14
Hamedzadeh (2013)-8A (Type D)	0.89	1593	1788	0.26	0.15	7	7
Hamedzadeh (2013)-8B (Type D)	0.89	1593	1788	0.26	0.15	7	7
Hamedzadeh (2013)-8C (Type D)	0.89	1593	1788	0.26	0.15	7	8
Rizaee (2015)-Wall 2-A	1.00	1800	1800	0.18	0.12	14	10
Rizaee (2015)-Wall 3-B	1.00	1800	1800	0.18	0.12	14	10
Rizaee (2015)-Wall 4-B	1.00	1800	1800	0.18	0.12	14	10
Rizaee (2015)-Wall 5-C	1.00	1800	1800	0.18	0.06	17	7
Rizaee (2015)-Wall 6-C	1.00	1800	1800	0.18	0.06	17	7
Rizaee (2015)-Wall 7-D	1.00	1800	1800	0.18	0.06	17	7

Wall ID	Aspect ratio H/L	Height H	Length L	Reinforcement ratio		Masonry comp. strength f'_m	Gross Axial stress/Masonry comp. strength, σ/f'_m
				Vertical ρ_v	Horizontal ρ_h		
	(Unitless)	(mm)	(mm)	(%)	(%)	(MPa)	(%)
Rizaee (2015)-Wall 8-D	1.00	1800	1800	0.18	0.06	17	7
Rizaee (2015)-Wall 9-E	1.00	1800	1800	0.18	0.06	17	7
Rizaee (2015)-Wall 10-E	1.00	1800	1800	0.18	0.06	17	7
Rizaee (2015)-Wall 11-F	1.00	1800	1800	0.18	0.06	12	10
Rizaee (2015)-Wall 12-F	1.00	1800	1800	0.18	0.06	12	10
Rizaee (2015)-Wall 13-G	1.00	1800	1800	0.18	0.03	12	10
Rizaee (2015)-Wall 14-G	1.00	1800	1800	0.18	0.03	12	10
Ramirez et al. (2016)-M1	0.90	1800	1990	0.33	0.04	7	8
Ramirez et al. (2016)-M3	0.90	1800	1990	0.33	0.10	7	8
Ramirez et al. (2016)-M4	0.90	1800	1990	0.33	0.10	7	8
Ramirez et al. (2016)-M6	0.39	1000	2590	0.18	0.10	7	8
Ramirez et al. (2016)-M7	0.39	1000	2590	0.18	0.06	7	0
Ramirez et al. (2016)-M8	1.82	1800	990	0.61	0.04	7	7
Ramirez et al. (2016)-M9	1.82	1800	990	0.61	0.10	7	7
Ramirez et al. (2016)-M10	1.82	1800	990	0.61	0.04	7	0

APPENDIX D: CAPACITY OF 247 NUMERICAL WALLS FAILED IN DIAGONAL SHEAR SELECTED FOR REGRESSIONS ANALYSIS

Wall ID	Flexural Capacity	Shear Capacity			Governing Capacity Mode	FE model Peak load
		Diagonal	Crushing of Comp. strut	Sliding		
	(kN)	(kN)	(kN)	(kN)		(kN)
BBW-3	117	100	135	348	Diagonal shear	97
BBW-12	137	116	135	441	Diagonal shear	108
BBW-21	167	133	135	534	Diagonal shear	119
BBW-30	133	120	165	394	Diagonal shear	119
BBW-39	172	145	165	534	Diagonal shear	146
BBW-42	155	145	165	470	Diagonal shear	138
BBW-66	206	172	190	627	Diagonal shear	179
BBW-69	187	172	190	564	Diagonal shear	169
BBW-83	376	239	250	619	Diagonal shear	254
BBW-84	376	185	250	619	Diagonal shear	223
BBW-86	313	239	250	491	Diagonal shear	227
BBW-87	313	239	250	491	Diagonal shear	227
BBW-90	239	181	243	364	Diagonal shear	178
BBW-93	454	216	250	792	Diagonal shear	250
BBW-96	397	216	250	664	Diagonal shear	238
BBW-99	338	211	243	537	Diagonal shear	229
BBW-102	522	247	250	965	Diagonal shear	271
BBW-105	471	247	250	837	Diagonal shear	261
BBW-108	422	241	243	710	Diagonal shear	245
BBW-110	442	277	306	705	Diagonal shear	325
BBW-111	442	223	306	705	Diagonal shear	297
BBW-113	374	277	306	578	Diagonal shear	287
BBW-114	374	223	306	578	Diagonal shear	273
BBW-116	298	272	298	450	Diagonal shear	245
BBW-117	298	218	298	450	Diagonal shear	236
BBW-120	572	269	306	965	Diagonal shear	342
BBW-123	510	269	306	837	Diagonal shear	325
BBW-126	448	263	298	710	Diagonal shear	315
BBW-137	504	312	353	792	Diagonal shear	377
BBW-138	504	257	353	792	Diagonal shear	363

* **BBW** means **W**alls reinforced with **B**ond **B**eam while **BJW** means **W**alls reinforced with **B**ed **J**oint

Wall ID	Flexural Capacity	Shear Capacity			Governing Capacity Mode	FE model Peak load
		Diagonal	Crushing of Comp. strut	Sliding		
	(kN)	(kN)	(kN)	(kN)		(kN)
BBW-140	433	312	353	664	Diagonal shear	343
BBW-141	433	257	353	664	Diagonal shear	333
BBW-143	356	306	344	537	Diagonal shear	302
BBW-144	356	252	344	537	Diagonal shear	296
BBW-147	685	319	353	1138	Diagonal shear	432
BBW-150	622	319	353	1010	Diagonal shear	410
BBW-153	557	312	344	883	Diagonal shear	399
BBW-163	2260	838	942	1432	Diagonal shear	750
BBW-164	2260	709	942	1432	Diagonal shear	671
BBW-165	2260	580	942	1432	Diagonal shear	609
BBW-166	1739	838	942	1113	Diagonal shear	639
BBW-167	1739	709	942	1113	Diagonal shear	607
BBW-168	1739	580	942	1113	Diagonal shear	577
BBW-170	1244	674	870	795	Diagonal shear	546
BBW-171	1244	545	870	795	Diagonal shear	521
BBW-172	2702	912	942	1844	Diagonal shear	947
BBW-173	2702	782	942	1844	Diagonal shear	861
BBW-174	2702	653	942	1844	Diagonal shear	756
BBW-175	2204	912	942	1525	Diagonal shear	861
BBW-176	2204	782	942	1525	Diagonal shear	805
BBW-177	2204	653	942	1525	Diagonal shear	712
BBW-179	1771	743	870	1207	Diagonal shear	752
BBW-180	1771	613	870	1207	Diagonal shear	720
BBW-182	3028	856	942	2256	Diagonal shear	945
BBW-183	3028	727	942	2256	Diagonal shear	844
BBW-185	2571	856	942	1938	Diagonal shear	882
BBW-186	2571	727	942	1938	Diagonal shear	803
BBW-188	2234	811	870	1619	Diagonal shear	819
BBW-189	2234	681	870	1619	Diagonal shear	782
BBW-190	2612	959	1153	1638	Diagonal shear	940

* **BBW** means **W**alls reinforced with **B**ond **B**eam while **BJW** means **W**alls reinforced with **B**ed **J**oint

Wall ID	Flexural Capacity	Shear Capacity			Governing Capacity Mode	FE model Peak load
		Diagonal	Crushing of Comp. strut	Sliding		
	(kN)	(kN)	(kN)	(kN)		(kN)
BBW-191	2612	830	1153	1638	Diagonal shear	854
BBW-192	2612	701	1153	1638	Diagonal shear	779
BBW-193	2085	959	1153	1319	Diagonal shear	826
BBW-194	2085	830	1153	1319	Diagonal shear	788
BBW-195	2085	701	1153	1319	Diagonal shear	763
BBW-196	1581	916	1066	1001	Diagonal shear	760
BBW-197	1581	787	1066	1001	Diagonal shear	749
BBW-198	1581	658	1066	1001	Diagonal shear	716
BBW-199	3356	1070	1153	2256	Diagonal shear	1336
BBW-200	3356	941	1153	2256	Diagonal shear	1210
BBW-201	3356	811	1153	2256	Diagonal shear	1057
BBW-202	2857	1070	1153	1938	Diagonal shear	1228
BBW-203	2857	941	1153	1938	Diagonal shear	1150
BBW-204	2857	811	1153	1938	Diagonal shear	996
BBW-205	2401	1018	1066	1619	Diagonal shear	1104
BBW-206	2401	889	1066	1619	Diagonal shear	1064
BBW-207	2401	760	1066	1619	Diagonal shear	1033
BBW-209	3948	1051	1153	2875	Diagonal shear	1367
BBW-210	3948	922	1153	2875	Diagonal shear	1213
BBW-212	3482	1051	1153	2556	Diagonal shear	1264
BBW-213	3482	922	1153	2556	Diagonal shear	1161
BBW-215	3118	991	1066	2238	Diagonal shear	1169
BBW-216	3118	862	1066	2238	Diagonal shear	1130
BBW-217	2954	1068	1332	1844	Diagonal shear	1124
BBW-218	2954	938	1332	1844	Diagonal shear	1071
BBW-219	2954	809	1332	1844	Diagonal shear	958
BBW-220	2423	1068	1332	1525	Diagonal shear	1022
BBW-221	2423	938	1332	1525	Diagonal shear	985
BBW-222	2423	809	1332	1525	Diagonal shear	950
BBW-223	1915	1016	1231	1207	Diagonal shear	959

* **BBW** means **W**alls reinforced with **B**ond **B**eam while **BJW** means **W**alls reinforced with **B**ed **J**oint

Wall ID	Flexural Capacity	Shear Capacity			Governing Capacity Mode	FE model Peak load
		Diagonal	Crushing of Comp. strut	Sliding		
	(kN)	(kN)	(kN)	(kN)		(kN)
BBW-224	1915	887	1231	1207	Diagonal shear	924
BBW-225	1915	757	1231	1207	Diagonal shear	906
BBW-226	3997	1215	1332	2668	Diagonal shear	1699
BBW-227	3997	1086	1332	2668	Diagonal shear	1557
BBW-228	3997	956	1332	2668	Diagonal shear	1337
BBW-229	3490	1215	1332	2350	Diagonal shear	1593
BBW-230	3490	1086	1332	2350	Diagonal shear	1472
BBW-231	3490	956	1332	2350	Diagonal shear	1274
BBW-232	3028	1152	1231	2031	Diagonal shear	1436
BBW-233	3028	1023	1231	2031	Diagonal shear	1399
BBW-234	3028	894	1231	2031	Diagonal shear	1342
BBW-236	4848	1233	1332	3493	Diagonal shear	1807
BBW-237	4848	1104	1332	3493	Diagonal shear	1595
BBW-239	4377	1233	1332	3175	Diagonal shear	1659
BBW-240	4377	1104	1332	3175	Diagonal shear	1546
BBW-242	3997	1159	1231	2856	Diagonal shear	1531
BBW-243	3997	1030	1231	2856	Diagonal shear	1486
BJW-3	117	100	135	348	Diagonal shear	83
BJW-12	137	116	135	441	Diagonal shear	94
BJW-21	167	133	135	534	Diagonal shear	102
BJW-30	133	120	165	394	Diagonal shear	106
BJW-38	172	152	165	534	Diagonal shear	135
BJW-39	172	145	165	534	Diagonal shear	123
BJW-42	155	145	165	470	Diagonal shear	118
BJW-56	151	146	190	441	Diagonal shear	131
BJW-57	151	138	190	441	Diagonal shear	125
BJW-65	206	179	190	627	Diagonal shear	166
BJW-66	206	172	190	627	Diagonal shear	153
BJW-69	187	172	190	564	Diagonal shear	145
BJW-82	376	239	250	619	Diagonal shear	233

* **BBW** means **W**alls reinforced with **B**ond **B**eam while **BJW** means **W**alls reinforced with **B**ed **J**oint

Wall ID	Flexural Capacity	Shear Capacity			Governing Capacity Mode	FE model Peak load
		Diagonal	Crushing of Comp. strut	Sliding		
	(kN)	(kN)	(kN)	(kN)		(kN)
BJW-83	376	198	250	619	Diagonal shear	206
BJW-84	376	185	250	619	Diagonal shear	192
BJW-85	313	239	250	491	Diagonal shear	213
BJW-86	313	198	250	491	Diagonal shear	197
BJW-87	313	185	250	491	Diagonal shear	188
BJW-89	239	195	243	364	Diagonal shear	191
BJW-90	239	181	243	364	Diagonal shear	181
BJW-92	454	229	250	792	Diagonal shear	228
BJW-93	454	216	250	792	Diagonal shear	218
BJW-95	397	229	250	664	Diagonal shear	224
BJW-96	397	216	250	664	Diagonal shear	212
BJW-98	338	225	243	537	Diagonal shear	218
BJW-99	338	211	243	537	Diagonal shear	209
BJW-102	522	247	250	965	Diagonal shear	237
BJW-105	471	247	250	837	Diagonal shear	233
BJW-108	422	241	243	710	Diagonal shear	230
BJW-109	442	277	306	705	Diagonal shear	300
BJW-110	442	236	306	705	Diagonal shear	272
BJW-111	442	223	306	705	Diagonal shear	259
BJW-112	374	277	306	578	Diagonal shear	276
BJW-113	374	236	306	578	Diagonal shear	261
BJW-114	374	223	306	578	Diagonal shear	249
BJW-115	298	272	298	450	Diagonal shear	244
BJW-116	298	232	298	450	Diagonal shear	253
BJW-117	298	218	298	450	Diagonal shear	238
BJW-119	572	283	306	965	Diagonal shear	313
BJW-120	572	269	306	965	Diagonal shear	298
BJW-122	510	283	306	837	Diagonal shear	305
BJW-123	510	269	306	837	Diagonal shear	295
BJW-125	448	277	298	710	Diagonal shear	298

* **BBW** means **W**alls reinforced with **B**ond **B**eam while **BJW** means **W**alls reinforced with **B**ed **J**oint

Wall ID	Flexural Capacity	Shear Capacity			Governing Capacity Mode	FE model Peak load
		Diagonal	Crushing of Comp. strut	Sliding		
	(kN)	(kN)	(kN)	(kN)		(kN)
BJW-126	448	263	298	710	Diagonal shear	283
BJW-136	504	311	353	792	Diagonal shear	367
BJW-137	504	271	353	792	Diagonal shear	337
BJW-138	504	257	353	792	Diagonal shear	322
BJW-139	433	311	353	664	Diagonal shear	333
BJW-140	433	271	353	664	Diagonal shear	321
BJW-141	433	257	353	664	Diagonal shear	310
BJW-142	356	305	344	537	Diagonal shear	298
BJW-143	356	265	344	537	Diagonal shear	308
BJW-144	356	252	344	537	Diagonal shear	292
BJW-146	685	332	353	1138	Diagonal shear	398
BJW-147	685	319	353	1138	Diagonal shear	383
BJW-149	622	332	353	1010	Diagonal shear	385
BJW-150	622	319	353	1010	Diagonal shear	375
BJW-152	557	325	344	883	Diagonal shear	379
BJW-153	557	312	344	883	Diagonal shear	359
BJW-163	2260	708	942	1432	Diagonal shear	665
BJW-164	2260	611	942	1432	Diagonal shear	621
BJW-165	2260	579	942	1432	Diagonal shear	594
BJW-166	1739	708	942	1113	Diagonal shear	609
BJW-167	1739	611	942	1113	Diagonal shear	574
BJW-168	1739	579	942	1113	Diagonal shear	551
BJW-169	1244	673	870	795	Diagonal shear	561
BJW-170	1244	577	870	795	Diagonal shear	527
BJW-171	1244	545	870	795	Diagonal shear	514
BJW-172	2702	781	942	1844	Diagonal shear	762
BJW-173	2702	685	942	1844	Diagonal shear	718
BJW-174	2702	653	942	1844	Diagonal shear	705
BJW-175	2204	781	942	1525	Diagonal shear	728
BJW-176	2204	685	942	1525	Diagonal shear	688

* **BBW** means **W**alls reinforced with **B**ond **B**eam while **BJW** means **W**alls reinforced with **B**ed **J**oint

Wall ID	Flexural Capacity	Shear Capacity			Governing Capacity Mode	FE model Peak load
		Diagonal	Crushing of Comp. strut	Sliding		
	(kN)	(kN)	(kN)	(kN)		(kN)
BJW-177	2204	653	942	1525	Diagonal shear	666
BJW-178	1771	742	870	1207	Diagonal shear	705
BJW-179	1771	645	870	1207	Diagonal shear	686
BJW-180	1771	613	870	1207	Diagonal shear	685
BJW-181	3028	855	942	2256	Diagonal shear	818
BJW-182	3028	759	942	2256	Diagonal shear	782
BJW-183	3028	726	942	2256	Diagonal shear	768
BJW-184	2571	855	942	1938	Diagonal shear	789
BJW-185	2571	759	942	1938	Diagonal shear	752
BJW-186	2571	726	942	1938	Diagonal shear	735
BJW-187	2234	810	870	1619	Diagonal shear	778
BJW-188	2234	713	870	1619	Diagonal shear	733
BJW-189	2234	681	870	1619	Diagonal shear	713
BJW-190	2612	829	1153	1638	Diagonal shear	876
BJW-191	2612	733	1153	1638	Diagonal shear	818
BJW-192	2612	701	1153	1638	Diagonal shear	787
BJW-193	2085	829	1153	1319	Diagonal shear	802
BJW-194	2085	733	1153	1319	Diagonal shear	755
BJW-195	2085	701	1153	1319	Diagonal shear	734
BJW-196	1581	786	1066	1001	Diagonal shear	743
BJW-197	1581	689	1066	1001	Diagonal shear	711
BJW-198	1581	657	1066	1001	Diagonal shear	691
BJW-199	3356	940	1153	2256	Diagonal shear	1079
BJW-200	3356	843	1153	2256	Diagonal shear	1018
BJW-201	3356	811	1153	2256	Diagonal shear	996
BJW-202	2857	940	1153	1938	Diagonal shear	1013
BJW-203	2857	843	1153	1938	Diagonal shear	966
BJW-204	2857	811	1153	1938	Diagonal shear	935
BJW-205	2401	888	1066	1619	Diagonal shear	979
BJW-206	2401	791	1066	1619	Diagonal shear	984

* **BBW** means **W**alls reinforced with **B**ond **B**eam while **BJW** means **W**alls reinforced with **B**ed **J**oint

Wall ID	Flexural Capacity	Shear Capacity			Governing Capacity Mode	FE model Peak load
		Diagonal	Crushing of Comp. strut	Sliding		
	(kN)	(kN)	(kN)	(kN)		(kN)
BJW-207	2401	759	1066	1619	Diagonal shear	978
BJW-208	3948	1050	1153	2875	Diagonal shear	1179
BJW-209	3948	954	1153	2875	Diagonal shear	1128
BJW-210	3948	922	1153	2875	Diagonal shear	1108
BJW-211	3482	1050	1153	2556	Diagonal shear	1114
BJW-212	3482	954	1153	2556	Diagonal shear	1073
BJW-213	3482	922	1153	2556	Diagonal shear	1054
BJW-214	3118	990	1066	2238	Diagonal shear	1054
BJW-215	3118	893	1066	2238	Diagonal shear	1066
BJW-216	3118	861	1066	2238	Diagonal shear	1039
BJW-217	2954	937	1332	1844	Diagonal shear	1092
BJW-218	2954	841	1332	1844	Diagonal shear	1001
BJW-219	2954	809	1332	1844	Diagonal shear	971
BJW-220	2423	937	1332	1525	Diagonal shear	991
BJW-221	2423	841	1332	1525	Diagonal shear	941
BJW-222	2423	809	1332	1525	Diagonal shear	917
BJW-223	1915	886	1231	1207	Diagonal shear	941
BJW-224	1915	789	1231	1207	Diagonal shear	896
BJW-225	1915	757	1231	1207	Diagonal shear	878
BJW-226	3997	1085	1332	2668	Diagonal shear	1399
BJW-227	3997	988	1332	2668	Diagonal shear	1310
BJW-228	3997	956	1332	2668	Diagonal shear	1267
BJW-229	3490	1085	1332	2350	Diagonal shear	1288
BJW-230	3490	988	1332	2350	Diagonal shear	1231
BJW-231	3490	956	1332	2350	Diagonal shear	1187
BJW-232	3028	1022	1231	2031	Diagonal shear	1267
BJW-233	3028	925	1231	2031	Diagonal shear	1284
BJW-234	3028	893	1231	2031	Diagonal shear	1255
BJW-235	4848	1232	1332	3493	Diagonal shear	1566
BJW-236	4848	1135	1332	3493	Diagonal shear	1494

* **BBW** means **W**alls reinforced with **B**ond **B**eam while **BJW** means **W**alls reinforced with **B**ed **J**oint

Wall ID	Flexural Capacity	Shear Capacity			Governing Capacity Mode	FE model Peak load
		Diagonal	Crushing of Comp. strut	Sliding		
	(kN)	(kN)	(kN)	(kN)		(kN)
BJW-237	4848	1103	1332	3493	Diagonal shear	1470
BJW-238	4377	1232	1332	3175	Diagonal shear	1434
BJW-239	4377	1135	1332	3175	Diagonal shear	1386
BJW-240	4377	1103	1332	3175	Diagonal shear	1363
BJW-241	3997	1158	1231	2856	Diagonal shear	1392
BJW-242	3997	1061	1231	2856	Diagonal shear	1417
BJW-243	3997	1029	1231	2856	Diagonal shear	1378

* **BBW** means **W**alls reinforced with **B**ond **B**eam while **BJW** means **W**alls reinforced with **B**ed **J**oint

APPENDIX E: DESCRIPTION OF 19 EXPERIMENTAL WALLS PROPERTIES SELECTED TO VALIDATE THE ACCURACY OF THE PROPOSED EQUATION

Wall ID	Aspect ratio H/L	Height H	Length L	Reinforcement ratio		Masonry comp. strength f'_m	Gross Axial stress/Masonry comp. strength, σ/f'_m
				Vertical ρ_v	Horizontal ρ_h		
	(Unitless)	(mm)	(mm)	(%)	(%)	(MPa)	(%)
Maleki et al. (2009)-Wall #1	1.00	3830	3830	0.19	0.05	19	4
Maleki et al. (2009)-Wall #5	1.48	5649	3830	0.19	0.04	19	4
Elmapruk (2010)-PG127-48I	0.54	1422	2642	0.33	0.07	15	1
Elmapruk (2010)-PG254-48	0.54	1422	2642	0.33	0.15	15	1
Minaie et al. (2010)-PCL 1	0.63	2438	3861	0.15	0.12	9	3
Minaie et al. (2010)-MC 2	0.63	2438	3861	0.15	0.12	7	0
Nolph et al. (2012)-PG085-48	0.85	2235	2631	0.46	0.05	12	1
Nolph et al. (2012)-PG169-48	0.85	2235	2631	0.46	0.09	12	1
Ramirez et al. (2016)-M2	0.90	1800	1990	0.33	0.04	7	8
Ramirez et al. (2016)-M5	0.39	1000	2590	0.18	0.06	7	8
Bolhassani et al. (2016b)-SR	1.00	3860.00	3860.00	0.08	0.08	17	0.40
Calder´on et al. (2021a)-BJRW-A	0.86	2270	2640	0.34	0.10	23	2
Calder´on et al. (2021a)-BJRW-B	0.86	2270	2640	0.34	0.10	23	2
Calder´on et al. (2021a)-BBRW	0.86	2270	2640	0.34	0.11	23	2
Calder´on et al. (2021a)-BJR+BBRW	0.86	2270	2640	0.34	0.09	23	2
Chapter 3-BB Squat	1	2600	2600	0.09	0.04	20.7	10
Chapter 3-BJ Squat	1	2600	2600	0.09	0.05	20.7	10
Vargas et al. (2023)-P1	1	2270	1020	0.34	0.10	19.3	2
Vargas et al. (2023)-P2	0.86	2270	2640	0.34	0.10	19.3	2

APPENDIX F: CAPACITY OF 25 NUMERICAL WALLS SELECTED TO VALIDATE THE ACCURACY OF THE PROPOSED EQUATION

Wall ID	Flexural Capacity	Shear Capacity			Governing Capacity Mode	FE model Peak load
		Diagonal	Crushing of Comp. strut	Sliding		
	(kN)	(kN)	(kN)	(kN)		(kN)
BBW-90-12.5	269	200	272	407	Diagonal shear	206
BBW-99-12.5	393	238	272	623	Diagonal shear	273
BBW-90-17.5	327	235	321	494	Diagonal shear	266
BBW-99-17.5	503	288	321	796	Diagonal shear	355
BBW-171-5	890	409	615	588	Diagonal shear	333
BBW-180-5	1134	443	615	795	Diagonal shear	389
BBW-189-5	1341	477	615	1001	Diagonal shear	419
BBW-171-7.5	1072	482	754	691	Diagonal shear	418
BBW-180-7.5	1455	533	754	1001	Diagonal shear	563
BBW-189-7.5	1789	584	754	1310	Diagonal shear	603
BBW-171-12.5	1413	603	973	898	Diagonal shear	619
BBW-180-12.5	2087	688	973	1413	Diagonal shear	882
BBW-189-12.5	2678	773	973	1928	Diagonal shear	955
BBW-171-17.5	1748	709	1151	1104	Diagonal shear	815
BBW-180-17.5	2715	828	1151	1825	Diagonal shear	1174
BBW-189-17.5	3557	947	1151	2547	Diagonal shear	1263
BJW-90-12.5	269	200	272	407	Diagonal shear	212
BJW-99-12.5	393	238	272	623	Diagonal shear	247
BJW-90-17.5	327	235	321	494	Diagonal shear	263
BJW-99-17.5	503	288	321	796	Diagonal shear	325
BJW-171-5	890	409	615	588	Diagonal shear	321
BJW-180-5	1134	443	615	795	Diagonal shear	358
BJW-189-5	1341	477	615	1001	Diagonal shear	380
BJW-171-7.5	1072	481	754	691	Diagonal shear	421
BJW-180-7.5	1455	532	754	1001	Diagonal shear	527

* **BBW** means **W**alls reinforced with **B**ond **B**eam while **BJW** means **W**alls reinforced with **B**ed **J**oint